W. A. Davis
VA Tech

NATIONAL ACADEMIES OF SCIENCE AND ENGINEERING

NATIONAL RESEARCH COUNCIL

of the

UNITED STATES OF AMERICA

UNITED STATES NATIONAL COMMITTEE

International Union of Radio Science

National Radio Science Meeting

5–8 January 1993

Sponsored by USNC/URSI
in cooperation with
Institute of Electrical and Electronics Engineers

University of Colorado
Boulder, Colorado
U.S.A.

National Radio Science Meeting
5-8 January 1993
Condensed Technical Program

Monday, 4 January

2000-2400
USNC-URSI Meeting — Broker Inn

Tuesday, 5 January

0835-1200
B-1 ANTENNAS — CR2-28

0855-1200
A-1 MICROWAVE MEASUREMENTS — CR1-46
D-1 MICROWAVE, QUASI-OPTICAL, AND ELECTROOPTICAL DEVICES — CR1-9
G-1 COORDINATED CAMPAIGNS AND ACTIVE EXPERIMENTS — CR0-30
J/H-1 RADIO AND RADAR ASTRONOMY OF THE SOLAR SYSTEM — CR2-26

1335-1700
B-2 SCATTERING — CR2-28
F-1 SENSING OF ATMOSPHERE AND OCEAN — CR2-6
G-2 IONOSPHERIC PROPAGATION CHANNEL — CR0-30
J/H-2 RADIO AND RADAR ASTRONOMY OF THE SOLAR SYSTEM — CR2-26

1355-1700
A-2 EM FIELD MEASUREMENTS — CR1-46
D-2 OPTOELECTRONICS DEVICES AND APPLICATION — CR1-9

1700-1800
Commission A Business Meeting — CR1-46
Commission C Business Meeting — CR1-40
Commission D Business Meeting — CR1-9
Commission G Business Meeting — CR0-30

Wednesday, 6 January

0815-1200
PLENARY SESSION — MATH 100

1335-1700
B-3 EM THEORY — CR2-28
D-3 MICROWAVE AND MILLIMETER AND RELATED DEVICES — CR1-9
F-2 PROPAGATION MODELING AND SCATTERING — CR2-6
H-1 PLASMA WAVES IN THE IONOSPHERE AND THE MAGNETOSPHERE — CR1-42
J-1 FIBER OPTICS IN RADIO ASTRONOMY — CR2-26

1355-1700
E-1 HIGH POWER ELECTROMAGNETICS (HPE) AND INTERFERENCE PROBLEMS — CR1-40

United States National Committee

INTERNATIONAL UNION OF RADIO SCIENCE

PROGRAM AND ABSTRACTS

National Radio Science Meeting
5-8 January 1993

Sponsored by USNC/URSI in cooperation
with IEEE groups and societies:

Antennas and Propagation
Circuits and Systems
Communications
Electromagnetic Compatibility
Geoscience Electronics
Information Theory
Instrumentation and Measurement
Microwave Theory and Techniques
Nuclear and Plasma Sciences
Quantum Electronics and Applications

NOTE:

Programs and Abstracts of the USNC/URSI Meetings are available from:

USNC/URSI
National Academy of Sciences
2101 Constitution Avenue, N.W.
Washington, DC 20418

at $5 for 1983-1993 meetings.

The full papers are not published in any collected format; requests for them should be addressed to the authors who may have them published on their own initiative. Please note that these meetings are national. They are not organized by the International Union, nor are the programs available from the International Secretariat.

MEMBERSHIP

United States National Committee
INTERNATIONAL UNION OF RADIO SCIENCE

Chairman:	Chalmers M. Butler*
Vice Chairman:	David C. Chang*
Secretary:	Charles M. Rush*
Immediate Past Chairman:	Sidney A. Bowhill*

Members Representing Societies, Groups, and Institutes:

American Geophysical Union	Dr. George W. Reid
American Astronomical Society	Dr. William J. Welch
IEEE Antennas & Propagation Society	Dr. W. Ross Stone
IEEE Microwave Theory and Techniques Society	Dr. A. A. Oliner
IEEE Geosciences and Remote Sensing Society	Dr. Robert E. McIntosh
American Meterological Society	Dr. Richard Hallgren

Members-at-Large:	Dr. Susan Avery
	Dr. Lewis Duncan
	Dr. Robert Mattauch
	Dr. R. M. Price
	Dr. David J. Thompson
	Dr. Donald Wilton

Liaison Representatives from Government Agencies:

National Telecommunications & Information Administration	Mr. Kenneth Allen
National Science Foundation	M. Kent Wilson
Federal Communications Commission	
Department of Defense	Mr. William J. Cook
Department of the Army	Mr. Earl J. Holliman
Department of the Air Force	Dr. Allan C. Schell

Chairmen of the USNC/URSI Commissions:

Commission A	Dr. Motohisa Kanda
Commission B	Dr. Ralph E. Kleinman
Commission C	Dr. Raymond Pickholtz
Commission D	Dr. James W. Mink
Commission E	Dr. Emil F. Soderberg
Commission F	Dr. Juergen H. Richter
Commission G	Dr. Haim Soicher
Commission H	Dr. William Taylor
Commission J	Dr. James M. Moran
Commission K	Dr. James C. Lin

* Member of USNC/URSI Executive Committee

Chairmen and Vice Chairmen of Commissions of URSI resident in the United States:	
Vice Chairman, Commission C	Dr. A. D. Wyner
Vice Chairman, Commission D	Dr. T. Itoh
Vice Chairman, Commission F	Prof. R. K. Moore
Chairman, Commission H	Dr. R. F. Benson
Foreign Secretary of the U.S. National Academy of Sciences	Dr. James B. Wyngaarden
Chair, Commission on Physical Sciences, Mathematics, and Applications, National Research Council	Prof. Richard N. Zare
Chair, Board on Physics and Astronomy, Commission on Physical Sciences, Mathematics, and Applications, National Research Council	Prof. Charles Kennel
Honorary Members	Dr. Harold H. Beverage Dr. Ernst Weber
Director, Board on Physics and Astronomy, Commission on Physical Sciences, Mathematics, and Applications, National Research Council	Dr. Donald C. Shapero
NRC Program Officer, U.S. National Committee for URSI	Dr. Robert L. Riemer

DESCRIPTION OF THE INTERNATIONAL UNION OF RADIO SCIENCE

The International Union of Radio Science is one of 18 world scientific unions organized under the International Council of Scientific Unions (ICSU). It is commonly designated as URSI (from its French name, Union Radio Scientifique Internationale). Its aims are (1) to promote the scientific study of radio communications, (2) to aid and organize radio research requiring cooperation on an international scale and to encourage the discussion and publication of the results, (3) to facilitate agreement upon common methods of measurement and the standardization of measuring instruments, and (4) to stimulate and to coordinate studies of the scientific aspects of telecommunications using electromagnetic waves, guided and unguided. The International Union itself is an organizational framework to aid in promoting these objectives. The actual technical work is largely done by the National Committee in the various countries.

The officers of the International Union are:

President:	E. V. Jull (Canada)
Past President:	Dr. A. L. Cullen (U.K.)
Vice Presidents:	Prof. J. Bach Anderson (Denmark) Dr. P. Bauer (France) R. L. Dowden (N.Z) Prof T. O'Koshi (Japan)
Secretary-General	J. Van Bladel (Belgium)
Honorary Presidents:	G. Beynon (U.K.) W. Dieminger (West Germany) W. Christiansen (Australia) W. Gordon (U.S.A.) F. L. H. M. Stumpers (Netherlands)

The Secretary-General's office and the headquarters of the organization are located at Avenue Albert Lancaster, 32, B-1180 Brussels, Belgium. The Union is supported by contributions (dues) from 38 member countries. Additional funds for symposia and other scientific activities of the Union are provided by ICSU from contributions received for this purpose from UNESCO.

The International Union, as of the XXth General Assembly held in Washington, DC in August 1981, has nine bodies called Commissions for centralizing studies in the principal technical fields.

Every three years the International Union holds a meeting called the General Assembly. The next is the XXIVth, to be held in August of 1993, in Kyoto. The Secretariat prepares and distributes the Proceedings of the General Assemblies. The International Union arranges international symposia on specific subjects pertaining to the work of one or several Commissions and also cooperates with other Unions in international symposia on subjects of joint interest.

Radio is unique among the fields of scientific work in having a specific adaptability to large-scale international research programs, since many of the phenomena that must be studied are worldwide in extent and yet are in a measure subject to control by experimenters. Exploration of space and the extension of scientific observations to the space environment are dependent on radio for their research. One branch, radio astronomy, involves cosmic phenomena. URSI thus has a distinct field of usefulness in furnishing a meeting ground for the numerous workers in the manifold aspects of radio research; its meetings and committee activities furnish valuable means of promoting research through exchange of ideas.

Session A-1 0855-Tues. CR1-46
MICROWAVE MEASUREMENTS
Chairman: Allen C. Newell, Electromagnetic Fields Division,
National Institute of Standards and Technology, Boulder, CO 80303

A1-1 0900 **A NEW ONE-WAY, TWO-PORT NETWORK ANALYZER CALIBRATION: REFLECT-THRU'-LINE (RTL)**

Prof. W.A. Davis*, Dr. D.M. Keller, & M.W. Ditz
The Bradley Department of Electrical Engineering
Virginia Polytechnic Institute and State University
Blacksburg, VA 24061-0111

Calibration of two-port systems for the measurement of non-linear characteristics is presented in this paper. Classically two-port measurement systems are calibrated for a source to be fed to both the input or the output of the system or alternatively requiring reversal of the device under test. A new form of calibration combines the concepts of the Thru'-Reflect-Line (TRL) form of calibration with the concept of load-pull measurement process common to power-amplifier measurements. Indeed, the basic measurements to be determined in such a calibration for large-signal, non-linear devices are the input reflection coefficient and the transmission coefficient (or gain) as a function of the input drive level and the load impedance or load reflection coefficient.

To implement such a measurement system, a one-way measurement structure is implied, rather than the often used two-source system. A set of two dual-directional couplers and a variable load may be used to construct this system along with a network analyzer type of measurement device. The error terms include the three input reflection coefficient terms, a transmission coefficient, a source-ratio term for determining the load, and associated cross-talk and directivity terms. The necessary cross-talk and directivity terms include the leakage from the source to both the transmission and source-ratio measurement ports as well as the leakage from the output and load ports to both the transmission and source-ratio measurement ports. The source-ratio measurement is simply the measurement of the incidence at the output port compared to the incidence from the source, resulting from reflection at the system terminating load.

The input reflection errors may be determined using either a standard reflection calibration or the RL^2 process presented in another paper, the latter process using a thru' and line as the two lines needed in the calibration. The cross-talk from the source to the two output ports of transmission and source-ratio are determined with the device ports disconnected, as in standard network analyzer calibration processes. The remaining four terms of the system are determined with a thru' reference and two discrete loads. Since the reflection system is already calibrated, the load reflection may be determined by reflection measurement as it appears at the reference plane. Thus the measurement of the transmission and source ratio using a thru' and two loads gives the necessary four equations to determine the remaining four system calibration parameters. A final step is required to calibrate the incident wave amplitude.

A example of the measurement of a two-port and the determination of the small signal scattering-parameters using two distinct terminations will be demonstrated in addition to the measurement of the large-signal transmission and reflection versus drive level.

A1-2
0920

Package Transmission Line Characterization

Roger B. Marks & Dylan F. Williams
National Institute of Standards and Technology
Mail Code 813.01, 325 Broadway
Boulder, CO 80303

M. P. Goetz
StratEdge Corp.
4393 Viewridge Ave.
San Diego, CA 92123

Abstract

Circuit interconnections, which play a central role in electronic packaging, are typically constructed from planar waveguides. The modes of such waveguides, even when non-TEM, may be characterized by four frequency-domain transmission line parameters, commonly known as *C*, *L*, *G*, and *R*, the magnitude and frequency dependence of which is critical to package performance. In this paper, we review theoretical expressions for the transmission line parameters and study their behavior numerically for lossy coaxial and coplanar waveguides. We then discuss measurement methods and compare the numerical results to experimental data from measurements of coplanar waveguide on GaAs over a broad spectrum of frequencies. Finally, we present measurements of various waveguide structures used in commercial ceramic microwave packages.

A1-3
0940

NETWORK ANALYZER REFLECTION CALIBRATION: REFLECT-LINE-LINE (RL^2)

Prof. W. A. Davis*
The Bradley Department of Electrical Engineering
Virginia Polytechnic Institute and State University
Blacksburg, VA 24061-0111

The problem of calibrating a network analyzer for precision measurements is not a new problem. For reflection, the open-short-load (OSL) and sliding short methods are common techniques for determining the calibration coefficients of the bi-linear transformation describing the reflection phenomena. This paper presents a new technique based on the concepts of the transmission-reflect-line (TRL) procedure used in 2-port systems. The technique uses two lines which are identical, except in length, and a reflection standard constructed at the desired reference plane on another identical line. This is similar to the use of the thru', reflection, and line standards of TRL and has the same advantage of including all connector effects as part of the measurement system. As a result, the removal of connector and adapter affects is already accomplished with the measurement rather than requiring additional effort to de-embed the desired device parameters. In this particular method, the reference phase is obtained from the known reflection standard rather than the thru' standard since no thru' measurements are included in the process.

To determine the coefficients with these standards, one needs three distinct loads for terminating the two lines. These may be the common open-short-load of OSL or another set of distinct loads, precise knowledge of the loads is not required. If we count the number of unknowns and related equations, we find the desired balance. There are three unknown calibration coefficients, three unknown loads, and an unknown differential propagation term relating the two lines for a total of seven unknowns. The seven equations are generated by measuring the reflection coefficient of the reflection standard as well as the two lines with each of the three loads. The difference between two lines leads to the same limitations due to potential resonance lengths found in the TRL calibration process.

The results of the calibration process will be demonstrated with measurements from an automated microwave network analyzer. A companion paper will consider the extension of this calibration process to a one-way, two-port measurement system useful in the measurement of large signal systems characteristic of power amplifiers and other nonlinear devices.

A1-4 **MEASUREMENT ACCURACIES FOR ON-WAFER AMPLIFIER NOISE**
1020

D. F. Wait
Electromagnetic Fields Division
National Institute of Standards and Technology
Boulder, CO 80303-3328 USA

The National Institute of Standards and Technology (NIST) has programs to develop amplifier noise measurements services. This paper will discuss the accuracy of measurements of noise for an on-wafer X-band (8 - 12 GHz) amplifier.

Four parameters are required to characterize the effective input noise temperature T_e of a linear amplifier as a function of the reflection coefficient of the source Γ_1. The measurements presented in this paper were implemented with cryogenic and ambient temperature primary standards. The measurement accuracy of the effective input noise temperature of low-noise amplifiers with coaxial connectors is about ± 7%. On-wafer noise measurements are significantly less accurate because measurements must be made though coaxial-to-wafer probes.

The noise available at the input port of the on-wafer amplifier is measured with various sources on the output port, then vice-versa. Fifteen ambient temperature standards with various impedances, a cryogenic standard, a cryogenic check standard, and a solid state noise check standard are used in the measurement. The impedance of these standards, and the scattering parameters of the probes and the amplifier under test were measured using a commercial automatic network analyzer.

The results of the on-wafer amplifier and the procedures used to assure the measurement will be discussed. The device we tested proved to have poor stability, so the potential accuracy of the measurement procedure is also addressed.

A1-5
1040

AN ERROR IN RADIOMETRIC MEASUREMENTS DUE TO FRONT-END TEMPERATURE VARIATIONS

Sunchana P. Pucic
Electromagnetic Fields Division
National Institute of Standards and Technology
Boulder, CO 80303

Radiometers measure the available noise temperature of an unknown noise source T_x, by comparing it to the available noise temperatures T_{s_1} and T_{s_2} of two noise standards. A simple 'radiometer equation', applicable to total power and switched (Dicke) radiometers, is given by

$$T_x = T_{s_2} + \frac{M_{s_1}}{M_x}(T_{s_1} - T_{s_2})\frac{Y_x - 1}{Y_{s_1} - 1}. \qquad (1)$$

where M_{s_1}/M_x is the mismatch correction at the input reference plane, and Y_x and Y_{s_1} are the measured power ratios.

The equation owns its simplicity partly to the fact that the radiometer input section is assumed to be at the same temperature as one of the two standards, *i.e.*, T_{s_2} in (1). A deviation ΔT from that requirement results in an error:

$$\epsilon = \left[\left|\frac{T_x - T_{s_2}}{T_{s_1} - T_{s_2}}\right|\left(\frac{M_{s_2}}{M_x} - \frac{M_{s_1}}{M_x}\right) - \left(\frac{M_{s_2}}{M_x} - 1\right)\right]\Delta T. \qquad (2)$$

The error can be substantive: in broadband, un-tuned systems having the temperature deviation of $\Delta T = 3$ K, on the order of 0.5 %.

A1-6 TRACKING FREQUENCY LASER GAUGE

1100 James D. Phillips, M. Charles Noecker, and Robert D. Reasenberg
Smithsonian Astrophysical Observatory
Harvard-Smithsonian Center for Astrophysics, MS 63
60 Garden St., Cambridge, MA 02138

A new class of laser distance gauges provides picometer (pm = 10^{-12} m) optical path accuracy, a factor 1000 better than the resolution of current instruments. The gauges have the advantages of absence of transmissive material from the interferometric path, which eliminates the associated thermally-induced path changes; resonance, which suppresses errors due to beam misalignment; the possibility for using the increased precision of the phase delay measurement to measure absolute distance and (using two or more colors) to correct for path errors due to air; and a readout in the form of an electrically measured frequency.

These distance gauges comprise a laser source, a modulator, and an interferometer. A single-mode polarization-preserving fiber couples light from the modulator to the interferometer. FM sideband locking is used in a null-finding arrangement to determine detuning from the cavity resonance, and optical frequency shifting to keep an optical carrier centered on the resonance under feedback control. The frequency shift required is the measure of optical phase change. When the frequency shifter nears the end of its range, a hop is introduced to cause the gauge to lock onto a neighboring cavity order. To measure absolute distance, the cavity free spectral range can be measured using an additional frequency-shifted, modulated beam locked to a nearby longitudinal order, or the Dual-Frequency Modulation method [DeVoe and Brewer, Phys. Rev. **A30**, 2827(1984)] can be used. These gauges can also employ a non-resonant interferometer.

The Tracking Frequency Gauge (TFG) was tested against a gauge that employed an alternating-frequency technique for null-finding. The beams from both gauges travelled along the same fiber and interferometer paths, and by means of feedback to a PZT the alternating frequency gauge maintained constant the optical path for the TFG. Variations in the TFG output revealed relative drifts. The gauges used a common ultrastabilized HeNe laser source. All beam paths were in air and thus the loop gain to the PZT had to be large to compensate for the path variations of ~0.1 μm. Spurious amplitude modulation introduced by reflections in the optical fiber was suppressed four orders by careful fiber termination. The TFG output showed a root-two-point variance ranging from 1 to 2 pm at averaging times from 1 min to 6 hr. For τ<1 min, the variance increased as $\tau^{-1/2}$, primarily due to incomplete averaging over vibrations. In this range, it is three orders above the shot noise limit. If the tested prototype gauge were used to measure a distance, and not in a comparison of distances measured with the same laser, its stability at long times would be limited by the stability of the laser.

These devices were developed in the course of work on POINTS, a proposed space-based microarcsecond astrometric optical interferometer, which is to be described in the Commission J session. During the laboratory development, the logarithm of the prototype gauge's variance showed fairly steady improvement, and the laboratory effort was suspended when the POINTS flight requirements were met. An application for a patent on the distance gauges has been filed.

B1-1
0840

METHODS TO IMPROVE THE APERTURE EFFICIENCY AND SIMPLIFY THE MECHANICAL MOTION OF SPHERICAL MAIN REFLECTOR SCANNING ANTENNAS

Bing Shen and Warren L. Stutzman
Satellite Communications Laboratory
Bradley Department of Electrical Engineering
Virginia Polytechnic Inst. & State University
Blacksburg, VA 24061-0111

Large reflector antenna systems with spherical main reflectors can be used in high gain, wide angle scanning applications. The performance of a spherical main reflector antenna system can be improved by using two subreflectors to correct for spherical aberration and to control the feed-to-aperture intensity mapping. However, due to the motion of the illuminated aperture area during scan, the aperture efficiency of a spherical main reflector system is limited. Moreover, the suboptics assembly, which consists of two subreflectors and the feed, must be translated and rotated during scan; therefore, the mechanical construction and operation of such systems is difficult. In this presentation we first introduce a method which maintains the illuminated aperture area constant during scan by designing subreflectors that correct for phase errors and produce an isotropic-to-uniform amplitude distribution mapping. In addition, the feed antenna is tilted during scan. We also demonstrate a new design which uses a flat mirror to create the image of the suboptics assembly and to simplify the mechanical motion for scan by fixing the suboptics assembly and rotating the mirror. Discussions on practical design situations and physical optics analysis results are also presented.

B1-2
0900

BEAM EFFICIENCY EVALUATION OF LARGE REFLECTOR RADIOMETER ANTENNAS

Bing Shen and Warren L. Stutzman
Satellite Communications Laboratory
Bradley Department of Electrical Engineering
Virginia Polytechnic Inst. & State University
Blacksburg, VA 24061-0111

Large reflector antennas are usually evaluated through performance parameters such as gain (G), side lobe level (SLL), cross polarization level (XPOL), beam efficiency (BE) and resolution (Δ). In radiometer applications beam efficiency and resolution are especially important. Of course, all of the above mentioned performance parameters need to be evaluated as well as beam efficiency and resolution. However, further information is required to accurately study antennas for radiometer applications. In this presentation the essential factors that determine the radiometer antenna temperature and signal-to-noise ratio are analyzed first, followed by a new approach that determines antenna performance accurately with only the following two parameters:

(1) Objective beam efficiency: The percentage of the co-polarized radiated power relative to the total radiated power of the antenna system within a specified main beam cone. The specified main beam cone angle is determined by the desired resolution and is independent of the antenna pattern.

(2) Integrated XPOL contribution: The percentage of the XPOL radiated power within the observation region of the radiometer relative to the total radiated power of the antenna system.

The method used to calculate these two parameters will be discussed. We conclude that the two parameters are sufficient for the evaluation of large reflector antennas used for radiometer applications.

B1-3
0920

ANALYSIS OF ISOLATED AND COUPLED SUPERQUADRIC LOOP ANTENNAS

M. A. Jensen and Y. Rahmat-Samii
Department of Electrical Engineering
University of California, Los Angeles
Los Angeles, CA, 90024-1594

The rapid expansion in the area of mobile communications has spurred the development of small, low-profile antennas suitable for implementation in portable equipment. In many devices such as pagers and hand-held transceiver units, the circular or non-circular loop antenna proves to be an effective radiator. Where packaging requirements limit the the possible loop shape and size, it is important to understand the effects of the antenna geometry on the input impedance and radiation characteristics. Furthermore, in applications where two loops are configured in an array or antenna diversity scheme, the effects of mutual coupling on the antenna impedance and diversity performance should be taken into account.

This work makes use of the mathematical construction of the superquadric curve to develop a very general formulation which allows modeling of a continuum of different loop geometries, including the well-known circular, square, and folded dipole configurations. The analysis capabilities allow investigation of the characteristics of isolated or coupled superquadric loops with different geometries, excitation, and relative orientation. The solution methodology employs a thin wire form of the electric field integral equation for arbitrarily shaped wires which is solved for the current distribution on the loop via a piecewise sinusoidal Galerkin moment method. The current obtained is subsequently used to find the input impedance, directivity, radiation pattern, and (in the case of coupled loops) self and mutual impedances for the antenna. In order to allow the use of curved wire segments, rather than the commonly employed piecewise linear segments, to construct the antenna geometry, a novel parametric form of the equation for the superquadric loop is developed. Both magnetic frill and delta gap source models are used to allow investigation of different possible feeding scenarios.

Application of the formulation to several superquadric loop configurations allows investigation of the variation of impedance and pattern characteristics with the antenna geometry. For the special case of the commonly-used circular loop antenna, the results are shown to agree favorably with previously computed results. The computations performed lead to some very useful curves which aid in the design of practical superquadric loop radiators. The results provided include the effects of antenna position, excitation, and geometry on the self and mutual impedance of two coupled loops. The current distribution on the coupled loops allows determination of the envelope correlation coefficients for signals received by antennas arranged in a diversity configuration. This computation provides a figure of merit of the system's ability to combat the effects of multipath fading in a typical mobile communications environment.

B1-4
0940

ANTENNA COUPLING AND NEAR-FIELD SAMPLING IN PLANE-POLAR COORDINATES

Arthur D. Yaghjian
Rome Laboratory/ERCT
Hanscom AFB, MA 01731, USA

During the past decade a substantial amount of work has been done and a number of fine articles have been written on the subject of planar near-field antenna measurements in polar coordinates. However, there appears missing from the published literature a rigorous sampling theorem with uniform radial spacing for plane-polar measurements and computations. The rigorous sampling theorem with $\lambda/2$ data point spacing for plane-rectangular scanning does not apply to the radial eigenfunction expansions of plane-polar scanning. Also, there appears absent from the literature a detailed formulation of probe-corrected plane-polar scanning from first principles directly in polar coordinates. The approach in the past has been to base the plane-polar derivations on the formulas from plane-rectangular near-field scanning. Thus, it is the purpose of this paper to derive, directly in plane-polar coordinates, rigorous formulas for near-field antenna coupling and sampling. (See Proc. 14th ESA Workshop on Antenna Measurements, Noordwijk, Netherlands, May 1991.)

The derivations are based on three fundamental theorems of antenna theory. One, the mutual coupling function between two antennas, which translate with respect to each other without rotation, satisfies the homogeneous wave equation when multiple interactions are neglected. Two, the output of a receiving antenna can be expressed as a linear differential operator converting the incident field and its spatial derivatives at a single point in space to an output voltage. Three, the mutual coupling function expanded in plane-polar as well as rectangular eigenfunctions is virtually bandlimited by the free-space propagation constant if the antennas remain outside their reactive zones.

The first theorem is applied to derive a vector plane-polar transmission formula and related expressions for the fields of the test antenna. The second is applied to determine the effect on the vector output of the probe of rotating the probe antenna with respect to the test antenna, or equivalently, the effect on plane-polar data of rotating the test antenna without co-rotating the probe. The third theorem is applied to derive a rigorous sampling-reconstruction theorem for straightforward evaluation of the plane-polar representation coefficients using $\lambda/2$ radial data-point spacing.

Comparisons are made with previous plane-polar expressions, and numerical results are presented for a hypothetical uniformly illuminated circular-aperture test antenna. Finally computer run times are discussed for different methods of processing the plane-polar near-field data.

B1-5
1000

GRADIOMETER ANTENNAS FOR DETECTION OF LONG CONDUCTORS OR CAVITIES

David A. Hill
Electromagnetic Fields Division
National Institute of Standards and Technology
Boulder, CO 80303

A common problem in electromagnetic detection of tunnels or other subsurface objects is that the scattered field is small compared to the primary field and is therefore difficult to detect. This problem occurs for detection of both empty tunnels and tunnels containing conductors. Several techniques have been used to attempt to suppress the primary field: (1) a large separation between the transmitting and receiving antennas in the detection of long conductors at low frequencies, (2) a receiving antenna that is polarized orthogonally to the primary field, and (3) a gradiometer receiving antenna. This paper will consider the gradiometer technique applied to detection of both long conductors and empty tunnels.

For analyzing low-frequency detection of long conductors, we consider a vertical magnetic dipole source in a lossy medium exciting a conductor of infinite length. The conductor can be either insulated or grounded. The gradiometer receiving antenna consists of two vertical magnetic dipoles displaced in the vertical direction and operated in the difference mode. In a parallel scan, the dipole source and the gradiometer are kept at the same height as they are moved vertically in separate boreholes. If the lossy medium is homogeneous, then the primary field is cancelled and the gradiometer receives only the field scattered by the long conductor. This type of scan produces a distinct signature as the gradiometer is moved past the conductor. The signature consists of two peaks separated by a deep null, and this signature has also been observed experimentally.

For analyzing detection of empty cavities, we consider a circular cavity excited by a plane wave of either vertical or horizontal polarization. For vertical (horizontal) polarization, the receiving gradiometer consists of two vertical electric (magnetic) dipoles displaced in the vertical direction and operated in the difference mode. In each case, the primary field is cancelled and only the field scattered by the empty cavity is received. When the gradiometer is scanned in the vertical direction (as in a borehole), the characteristic signature of two peaks separated by a deep null is obtained. The sum output of the two dipoles has also been computed, and this quantity also contains useful information that is similar to the output of a single receiving dipole.

B1-6
1040

COMPUTATIONAL TECHNIQUES FOR SYNTHESIS OF OFFSET DUAL REFLECTOR ANTENNAS

Professor Vladimir Oliker*
Department of Mathematics and Computer Science
Emory University, Atlanta, GA 30322

The geometric optics approximation is used in design of offset single and dual nonaxially symmetric reflector antennas when it is required to control the field amplitude and/or phase on the far field or on the output aperture. The formulation of the problem consists of two steps: (a) using Snell's law one derives the ray tracing equations and (b) using the energy conservation law one derives the relation between the primary feed and output power distribution. In step (b) one needs to compute the Jacobian of the map established by the ray tracing equations. This can be done in different ways which, while expressing the same physical principles, lead to different differential equations. Then, when solving the problem numerically, one may get different results with different sources of errors.

There have been, essentially, two approaches to the problem. B. Kinber in the former USSR and V. Galindo-Israel and his coauthors in USA formulated the problem as a nonlinear system of first order PDE's. This system is solvable only if some integrability conditions are satisfied. These conditions may not always hold and then the solution does not exist. Numerically, however, one still may construct a "solution" which will only approximately satisfy the energy and/or boundary conditions and the errors could be substantial. Another approach, due to F. Brickell and B. Westcott in England, is based on formulating the problem as a complex second order nonlinear PDE for a complex valued quasi-potential defined on the output aperture. The corresponding boundary value problem has to be solved on the output aperture. This adds substantial "rigidity" to the problem, since the output aperture can not serve as a flexible control parameter.

Recently, we proposed an alternative approach to formulating and solving the synthesis problem. We derive a new nonlinear second order PDE describing simultaneously steps (a) and (b). This equation is in real valued form and its solution is the polar radius of the subreflector. The shape of the output aperture is an easily adjustable control parameter. To solve the problem numerically, we convert it into a nonstationary one solved by an implicit iterative scheme.

---

* This research was sponsored by AFOSR(AFSC) under contracts F49620-91-C-0001 and F49620-92-C-0009

B1-7
1100

RADIATION FIELDS FROM TWO WIRE TRANSMISSION LINE ANTENNAS

Albert W Biggs* and Ernest A. Baca
Phillips Laboratory, Kirtland AFB, NM

The family of antennas analyzed and described here originate with two parallel linear perfectly conducting, infinitely thin wires. Spacing between antenna elements is much less than the source wavelength. Excitation currents are constant along the wires, flowing in opposite directions.

Families of these antennas are formed by varying the length of the two wire lines. When length is small compared with the source wavelength, the antenna becomes a pair of infinitesimal or Hertzian dipoles. With longer lengths, they are similar to wave antennas (H.H. Beverage et al, AIEE Trans., 42, 215-266, 1923, transmission line antennas, and horizontal antennas buried in Antarctic ice and snow (A.W. Biggs, IEEE Trans. AP-16, 201-208, 1968. Wave antennas, or Beverage antennas, are single long low wires above the earth's surface, first erected on Long Island and in Scotland in 1923.

Transmission line antennas are single wires above perfectly conducting ground planes so that the lines and their images form a two wire transmission line. These are encountered with coaxial feeds on aircraft, where outer conductors terminate on the aircraft surface and the inner conductor continues slightly and then bends to be parallel with the surface. Terminations may be short or open circuits and mismatched or matched loads, Matched loads simulate constant current excitation, while other loads introduce standing waves.

When lengths increase to several wavelengths, broadside or main lobes increase in magnitude, side lobes increase in number and magnitude, and mainlobe and sidelobe beamwidths decrease. As antenna lengths reach infinity, mainlobe and sidelobe beamwidths reach zero, and the mainlobe increases in the form of Dirac Delta functions.

Antenna patterns are presented for the above varying lengths.

*Visiting Faculty at Phillips Lab until 15 Sept 92, then Elect and Compu Engr Department, University of Alabama in Huntsville, Huntsville, AL 35899

B1-8
1120

ANALYSIS OF THE QUADRIFILAR HELIX USING AN ENERGY PROPAGATION MODEL APPLICATION DISTANCE MEASUREMENT SYSTEMS

J. M. Tranquilla and Radha Telikepalli (Graduate Student)
Radiating Systems Research Laboratory
Department of Electrical Engineering
University of New Brunswick
Fredericton, New Brunswick, Canada, E3B 5A3
(506)453-4561

The concepts of phase and group velocity have important applications in satellite-based distance determination systems using code and carrier phase measurements. This work presents a geometrical representation of electromagnetic energy flow from the quadrifilar helix antenna by means of the Poynting vector flow lines. Deviations of the energy flow lines from the (assumed) straight radial lines results in range errors in distance measurement systems. Amplitude and phase characteristics, phase centre and phase/group velocities are calculated using the energy flow concept from the feed point through the far field region.

B1-9
1140

DESIGN OF ACTIVE MICROSTRIP PATCH ANTENNAS USING THE MULTIPORT NETWORK MODEL

Rajan P. Parrikar and K. C. Gupta*
Department of Electrical and Computer Engineering
University of Colorado at Boulder
Boulder, Colorado 80302

The design of conventional microstrip patch antennas employs passive feed network and separate sources for excitation of the antenna elements. Recent developments have demonstrated the feasibility of combining active devices (Gunn diodes, MESFETS etc.) to generate and feed microwave power to microstrip patch antennas. These "active antenna" configurations provide a compact antenna system wherein the radiating elements and the sources are integrated together to form one component. When an array of these active antennas is used, the power combining takes place spatially and the need for a single high power source is eliminated.

This paper reports experimental investigations of microstrip patch antennas integrated with Gunn diodes as oscillators placed underneath the radiating patch. The Multiport Network Modeling (MNM) approach, which has been used extensively for passive microstrip antenna design, is extended to the design of active antennas. The location of the Gunn diode underneath the patch is an important factor in the design of these oscillator-antenna modules. The MNM technique is used to find the optimum location for the Gunn diode. Also investigated are configurations that use Gunn diodes in conjunction with varactor diodes. These configurations provide a capability for tuning the resonant frequency of active antennas. Again, the MNM approach is used to determine the Gunn and the varactor diode locations.

The paper will discuss design procedures and present sample experimental results.

Session D-1 0855-Tues. CR1-9
MICROWAVE, QUASI-OPTICAL, AND ELECTROOPTICAL DEVICES
Chairmen: James W. Mink, U.S. Army Research Office, Research Triangle Park, NC 27709; and
Z.B. Popovic, Dept. of Electrical and Computer Engineering,
Univ. of Colorado at Boulder, Boulder, CO 80309-0425

D1-1
0900

Frequency Filtered Free-Space Power Combining

Jan McKinnis* Scott Bundy Zoya Basta Popović

Department of Electrical and Computer Engineering
University of Colorado, Boulder, Colorado 80309

A planar transistor grid oscillator is a quasi-optical power combining device ("A 100 MESFET Planar Grid Oscillator," Z. B. Popović, et al., IEEE-MTT Vol. 39, February 1991). To obtain power at higher frequencies, a second planar grid acting as a frequency multiplier can be placed in front of the oscillator ("Milli-meter Wave Diode Grid Frequency Doubler," C. F. Jon, et al., IEEE-MTT Vol. 36, November 1988, and Nonlinear Microwave Circuits, Stephen A. Maas, 1992). The combination of the oscillator and multiplier grids will radiate power at the design frequency as well as at undesired harmonics. A band pass frequency selective surface (FSS) can be used to attenuate the power transmitted at the undesired frequencies ("Techniques for Analyzing Frequency Selective Surfaces - A Review," R. Mittra, et al., Proceedings of the IEEE, Vol. 76, 1988). By setting up the grids and FSS as shown in Figure 1, most of the power transmitted by the FSS will be at the design frequency. To produce a band pass filter, a low pass and a high pass filter were combined. The low pass filter consists of an array of dipoles, and the high pass filter is an array of slots. A bandpass FSS with a resonant frequency at 6 GHz was used with a MESFET grid oscillator that locks at 3 GHz. Between 10 and 15 dB of attenuation was observed at 3 and 9 GHz, and 2 dB of attenuation was measured at the design frequency of 6 GHz.

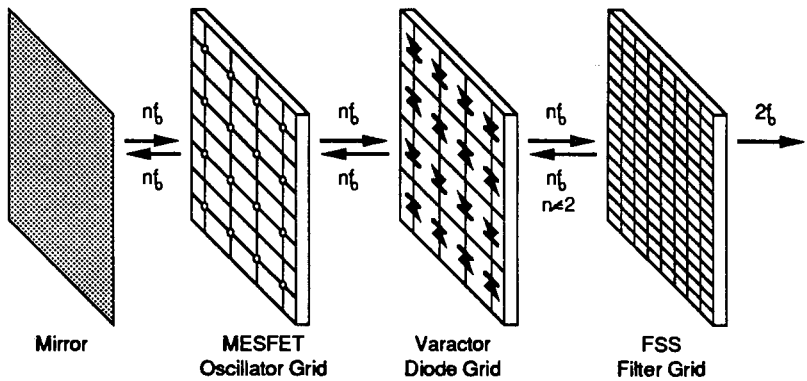

Figure 1: Configuration of the Free-Space Frequency Filtered Sytem.

D1-2
0920

CURRENT AND FIELD DISTRIBUTION ACROSS A 25-HEMT GRID OSCILLATOR

Kuang Yi Chen*, Paul Biernacki
Zoya B. Popović, Alan R. Mickelson,

Department of Electrical and Computer Engineering
University of Colorado at Boulder, Boulder, CO 80309-0425

A grid oscillator is a planar quasi-optical power-combining device ("A 100-MESFET Grid Oscillator," *IEEE MTT-39,* February 1991). The nature of the current and field distribution as well as self-locking properties are not yet understood. We have fabricated a hybrid 25 high electron mobility transistor (HEMT) grid on a GaAs electrooptic substrate. Electrooptic sampling results at a locking frequency of 6 GHz give the current distribution along the radiating drain and gate leads as well as the bias lines. Figure 1(a) shows the HEMT grid oscillator geometry. Figure 1(b) shows the electrooptic sampling measurement of the potential distribution along the gate leads labeled in Figure 1(a). The measured potential distribution is used to find the current distribution, which is then used to find the radiated electric field distribution in the roughly half-wavelength long Fabry-Perot cavity, taking into account the full near-field Green's function.

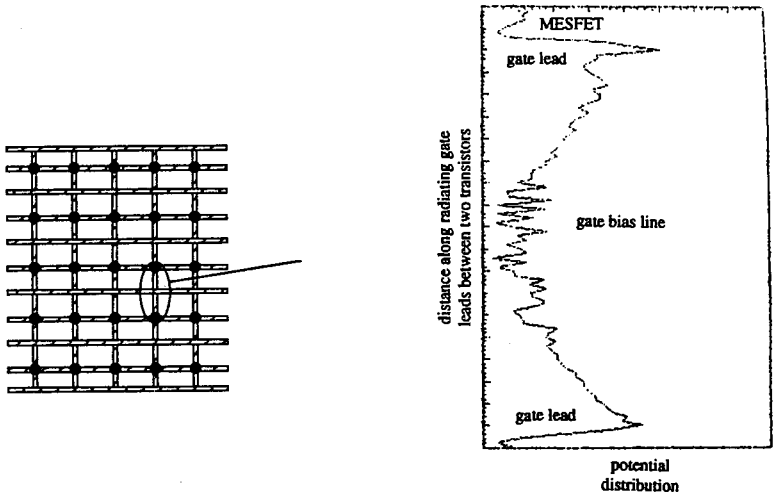

Figure 1. (a) The 25-HEMT grid oscillator geometry. (b) Electrooptical sampling results for the potential along two adjacent radiating gate leads.

D1-3
0940

Quasi-Optical Bar Grid Amplifier

Jon Schoenberg* Thomas Mader Zoya Basta Popović

Department of Electrical and Computer Engineering
University of Colorado, Boulder, Colorado 80309

A new planar bar grid MESFET amplifier is presented. As shown in Figure 1, a low-power input plane wave incident on one side of the grid is amplified and a high-power plane wave is reradiated on the other side of the grid. The bars act as TEM waveguides which couple the free-space plane wave to the transistors in the grid and provide isolation between the input and output waves. In a previously demonstrated grid amplifier, the input and output waves were polarization isolated ("A Grid Amplifier," M. Kim, et al., IEEE-MGWL Vol. 1, November 1991). The structure presented here preserves the polarization between the input and output and also acts as an efficient heatsink. In the bar-grid amplifier, the transistors are placed a small fraction of a wavelength apart, making high power amplification possible with many devices in a small array. The concept of using metal bars to provide good heatsinking was originally demonstrated in a bar grid oscillator by Popović, et al. ("Bar-Grid Oscillators," Z. B. Popović, et al., IEEE-MTT Vol. 38, March 1990). A transmission line circuit model is proposed for predicting the electrical characteristics of the amplifier in which the output power is maximized.

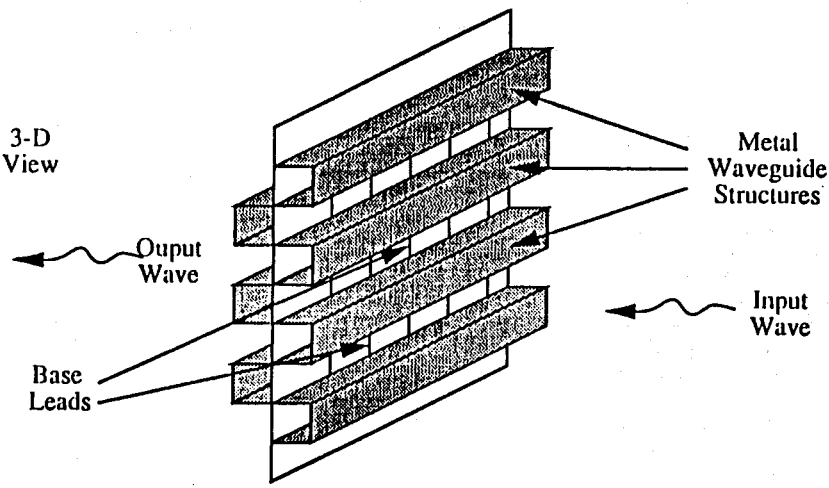

Figure 1: Quasi-optical high-power bar grid amplifier.

D1-4
1000

FINITE DIFFERENCE TIME DOMAIN ANALYSIS OF ANTI-RESONANCE OPTICAL MASKS

El-Badawy El-Sharawy
Department of Electrical Engineering
Arizona State University
Tempe, AZ 852870

Phase shifting masks have recently received considerable interest due to their potential to produce 64 Mb chips with the current i-line lithography. These masks may be the only feasible approach to produce the 256 Mb chips utilizing deep ultraviolet light (h-line). There are two types of phase shifting masks; symmetric (alternating) and asymmetric masks. Alternating masks require periodic structures and thus are disposed to memories. Asymmetric phase shifting masks can be used in nonperiodic structures. However, asymmetric masks such as attenuating and the rim phase shifting mask (M. Levenson,SPIE vol. 1496, pp 20-26, 1990) tend to create sidelobes and decrease depth of focus. In addition, fabrication of this type of masks is usually difficult.

This paper presents a finite difference time domain (FDTD) analysis of a new type of phase shifting masks. The objectives of the new mask are: (1) to improve the image contrast without sacrificing the depth of focus or sidelobe level, and (2) ease of fabrication and repair

The above goals are achieved by adding a second layer of opaque chrome (Figure 1) and controlling the phase of diffraction from the second mask to cancel the diffraction from the first mask. Also, the diffracted light from the top mask decays gradually which reduces the sidelobe level. The new mask is called "the anti-resonance mask". To suppress fields between the two chrome layers and reduce coupling between different nearby lines or opening in the mask, the electrical spacing between the chrome layers is chosen to be $n\pi/4$, n=3,5,7. Combining the anti-resonance and the phase shifting effects, the thickness and refractive index of the dielectric must be chosen to produce a phase difference of π between the free and the dielectric paths. The present analysis shows a contrast improvement of 10-15% for perfectly coherent light without increasing the sidelobe level. Simulation for partially coherent light is underway.

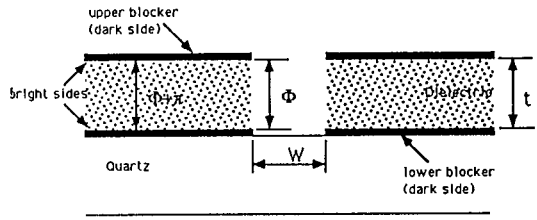

Figure 1. Anti-Resonace Phase Shifting Mask

D1-5
1040

EXPERIMENTALLY VERIFIABLE MODELING OF PARASITICS IN COPLANAR WAVEGUIDE

Dag R. Hjelme*, Vesna Radišić
Zoya B. Popović, Alan R. Mickelson,

Department of Electrical and Computer Engineering
University of Colorado at Boulder, Boulder, CO 80309-0425

Parasitic reactances at microwave and millimeter-wave frequencies due to active device electrodes present a difficult problem with respect to analysis and scaling. Rigorous characterization of these parasitics require a full-wave analysis. However, generally the line dimensions are such that the local field distributions are dominated by the static field. A characterization technique based on these local static fields, as well as a discretized transmission line equation that recovers the dynamics, will be presented. A multiple scales expansion is developed to justify the analysis algorithm. Several passive devices on GaAs substrates with discontinuities and parasitics are fabricated, analyzed and the models are verified using network analysis and a unique optical sampling technique. Figure 1 shows an example of a double step in impedance in CPW, with a plot of the charge distribution on a transverse cross section. The theoretical charge distribution used in the analysis is shown in solid line, and the results from optical sampling measurements are superimposed and show good agreement.

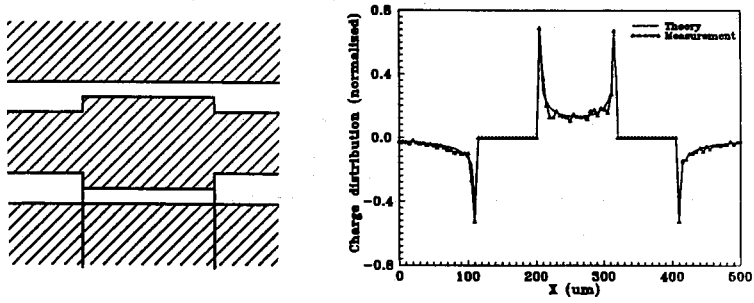

Figure 1. A step in impedance CPW test structure (a) and the theoretical and measured charge distribution on a transverse cross section (b).

D1-6
1100

CROSSTALK REDUCTION USING TRANSPOSED CONDUCTORS

Robert H. Voelker
Dept. of Electrical Engineering
and Center for Electro-Optics
University of Nebraska
Lincoln, NE 68588-0511

The technique of transposing conductors within signal buses is analyzed for reduction of nearest-neighbor crosstalk. This method is applicable to buses in high speed digital and microwave pulse integrated circuits. Conductor transposition provides higher wiring density and less signal distortion and delay than other crosstalk reduction approaches.

Conductors are periodically transposed in a bus to increase the average spacing of conductors which would normally be nearest neighbors in a conventional parallel bus. The increased average spacing reduces capacitive and inductive coupling and thus nearest-neighbor crosstalk compared with an ordinary bus. Additionally, the conductors between a driven line and a coupled line act as shields. A general transposition algorithm is developed for an N-conductor bus. This pattern intertwines all conductors so that a conductor is a nearest neighbor of any other conductor for no more than a fraction of the bus length. Transposition spreads and dilutes the crosstalk signal energy among all conductors, so that an individual neighboring conductor has less crosstalk than in a conventional bus.

A five conductor aluminum bus on a 0.5 mm thick GaAs substrate is analyzed for mutual inductance and capacitance. SPICE simulations using lumped LCR models for the lines are performed for parallel and transposed buses. Simulations show that nearest-neighbor crosstalk is reduced by roughly 30% when a transposed line bus is used. This reduction is possibly useful in high-speed GaAs direct-coupled FET logic (DCFL) digital circuits which have small noise margins. When many lines are driven simultaneously, the crosstalk accumulates on all coupled conductors. However, if it is known beforehand that few conductors will switch simultaneously, such as for a Gray code signal, transposed lines are effective in reducing crosstalk.

Conductor transposition has roughly twice the wiring density compared with other crosstalk reduction techniques such as using grounded conductors between signal lines, fabricating widely spaced lines, or placing a second ground plane immediately above the bus (J. Chilo and T. Arnaud, IEEE Trans., ED-31, 347-352, 1984). Additionally, conductor transposition has less signal distortion and delay than placing a second ground plane above a parallel bus.

D1-7
1120

MODIFIED HARDFET MODULATOR

Istvan Nogradi, Senior Research Engineer
Georgia Tech Research Institute
Georgia Institute of Technology
Atlanta, GA 30332

Commercial, military and planetary pulsed radar systems are configured with "hard-switch" (hard-tube), "line type," and solid-state modulators. Recently, the "Hardfet" concept [1,2,3,4] was added to this selection, with advantages that enhanced the desirable attributes of these classic modulating methods [2]. This paper introduces the concept of a "Modified Hardfet" modulator, presents theoretical considerations, and suggests some configurations and specialized applications.

In the Modified Hardfet concept, the storage capacitors of the original Hardfet modulator are replaced with storage-battery banks [5], but the storage modules are still charged in parallel and partially discharged in series. The parallel-to-series transition can be achieved in a precharacterized and controlled sequence to accommodate possible rate-of-rise-of-voltage (RRV) specifications [6]. This may be accomplished with either solid-state or vacuum switching devices depending on risetime, falltime, pulsewidth, and total rf pulse energy requirements. The switching process is performed via fiber optics and associated circuitry.

The Modified Hardfet approach offers a novel but practical solution to specialized commercial, military, and planetary radar transmitters, with promising possibilities for space application also. Technical advantages lie in their nonexistent ripple, consistent droop, relatively low standby voltages, ease of maintenance, and relatively high safety. The concept eliminates the need for noisy high-voltage dc/dc converters, and for planetary radars it offers feasible implementation without dedicated high power generating systems. Depending on the application, the Modified Hardfet storage banks may be charged/recharged from commercial power sources, local generators, or solar panels.

References:

1.2.3. Nogradi, Istvan:
"Hardfet Radar Modulator" *High-Voltage Workshop. IEEE & DoD October 1989, Session VI-2.*
"Hardfet Modulator" *Twentieth Power Modulator Symposium. IEEE & DoD June 1992, Session 6-26.*
"A Quiet Expendable Signal Source" *High-Voltage Workshop. IEEE & DoD October 1992, Session VII-3.*

4. *D. L. Harris & G. L. Richardson,* ***"A 100 KW Hardfet Modulator"*** *High-Voltage Workshop. IEEE & DoD October 1992, Session VII-4.*
5. *Vankatesan, S., et al.,* ***"Advances in the Development of Ovonic Nickel Hydride Batteries for Industrial and Electrical Vehicles"*** *26th Intersociety Energy Conversion Conference, Boston, MA, August 1991.*
6. *Nogradi, Istvan,* ***"The Envelope Technique for Trigger Amplifiers"*** *Nineteenth Power Modulator Symposium. IEEE & DoD June 1990, Session 2-7.*

G1-1
0900

MULTITECHNIQUE DIAGNOSTICS OF PLASMA DENSITY AND DRIFT STRUCTURES IN THE DAYSIDE CUSP/CLEFT REGION

Su. Basu and C.E. Valladares *(Institute for Space Research, Boston College, Newton, MA 02159)*
S. Basu and J. Buchau *(Phillips Laboratory, GPIA, Hanscom AFB, MA 01731)*
B.W. Reinisch *(Center for Atmospheric Research, University of Massachusetts, Lowell, MA 01854)*

Several campaigns were conducted under the auspices of the CEDAR High Latitude Plasma Structure (HLPS) Working Group and its international counterpart STEP Global Aspects of Plasma Structure (GAPS) Group to investigate the processes by which mid-latitude plasma get access to the polar cap through the dayside cusp/cleft region usually when the interplanetary magnetic field (IMF) has a southward component. This paper will present observations made in Greenland when the Sondrestrom radar made azimuth and elevation scans of the plasma density and convection in the region of entry of enhanced densities. Corroborating evidence for the existence of discrete density enhancements was provided by the digisondes at Sondrestrom and Qanaq. Spaced receivers for scintillation measurements were able to determine the spectral characteristics of km-scale plasma structures and drift characteristics in the region of entry near Sondrestrom and the evolution of these irregularity characteristics in the central polar cap at Thule. It was found that a vortex-like structure in the convection pattern accompanied by rapid eastward flows were probably instrumental in the break-up of the convected enhanced density sub-auroral plasma into discrete density structures of dimensions several hundred km known as polar cap patches. A companion paper presents a modeling of such patch structures based on many of the measured parameters presented in this paper.

G1-2
0920

MODELING POLAR CAP F LAYER PATCHES

Dwight T. Decker, Institute for Space Research, Boston College, 885 Centre St., Newton, MA 02159
C.E. Valladares, Institute for Space Research, Boston College, Newton, MA 02159
R. Sheehan, Physics Dept., Boston College, Chestnut Hill, MA 02167
D.N. Anderson, Phillips Laboratory, GPIM, Hanscom AFB, MA 01731
R.A. Heelis, Center for Space Research, University of Texas at Dallas, Dallas, TX 75083-0688

A comprehensive, time-dependent, high latitude, one species F region model has been developed to study the various physical processes which are believed to affect the polar cap plasma density distributions as a function of altitude, latitude, longitude, and local time. These processes include production of ionization by solar extreme ultraviolet radiation and particle precipitation; loss through charge exchange with N2 and O2; and transport by diffusion, neutral winds, and convection E X B drifts. In our initial calculations, we are investigating various scenarios for creating structure in a simulated ionosphere. Specifically, the roles of particle precipitation, time stationary convection patterns, and time varying convection patterns are being assessed in the generation and transport of polar cap F region patches of enhanced ionization. In this presentation, we will describe details of the model, its present status and anticipated near-term improvements. We will also show our initial attempts to simulate F region structures.

G1-3
0940

AN EVALUATION OF THE ROLE OF COORDINATION IN MULTI-INSTRUMENT GEOPHYSICAL STUDIES

Raymond A. Greenwald
The Johns Hopkins University
Applied Physics Laboratory
Johns Hopkins Road
Laurel, MD 20723

Since the Goose Bay HF radar was put into operation in 1983 and the Halley, Antarctica HF radar was put into operation in 1988, these radars have been used in a number of colloborative investigations many of which have involved active and passive coordination. The coordinated efforts have involved investigators at Sondrestrom, Millstone Hill and South Pole. While many of these activities have led to interesting and significant scientific results, it is noteworthy that numerous other uncoordinated collaborative studies have also used the HF radar data during the same period. The purpose of this presentation is to consider the relative merits and shortcomings of the two approaches and to identify those factors that are necessary for successful scientific collaborations.

G1-4
1000

THE MISETA INITIATIVE FOR EQUATORIAL ELECTRODYNAMIC STUDIES

Prof. John W. Meriwether, Jr.
Department of Physics and Astronomy
Clemson University
Clemson, SC 29634-1911

A new CEDAR initiative, **M**ulti-instrument studies of the **e**quatorial **t**hermosphere **a**eronomy (MISETA), has been started to expand the diagnostic instruments available in Peru for long term studies of the equatorial electrodynamics near the magnetic equator. MISETA key instruments now operational in Peru are the Fabry-Perot interferometer operating automatically at Arequipa, Peru, and the 50 MHz incoherent radar observatory operated on a campaign basis at Jicamarca, Peru. Thermosphere neutral winds and temperatures and the zonal plasma drifts are routinely observed with these instruments, but a variety of factors has limited simultaneous observations to only a few nights. The MISETA initiative would expand the list of diagnostic instrumentation to include an optical all sky imaging system located at Arequipa, a digital ionosonde constructed by Prof. Reinish (U. of Lowell) and located at Jicamarca, and a scintillation plasma drift receiver system located at Ancon constructed by the Air Force and the Boston College group (Dr. Cesar Valladares). These instruments are intended to operate automatically and routinely. The all sky system, constructed by Prof. Mendillo and Dr. Baumgardner (Boston University), would observe the morphology of the 630 nm airglow. The ionosonde system would provide data on the nighttime zonal and meridional plasma motions for the F region. The scintillation plasma drift instrument would provide data on the zonal plasma drifts with excellent temporal and spatial resolution. It would also provide information on the power and structure of the scintillations that relates to the development of the F region plasma irregularities. The Jicamarca radar would have the important role of validation of these two instruments through occasional long period series of measurements.

While except for the Jicamarca radar, these instruments would run automatically, focus would be applied to the data for the April to June period. This period features succession of quiet and active periods of scintillation activity for similar solar and magnetic conditions. The results from this analysis campaign would address one of the several major themes of MISETA, which is to understand what are the geophysical controlling factors that distinquish periods of active and quiet nights for scintillation activity. Dr. Cassandra Fesen (Dartmouth College) would provide theoretical modelling support to the MISETA initiative by providing TIEGCM runs for specified conditions set by the observations obtained during the analysis campaign efforts.

G1-5
1040

REVIEW OF NASA/CRRES PROJECT EL COQUI: COORDINATED EXPERIMENTAL CAMPAIGN AT ARECIBO USING ROCKETS, RADARS AND OPTICAL MEASUREMENTS

L. M. Duncan[1], P. A. Bernhardt[2], F. T. Djuth[3], M. C. Kelley[4], R. F. Pfaff[5], E. P. Szuszczewicz[6], E. J. Weber[7]

[1]College of Engineering and Applied Sciences, University of Tulsa, Tulsa, OK 74104-3189; [2]Naval Research Laboratory, Code 4780.1, Washington, DC 20375-5320; [3]Geospace Research, Inc., 550 N. Continental Blvd., El Segundo, CA 90245; [4]Cornell University, Elec. Eng. Dept., Ithaca, NY 14853; [5]NASA/GSFC, Code 696, Greenbelt, MD 20771; [6]SAIC, 1710 Goodridge Dr., McLean, VA 22102; [7]Phillips Laboratory, GPIA, Hanscom AFB, MA 01731-5000

The NASA/CRRES El Coqui experimental campaign was conducted in Puerto Rico from May through July, 1992. Eight sounding rockets were successfully launched from the north coast of Puerto Rico near the facilities of the Arecibo Observatory. These rockets carried chemical releases and/or *in situ* instrumentation, and were supported by a large array of ground-based radar, rf propagation, and both ground-based and airborne optical measurements. The campaign was designed to study high-power HF ionospheric modification phenomena, including HF interactions with barium plasma clouds and SF_6 ionospheric depletions, E-region image structures accompanying F-region barium releases, other chemical release interactions with the ionosphere, and natural sporadic-E effects. As a coordinated campaign, Project El Coqui included scientists from more than a dozen universities and research institutions sharing observational data on the eight rocket experiments. This presentation provides an overview of the campaign program, and a brief summary of the principal objectives and results of each experiment.

G1-6
1100

PRELIMINARY RESULTS FROM THE IONOSPHERIC FOCUSSED HEATING EXPERIMENT DURING THE CRRES ROCKET CAMPAIGN AT ARECIBO

P.A. Bernhardt[1], H.A. Romero[1], P. Rodriguez[1], C.L. Siefring[1], F.T. Djuth[2], L.M. Duncan[3], D.E. Hunton[4], C.J. Pollack[5]
[1]Space Plasma Branch
Code 6780, Plasma Physics Division
Naval Research Laboratory
Washington, DC 20375-5000
[2]Geospace Research, Inc.
El Segundo, CA 90245
[3]University of Tulsa
Tulsa, OK 74104-3289
[4]Phillips Lab/LID
Hanscom AFB, MA 01731
[5]NASA/MSFC Code ES53
Hustsville, AL 35812

The NASA sponsored Ionospheric Focussed Heating (IFH) experiment was launched from the north coast of Puerto Rico on 29 May 1992. The sounding rocket carried an instrument and chemical payload along a trajectory that crossed the intersection of the incoherent scatter radar and the HF facility near Arecibo. The release of 30 kg of CF_3Br into the F-region at 285 km altitude produced an ionospheric hole that acted like a convergent lens to focus the 5.1 MHz HF transmissions. The equivalent radiated power inside the radio beam was raised from 60 MW to over 6000 MW by the action of the 30 km diameter lens. In situ measurements of Langmuir waves, electron densities and temperatures, and energetic electron fluxes were performed on the rocket payload. Small scale (~ 10 meter) density reductions were observed within 10 km of the release. The wave spectra around the HF pump frequency broadened following the release. Six minutes after the release, the ion acoustic and electron plasma wave turbulence observed with the radar backscatter was 100 to 1000 times stronger than observed before the release. Raytracing through a model of the modified ionosphere shows that at this time the rays entering the ionospheric hole are focussed to the reflection surface at the top of the hole. The simultaneous action of the Airy pattern near the plasma frequency resonance and the diffraction pattern at the focal point combine to produce unusually large electromagnet fields. These fields drive the Langmuir turbulence responsible for the enhanced waves.

G1-7
1120

RADAR STUDIES OF THE LIGHTNING-INDUCED PLASMAS WITH POTENTIAL APPLICATIONS TO RADIO COMMUNICATIONS AND SPACE SURVEILLANCE

Y.R. Dalkir and M.C. Lee
Plasma Fusion Center, MIT, Cambridge, MA 02139

The scattering of radio waves from perfectly conducting rough plasma surfaces is investigated. Cylindrical plasma channels created by lightning discharges and disk-shaped plasmas generated by a single radio beam are examined. The surface density irregularities of the plasmas are modeled as random perturbations of the constant density background, characterized by either a Gaussian or power-law type spectrum. The theoretical wavelength dependence of the radar reflectivity of the lightning plasmas is compared to experimental results obtained with the MIT C-band, S-band, and the Millstone UHF radars. The rough surface scattering model can adequately account for the $1/\lambda^2$ wavelength dependence of the radar reflectivity observed in the MIT-Millstone Hill experiments, if the surface density irregularities have a power-law type spectrum. The efficiency of reflection of radio waves from an artificially generated plasma disk in both monostatic and bistatic radar geometries is discussed. In radio communication and space surveillance applications, the surface density irregularities may significantly affect the reflectivity of the artificial plasma patch, depending on the power spectrum of the plasma density irregularities.

G1-8
1140

VLF HEATING OF THE LOWER IONOSPHERE

U. S. Inan and Y. Taranenko
Space, Telecommunications and Radioscience Lab
Stanford University
Stanford, California 94305

A number of new results have recently emerged concerning the heating of lower ionospheric electrons by VLF radiation from ground-based sources, either VLF transmitters or lightning discharges. It appears that VLF radiation is particularly efficient in heating the lower ionosphere as compared for example to HF radiation. In this paper, we discuss recent results and compare VLF versus HF heating at a fundamental level. We also briefly review the implications of the VLF heating phenomena in the context of lightning discharges.

J/H1-1
0900

HEAT FLOW AND VERTICAL STRUCTURE IN MERCURY'S REGOLITH

David L. Mitchell and Imke de Pater
Radio Astronomy Laboratory
University of California
Berkeley, CA 94720

We have imaged Mercury's thermal emission at wavelengths of 0.3, 1.3, 2.0, 3.6, 6.2, 18.0, and 20.5 cm. These observations probe to depths ranging from a few centimeters to ~4 meters below the surface and are thus well-suited to the study of diurnal temperature variations, which diffuse tens of centimeters into the regolith. We have used these observations, together with Mariner 10 surface temperature measurements, to constrain a detailed thermophysical model of Mercury's regolith. Analysis of the Mariner 10 data and the night-side radio spectrum reveals that the regolith of Mercury, like that of the Moon, consists of a thermally insulating surface layer overlying a medium of much higher thermal conductivity. This structure is expected to result from bombardment by small meteorites, which maintains the top layer at a very low density while compacting deeper layers. We find that the thickness of the insulating surface layer on Mercury is ~10 cm.

The highly conducting medium below 10 cm greatly reduces temperature gradients that result from internal heat sources such as radioactive decay and differentiation. If the thermal conductivity of Mercury's compacted layer is similar to that of the Moon's, then the observed night-side radio spectrum sets an upper limit of ~10 μW cm^{-2} for Mercury's heat flow. This allows for models of Mercury's formation in which a significant amount of heat is generated by core-mantle differentiation.

J/H1-2
0920

RADAR MAPPING OF MERCURY AT ARECIBO

John K. Harmon
Arecibo Observatory
P.O. Box 995
Arecibo, PR 00613

Results are reported on some of the Mercury radar mapping work that has been done at Arecibo during the last two years. All of the mapping has been done in the monostatic mode using the delay-Doppler technique. The mapping has been of two types: (1) high-resolution mapping of the subradar region using a conventional cyclic code with short (4μs) baud, and (2) low-resolution mapping of the entire disk using a random code with long (100μs) baud.

High-resolution maps of the polarized (OC) component are dominated by specular reflections from high-relief structures such as crater rims. We will present a sequence of such maps covering part of the equatorial zone of the unimaged hemisphere. Among the features revealed by these maps is a heavily-cratered plateau located adjacent to a craterless lowland. These are the first Mercury maps of this type to be made with Arecibo data.

The purpose of the low-resolution mapping work was to obtain full-disk images (especially of the depolarized component) and to try to identify and map some of the large-scale reflectivity features that were first seen by Goldstein in depolarized Doppler spectra. The observations used a random-code or coded-long-pulse technique to mitigate the effects of overspreading. This technique was originally developed for ionospheric radar work and was used to make the first delay-Doppler radar maps of Mars in 1990. The new Mercury maps reveal several radar features, including Goldstein's features, showing modest reflectivity enhancements reminiscent of those seen in radar maps of the Moon. In addition, anomalously bright radar features were seen at the north and south poles. The north polar anomaly, which was first seen in VLA synthesis maps, has been accurately positioned on the Mercury globe with the Arecibo delay-Doppler data. At the same time, the maps have enabled us to place some new constraints on the polar obliquity. The smaller south polar anomaly is mostly confined to the floor of crater Chao-Meng Fu. The small polar obliquity ensures that the floor of this polar crater is permanently shaded, which lends support to the notion that the polar radar anomalies are associated with some sort of enhanced backscatter from frozen volatiles, possibly water ice.

J/H1-3
0940

MAGELLAN MISSION PROGRESS REPORT

Thomas W. Thompson
Jet Propulsion Laboratory
California Institute of Technology
Pasadena, California

The Magellan spacecraft was launched from Cape Kennedy on May 4, 1989 and was inserted into orbit around Venus on August 10, 1990. Radar mapping of the Venusian surface commenced on September 15, 1990 and continued until September 15, 1992. Some 99 percent of the surface has been mapped with resolutions on the order of 120 meters. In fact, Magellan has generated more digital planetary image data than all previous missions.

Magellan has shown that Venus has tectonic and volcanic styles that are both the same and different from those here on Earth. On a global scale, Venus and Earth are different since Venus does not have the plate tectonics that characterizes Earth. On a sub-global scale, Venus has rift valleys like those on Earth. The most common tectonic features on Venus arise from mantle plumes which occur infrequently on Earth. Venus has thousands of volcanic constructs and flows. Many of these Venusian volcanic features are similar to those on Earth.

Magellan also revealed over 800 impact craters. The number and distribution of these craters on the surface likely indicate that most of the Venusian surface is about 500 million years old. This is about 12 times older than average age of the earth's surface and ten times younger than the surfaces on Mercury, Mars and the Moon. Larger Venusian crater with diameters from about 60 kilometers up to about 200 kilometers tend to have double crater rims like larger impact craters on other surfaces in the inner solar system. Craters with diameters of a few tens of kilometers tend to have characteristics that are like those of similar sizes on Mars, Mercury and the Moon. However, the thick Venusian atmosphere disrupts the kilometer sized impactors resulting in smaller multiple impact craters as well as circular surface shock features.

J/H1-4
1000

VENUS SURFACE RADIO/RADAR ANOMALIES; WHAT CAUSES THE HIGH REFLECTIVITY AND LOW EMISSIVITY?

Gordon.H. Pettengill and Peter G. Ford
Center for Space Research
Massachusetts Institute of Technology
Cambridge, MA 02139

Magellan spacecraft observations have confirmed earlier findings that a few regions on Venus, primarily located at high elevations, possess unexpectedly low values of radiothermal emissivity, occasionally reaching as low as 0.3; associated values of radar reflectivity rise to over 0.6.

Two possible explanations for these unexpected values have been advanced: (1) emission or reflection from a highly reflective single interface between the atmosphere and a surface material having a bulk dielectric permittivity of order 80; or (2) emission or reflection from the surface of a low-loss medium having a permittivity of order 5, but which contains many voids permitting efficient internal multiple scattering. Distinguishing between these hypotheses is difficult with the data presently available. However, measurements of emission and reflection where two orthogonal components of the observed power are simultaneously available could distinguish between the two mechanisms. Of particular significance would be the simultaneous observation of two orthogonal circularly polarized components of backscattered radar power.

J/H1-5
1040

SCATTERING FUNCTIONS FOR PLANETARY SURFACES

R.A. Simpson, G.L. Tyler, M.J. Maurer, and C.-M. Wang
Center for Radar Astronomy
Stanford University
Stanford, CA 94305-4055

Scattering functions for planetary surfaces vary, depending on both topographic relief and texture at wavelength and larger scales. For surfaces hidden by clouds or haze, measurements from orbiting radars uniquely characterize surface properties. In these cases, inference of geology and physical processes depends critically on our ability to interpret the scattering results.

Early radar remote probing of the moon yielded estimates of rms slopes and Fresnel reflectivity, which were consistent with models of a gently undulating surface composed largely of soil. Tyler *et al.* (*J. Geophys. Res.*, *76*, 2790-2795, 1971) found that quasi-specular scattering measurements at radar wavelengths of 2.2 m were consistent with slopes obtained from photoclinometry and photogrammetry at scales about 200 times larger. Inversions of measurements from both lunar (Parker and Tyler, *Radio Science*, *8*, 177-184, 1973) and Mars (*J. Geophys. Res.*, *89*, 10385-10404, 1984) experiments gave scattering function shapes, as well as rms slopes, from quasi-specular echoes.

The Magellan radar system includes both a nadir-viewing sounder for altimetry and a side-looking SAR for imaging, providing data in two distinct scattering regimes. Composite scattering functions, combinations of both altimetry and SAR results, are being constructed from the Magellan data Tyler *et al.*, *J. Geophys. Res.*, *97*, 13115-13139, 1992). Although preliminary geologic mapping will be based on SAR mosaics, availability of complete scattering data (including azimuthal variations for scenes imaged two or more times) is expected to improve our final understanding of Venus' surface and the processes which have controlled its evolution.

J/H1-6
1100

PROPAGATION OF ELECTROMAGNETIC WAVES IN THE NIGHTSIDE VENUS IONOSPHERE

J.D. Huba, H.L. Rowland, and P.A. Bernhardt
Space Plasma Branch
Code 6780, Plasma Physics Division
Naval Research Laboratory
Washington, DC 20375-5000

A theory for the electric field fluctuations observed in the nightside venus ionosphere is presented. The special case of propagation parallel to the magnetic field is considered. The model assumes a source of electromagnetic radiation in the Venus atmosphere, such as produced by lightning, and addresses wave propagation in the altitude range z = 130 to 180 km. Four frequencies detectable by the Pioneer Venus Orbiter (100 Hz, 730 Hz, 5.4 kHz, and 30 kHz) are considered. The f_0 = 100 Hz and 730 Hz waves can propagate as whistler waves provided that $f_0 < f_{ce}$ where f_{ce} is the electron cyclotron frequency, and provided that the ionospheric electron density is sufficiently small so that the waves are not strongly attenuated by the Pedersen conductivity. The waves are found to propagate most easily for high magnetic field and low electron density conditions (i.e., ionospheric holes); this result is consistent with the observations. The 5.4 kHz and 30 kHz waves cannot propagate because $f_{pe} > f_0 > f_{ce}$.

J/H1-7
1120

INITIAL RADIO AND PLASMA WAVE RESULTS FROM THE SECOND GALILEO ENCOUNTER OF EARTH

W. S. Kurth, D. A. Gurnett, and A. E. Keller
Department of Physics and Astronomy
The University of Iowa
Iowa City, IA 52242

The Galileo spacecraft is scheduled to encounter Earth for the second time on December 8, 1992 on its journey to Jupiter. Included in the scientific payload is a radio receiver designed to study plasma waves and radio waves in the frequency range from 5.6 Hz to 5.6 MHz. Based on the first flyby of Earth in December 1990, we anticipate a second opportunity to observe auroral kilometric radiation and continuum radiation from Earth, solar type III radio bursts, and a broad range of plasma wave phenomena related to the solar wind interaction with the magnetosphere and numerous processes in the magnetosphere, itself. Unique to this encounter is a crossing of the downstream region at a distance of some 3500 R_E, although at somewhat high latitudes ($\sim 15°$). It is possible that this trajectory would allow for observations of the very distant magnetotail. The encounter sequence also provides for a unique opportunity to study Langmuir waves in the Earth's foreshock with heretofore unequaled temporal resolution. We will collect several brief samples of wideband data in an 80-kHz bandwidth at 806 kbps in order to study the nonlinear aspects of the Langmuir waves. In addition, we will observe the full range of magnetospheric plasma wave phenomena one might expect, including broadband electrostatic waves in the magnetotail and near the magnetopause; electron cyclotron harmonic emissions; whistlers, chorus, and other whistler-mode emissions; wave turbulence associated with the bow shock, and a second opportunity to study a poorly-understood phenomena near closest approach which was evident during the first encounter. This phenomenon produces intense, spin-modulated noise which we believe to be the result of an interaction between the spacecraft and the cold, dense, magnetized plasma in the ionosphere and plasmasphere.

We will also review the prospects of data return from Jupiter in the event that the high gain telemetry antenna fails to deploy. Recent experimentation with various data compression techniques leads us to the conclusion that a reasonable science return is feasible, even under the severely-constrained data return prospects associated with using Galileo's low gain telemetry antenna.

J/H1-8
1140

OBSERVATIONS OF JUPITER SYNCHROTRON RADIATION

S.J. Bolton[1], C. Heiles[2], I. de Pater[2],
S. Gulkis[1], M.J. Klein[1]
[1]Jet Propulsion Laboratory
California Institute of Technology
Pasadena, California 91009
[2]University of California, Berkeley

The short term time variability of Jupiter's synchrotron emission is investigated using observations from U.C. Berkeley's Hat Creek 85 foot radio telescope operating at 1400 MHz. The investigation focuses on the short term variability (days to weeks) through the analysis of high time resolution observations obtained approximately every other day over the course of a few months surrounding Jupiter opposition. Individual measurements are obtained for up to a full Jupiter rotation providing an accurate estimate of the daily average peak flux. Daily peak flux measurements are compared to investigate the possibility of short term variability.

Session A-2 1355-Tues. CR1-46
EM FIELD MEASUREMENTS
Chairman: Keith D. Masterson, Electromagnetic Fields Division,
National Institute of Standards and Technology, Boulder, CO 80303

A2-1
1400 **AN OPTICALLY LINKED THREE LOOP ANTENNA SYSTEM FOR MEASURING THE RADIATION CHARACTERISTICS FROM A SMALL ELECTRIC SOURCE**

David R. Novotny, Keith D. Masterson, Motohisha Kanda
Electromagnetic Fields Division
National Institute of Standards and Technology
Boulder, Colorado 80303

We present the experimental results for a three loop method for determining the radiation characteristics of an electrically small source such as a VDT or computer. Because of the vast proliferation of these devices and the current concerns about EMI radiation effects on other electronic devices and their users, we have developed a system to measure and characterize these emissions.

We first review the theory (Kanda, *IEEE Transactions on Electromagnetic Compatibility, Vol. EMC-26*, NO.3, 1984) and give the experimental results for a single 1 m diameter loop antenna with two diametrically opposite, identically loaded gaps. The electric and magnetic fields are determined from the difference and sum of the electrical currents in the loads. Optical signals proportional to the currents are generated at the gaps and transmitted down a fiber to a remote detector where the appropriate sum and difference are taken. The plane wave verification of the theory was done in a TEM cell, and the data agrees with theory to within 1 db.

We have constructed a measurement system using three concentric, orthogonal loops. We used the system to determine the electric and magnetic dipole moments of a small standard dipole radiator and a commercial VDT (Kanda and Hill, *IEEE Transactions on Electromagnetic Compatibility, Vol. EMC-34*, NO.1, 1992). The radiation characteristics measured for the standard radiator are compared with theory.

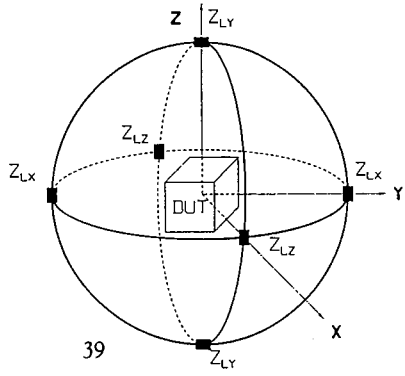

Geometry of the three loop antenna system.

A2-2 1420 REDUCTION OF MAGNETIC FIELDS ASSOCIATED WITH POWER LINES AND TRANSFORMERS

Frank S. Barnes, Ashim K. Banerjee and Peter J. Hartwick

Recently, there has been considerable concern expressed in the media and by the general public about the possibility of harmful effects for the fields emanating from power lines and transformers. In this paper we review several possible techniques for reducing these fields. First, we present the results of computer simulations for the magnetic fields as a function of distance for the cases of a number of well known power line geometries, including a dipole pair, several three and four wire three-phase geometrys and a six wire arrangement. We also show theoretically that we should get zero magnetic fields for $r > a$ for multiple coaxial systems.

Next, we examine the effects for the shielding of the fields around transformers with soft iron and by the use of copper straps which use the fringing fields to generate counter currents. Measurements of the magnetic fields associated with a transformer are made using a standard inductive coil. Magnetic field levels, as a function of distance, in conventionally packaged transformers are compared with magnetic field levels measured when the same transformer is fitted with a copper strap, acting as a shield, in various configurations.

A2-3
1440

BACK-SCATTERED REFLECTION OF ABSORBING MATERIALS FROM 30 TO 1000 MHz

Robert Johnk, Arthur Ondrejka,
and Motohisa Kanda
Electromagnetic Fields Division
National Institute of Standards
and Technology (NIST)
Boulder, CO 80303-3328

A wideband time-domain reflectometer has been used to characterize the back-scattering coefficient of rf/microwave absorbers as a function of angle of incidence. Measurements were made on 30 cm pyramidal absorber material at angles of incidence of 0°, 30°, and 45°, in the frequency range of 30 to 1000 MHz. At these frequencies, the backscatter is a strong function of the size of the illuminating spot on the absorber. The measurement technique uses two broadband antennas to transmit an impulsive signal. The measurement procedure requires that both antennas also receive the reflected signal. This permits the removal of undesired system reflections along with the associated errors. The technique is described and the measurement results are reported.

A2-4
1520

A PROVISIONAL BUILDING ATTENUATION MODEL FOR TELECOMMUNICATION SYSTEM ANALYSIS

H.K. Kobayashi
National Telecommunications and
Information Administration
Spectrum Engineering & Analysis Div.
179 Admiral Cochrane Drive
Annapolis, MD 21037 (410) 224-4302

With the increased use of radio telephones and other easily portable telecommunication devices, an estimate of building penetration loss is becoming a necessary part of radio interference and spectrum sharing studies.

This paper discusses two preliminary graphical models developed by NTIA for commercial and residential buildings spanning 1 MHz to 30 GHz. The models are linear least-square fits to measurements selected from the open literature including those of the Institute for Telecommunication Sciences, NTIA. The mean attenuation through the exterior wall of buildings can be estimated for the frequency range of the model. The effect of windows and building height are examined.

Details of this presentation can be found in a recent publication (Kobayashi, H.K. and G. Patrick, NTIA Technical Memorandum 92-155, May 1992). A measurement plan for verifying and improving the models is outlined in the memorandum. Also included is a literature review with summary tables cross-referenced to primary sources of measurement data.

A2-5
1540

MEASUREMENT OF SE OF RF GASKETS

John W. Adams
National Institute of Standards and Technology
Electromagnetic Fields Division
Boulder, Colorado 80303

The need for an accurate measurement for the electromagnetic shielding effectiveness (SE) of rf gaskets has been a long-standing problem. The present techniques give poor repeatability, partly due to poor definitions and separation of effects. A new technique that takes advantage of the clear definition of the ASTM Standard D 4935 (ASTM D 4935-89, Standard Test Method for Measuring the Electromagnetic Shielding Effectiveness of Planar Materials, ASTM, Philadelphia) and that uses a modification of its sample holder is described. The procedure requires two relative measurements of power (at each frequency), with and without the gasket present. No reference standard is needed, only a stable power source. Pressure is controlled by shims of various thicknesses.

The major challenge in this modification is to match impedance of the enlarged 50 Ω transmission line of the D 4935 holder to a radial transmission line that holds the gasket.

The radial wave impedance is given by Bessel functions of the third kind (Ramo and Whinery, Fields and Waves in Modern Radio, John Wiley and Sons, NY, NY, 1959). These wave impedances are used to calculate the characteristic impedance of radially inwardly- and outwardly- propagating waves. There are frequency and shim-thickness dependencies that must be analyzed in order to minimize mismatches that reduce dynamic range in the sample holder. Additional taper sections are needed to achieve this match. A cross-sectional view of the structure is shown in the figure.

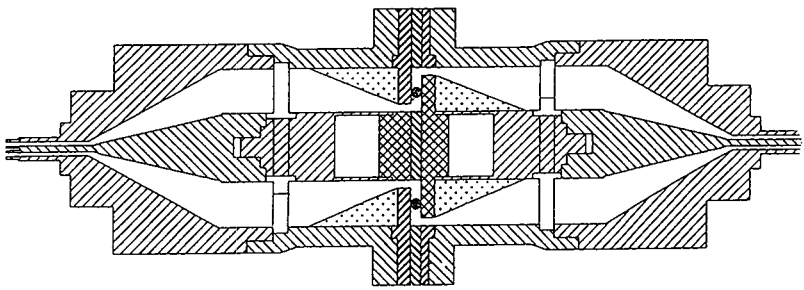

A2-6
1600

Predicting Complete Response for Unknown Linear Systems based on Measured CW Magnitude

M. T. Ma

Electromagnetic Fields Division
National Institute of Standards and Technology

Boulder, CO 80303

Abstract

A method is presented for predicting the total response, in both frequency and time, of an unknown linear system when only the measured cw magnitude response is available. The approach is to approximate the given magnitude by a ratio of two polynomials with real coefficients, from which various system transfer functions in terms of complex frequency are deduced. These transfer functions may or may not be at minimum phase. The corresponding impulse response in time is then obtained by taking the inverse Laplace transform of the transfer function. The first maximum of the impulse response and the energy content are shown to be the greatest during the initial period of excitation when the transfer function is at minimum phase.

Session B-2 1335-Tues. CR2-28
SCATTERING
Chairman: John A. DeSanto, Dept. of Mathematical and Computer Science, Colorado School of Mines, Golden, CO 80401

B2-1
1340

ELECTROMAGNETIC SCATTERING FROM ROUGH DIELECTRIC INTERFACES USING DIFFERENT BOUNDARY UNKNOWNS

John A. DeSanto
Department of Mathematical and Computer Sciences
Colorado School of Mines
Golden, CO 80401

One of the standard representations used to describe electromagnetic scattering from a dielectric interface is the Stratton-Chu formalism. The result is six coupled integral equations to solve for the six boundary unknowns, the electric field vector and the magnetic current vector. We formulate the theory using the spectral-coordinate techniques (J.A. DeSanto, J. Opt. Soc. Am. **A2**, p.2202, 1985). This is a mixed representation which describes the operator matrix to be inverted in terms of rows sampled in Fourier transform (spectral) space and the columns sampled in coordinate space. The formalism has proved very useful for the scalar inverse problem of surface reconstruction (R.J. Wombell and J.A. DeSanto, Inv. Pbs. **7**, p.L7, 1991, and J. Opt. Soc. Am. **A8** , p.1892, 1991).

The operator matrix to be inverted is a 6×6 matrix. This can be decomposed into four 3×3 block matrices. In Stratton-Chu, two of these 3×3 matrices are diagonal. The remaining two non-diagonal matrices describe the coupling.

The question arises as to whether this coupling can be reduced. The answer is yes. We describe a new alternate equivalent formalism using different boundary unknowns in which three of the four 3×3 matrix blocks are diagonal. All the coupling resides in the fourth block.

B2-2
1400

VERTICALLY POLARIZED BISTATIC RADAR CROSS SECTIONS FOR RANDOM ROUGH SURFACES - FULL WAVE, PERTURBATION AND PHYSICAL OPTICS SOLUTIONS

Ezekiel Bahar and Bom Son Lee
Electrical Engineering Department
University of Nebraska-Lincoln
Lincoln, NE 68588-0511

Full wave solution for the vertically-polarized incoherent diffuse bistatic scattering cross sections are evaluated for one-dimensionally rough surfaces that are characterized by four-dimensional Gaussian joint probability density functions for the surface heights and surface slopes at two points. The expression for the diffuse scattered field that is used to obtain the random rough surface cross sections does not include the diffraction term. The small perturbation solution developed by Rice also does not include the diffraction term; however, the physical optics solution based on the Kirchhoff approximations does include the diffraction term.

These full wave results for the vertically-polarized waves are compared with the corresponding small perturbation solutions, physical optics solutions, as well as with the earlier full wave results that are based on the apriori assumption that the surface heights and slopes are uncorrelated. The impact of self shadow expressed by the unit step functions is also considered in this work.

For surfaces with small Rayleigh roughness parameters and very small mean square slopes (compared to unity), it has been shown that the leading term of the full wave solution is the same as the (low frequency) first order small perturbation solution, while in the high frequency limit the same expression for the full wave solution reduces to the physical optics solution if the major contributions to the scattered fields come from the neighborhood of the stationary phase (specular) points.

B2-3
1420

THE ENHANCED BACKSCATTERING OF LIGHT FROM DETERMINISTIC QUASIPERIODIC SURFACES

A. A. Maradudin
Department of Physics
and Institute for Surface and Interface Science
University of California
Irvine, CA 92717
E. R. Méndez
División de Física Aplicada
CICESE, Apdo. Postal 2732
Ensenada, Baja California, México

It is usually assumed that some randomness of a surface is required for the occurrence of the enhanced backscattering of light from it. In this paper we study numerically the scattering of s-polarized light from a quasiperiodic, perfectly conducting, surface. We find that under certain conditions the angular distribution of the intensity of the light scattered by this deterministic surface displays a peak in the retroreflection direction – enhanced backscattering. This phenomenon is shown to be a multiple-scattering effect.

B2-4
1440

ENHANCED FORWARD SCATTERING OF LIGHT FROM RANDOM SURFACES THAT ARE PERIODIC ON AVERAGE

A. D. Arsenieva and A. A. Maradudin
Department of Physics
and Institute for Surface and Interface Science
University of California
Irvine, CA 92717
A. R. McGurn
Department of Physics
Western Michigan University
Kalamazoo, MI 49008

By perturbation theory we have calculated $\langle \partial R_p/\partial\theta_s\rangle_{incoh}$, the contribution to the mean differential reflection coefficient from the incoherent (diffuse) component of p-polarized light, scattered from a one-dimensional, random, metal surface that is periodic on average rather than planar. The plane of incidence is perpendicular to the generators of the surface. In the present calculations we have modeled the randomly rough surface by a position-dependent impedance boundary condition on a planar surface. Due to the fact that the surface is periodic on average rather than planar we find that, for a fixed angle of incidence θ_0, $\langle \partial R_p/\partial\theta_s\rangle_{incoh}$ as a function of the scattering angle θ_s can display sharp peaks at values of θ_s given by $\sin\theta_s = -\sin\theta_0 + n(\lambda/d)$, where n is an integer, λ is the wavelength of the incident light, and d is the period of the average surface profile function. The peak corresponding to $n = 0$ is due to enhanced backscattering; the peaks corresponding to $n \neq 0$ are called enhanced forward scattering peaks, because at least some of them can occur at positive values of θ_s. Enhanced forward scattering is a multiple-scattering phenomenon that is caused by the coherent interference between a surface plasmon polariton scattering sequence and its time-reversed partner.

B2-5
1500

THE USE OF THE SAMPLING THEOREM TO SPEED UP NEAR-FIELD PHYSICAL OPTICS SCATTERING CALCULATIONS

P. W. Cramer and William A. Imbriale
Jet Propulsion Laboratory
California Institute of Technology
4800 Oak Grove Dr., Pasadena CA 91109

The analysis of large (34 meters and above) beam waveguide antennas at Ka-band using physical optics techniques requires an excessive amount of computer time that needs to be reduced. On a Cray Y-MP2 computer, computation times on the order of 12 hours is typical. The excessive amounts of time result from the multiple scattering calculations that must be made — in our case five surfaces. Using physical optics, a complete double integration over one surface is required to determine each integration point on the next scattering surface. If each scattering surface is the same size, then the number of evaluations is on the order of the number of linear sample points to the fourth power. If the number of current evaluations on the next scattering surface can be reduced significantly and the intervening points filled in by an efficient interpolation algorithm, then the primary contributor to the computation time is the number of sampling points on the first surface to the second power, a significant improvement.

Typically, the density of current samples needed on a scattering surface is determined by the surface current phase characteristics and its impact on the physical optics integral. It was anticipated that the number of surface current samples actually needed to accurately define the currents over a surface should be far less than required by the physical optics integral. The application of the sampling theorem was investigated and was found to significantly reduce the number of points needed on the second surface, reducing the number of integrations over the first surface. The number of sample points needed is a function of the first surface diameter and the angle subtended by the second surface. In one example the number of points required was reduced from 120,000 to 6000. To enable interpolation in the near field, the sampling was done over a pair of spherical surfaces, the origins of which are located at the least-squares best-fit phase center of the first surface's scattered fields. The two spherical surfaces were selected such as to enclose the second scattering surface. The interpolation on the spherical surfaces was provided by Sinc functions, with the coefficients obtained by the sampling theorem. The desired value on the second scattering surface was then obtained by a second-order radial interpolation between the spherical surfaces.

Including the computer program overhead required to locate the phase centers and the need to evaluate the sampling theorem over two surfaces, the net computational time improvement was a factor of 4.4 for a pair of 3- and 2.5-meter surfaces at Ka-band.

The research described in this paper was carried out at the Jet Propulsion Laboratory, California Institute of Technology, under a contract with the National Aeronautics and Space Adminstration.

B2-6
1540

USE OF AN MFIE FORMULATION TO OVERCOME THE SLOW CONVERGENCE EXHIBITED BY A CLASS OF EFIE SOLUTIONS

F. Falco, M. Orman,* D. Koppel
Riverside Research Institute
330 West 42nd Street
New York, NY 10036

A. Glisson
Dept. of Electrical Engineering
University of Mississippi
University MS. 38677

In implementing a 3D moment-method code that employs an impedance boundary condition (IBC3D), we have found that the EFIE can give rise to erroneous or slowly convergent solutions when signals are incident on thin coated edges. These problems occur when the wave propagates in or near the plane of the edge, with the electric field nearly perpendicular to the edge. For such cases, we have found that the MFIE provides more rapid convergence to the correct solution, and is therefore the method of choice. The difficulty with the EFIE appears to stem from the relatively large magnetic currents (by comparison to their electric counterparts) for the problematic cases. This apparently results in very slow convergence in the EFIE formulation when the magnetic currents are not directly calculated. Similar difficulties, it should be noted, were previously encountered by Knott and Senior when they developed a 2D moment method code using an impedance boundary condition.

In the present paper, we demonstrate the aforementioned difficulties by showing EFIE predictions from the IBC3D code for a thin, finite-length, ogival cylinder. By employing duality, we also use the code to perform MFIE calculations that are shown to resolve the problem cases. The duality procedure used in this analysis interchanges TE and TM polarizations, and replaces the surface impedance by its inverse ($\underline{Z}_s \rightarrow \hat{n} \times \underline{Z}_s^{-1} \times \hat{n}$ for the tensor case). However, this approach may experience difficulties if portions of the object are conducting since $Z_s \rightarrow 0$. We are therefore presently investigating an alternative MFIE formulation that employs a mixed current representation; i.e., magnetic current unknowns over coated regions and electric current unknowns for the conducting regions.

B2-7
1600

A COUPLING OF THE MOMENT METHOD AND THE EDGE-ELEMENT METHOD IN SCATTERING FROM GENERAL INHOMOGENEOUS CYLINDERS

Djordje Jankovic, Michael S. LaBelle, David C. Chang,
John M.Dunn, and Richard C. Booton, Jr.
Department of Electrical and Computer Engineering
University of Colorado at Boulder
Boulder, CO 80309-0425

Usually electromagnetic problems fall into two classes: those that are solved using the integral equation methods (moment methods) and those that are solved using finite methods (finite difference method, finite element method, edge-element method). The moment method is more suitable for solving unbounded homogeneous problems, such as scattering from conducting cylinders where the Green's function is easily found. On the other hand, finite methods are usually used in bounded inhomogeneous regions for finding field distributions. Both methods are well suited for certain classes of problems, but they have limitations. For example, as soon as an object becomes slightly inhomogeneous (perhaps only partially covered with conductors) a moment method is more difficult to implement. We can extend the range of problems involving scattering by treating the region exterior to the scatterer with a moment method. Interior to the object, where there may be regions of inhomogeneity, it is better to use a finite method.

In this paper we will present two formulations that couple a moment method with the edge-element method in the solution of two dimensional scattering from inhomogeneous objects partially covered by conductors. In both cases a moment method is used to solve for the fields exterior to the object, and an edge-element method is used in the interior. In the first formulation, an equivalent problem is posed such that the free space Green's function is used in the exterior by removing all metal from the object. Two coupled integral equations will result. In the second case, the object is completely metalized and a numerical Green's function is found for the exterior region, yielding a single integral equation. Several examples will be presented.

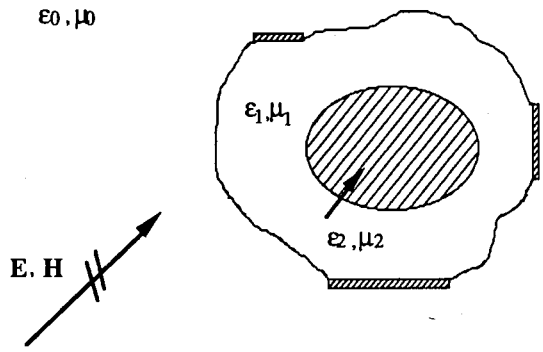

B2-8 1620 **SURFACE INTEGRAL EQUATIONS FOR ELECTROMAGNETIC SCATTERING PROBLEMS INVOLVING THIN SHEETS OF COMBINED DIELECTRIC AND MAGNETIC PROPERTIES**

E. Bleszynski*, M. Bleszynski† and H. B. Tran*

* NAA, Rockwell Int., P.O. Box 92098, Los Angeles, CA 90009
† Science Center, Rockwell Int., P.O. Box 1085, Thousand Oaks, CA 91360

There is a significant interest in scattering from thin layers of lossy materials for radar cross section reduction purposes. Calculations of fields scattered by such systems become computationally significantly less intense if the layers are modeled by infinitesimally thin sheets of electric and magnetic currents and hence the volume integral equations are reduced to the surface integral equations. We derive such surface integral equations for electromagnetic scattering problems involving thin penetrable layers of combined dielectric and magnetic properties as well as impenetrable sheets with two different face impedances.

Our formulation is based on the following surface integral representation for the fields outside a thin material layer in terms of two surface polarization currents $\mathbf{J}$ and $\mathbf{M}$

$$\mathbf{E}(\mathbf{r}) = \mathbf{E}^{(\mathrm{in})}(\mathbf{r}) + \mathrm{i}\omega\mu_0 \int \mathrm{d}S(\mathbf{r}')\widetilde{G}(\mathbf{r},\mathbf{r}')\mathbf{J}(\mathbf{r}') - \mathrm{i}k_0 \int \mathrm{d}S(\mathbf{r}')\Gamma(\mathbf{r},\mathbf{r}') \times \mathbf{M}(\mathbf{r}'),$$

$$\mathbf{H}(\mathbf{r}) = \mathbf{H}^{(\mathrm{in})}(\mathbf{r}) + \mathrm{i}\omega\epsilon_0 \int \mathrm{d}S(\mathbf{r}')\widetilde{G}(\mathbf{r},\mathbf{r}')\mathbf{M}(\mathbf{r}') + \mathrm{i}k_0 \int \mathrm{d}S(\mathbf{r}')\Gamma(\mathbf{r},\mathbf{r}') \times \mathbf{J}(\mathbf{r}'),$$

where $\widetilde{G}$ and Γ are the tensor and vector Green functions, $\omega = k_0/\sqrt{\epsilon_0\mu_0}$, and $\mathbf{E}^{(\mathrm{in})}$ and $\mathbf{H}^{(\mathrm{in})}$ are the incident fields. By evaluating the fields values following from this representation on two sides of the layer and subjecting them to the boundary conditions in a form of generalized "Ohm's laws" for the polarization currents, we obtain a set of two coupled surface integral equations for $\mathbf{J}$ and $\mathbf{M}$. Depending on the problem of interest, the generalized "resistivity" coefficients appearing in the "Ohm's laws" depend on the material properties of the layers or on the values of surface impedances. For some particular cases, the integral equations decouple.

In our formulation, the $\mathbf{J}$ and $\mathbf{M}$ currents contain components both tangential and normal to the sheet. While simulation of thin sheets by currents with tangential components only yields accurate results for near normal incidence, the inclusion of normal components of the currents substantially improves the thin sheet approximation for the near grazing incidence. Also, our formulation is valid for inhomogeneous layers with position-dependent material properties.

B2-9
1640

EM SCATTERING BY HETEROGENEOUS MEDIA†

Mark Shu, Research Associate, Ramesh K. Agarwal, Program Director
McDonnell Douglas Corporation
P.O. Box 516
St. Louis, MO 63166-516

A finite–volume method has been developed to compute wave scattering by heterogeneous objects in two dimensions. Wave interaction is simulated by solving the Maxwell equations which are written in conservation–law form in the curvilinear coordinates system. Further simplification is obtained by assuming a harmonic incident wave and transforming the solution space to the frequency–domain. A pseudo–time variable is introduced to obtain a hyperbolic form.

The numerical method is based on technology developed for computational fluid dynamics and aeroacoustics, and has been validated by computing scattering by various perfectly conducting objects (K. S. Huh *et al.*, 1992 IEEE-APS International Symposium Digest, 1976–1979). The numerical scheme employs dispersion–preserving high–order differencing in both space and time. The compact spatial discretization is based on Padé approximants and is fourth–order accurate for smooth grids. The Padé scheme acheives two to three times the resolution of centered second–order schemes using the same grid. The discrete equation set is integrated in the frequency–domain using an explicit four–stage Runge–Kutta (RK4) scheme with point–implicit treatment of the real–time term. The RK4 scheme has a stability limit of cfl$\leq 2\sqrt{2}$ while the point–implicit treatment alleviates the stiffness resulting from the real–time term. The numerical techniques are used in combination to increase the convergence rate of the time integration scheme. A zonal methodology is used in defining the computational space, facilitating application to complex geometries. A novel treatment of the radiation boundary condition is used to minimize the size of the computational domain. Material interface boundary conditions are explicitly enforced and are derived from the nonreflecting boundary conditions of Trefethen (L. N. Trefethen, MIT 18.336 Class Notes, 203-208, 1989).

The method has been applied to compute scattering by various heterogeneous and dielectric objects. A typical calculation is shown below. The scattered fields are computed accurately with a high level of resolution. Results are compared with analytical solutions and the results of other investigators.

Scattering by a Coated Ogive

Contours of Amplitude of Scattered Hz
TE Polarization 257x140 Grid
Dielectric constants: ε=2 μ=1

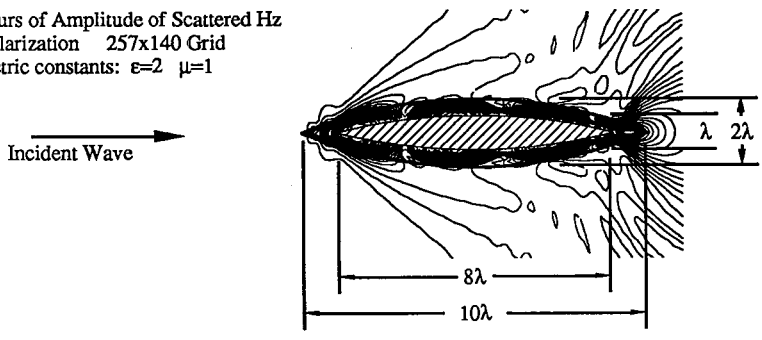

† This research was conducted under the McDonnell Douglas Independent Research and Development Program

Session D-2 1355-Tues. CR1-9
OPTOELECTRONICS DEVICES AND APPLICATION
Chairmen: Alan R. Mickelson, Dept. of Electrical and Computer Engineering, Univ. of Colorado, Boulder, CO 80309-0425; and F. Schuermeyer, Wright Laboratory, Wright-Patterson AFB, OH 45433-6543

D2-1 1400 **OPTICAL WAVEGUIDE LENSES FOR INTEGRATED OPTICAL COMPONENTS**

Stephen L. Kwiatkowski*, Dag R. Hjelme and Alan R. Mickelson
Department of Electrical and Computer Engineering
University of Colorado
Boulder, Colorado 80309-0425

Efficient integrated optical waveguide components have the potential to be an integral part of future large capacity communication systems. One such component is the integrated acousto-optic interconnect. To realize efficient integrated acousto-optic interconnects it is necessary to design and fabricate high performance waveguide lenses. Waveguide lens performance issues include focal length, aberration control, insertion loss, and propagation loss. These performance issues are highly dependent on the effective mode index of the waveguide lens. Thus it is important to control the effective mode index during the fabrication process.

Numerical simulation of titanium indiffused lithium niobate, (Ti:LiNbO3) planar waveguides reveals a region in fabrication parameter space where the change in mode effective index as a function of diffusion time is zero. This region of zero slope may be used to ease the fabrication tolerances of high performance waveguide lenses. Several y-cut Ti:LiNbO3 planar waveguides are fabricated. Preliminary measurements of mode effective index verify the existence of the zero slope region.

D2-2
1420

A NOVEL INTERCONNECTION AND ISOLATION SCHEME FOR OEICS

K. Y. Hur, M. M. Gitin, F. W. Wise*, and R. C. Compton
School of Electrical Engineering
School of Applied and Engineering Physics*
Cornell University, Ithaca, NY 14853

Key fabrication issues in optoelectronic integrated circuits (OEIC) include the development of uniform and reliable interconnection schemes to accommodate continuous metallization among different device layers as well as isolation schemes to provide electrical and physical separation among discrete devices. A unique interconnection and isolation scheme for multilayer device and circuit integration, using reactive ion etching (RIE) and chemically assisted ion beam etching (CAIBE) techniques will be presented. As a demonstration of this approach a GaAs OEIC receiver has been fabricated and tested.

The receiver consists of a Schottky barrier photodiode followed by a single stage 0.2 μm-gate metal-semiconductor field effect transistor, as pictured below. For the photodiode, anisotropic CAIBE defines the photosensitive active area. Isotropic RIE is used to create free-standing-metal airbridge interconnections for total spatial isolation of the active areas on the diode and FET. The free-standing-metal airbridge technique is desirable for high-speed device applications for many reasons. Compared to wet chemical etching, the RIE process provides uniform and crystal-orientation-independent etch characteristics with improved reliability. In addition, the airbridge formation results in smaller parasitic effects. To interconnect between the top photodiode layer and the bottom MESFET active layer a 45° CAIBE interconnect ramp is etched.

Optical response of the receiver was obtained by illuminating the photodiode with a mode-locked Ti-Sapphire laser operating at 780 nm (100 femtosecond pulse duration). The receiver's frequency response was obtained by observing the power output on a spectrum analyzer. Absolute calibration was performed by comparing the output to that of a 100 GHz airbridged photodiode. The receiver has 9 dB of gain at 4 GHz and gain up to 10 GHz.

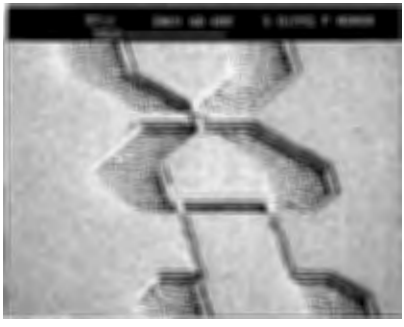

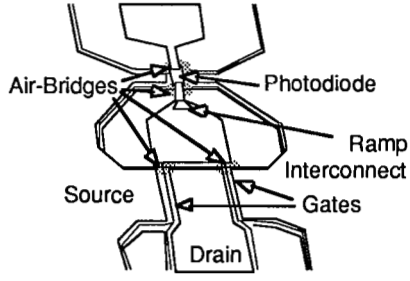

SEM of integrated GaAs photodiode and FET. The ramp produces a well controlled transition from the photodiode layers to the MESFET layers.

D2-3
1500

MICROWAVE CHARACTERIZATION OF POLYMERIC MATERIALS FOR ELECTRO-OPTIC DEVICES

Lori E. Primas*, Vladan Jevremovic,
Alan R. Mickelson and Zoya Popovic
Department of Electrical and Computer Engineering
University of Colorado
Boulder, Colorado 80309

The integration of electro-optic organic materials and coplanar waveguide circuit drivers in electro-optic devices for multi-layer structures could solve many of the demands of optical switching and interconnects. The University of Colorado and IBM have recently joined efforts towards the synthesis, processing and fabrication of organic thin film materials. The ultimate goal is to build optoelectronic integrated devices and a CAD tool that will model the optical and microwave properties for a given set of fabrication parameters.

The optical and microwave properties of nonlinear polymeric materials will be discussed. Fabrication and optical measurements of the NLO materials, as well as measurement of the microwave properties of such materials lead to optical waveguide and microwave modulator circuit design. It is our goal to help predict the speed limitations of high-speed modulators and switches. The first step is to measure the microwave properties of such materials. This is being done with 50 ohm TRL calibration standards placed on multiple layers of these materials. These NLO materials are tested on GaAs, LiNbO3, fused quartz and high resistivity silicon substrates. Once the basic microwave properties of the materials are determined, active microwave electro-optic modulators are designed.

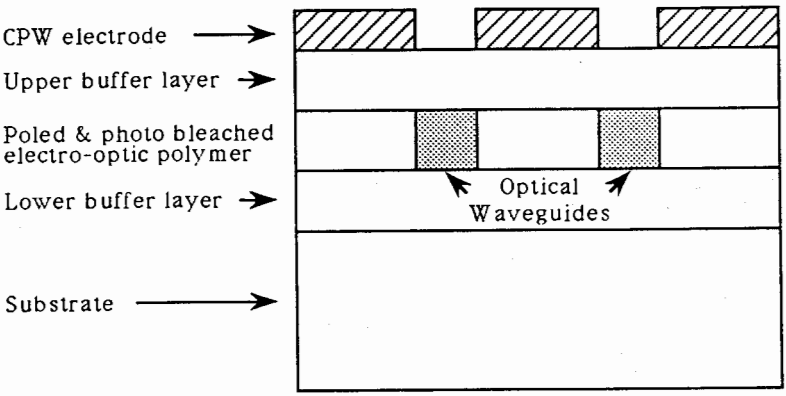

D2-4
1520

POLYMERIC MATERIALS PROCESSING AND OPTICAL PROPERTIES OF HIGH SPEED MODULATORS

S. Lin, W. Feng
H.B. Hooker, Z.B. Popovic, A.R. Mickelson

Department of Electrical and Computer Engineering
University of Colorado
Campus Box 425
Boulder, Colorado 80309

Nonlinear optical polymers have potentially large electrooptic (EO) coefficients, low dielectric constants, and flat frequency response from DC to optical frequencies. Compared with inorganic EO materials, such as $LiNbO_3$, the organic EO polymer materials exhibit attractive properties for use in optoelectronic devices. Using organic EO polymer materials can solve the problem of phase mismatch between the driving electrical wave and guided optical wave in the optical waveguide, which is severe in many inorganics with far IR resonances, such as $LiNbO_3$.

In this paper, we report our recent results on different nonlinear optical polymers. We have developed different processing techniques for different polymers. Their thermal stability and optical properties have been investigated. We have used the second harmonic generation measurement and optical loss measurement to characterize the optical properties. The poling and photo bleaching effects on optical properties have been studied.

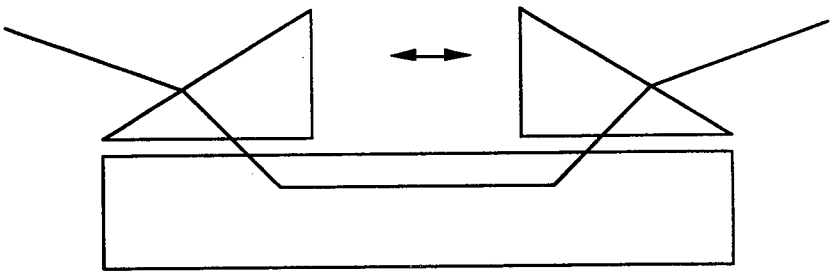

Loss Measurement - Two Prism Technique

D2-5
1540

APPLICATION OF FERRITE LOADED DETECTION SCREENS TO THE INFRARED MEASURMENTS

Amir Matini, Prof. Ronald Sega, Prof. John Norgard
Department of Electrical and Computer Engineering
Colleg of Engineering and Applied sciences
University of Colorado
Colorado Springs, CO 80933-7150

Ferrites interact with microwave fields and heat due to the coupling of dynamic magnetic fields. A mixture of ferrite powder and epoxy compound formed into a thin screen may be used as an absorber for infrared detection of metallic surface currents. The screen absorbs the microwave energy on a metallic surface and creates a thermal pattern of the surface current, visible to an infrared camera.

The method of infrared detection of metallic surface currents introduced by this work can be a valuable tool to study antennas, current balancing networks (baluns), induced currents on scatterers, and radar cross sections. This method would be of most value in the study of surfaces with exotic shapes whose patterns of surface current distributions may not be found easily using theoretical methods.

Session F-1 1335-Tues. CR2-6
SENSING OF ATMOSPHERE AND OCEAN
Chairman: Earl E. Gossard, CIRES, Univ. of Colorado, Boulder, CO 80309

F1-1
1340

VARIABILITY OF COASTAL ATMOSPHERIC REFRACTIVITY

Richard A. Paulus
Tropospheric Branch, Code 543
Naval Command, Control and Ocean Surveillance Center, RDT&E Division
San Diego, CA 92152-5000

In 1944, the U.S. Navy Radio and Sound Laboratory conducted a radio-meteorological experiment along the coast of southern California (D. E. Kerr, Propagation of Short Radio Waves, New York, McGraw-Hill Book Co., Inc., 1951, pp. 328-335) that showed a high correlation between UHF signals and the base of the temperature inversion. A re-analysis of this experimental data with a recently developed hybrid propagation model (H. V. Hitney, "Remote Sensing of Refractivity Structure by Direct Radio Measurements at UHF," in Remote Sensing of the Propagation Environment, AGARD-CP-502, February 1992, pp. 1-1 to 1-5) confirmed this correlation and proposed a method to remotely sense the refractive structure. Out of this proposal, an experiment called Variability of Coastal Atmospheric Refractivity (VOCAR) was designed. VOCAR is a multi-year experimental effort to investigate the mesoscale variability of atmospheric refractivity with emphasis on the coastal zone. The experiment is being conducted jointly with the Naval Air Warfare Center Weapons Division, Point Mugu, CA, the Naval Research Laboratory (Washington, DC and the Monterey Detachment), and the Naval Postgraduate School. In addition, the NOAA Wave Propagation Laboratory and Penn State University/Applied Research Laboratory are participating in the measurement phase of VOCAR. The objective of VOCAR is to provide an assessment capability for horizontally varying refractivity conditions in a coastal environment and to develop a remote sensing capability.

The propagation measurements to be made during VOCAR consist of monitoring signal strength variations of VHF/UHF transmitters in the southern California coastal region. The Automatic Terminal Information System (ATIS) transmitters located at many airports provide a variety of propagation path geometries. With receiver systems located at Point Loma in San Diego and at Point Mugu near Oxnard, primary interest will be on the over-water paths between each receiver site to San Clemente Island. These paths are very nearly equal in length. Differences in signals over these two paths will provide data on the inhomogeneity of the refractive structure. Secondarily, paths to ATIS transmitters in Orange County will provide information on signal propagation intersecting a coastline. An alternate receiver site is on San Nicolas Island, which would provide several nearly perpendicular paths of varying length from the two receivers to ATIS transmitters in the Los Angeles basin. Preliminary propagation data will be presented. Long-term signal strength measurements will be conducted throughout FY93.

F1-2
1400

GROUND-BASED SENSING OF HEIGHT PROFILES OF REFRACTIVE INDEX AND HUMIDITY

Earl E. Gossard
CIRES, Campus Box 449
University of Colorado
Boulder, CO 80309

Under clear-air conditions, it is possible, in principle, to retrieve profiles of refractive index and humidity from Radio Acoustic Sounding System (RASS) data by using the temperature profile along with the backscattered power from the radar and from the acoustic sounder received at the ground.

This paper evaluates the method by comparing tower-measured gradients of humidity and refractivity with those calculated from in-situ C_T^2 and C_N^2 values measured on a 300-m tower. We also present simulations, based on aircraft soundings off Southern California, to assess the errors in the method and to discuss possible calibration procedures.

F1-3
1420

REMOTE SENSING OF SMALL DROP SPECTRA WITH A CLEAR-AIR RADAR

Earl E. Gossard
CIRES, Campus Box 449
University of Colorado
Boulder, CO 80309

Vertically pointing Doppler radars sense the fall velocity spectra of precipitating particles which have substantial fall velocity. From the fall velocity spectra, drop-size spectra can be calculated if the vertical velocity of the atmosphere in which the droplet population is embedded can be removed. Clear-air radars sense the movement of the refractive index perturbations, so the atmospheric movement can be separately sensed and removed. However, small cloud droplets have essentially no fall velocity and act as tracers of the air motion. For dense clouds, the droplet backscatter can compete with the "clear-air" backscatter and cannot be effectively separated from it with a single radar. In this case, atmospheric turbulent smearing broadens the droplet spectrum so that it looks much like a clear air turbulence spectrum.

In this paper, we deconvolve the droplet spectrum with the PDF of the turbulent velocity to recover the droplet spectrum needed to produce the radar-observed spectrum. The result provides insight into the proper interpretation of Doppler spectra in the presence of clouds and precipitation.

F1-4
1440

ESTIMATING MIXING DEPTH AND CLOUD DEPTH USING RADAR REFLECTIVITY DATA

Allen B. White[1] and C. W. Fairall[2]
[1]Cooperative Institute for Research in Environmental Sciences
University of Colorado
Boulder, CO 80309
[2]Wave Propagation Laboratory
National Oceanic and Atmospheric Administration
Boulder, CO 80303

During the past few years, the Wave Propagation Laboratory of the National Oceanic and Atmospheric Administration has deployed a number of 915-MHz boundary layer radar wind profilers in a wide range of atmospheric research applications, over land, sea, and ice. Although these radars were designed primarily to measure wind speed and direction in the lower troposphere, much additional information concerning planetary boundary layer structure or marine boundary layer structure can be deduced using radar reflectivity data.

In this paper, we examine an objective algorithm for determining the mixing depth in the clear convective planetary boundary layer. For verification of the technique, intensive rawinsonde launches were performed at the radar sites. In addition, we present preliminary results that suggest the potential for using radar reflectivity data in conjunction with ceilometer data to estimate cloud depth. The data used in this part of the study were collected in an equatorial marine boundary layer using a specially designed shipboard radar. Both of these techniques are based on the observed/theoretical behavior of the refractive index structure parameter, C_n^2, in clear air and in clouds. The radar provides information on C_n^2 through the signal-to-noise ratio, together with the appropriate radar operating parameters.

F1-5
1520

TEMPERATURE AND HUMIDITY PROFILES OBTAINED FROM INTEGRATION OF RASS, RADIOMETER, ACARS AND SATELLITE DATA USING THE ITPP

B. B. Stankov, J. A. Schroeder, and E. R. Westwater
NOAA/ERL/Wave Propagation Laboratory, Boulder, CO
D. Kim
CIRES/University of Colorado/NOAA, Boulder, CO

Radio Acoustic Sounding System (RASS) provides high-resolution vertical profiles of virtual temperature up to about 5 km AGL. To extend this coverage to the top of the atmosphere, we used the "physical" retrieval algorithm provided by the International TOVS Processing Package (ITPP). ITPP allows for use of the information from the polar-orbiting satellite, RASS, the two-channel radiometer, and the commercial aircraft ACARS data. Regression coefficients computed from a 15-year record of rawinsonde data for Denver, Colorado, together with the RASS, ACARS, and two-channel radiometer data, were used to construct the first guess for the ITPP at the pressure levels it required. Figure 1 shows the results in a time-height cross-section analysis of potential temperature for a 26-h period with a temperature profile given every 20 m. The thick dashed line represents the height coverage of the RASS profiler, and the shaded area represents ACARS flight levels. The merger of these diverse data sets allows construction of profiles that are more complete and accurate than those from single sources.

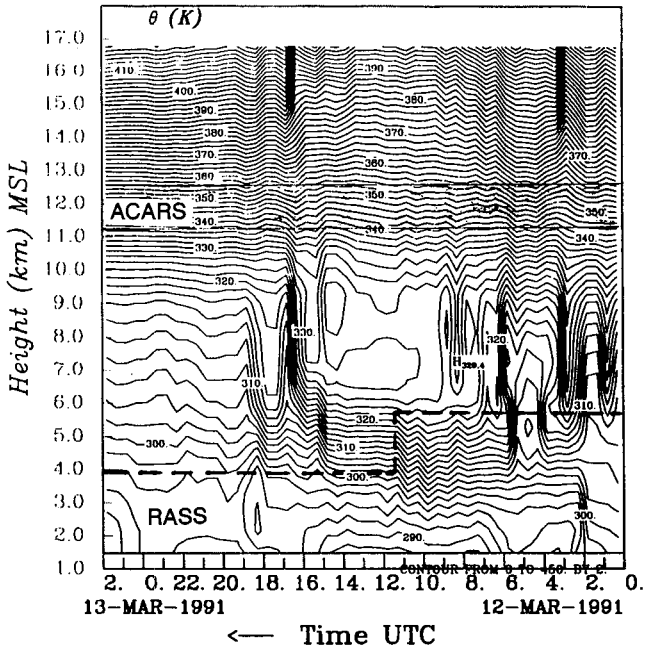

F1-6 1540 WIND PROFILER, RASS, AND MICROWAVE RADIOMETER PERFORMANCE

B.E. Martner[1], D.B. Wuertz[1], B.B. Stankov[1], E.R. Westwater[1], R.G. Strauch[1], K.S. Gage[2],W.L. Ecklund[2], C.L. Martin[3], and W.F. Dabberdt[3]

[1]NOAA/Wave Propagation Laboratory, Boulder, CO
[2]NOAA/Aeronomy Laboratory, Boulder, CO
[3]National Center for Atmospheric Research, Boulder, CO

Several ground-based remote sensors were operated together in Colorado in February-March 1991 to obtain continuous profiles of the kinematic and thermodynamic structure of the atmosphere. The instruments included five distinctly different wind profilers, each equipped with Radio Acoustic Sounding System (RASS) capability for measuring virtual temperature profiles. This was the first side by side test of the three most common wind profiler frequencies: 50, 404, and 915 MHz, and included a NOAA Wind Profiler Demonstration Network (WPDN) unit. Dual-frequency microwave radiometers were also operated to measure the path-integrated water vapor and liquid content of the atmosphere overhead. Frequent rawinsonde launches from the remote sensor sites provided an extensive set of in situ measurements for comparisons.

The Colorado wintertime operations provided a severe test of the profiler/RASS capabilities because atmospheric scattering is relatively weak and acoustic attenuation is relatively strong in these dry and cold conditions. Nevertheless, the lower frequency units exhibited impressive height coverage for wind and virtual temperature profiling, whereas the high frequency units provided measurements with greater vertical resolution near the surface. Good wind measurements were obtained 90% of the time to heights of 10 km above ground level for the WPL 50 MHz system, to 13 km for the WPDN 404 MHz system, to 1.4 km for the WPL high-power 915 MHz system, and to 0.6 km for the AL 915 MHz boundary layer system. Virtual temperature profiles were obtained 90% of the time to heights of 4.4 km for the WPL 50 MHz system, 2.7 km for the WPDN 404 MHz system, 1.3 km for the WPL 404 MHz system, 0.95 km for the WPL high-power 915 MHz system, and 0.4 km for the AL boundary layer 915 MHz RASS. As expected, the height coverage of RASS decreased significantly with increasing frequency because of more severe acoustic attenuation at higher frequencies.

Extensive comparisons of the remote sensor data with those of collocated rawinsondes indicate very good to excellent agreement between the remote and in situ measurements. Mean differences between sonde and remote sensor were less than 1 m/s for horizontal wind components and less than 0.3°C for virtual temperature on most systems. Standard deviations of the differences were about 3-4 m/s for wind speed components and about 1°C for virtual temperature. Microwave radiometer measurements of the precipitable water vapor had an RMS difference of 1.1 mm from the data of 121 sonde launches. This is close to the theoretical limit of accuracy of 0.7 mm for the radiometer.

F1-7
1600

915 MHz LOW-LEVEL WIND PROFILERS: 3 YEARS IN THE FIELD

Daniel E. Wolfe, Clark W. King, and John E. Gaynor
Dept of Commerce, NOAA/ERL/WPL
325 Broadway
Boulder, CO 80303

January of 1993 marks the 3-year anniversary of the deployment of NOAA Wave Propagation Laboratory's (WPL) first low-level wind profiler (W. L. Ecklund et al., *Radio Sci.* **25**, 899-906, 1990). Since operating the first three radars in Arizona during the 1990 Grand Canyon Visibility Study, over 14 additional field studies involving more than 50 separate profiler sites have taken place. Operating conditions have ranged from the deserts of the southwestern United States to the northern Arctic, on-board ships in both the Atlantic and Pacific oceans, and throughout California and its small coastal islands.

The demand for these profilers is due to their portability and capability to measure continuous winds in the lowest 3-5 km of the atmosphere. This flexibility allows experiments to be designed using multiple wind profilers located in areas where knowledge of continuous wind patterns is desired. Studies to date have been dominated by, but not limited to, pollution transport questions.

A summary of WPL's low-level wind profiler and Radio Acoustic Sounding System (R. G. Strauch et al., *NOAA Tech. Memorandum ERL WPL-158*, 1988) deployment and development will be shown. Results from several field experiments, including the Fresno eddy, pollution transport patterns in the southwestern United States, and boundary layer growth in the southeastern United States will be presented. Data reliability and improvements to hardware and software made over these last three years will also be discussed.

F1-8
1620

A SHIPBOARD METEOROLOGICAL MEASUREMENT SYSTEM FOR CHARACTERIZING LOW ALTITUDE REFRACTIVITY: MEASUREMENTS AND RESULTS

John Rowland
James Meyer
Robert Miller
The Johns Hopkins University
Applied Physics Laboratory
Johns Hopkins Road
Laurel, MD 20723-6099

A system designed to characterize the low altitude refractivity environment over the ocean has been built and has undergone preliminary testing aboard a ship operating off the coast of California. The system is used to gather data from multiple sources and perform computations to describe the refractivity profile from the surface to an altitude of 500 m. Characterization of this region is essential for describing the effects of refractivity on shipboard radar and communications systems.

Multiple fixed sensors on the ship, as well as a rocketsonde system for upper air measurements and a disposable buoy for surface measurements have been developed using commercially available hardware. Data acquisition and analysis are accomplished within a small multitasked desktop computer. Output of data for a quick look, computation of boundary layer models, and propagation modeling are all done simultaneously.

The purpose of this paper is to describe the system and to summarize the results of an extended test conducted during the summer of 1992.

F1-9
1640

CO-POLAR CORRELATION COEFFICIENT AT VERTICAL INCIDENCE

D.S. Zrnic
NOAA/Environmental Research Laboratories
National Severe Storms Laboratory
Norman OK, 73069

The paper discusses utility of polarimetric measurements at vertical incidence. In particular the correlation coefficients between linear co-polar components is examined and measurements, obtained with the NSSL S-band polarimetric radar, are presented. The data are from a well defined bright band, from a stratiform region behind convective cells and from a convective cell. A sharp decrease of the correlation coefficient, confined to a height interval smaller than 150 m, marks the bottom of the bright band. In some cases the decrease coincides with the change in Doppler velocity and spectrum width, at other times it is offset from the change in these two variables. The decrease is in the transition region between mixed phase hydrometeors and rain; it appears that either large aggregates before collapse or water drops with ice cores cause this signature.

G2-1
1340

ALTAIR UHF OBSERVATIONS OF BACKSCATTER ENHANCEMENT

Dennis L. Knepp
Mission Research Corporation
2300 Garden Road, Suite 2
Monterey, California 93940

ABSTRACT

During the Defense Nuclear Agency (DNA) PEAK (Propagation Effects Assessment - Kwajalein) experiment in August 1988, the ALTAIR VHF/UHF wide bandwidth radar was used to track spherical satellites in low-earth orbit. The purpose of the experiment was to obtain radar data during the most severe propagation disturbances available naturally. The PEAK experiment has been quite successful, giving many measurements of strong scintillation as well as the first measurements of frequency-selective fading on propagating radar pulses.

In this paper the experimental results are used to demonstrate an enhancement in the average received power that is observed during severe scintillation. The observed statistics of the enhancement are discussed for several passes of a Soviet calibration satellite and are compared to analytic calculations using the Nakagami-m distribution with very good agreement. The enhancement is important for both ground and space-based radars that have to operate during scintillation, since as much as a 3 decibel increase in the target (and clutter) signal-to-noise ratio is possible, depending on the severity of the scintillation and on the radar transmit/receive geometry.

G2-2
1400

FINITE DIFFERENCE - TIME DOMAIN PROPAGATION IN RANDOMLY STRUCTURED IONIZATION

L. J. Nickisch
Mission Research Corporation
2300 Garden Road, Suite 2
Monterey, CA 93940-5326
P. M. Franke
University of Illinois at Urbana-Champaign
Department of Electrical and Computer Engineering
Urbana, IL 61801-2991

Much progress has been made over the last two decades in our understanding of the scattering of electromagnetic waves from small scale ionization structure. This progress has been made by taking advantage of a sequence of approximations which render the random media propagation calculations tractable, at least numerically. However, regimes of interest exist for which the limits of validity of these approximations are exceeded and suitable extensions cannot be found. Thus, for lack of an alternative, the results of computations performed under these approximations are being applied in the invalid regime with the hope that the breakdown of the approximations is more or less graceful. An example is provided by the case of HF propagation through highly structured ionization. In this case the stochastic signal component is usually studied using the parabolic wave equation, an approximation to the scalar Helmholtz wave equation (itself an approximation to the true vector wave equation) which is tractably soluble but which neglects terms which can be significant when the signal correlation length approaches or gets smaller than the signal wavelength. Yet measurements implying the violation of this condition are typical of high latitude HF propagation.

A tool now exists which can allow the limits of validity of the standard random media propagation theory approximations to be explored. We have recently shown that the Finite Difference - Time Domain (FDTD) method can be extended to account for the effects of temporal dispersion in frequency dependent media, and can therefore be applied to ionospheric propagation. The FDTD method solves the Maxwell equations directly in the time domain by temporal integration. No approximations beyond that of finite differencing are necessary, although the direct enforcement of certain approximations is possible. By doing so the method can be used to explore the breakdown of the standard random media propagation approximations. We discuss the issues involved in such an analysis and present some preliminary results.

G2-3
1420

PROPAGATION AND SCATTERING OF ELECTROMAGNETIC WAVES BY THE IONOSPHERIC IRREGULARITIES

Antony. Y. Ho and S. P. Kuo
Weber Research Institute, Polytechnic University,
Route 110, Farmingdale, NY 11735
M. C. Lee
Plasma Fusion Center, Massachusetts Institute of Technology,
Cambridge, MA 02139

The problem of wave propagation and scattering in the ionosphere is particularly important in the areas of communications, remote-sensing and detection (K. C. Yeh and C. Liu, Proc. of IEEE, 70, 4, 1982). The ionosphere is often perturbed with coherently structured (quasi-periodic) density irregularities. Experimental observations suggest that these irregularities could give rise to significant ionospheric effect on wave propagation such as causing spread-F of the probing HF sounding signals (S. P. Kuo et al., Radio Science, 20, 3, 1985) and scintillation of beacon satellite signals (S. Basu et al., J. Geophys. Res., 91 (A1), 1986).

In this work a quasi-particle theory is developed to study the scintillation phenomenon. A Wigner distribution function (H. Bremmer, Radio Science, 8, 6, 1973) for the wave intensity in the (k,r) space is introduced and its governing equation is derived with an effective collision term giving rise to the attenuation and scattering of the wave. This kinetic equation leads to a hierarchy of moment equations in r space. This systems of equations is then truncated to the second moment which is equivalent to assuming a cold quasi-particle distribution. In this analysis, the irregularities are modeled as a two dimensional density modulation on an uniform background plasma. The analysis shows that this two dimensional density grating effectively modulates the intensity of the beacon satellite signals. This spatial modulation of the wave intensity is converted into time modulation due to the drift of the ionospheric irregularities, which then contributes to the scintillation of the beacon satellite signals. The modulation is due mainly to the transverse (to the wave propagation) grating which has a much larger grating vector. The analysis also shows that the functional dependence of the required distance leading to a fixed amount of intensity modulation on the wave frequency follows a power law of distance $\propto$ frequency$^{\alpha}$ where $\alpha \approx 2$. This is consistent with the fact that the plasma is modeled as a dielectric with a $1/\omega^2$ frequency dependence.

G2-4
1440

SELF-ABSORPTION OF HIGH POWER HF RADIO WAVES IN THE IONOSPHERE

G.S. Sales and Y. Huang
University of Massachusetts Lowell
Center for Atmospheric Research
450 Aiken Street
Lowell, MA 01854

J. Hecksher
Geophysics Directorate
Phillips Laboratory
Hanscom AFB, MA 01733

Changes in the nighttime E-region and F-region caused by high power obliquely incident HF radio waves are analyzed. These changes include the electron temperature, electron density, collision frequency and the resultant heater-induced absorption is calculated for both the high power signal and a relatively low power probe signal that passes through the disturbed region. Equations are developed that describe the relationship between the effective radiated power (ERP), the HF field strength and the incidence angle of the radio wave in the ionosphere to the changes in the electron temperature. This heating theory is applied to the results of an ionospheric modification experiments carried out in May in 1991 in the southwest U.S. using VOA transmitting system with a ERP. Good agreement between the theoretical calculations and these experiments are found based on the heating of nighttime sporadic-E layers. Using this theory, comparison is made with other earlier Soviet oblique heating experiments. Finally, for higher power HF communications and radar systems, the calculations indicate that they can become self-limiting because of induced absorption.

G2-5
1520

SOME FIRST RESULTS WITH THE NEW DIGITAL IONOSONDE IN SAN DIEGO

Adolf K. Paul
7455 Brockway Dr.
Boulder, Colorado 80303
Richard A.Sprague
NRaD,Code 542
San Diego,Ca 92152-5000

The new digital Ionosonde (Dynasonde) became operational in early March 1992. The system takes ionograms in five minute intervals and the data are processed extracting F-region profile and propagation parameters (Adolf K. Paul, NOSC Tech. Doc. 529 1982) on a routine basis. The data verify earlier findings in Boulder, that a minimum sampling rate of twelve ionograms per hour is necessary to avoid aliasing.

The most surprising result was the observation of large variations (of the order of 100 km) of the height of the F-layer maximum during the nighttime hours on many otherwise undisturbed days in late March and early April. The height variation are quasi-periodic with periods of two to three hours. The height variations appear to have little effect on the F-layer maximum density.

G2-6
1540

A SMALL DIGITAL IONOSONDE FOR VERTICAL AND OBLIQUE SOUNDING

B.W. Reinisch, D.M. Haines and W. Kuklinski
University of Massachusetts Lowell
Center for Atmospheric Research
450 Aiken Street
Lowell, MA 01854

A small digital ionosonde has been developed which uses 500μs wide pulses at 10% duty cycle for vertical sounding, and 4,200μs pulses at 50% duty cycle for oblique sounding. Intrapulse coding and pulse compression result in a 67μs resolution for both waveforms. In the oblique mode of operation, the sounder operates as a channel probe testing propagation paths for optimal frequencies, Doppler and range spread, and multipath propagation. Proven real time autoscaling and profile inversion techniques for the vertical ionograms establish the ionospheric conditions at the sounder locations. We have now developed new autoscaling methods for the oblique ionograms that invert the oblique echo traces into midpoint electron density profiles that are modeled as a sum of quasiparabolic layers.

G2-7
1600

PROPOSAL FOR STANDARDIZATION OF IONOGRAM PROCESSING

Adolf K. Paul
7455 Brockway Dr.
Boulder, Colorado 80303

Different methods for computing electron density profile parameters are being used by different investigators and the results vary significantly in accuracy. This situation limits severely the value of empirical models or the comparison of theoretical models with observed data, when data from a variety of sources have to be used. Standardization of ionogram processing for routine production is highly desirable.

It is proposed that foF2 is obtained by extrapolation using the inverse slope method and that the height of the maximum and the half-thickness parameter are obtained by fitting a parabola to the F-region peak. Both processes are relatively simple and stable. Standardization of several other characteristics, e.g MUF(3000) and sporadic E will be discussed.

G2-8 1620 AN AURORAL-E HF PROPAGATION EXPERIMENT IN ALASKA:RESULTS FROM THE FIRST YEAR DATA ANALYSIS

Robert D. Hunsucker, RPC-Fairbanks(1)
Robert B. Rose, NRaD/NCCOSC-San Diego
Richard W. Adler, Naval PG School
-Monterey Gus K.Lott, Naval PG School

We have implemented a relatively simple HF propagation experiment between Wales and Fairbanks, Alaska (D=960km) in order to obtain data on the characteristics of Auroral E Ionization on trans-auroral paths and to use these data to verify high latitude HF propagation prediction codes. The Wales beacon transmitter puts 100 watts into a halfwave dipole antenna oriented broadside to Fairbanks on a frequency of 25.545 MHz using CW identified with the Morse letter R every 5 seconds. The midpoint of the one-hop propagation mode lies within the auroral oval for several hours per day for Kp > 3+.

The circuit has been in continuous operation since mid-August 1991, and we plan to operate for at least half a sunspot cycle. The signal is characterized by an extremely "bursty" nature, with burst duration from 1 minute to over 3 hours, and averages about 11 minutes.

Signal amplitude and duration seem,in general to be highly correlated with the location of the auroral electrojet in relation to the path reflection point. Their are five or six distinctive "signatures" of the Wales signal recorded at Fairbanks: 1.) A strong onset of signal coinciding with the electrojet reversal near local magnetic midnight, 2.)Strong onset and extreme variation of signal during magnetic storms,3.) Significant bursts of signal during locally quiet magnetic times,4.) Isolated bursts with sharp onset and slow decay during quiet times,5.) Long duration signals in the summer, seemingly related to isolated increases in magnetic activity,and 6.) Quasi-periodic (6-9 minute) bursts during quiet times. These results and diurnal, seasonal and sunspot cycle behavior will be discussed.

1.)RP Consultants/1618 Scenic Loop/Fairbanks, Alaska 99709 (Commission G)

J/H2-1
1340 MAPPING WATER IN THE MARS ATMOSPHERE WITH THE VERY LARGE ARRAY

C. Todd Clancy, Research Associate
University of Colorado @ Boulder
LASP, CB 392
Boulder, CO 80309-0392

We employed the Very Large Array (VLA) to obtain the first radio measurements of water vapor in a planetary (non-terrestial) atmosphere on December 3/4 and 6/7 of 1990. The key elements of this experiment are the operation of the VLA in the spectral line mode at the 22.2 GHz (1.35 cm) rotational transition of H_2O and the 1 arcsecond angular resolution of the VLA in the C configuration. This allows observation of the atmospheric limb emission from Mars water vapor, with sufficient sensitivity to derive the latitudinal and diurnal distributions of water vapor from variation in the measured line emission around the atmospheric limb of Mars. The observed line width of the H_2O emission is determined by pressure broadening, such that the measured line shapes constrain the mixing profile of Mars atmospheric water for altitudes from 0 to 50 km.

The initial December 1990 experiment revealed a very dry Mars atmosphere relative to Viking observations in 1977, suggesting large interannual variations in the water content of the Mars atmosphere. We are currently scheduled to repeat the VLA Mars water vapor observations for three separate periods during the 1992-1993 opposition of Mars.

J/H2-2
1400

BISTATIC RADAR OBSERVATIONS OF ASTEROIDS 324 BAMBERGA, 7 IRIS, AND 1991EE

I. de Pater and D.L. Mitchell (U. C. Berkeley),
P. Palmer (U. Chicago), L.E. Snyder (U. Illinois),
S. J. Ostro and D. K. Yeomans (JPL)
Radio Astronomy Laboratory
University of California
Berkeley, CA 94720

In recent years D. Muhleman and his colleagues have utilized the Goldstone-VLA bistatic radar system to image planets and satellites. The main advantage of using this system over a more conventional monostatic system is that the VLA provides unambiguous spatial resolution of the radar echoes on the plane of the sky, with an angular resolution as fine as 0.25". A second advantage is increased sensitivity for targets whose echo bandwidths are at least as large as the finest frequency resolution available with the VLA's receiving system.

Monostatic radar observations (e.g., Harmon et al., 1989, Ap. J. **338**, 1094) have shown that some comet nuclei are surrounded by a cloud of particles that backscatter significantly at centi-to-decimeter wavelengths. We plan to use the Goldstone-VLA radar system to image a comet whenever there is a good opportunity. However, an experiment like this is not trivial because of near- field corrections and the fast motion of a comet. Last year we "practiced" on two main belt asteroids, 324 Bamberga and 7 Iris, and on an Earth – crossing asteroid, 1991EE.

Our observations were carried out in Sep/Oct 1991 and yielded echoes from all three targets. The resulting angular resolution was ~ 0.5 arcsec, permitting absolute angular position determinations with errors ~ 0.1 arcsec. To aid in the physical interpretation of the radar reflectivity in terms of asteroidal composition, we also imaged the thermal emission of Bamberga at the radar wavelength, 3.5 cm, and coordinated the bistatic observations with monostatic Goldstone and Arecibo observations.

This work was supported by NASA grant number NAGW-1131 to the U. of Illinois.

J/H2-3
1420

JOVIAN RADIO SOURCE LOCATIONS DETERMINED BY THE ULYSSES RADIO RECEIVER

M. J. Reiner, J. Fainberg and R.G. Stone
Code 690.2, NASA/Goddard Space Flight Center
Greenbelt, MD 20771

Low frequency (1kHz - 5MHz) interplanetary and planetary radio emissions have been observed by spaceborne radio receivers for decades. From spinning spacecraft, the modulation in the radio signal has been used to locate these radio sources (J. Fainberg, L. G. Evans and R. G. Stone, *Science*, **178**, 743, 1972). The Ulysses radio receiver (R. Manning and J. Fainberg, *Space Sci. Instr.*, **5**, 161, 1980) combines signals from both spin plane and spin axis antennas to permit a determination of both the direction and complete polarization state (4 Stokes parameters) of a remote radio source.

Jupiter is the source of a number of distinct radio emissions. Three main low frequency Jovian emissions, observed by spacecraft, have been identified: hectometric (HOM) emission in the frequency band ~200 kHz - 3 MHz, kilometric emissions consisting of broad-band emission (bKOM) in the frequency band ~20 - 300 kHz and narrow-band emission (nKOM) in the band ~100 - 200 kHz, and continuum emission below ~20 kHz. It has been inferred from analyses of the Voyager data that HOM emission originates from the Jovian auroral regions; nKOM emission from near the Io plasma torus. Both of these radio sources are circularly polarized.

We present examples of new observations and analyses of these Jovian radio sources made during the Ulysses-Jupiter fly-by in February 1992. Ulysses observed individual nKOM radio sources, at various Jovian longitudes, which are found to be in rotational motion around the planet. Model analysis of these data provide the locations of these nKOM sources in the region of the Io plasma torus. An analysis of the HOM emission observed during the Ulysses-Jupiter encounter provides confirmation that this Jovian radio emission component originates from the northern and southern polar regions of the planet. These results demonstrate the unique direction-finding and polarization capabilities provided by the Ulysses antenna/receiver system.

J/H2-4
1440

RADIO AND PLASMA WAVE OBSERVATIONS OF JUPITER OBTAINED DURING THE ULYSSES FLYBY

R.J. MacDowall and R.G. Stone
Lab. for Extraterrestrial Physics
NASA/Goddard Space Flight Center
Greenbelt, MD 20771, USA

The Ulysses spacecraft will be the first to explore the high-latitude interplanetary medium over the poles of the Sun. In order to achieve its high inclination orbit, a gravitational assist was obtained from a close flyby of Jupiter. During the encounter with the Jovian magnetosphere, the Unified Radio and Plasma Wave Experiment (URAP) measured plasma waves in the frequency range <1 Hz to >100 kHz. The sensitive radio receivers, which make up part of the URAP experiment, have observed Jovian radio emissions in the frequency range 1 kHz – 1 MHz since shortly after launch.

Among the radio emissions observed by URAP are hectometric (HOM), narrow-band kilometric (nKOM), broad-band kilometric (bKOM), and continuum emissions. URAP also routinely observed broad-band, short duration, quasi-periodic bursts. The URAP receivers use spacecraft spin and summation of signals from separate antennas to permit determination of the source direction and polarization of the radio emissions.

Plasma wave observations include electrostatic waves upstream of and at the bowshock, electromagnetic bursts immediately downstream of the bowshock and in the magnetosheath, a variety of waves in the vicinity of the Io torus, and the first observations of auroral hiss emission from the Jovian polar cap. The URAP experiment provides the first search coil measurements of AC magnetic fields (up to 450 Hz) in the Jovian magnetsophere. In this talk, we will present an overview of the URAP observations of Jupiter.

J/H2-5
1520

RADIO AND RADAR STUDIES OF TITAN'S SURFACE

A. W. Grossman
Department of Astronomy
University of Maryland
College Park, MD 20742
D. O. Muhleman
Division of Geological and Planetary Sciences
California Institute of Technology
Pasadena, CA 91125

Four years of radar observations of Titan near opposition reveal a surface whose radar properties are not compatible with a putative global ethane-methane ocean. The observed mean radar reflectivity is near 30% ± 5%, which is much greater than would be expected for a several–hundred–meter deep ocean. Instead, the observed reflectivity and circular polarization ratio are similar to the icy Galilean satellites. However, the individual observations are highly variable in amplitude and polarization from day-to-day, and suggest a real spatial variability of surface properties.

We observed the 3.5 cm radio emission from Titan with the NRAO Very Large Array (VLA) interferometer in an attempt to detect the rotational modulation of the emission light curve. Hour-long, snapshot observations were obtained during 17 nights of February 1992. A total of 11 distinct longitudes were observed, and 6 longitudes were repeated on a second orbit, assuming a 15.95 day synchronous rotation period. Synthesis images techniques were applied to yield maps of sky brightness with 3 arcsecond resolution. Although, this was not sufficient to resolve Titan's disk, it did allow for spatial removal of confusing flux from Saturn.

The weighted mean observed brightness temperature is 80.4 ± 0.6 K, with an absolute uncertainly of 2.5 K. This measurement represents the most accurate published centimeter brightness temperature to date. Remarkably, the individual observations exhibit a 3.1 K rms deviation about this mean, and show no significant evidence for rotational modulation. This suggests that the subsurface, to depths of a meter, is homogeneous with respect to longitude on large spatial scales.

The weighted mean of all previously published centimeter-wavelength brightness temperatures is 81.7 ± 2.6 K, which compares favorably with our result. Applying the often-neglected correction for background sources of radiation, and assuming a surface temperature of 94 K, yields an emissivity of 0.88 ± 0.03. This corresponds to emission from a smooth dielectric sphere with dielectric constant $\epsilon = 2.9 \pm 0.6$. This determination tends to argue against the global ethane-methane ocean hypothesis, which requires a dielectric constant in the range 1.6–1.8 which would yield an observed brightness temperatures of 85.0 K. Water ice, with $\epsilon = 3.1$, is one possible constituent that is consistent with the observations, however, there are many candidate materials and mixtures which satisfy the observational constraints on dielectric properties of the surface.

J/H2-6
1540

MODELING OF RADIO EMISSION AT URANUS AND NEPTUNE

J. D. Menietti
Dept. of Physics and Astronomy
University of Iowa
Iowa City, IA 52242

R. M. Winglee and D. B. Curran

Observations of radio emission at Uranus and Neptune obtained by the planetary radio astronomy instrument on board Voyager 1 and 2 have produced a wide variety of spectral types at each planet. These include broadbanded, narrowbanded, smooth and bursty emission. We have modelled these emissions using ray tracing as weii as P-I-C simulations. Broadbanded smooth radio emission observed on the nightside of Uranus is consistent with RX mode radiation generated by the cyclotron maser instability and has a source region near the magnetic pole. This region corresponds well with the location of ultraviolet emissions. The Uranian emissions observed on the dayside are narrowbanded smooth and bursty radiation, including O-mode as well as possible second harmonic gyroemission with a source near the magnetic equator. The broadbanded bursty radio emission observed on the nightside of Uranus occurs almost exclusively of the smooth emission and has a source region that is at lower latitudes. The most unusual radio emission at Neptune is very narrowbanded and discrete bursty radio emission. We find the bursty emissions at both Uranus and Neptune may be generated by a temperature anisotropic beam instability (TABI). RX mode, broadbanded smooth and possible second harmonic gyroemission at Neptune appear to have sources near the magnetic poles.

J/H2-7
1600

RADIO OBSERVATIONS OF COMETARY MOLECULES

Lewis E. Snyder
Department of Astronomy
University of Illinois
Urbana, IL 61801

Comets are believed to be relatively pristine samples of the debris left from the formation of the solar system and may have been the carrier between interstellar and terrestrial prebiotic chemistries. Observations of Comet Halley and other comets have given us an excellent opportunity to study the relationship between interstellar molecular chemistry and cometary chemistry. Many interesting questions can be addressed using cometary spectroscopy. Which molecular species are firmly identified as cometary species and which are not? How many cometary molecular species are also interstellar species? How may excitation effects in comets bias our interpretation of the observational data? Current radio spectroscopic studies of comets are especially important because they are beginning to provide answers for these questions.

This research was supported by NASA grants NAGW-1131 and NAGW-2299 to the University of Illinois.

0815-Weds. Math 100
PLENARY SESSION

0815 Introduction

Student Paper Competition

SDI—ITS PAST AND FUTURE: Henry F. Cooper, The Strategic Defense Initiative Organization

Session B-3 1335-Wed. CR2-28
EM THEORY
Chairman: Ralph E. Kleinman, Dept. of Mathematical Sciences, Univ. of Delaware, Newark, DE 19716

B3-1
1340

LOW-FREQUENCY IMAGE THEORY FOR THE DIELECTRIC SPHERE

I.V. Lindell[1], R.E. Kleinman[2]
[1] Electromagnetics Laboratory
Helsinki University of Technology, Espoo, Finland, 02150
[2] Department of Mathematical Sciences
University of Delaware, Newark, Delaware

The well-known static Kelvin image theory for the conducting sphere was recently generalized to the dielectric sphere, magnetic sphere, layered dielectric sphere, bi-isotropic sphere and two dielectric spheres by one of the present authors with colleagues [see e.g., *Radio Sci.* **27** (1) 1-8,1992]. However, since then, it has been found that a similar basic solution for the magnetic sphere already existed in the appendix of a book by Carl Neumann (*Hydrodynamische Untersuchungen*, Leipzig: Teubner, 1883), ignored by the electromagnetics community for 110 years. Henceforth, the static image for a material sphere will be labeled as the Neumann image.

In the present paper, the Neumann image for the dielectric sphere is generalized to correspond to a current dipole in low-frequency approximation. It is seen that the image corresponding to a current dipole directed radially away from the sphere consists of a dipole plus a radial line current while the image corresponding to a transverse current dipole is a combination of a transverse line current plus a radially directed bifilar line current. These new image currents can be interpreted as arising from the Neumann image of a static dipole set in a suitably defined harmonic motion. The theory is tested through some known special cases.

B3-2
1400

FOCUSSING OF ELECTROMAGNETIC WAVES THROUGH A CONDUCTING SHEET INTO A LOSSY DIELECTRIC

James R. Wait
2210 East Waverly
Tucson AZ 85719
K.A.Nabulsi
EM Laboratory, ECE Dept.
University of Arizona
Tucson AZ 85721

The ability to focus electromagnetic fields into a lossy dielectric region is considered for the case where a highly conducting sheet is located between the source aperture and the observer. An exact formulation is presented for the aperture illumination that may be any function of the horizontal (x,y) coordinates. The resulting expressions for the fields in the homogeneous lossy dielectric region , above or below the thin conductive sheet , are developed numerically for selected cases. In particular, it is shown that the presence of the sheet does not impair the quality of the focus to any major extent, but the amplitude of the amplitude of the field is diminished significantly.The double numerical integration routines are validated by developing relatively simple asymptotic expressions for the fields that can also be employed as dependable field predictors for the regions not near the array .

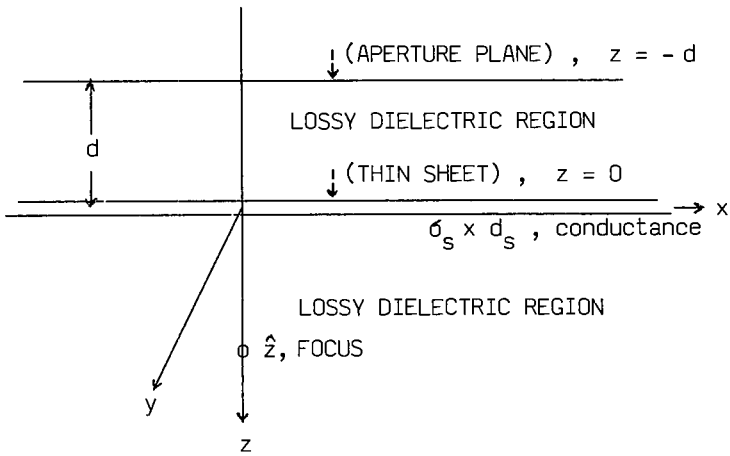

B3-3
1420

ANALYSIS OF LINEAR AND NONLINEAR ELECTROMAGNETIC RESPONSE BY MAXIMUM-ENTROPY METHODS

James Baker-Jarvis
Electromagnetic Fields Division
MS 813.02
National Institute of Standards and Technology
Boulder, CO 80303

Linear and nonlinear-response theory are reviewed using classical and maximum-entropy approaches. Expressions for the electric polarization of a material are developed in terms of covariance functions. Expressions are derived for linear and nonlinear-responses to simultaneously applied electric, magnetic, stress, and temperature fields. It is shown that the time evolution of the electric polarization vector can be separated into a relaxation term and an external source term. Expressions for time-dependent entropy and entropy production are developed and analyzed. The statistical mechanical theories of dynamically and thermally driven systems (B. Robertson and W.C. Mitchell, J. Math Phys., 12, 563-568, March 1971) are used to obtain a generalized equation of evolution for the polarization vector.

In the very special case of the *relaxation approximation*, commonly used in the Boltzmann equation the result reduces to Debye's equation. In a linear approximation the Kubo expression (R. Kubo, Statistical Mechanics of Equilibrium and Nonequilibrium. Amsterdam: North-Holland, 1965) for the polarization is obtained. Driven polarization phenomena coupled to mechanical relaxation are studied using the developed formalism. Constitutive relations are given for electro-acoustic interactions. A novel application, based on the kinetic theory of fracture, is made of coupling of electrodynamic polarization phenomena to microscopic fracture damage in polymers.

B3-4
1440

MECHANICAL PROPULSION FROM UNSYMMETRICALLY INDUCED MAGNETIC FIELDS

Rex L. Schlicher
8230 Stationhouse Ct
Lorton, Virginia 22079
Albert Biggs*
Phillips Lab/WSL
Kirtland AFB, NM 87117

Electromagnetic interactions are described for a unique system for vehicular propulsion, known as the **N**onlinear **E**lectro**M**agnetic **P**ropulsion **S**ystem, or **NEMPS**, which generates mechanical propulsion from unsymmetrically induced magnetic flux densities.

NEMPS has an array of three dimensional Extremely Low Frequency (ELF) loop antennas that link magnetic flux in a region partially enclosed by flat strip conductors.

NEMPS is designed with physical boundary conditions which generate an unsymmetrical magnetic flux density **B** when excited with source currents **I**. Lorentz forces **F**,

$$\mathbf{F} = \mathbf{I} \times \mathbf{B}\, \mathbf{dl},$$

between the magnetic flux density **B** and the currents **I** in the flat strip conductors with lengths **dl** results in a net mechanical force on the conductors for acceleration of **NEMPS**.

After describing electromagnetic interactions, models of the ELF antenna array are presented. Calculations are derived for Lorentz forces on the flat conductors, with discussions and estimations of canceling forces. The net force is then found by adding individual forces.

*AFOSR Summer Faculty Program at Phillips Laboratory until 15 Sept 1992, then Electectrical and Computer Engineering Department, University of Alabama in Huntsville, HVL, AL 35899

B3-5 1500 DIELECTRIC AND MAGNETIC CHARACTERIZATION OF COMPLEX MEDIA

Richard G. Geyer
Electromagnetic Fields Division
MS 813.02
National Institute of Standards and Technology
Boulder, CO 80303

Dielectric and magnetic materials have complex permittivity and permeability properties that are limited by their physical composition. Frequently, spectral characteristics for the dielectric and magnetic properties are needed that differ from those of individual constitutive materials. Hence it is necessary to "engineer" the material's electromagnetic properties according to some prespecified behavior. This may be accomplished by making multi-phase uniform mixtures, where the loading constituent within a matrix may take the form of spheres, ellipsoids, platelets, rods or other shapes.

Effective medium theory has a long history. In this paper we evaluate the effective propagation constant and impedance of a two- phase mixture by considering plane-wave scattering from a uniform lattice of spheres embedded in a matrix material. The electromagnetic field components may be expressed in terms of excited dipoles of electric and magnetic types. In the limiting case where the sphere size is less than the wavelength in the matrix, the mathematical formalism markedly simplifies.

In general, the bulk properties of the composite will not be a symmetric function of the dielectric and magnetic constants of the matrix and loading materials. Structural effects may also be imposed on the behavior of the composite material that are not due to special physical properties of the constituents.

D3-1
1340

STUDY OF HOT-ELECTRON GATE CURRENTS IN COMPLEMENTARY HETEROSTRUCTURE FIELD EFFECT TRANSISTORS

(Student Paper)

E. Martinez*+, M. Shur*, F. Schuermeyer**, D. Grider***, P. Bauhahn***

*Dept. of Electrical Engineering, University of Virginia,
Charlottesville, VA 22903-2442, (804) 924-6092
+on leave from Wright Laboratory,
Wright-Patterson AFB, OH 45433-6543
**Wright Laboratory,
Wright-Patterson AFB, OH 45433-6543
***Honeywell, System and Research Center,
Bloomington, MN 55420

Complementary Heterostructure Field Effect Transistor Technology (C-HFETs) has attracted a great deal of attention recently, for digital applications where ultra-high speed and low power consumption are required (Akinwande *et al.*, IEDM'90 pp 983-986, 1990). In contrast to CMOS technology, the gate current in C-HFETs is still a major limitation for this technology to be incorporated in real applications. In recent studies (Schuermeyer *et al.*, DRC'92, pp. 3A-III, 1992), the gate currents in C-HFETs were analyzed not considering the effects of high drain-to-source bias that might affect the magnitude of the gate current. The purpose of this work is to present the analysis of hot-electron gate currents in a large variety of $Al_xGa_{1-x}As/In_yGa_{1-y}As/GaAs$ and $Al_xIn_{1-x}As/In_yGa_{1-y}As/InP$ C-HFETs over a temperature range from -75 °C to 125 °C. The results of our studies show that hot-electrons effects not only play an important role in all devices at high drain voltages, but they are dominant factors in devices with AlAs mole fraction greater than 0.45. The hot-electron effects lead to a considerable amount of real-space electron transfer over the barrier. In addition, the gate currents, under the influence of high drain bias, are considerably larger than the gate-leakage current at zero drain bias, in contrast to p-channel devices, where hot-hole effects have been observed, or in n-channel devices with a relatively small AlAs mole fraction in the barrier layer. The extreme case has been observed in $In_xAl_{1-x}As/In_yGa_{1-y}As/InP$ HFETs, where the conduction-band discontinuity is higher and the hot-electron gate current increases almost four times greater than the gate-leakage current at zero drain bias.

This dependence of the gate current on the drain-to-source voltage exhibits three regions. In the first region (low drain voltages), the gate current decreases with the increase in the drain voltage. As expected the magnitude of the gate current depends on the conduction band discontinuity between the channel and the barrier layer. In the second region, the gate current rapidly increases with the drain voltage due to the electron heating. Finally at large drain voltages (region 3), the gate current practically saturates. An increase in the device temperature makes the hot-electron effects less pronounced, with a peak-to-valley ratios decreasing linearly with temperature.

The theory of hot-electron gate currents is developed based on a CHINT-like model for the real-space electron transfer. In this model, the saturation of the hot-electron currents is explained by the rapid drop in the effective electron-energy relaxation time caused by the real-space transfer of hot electrons. Our results completely change the usual interpretation of the switching in C-HFET inverters and have to be accounted for in the designing of C-HFET ICs.

D3-2
1400

NEW HIGH SPEED METAL/2-DEG JUNCTION DEVICES

W.C.B. Peatman, P.J. Koh, T. W. Crowe and M. Shur
Semiconductor Device Laboratory
Department of Electrical Engineering
University of Virginia
Charlottesville, VA 22903

Recently, a new Schottky diode was investigated for use as a multiplier element in the millimeter and submillimeter wavelength regions. The new diode is based on the Schottky contact at the edge of a 2-dimensional electron gas (2-DEG). As a negative voltage is applied to the Schottky contact, the depletion layer between the Schottky contact and the 2-DEG expands and the junction capacitance decreases, resulting in a non-linear capacitance-voltage characteristic. Preliminary tripler results of a prototype device at 225 GHz included an output power of 500 μW with an efficiency of 0.5 percent.

The metal/2-DEG junction can also be used as a gate in Field Effect Transistors (FETs). Two new FETs are being investigated. The first is a Quantum HFET in which the gate voltage is used to establish a "quantum wire". Another 3-terminal device which uses the new metal/2-DEG junction is a resonant tunneling transistor (RTT). In this device, the gate controls the current through the double-barrier structure. In this paper, the theory, design, fabrication and testing of these devices will be summarized.

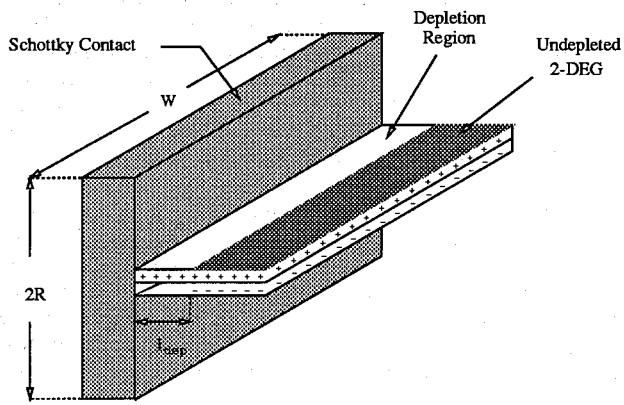

D3-3
1420

RF PERFORMANCE OF $In_xGa_{(1-x)}As$ MIXER DIODES FOR SPACE-BASED APPLICATION*

R. J. Mattauch, Y. Li, U. V. Bhapkar, and P. Siegel**
Semiconductor Device Laboratory
Department of Electrical Engineering
University of Virginia, Charlottesville VA 22903-2442
**Jet Propulsion Lab, Pasadena CA 91109

Providing of local oscillator, LO, power in the terahertz frequency range for heterodyne receivers in space-based application remains a challenge. While solid state sources along with multiplier chains are desired as LO sources, their power decreases monotonically with increasing frequency due to attendant decreasing output of fundamental sources and decreasing efficiency of multipliers. Subharmonic mixing has been proposed to help alleviate this problem by requiring LO power at approximately half the signal frequency. This techniques requires a mixing element exhibiting a centrally symmetric electrical characteristic.

Modeling of both the conduction mechanisms of a Schottky mixer element having a decreased barrier, and the performance of such an element in a mixer configuration have been carried out and presented (R. J. Mattauch, et al., Nat. Radio Sci. Meeting, Jan. 1992). These results, which predicted a marked decrease in required LO power along with slight increase in conversion loss, will be reviewed. The material of choice in such an application is $In_xGa_{(1-x)}As$ since the Schottky barrier height decreases monotonically with increasing In mole fraction. A diode fabrication technology has been developed, reported upon previously, and will be reviewed briefly. That technology has been adapted for incorporation in fabrication of a surface channel antiparallel diode pair. This report will describe that fabrication process, its application in a diode substrate removal process, and present results of each. Finally, RF performance of resulting $In_xGa_{(1-x)}As$ diode pairs fabricated on a semi-insulating InP substrate and with that substrate removed will be presented. Included will be mixer conversion loss, noise temperature, and input impedance as a function of frequency from 200 to 230 GHz.

* This work was supported in part by NASA through the University of Michigan Space Terahertz Technology Center under grant Z-25251, and by the National Science Foundation under Grant ECS-91131232.

D3-4
1440

Millimeter Wave Oscillators with Several Tunneling Devices in Series

Olga Boric Lubecke, Dee-Son Pan and Tatsuo Itoh
University of California, Los Angeles
School of Engineering and Applied Science
Electrical Engineering Depatement
405 Hilgard Av.
Los Angeles, CA 90024

The quantum well diode has a potential of generating very high frequency oscillations, order of THz. However, generated power from these devices has been very low so far, with the best result of order of mW. One way to increase the generated power is to integrate several (N) diodes in series. If biased properly, such a device exibits an I-V curve, that looks like the I-V curve of a singe devices, but is streched N times along V-axes. Therefore, for the same current, the voltage swing acrross the device is going to be N times larger, and the generated power N^2 times larger. The bias voltage has to be applied very abruptly in order for it to be devided equally among the diodes. The required rise time depends on the single diode capacitance, the number of diodes, and the difference in peak currents for single devices.

This principle has been demonstrated for tunnel diodes in the past, at frequency of several KHz. We have demostrated it at several MHz, also using tunnel diodes. The voltage swing obtained from the oscillator that had two diodes connected in series was about two times larger than for one diode, and the frequency of oscillation increased from 5 MHz to 9.4 MHz.

Further efforts are being made to do the same experiment at higher frequencies, and also with quantum well diodes. Since tunnel diodes and quantum well diodes are using a very simmilar mechanism to generate the negative resistance, we expect to observe a simmilar behavior for quantum well oscillators. All experiments done so far were done using several beam-lead devices connected in series, but an experiment with one device with several integrated quantum wells in series is also intended. The estimated power of the oscillator of 10 devices integrated in series at 100 GHz is .1W, with the dc-to-RF conversion efficiency of 8%.

D3-5
1520

CONCENTRIC ELECTRODE METAL-SEMICONDUCTOR-METAL (MSM) PHOTODETECTORS

J. A. McAdoo and Prof. E. Towe
Department of Electrical Engineering
Thornton Hall E214
University of Virginia
Charlottesville, VA 22903-2442

Metal-semiconductor-metal (MSM) photodetectors have recently received widespread attention because of their superior temporal response characteristics and the compatibility of their fabrication technology with that of FETs. Operating bandwidths as high as 480 GHz have been reported. (Y. Liu *et al*, IEEE 50th Annual Device Research Conference, June 22-24, 1992, MIT). The large bandwidths, however, have been achieved by reducing the interdigitated electrode spacing to below half-a-micron. This requires direct e-beam writing lithography, an expensive process with low throughput. It would therefore be highly desirable to produce devices which can achieve faster response times and still be fabricated using conventional optical lithography.

We are proposing a novel device structure which should allow faster response times with larger feature sizes. This structure is an MSM photodetector which has concentric Schottky electrodes instead of the conventional rectangular interdigitated pattern. The advantage of this electrode geometry is that it has desirable symmetry properties. This eliminates the non-ideality of electric fields associated with the sharp corners of the interdigitated rectangular contacts. This, in turn, should lead to higher breakdown voltages and faster response times. An important aspect of this structure is a circular disk electrode at the center which is biased with the rest of the others. This disk is necessary to preserve high-speed operation because photo-generated carriers inside the innermost contact would encounter low fields in its absence. They would, accordingly, be transported much more slowly than carriers in the other regions.

We present a model for calculating the I-V characteristics as well as the temporal response of the concentric electrode MSM photodetectors. The temporal response is modeled accounting for both the intrinsic transit time and the device capacitance in an external circuit. This model is valid only for first-order analysis because of the nature of approximations made. Although the model is fully two-dimensional, it assumes that the optically active semiconductor layer is infinitely thick. Furthermore, the effects of the interconnects of the structure to the external circuit are ignored. In practice, these effects can lead to additional parasitics. These, however, are not important to the fundamental physics issues of the device.

In our model, the effects of several device parameters are explored. The first two are the electrode size and the radial inter-electrode spacing. Another parameter is the number of electrodes, or equivalently, the active area of the device. Finally, the role and the size of the central electrode is analyzed in detail. The size of this disk (electrode) is important for several reasons. As the areal size of the disk is increased, the relative area of the active region obscured from incident light increases correspondingly, and the external quantum efficiency decreases. Also, the dark current and capacitance associated with this electrode vary in direct proportion with its size. This electrode, however, cannot be too small; otherwise, the electric field near the disk can become excessive and may lead to a reduced breakdown voltage. The size of this electrode represents a compromise amongst the values of the other parameters. We present a comparative analysis of the new device and the conventional interdigitated electrode MSM structure.

D3-6
1540

SPREADING RESISTANCE OF A ROUND OHMIC CONTACT.

Boris Gelmont*+ and Michael Shur*
*Department of Electrical Engineering, University of Virginia, Charlottesville, VA 22903-2442
+A. F. Ioffe Institute of Physics and Technology, St. Petersburg, Russia

We calculate the spreading resistance of ohmic contacts for two important geometries -- an ohmic contact stripe and disk separated by a semiconductor from a parallel ground plane. The solution of these problems also apply to the problem of the capacitances between metal contacts of the same geometry separated by a dielectric. For a disk contact, our calculation corrects the classical theory developed by Brooks and Mattes. Fig. 1 shows the dependence of $C/(\varepsilon a)$ versus b/a ratio (solid line) by solving an integral equation for the charge density. The dashed line shows the same dependence predicted by a commonly used interpolation formula

$$C = 2\pi\varepsilon a / \tan^{-1}\left(\frac{2b}{a}\right)$$

Here a is the disk radius, b is the distance between the disk and the ground plane.
As can be seen from this comparison, the approximate formula leads to a considerable error for values $0.5 < b/a < 3$, i. e. exactly in the range of value of b/a where simple limiting cases do not apply. (The calculated values of the capacitance for $b/a < 0.5$ are fairly close to the sum of the parallel plate capacitance and fringing capacitance.)

This work is partially supported by the Office of Naval Research under the contract # N00014-90-J-4006.

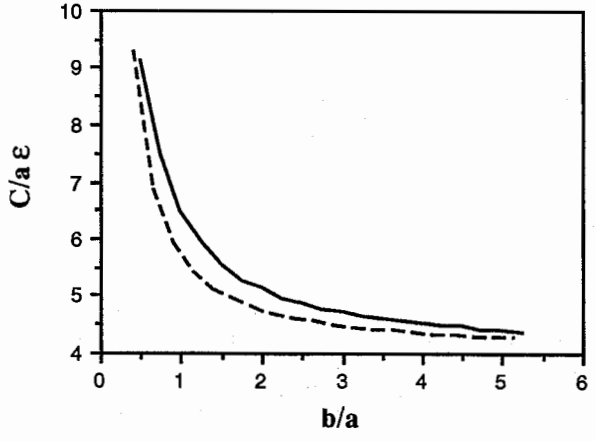

D3-7
1600

ENHANCED SNR AND STABILITY OF MICROWAVE MESFET OSCILLATORS VIA OPTICALLY INJECTED SIGNALS

Sheryl M. Genco, John Buetow, Zoya Popovic
and Alan Mickelson
Department of Electrical and Computer Engineering
University of Colorado
Boulder, CO 80309-0425

Optoelectronic techniques to control microwave devices have been studied here at the University of Colorado for some time ("Quasi-optical MESFET VCO's", S. Bundy, et al., SPIE Proceedings, vol. 1475). Through optical techniques, microwave oscillator stability can be enhanced. Optical injection of microwave devices has been reported for use in phase locking, and oscillator stabilization. Most previous work had centered around the use of simple LED systems as the source of optical power ("Analytical Model for Optically Generated Currents in GaAs MESFETs", A. Madjar, et al., IEEE Transactions on Microwave Theory and Techniques, vol. 40, no. 8, August 1992) with low coupling into the FET active region. Our work takes advantage of lasers locked to a reference laser for mode stability with the direct current modulated at RF frequencies and heterodyned prior to injecting the microwave devices. The microwave devices act as optical detectors. Microwave oscillators are tuned to the modulated RF frequency of the optically heterodyned signal. Microwave amplifier gain is enhanced by the increased transconductance.

We plan to present a study of the optical locking problem both theoretically and experimentally. This will include bit error rate studies for use of FET receivers as well as studies of ways of increasing injected driver power.

D3-8 1620 A RIGOROUS TECHNIQUE FOR THE ANALYSIS OF THE DISPERSION CHARACTERISTICS OF SUPERCONDUCTING MICROSTRIP LINES.

Mohamed A. Megahed, and Samir M. El-Ghazaly
Department of Electrical Engineering
Arizona State University
Tempe, AZ 85287-5706

High T_c superconductor can be deposited in a thin film form on appropriate dielectrics, which makes them very promising for microwave and millimiter-wave device applications. Better understanding of the conduction mechanism inside the superconductors is crucial. Losses and non-linearity behavior need to be addressed. Standard technics are not suitable for the analysis of the superconducting devices as a result of approximations made,(S.M. El-Ghazaly et al., IEEE MTT, 40,499-508, 1992).

A finite-difference technique is used to evaluate the dispersion characteristics of a microwave transmission lines, which include a.high T_c superconductor material. A rigorous full-wave solution is developped, which incorporates the physical aspects of high T_c superconductor materials, and satisfies all the electromagnetically required boundary conditions in the structure. The end result of this procedure is an eigen system of equations, that is solved for the propagation constant along the transmission line.

E1-1
1400

EFFECTS OF MAN-MADE NOISE ON THE MEASUREMENT OF ATMOSPHERIC RADIO NOISE IN GREENLAND

David B. Sailors
Naval Command, Control and Ocean Surveillance Center
Research, Development, Test and Evaluation Division
Code 542
San Diego, CA 92152-5000

An experiment is planned to measure both components of the atmospheric radio noise in Greenland at VLF frequencies. An important concern in such a measurement is man-made noise. If man-made noise is present, how can that be determined? What procedures can be followed to avoid the possibility of man-made noise?

Man-made noise sources in both the near field and far field were considered. As one moves from the near field to the far field, the man-made radio noise begins to become the collective radiation from a vast ensemble of electrical devices and equipment that pulse, arc, spark, or switch on and off. Depending upon the distance and coupling mode between a radiation noise or signal source and the affected receiving equipment, the incoming interference can be classified as conductive, inductive or radiative. Because of the uniqueness of the location of the experiment at Greenland's summit, some sources of man-made noise such as automobile sources do not need considering. Radio noise emitted by rotating machinery, particularly generators, are of concern. In alternators, noise is generated due to contact between brushes and slip rings. In direct current machines, the disturbances are worse than for alternators. Transients are generated by commutation. This disturbance is likely to be coupled into power lines. The use of laminated brushes and power line filtering can be used to reduce the effect of these transients. Other sources of concern are consumer products and lighting systems.

The properties of the amplitude probability distribution (APD) of atmospheric noise can be used to differentiate between man-made noise and atmospheric noise in the far field. Contamination by man-made noise will cause the value of L_d to be less than it would have been had the recorded value been only atmospheric noise. Crichlow et al. (NBS J. of Res.-D, Radio Propagation, 64D,49-56,1960) found that for a given V_d only a certain range of values of L_d will result in an APD of the form expected for atmospheric noise. For a given V_d there is a minimum value of L_d that will give the required form. Therefore, the measured values of V_d and L_d can be used to determine contamination by man-made noise.

E1-2
1420

MARK 0 PHASER

D.V. Giri, Pro-Tech, 3708 Mt.Diablo Boulevard, #215, Lafayette, CA 94549-3610
Y.Rahmat-Samii, Department of Electrical Engineering, UCLA, Los Angeles, CA 90024

Various considerations in the design of a possible high-power microwave (HPM) weapon (phaser) have been addressed in the past. The term " phaser " stands for pulsed high -amplitude sinusoidal electromagnetic radiation. Mark 0 Phaser is a system with 1 GW of average power from the HPM source. This power refers to the useful power from the source in the lowest order mode of a waveguide (e.g., the dominant mode of a standard rectangular waveguide) with an operating frequency below the cut off frequencies of other modes.

The objective of this paper is to describe in detail the design considerations of a Mark 0 Phaser. It is emphasized that we are concerned with single-shot operation of the phaser with the purpose of causing a functional upset in the target system. Phasers are not intended to destroy the target system but deny a successful mission. The Mark 0 Phaser described here is a 1.1 GHz, 1 GW average power, 100ns pulse duration system that can be assembled. The design details consisting of the choice of waveguide, flanges, bi-directional couplers, the feed horn and a single parabolic reflector will be dealt with. The high- field levels in and around the feed and antenna systems require the use of appropriate insulating media. Far field quantities, such as the power densities, field strengths and energy densities have also been computed and will be presented along with some preliminary target coupling estimates.

E1-3
1440

THE PHILLIPS LABORATORY BROAD BAND, HIGH FREQUENCY CW SIMULATOR

Donald McLemore, and Joe Martinez
Kaman Sciences Corporation
6400 Uptown Blvd NE, Suite 300E
Albuquerque, NM 87110

Gary Sower
EG&G Special Projects, Albuquerque Operations
2450 Alamo Ave SE
Albuquerque, NM 87106J

Carl Baum, Tyronne Tran and William Prather
Phillips Laboratory
Kirtland Air Force Base, NM 87117

The Phillips Laboratory has developed a new CW broad band, high frequency simulator which has the normal characteristics desired for a hybrid EMP simulator, e.g.

- The early time fields (high frequency) are radiated from a relatively small source region on the antenna
- For low frequency fields, the antenna forms a loop for current to flow around the test object which includes resistive loading such that the resistance per unit length, R', is chosen so that the low frequency E/H ration is Zo (≈ 377 Ω) in the case of a full loop (antenna plus image with zero image source voltage)
- The antenna is slender so that at intermediate frequencies the energy is allowed to radiate away and not produce significant resonances.

This new design achieves these criteria using a coaxial cable for the antenna wire with a small-gap source located overhead at the apex of the antenna. This permits the interior section of the coaxial cable of one leg of the antenna to be used to supply current for the small-gap source. The resistive loading for this antenna is achieved using ferrite beads (material #77 - manganese/zinc) which have resistors connected in loops around them. Additionally, an impedance matching network (balun) has been designed which can be used for this unusual feed topology.

A resistive loading was achieved on the coaxial cable using one torroid/resistor combination every 0.5 meters on the antenna. The ferrite torroids had four, 40 Ω resistors connected around the bead, making four equally spaced loops. The overall resistance presented to the antenna by each torroid/resistor combination was approximately 7 Ω over the frequency range of approximately 300 kHz to 500 MHz. Measured impedance curves, showing a single ferrite torroid impedance without resistor loading, and the effects of loading the beads with various parallel combinations of resistors (all having an equivalent resistance of ≈ 10 Ω) were obtained.

A matching circuit to match the coaxial cable feed and the antenna impedance was designed for this simulator. This balun, in many ways much like past coaxial cable balun designs, was significantly different because of the design of the intermediate transmission lines. Essentially, tilted moncones over a bicone ground plane were used to achieve the 100 Ω requirement.. Design criteria used to achieve this impedance requirement were calculated for ranges of the angle of the tilted monocones from the ground plane, half angles of the monocones and half angles of the bicone ground planes.

Electric and Magnetic fields produced by this antenna were measured within the working volume from 300 kHz to 1 GHz with an HP 8753C network analyzer. The results illustrate fields similar to other hybrid EMP antennas over this frequency range in the working volume, which recommends its use as a CW simulator to determine low level coupling data for large test objects. This antenna was also used to measure cable currents on a testbed aircraft. Results from this test will also be presented.

E1-4
1500

EM RADIATION FROM A SERIES OF SHARP X-RAY PULSE

R. L. Gardner
Phillips Laboratory/WST
Kirtland AFB, NM 87117

X-rays incident on a metal surface scatter electrons from the plate. As the electrons leave the plate, the fields at the metal surface due to the electrons that have been emitted earlier attract the electrons back to the surface. These accelerating electrons transmit electromagnetic fields. The equation of motion of electrons caused by an x-ray pulse long in duration compared to electron lifetimes above the plate is difficult to solve and requires application of numerical techniques.

A series of x-ray pulses each with short time duration lends itself readily to application of analytical techniques. Enabling the solution is the gravitational approximation. Spot sizes for this solution must be large compared to the turn around distances associated with the electrons. The equation of motion for each sheet of electrons can then be solved analytically. The resulting second derivative of the dipole moment leads directly to the electromagnetic fields from the accelerating electrons.

E1-5
1540

MULTIPOLE MODEL FOR COUPLING BETWEEN CORONA DISCHARGES AND WIRES

Steven D. Schennum
Department of Electrical Engineering
Gonzaga University
Spokane, WA 99258

Robert G. Olsen
School of Electrical Engineering and Computer Science
Washington State University
Pullman, WA 99164-2752

An analytic model for the motion of charge in a corona streamer is developed. Using this model as a basis, a multipole expansion for the fields generated by the streamer is written. It can be shown that the far fields of this streamer are well approximated by the first (i.e. dipole) term of the multipole expansion. More terms of the expansion are needed, however, to accurately represent the near field. Since the near fields are responsible for coupling between the streamer and the wire on which it resides, the dipole term is not a sufficient model for quantifying the coupling. In this research, the multipole expansion is used to develop a more correct model for coupling between a streamer and a wire. A zeroth order model for the coupling which provides some justification for modeling the streamer as an "equivalent" dipole is found. This model can be used to provide insight into the generation of electromagnetic interference from corona on power lines. It can also be used as a foundation for the study of radiation from electrostatic discharges between wires.

E1-6
1600

RADIATION LOSSES FROM TEM TRANSMISSION LINE ANTENNA FEEDS

Albert W. Biggs* and Ernest A. Baca
Phillips Laboratory, Kirtland AFB NM 87117

TEM transmission line antenna feeds discussed here are grouped into open wire lines, shielded wire lines, strip lines, and conical lines . Although pairs of conductors and multiplicities of conductors are open wire lines, only two wire lines are considered because the application is feeding short dipoles, half wave and full wave antennas, loop antennas, helical antennas, biconical antennas, and TEM horns. Although open wire lines are simple and economical, they are unusable at high frequency because of excessive radiation loss. Shielded wire lines, such as coaxial lines, overcome the radiation problem.

Strip transmission lines have conductors in the form of flat parallel plates or strips, but open structures also suffer radiation problems at higher frequencies. As the strip width approaches zero, the two wire line configuration is approached. As the width approaches infinity, losses approaches zero, but this is not realistic.

Several antenna feeds are associated with conical lines. One line has two conductors each resembling an Alpine-type horn used by Swiss mountaineers. When the curved conductors are straightened into regular cones, they become a V-shaped conical feed. When aligned colinearly, a biconical feed is formed. If the lower cone angle increases to 180 degrees, a feed with a conical section above a ground plane is reached.

Other variations include a right cylindrical cone cut by two planes passing through the apex, forming a rectangal at the base of the cone. The two conductors can be the isosceles triangles in the two planes cut by the cone or the curved cone sections cut by the planes. These feeds provide wide band coupling to TEM horn antennas because a constant characteristic impedance is maintained as the feed cross section increases or decreases.

This evaluation was made because losses due to radiation from antenna feeds is usually neglected, but with higher frequencies in pulsed waveforms and high power microwave sources, these are no longer negligible. Losses are calculated for two wire, parallel strip, and conical TEM feed lines, with associated fields.

*Visiting Faculty at Phillips Lab until 15 Sept 92, then Electrical and Computer Engineering Department, University of Alabama in Huntsville, AL 35899.

E1-7
1620

A CANONICAL SCATTERER FOR TRANSIENT SCATTERING RANGE CALIBRATION

Everett G. Farr
Farr Research
614 Paseo del Mar NE
Albuquerque, NM 87123

Carl E. Baum
Phillips Laboratory
Kirtland AFB, NM 87117-6008

We describe here a simple process for calibrating a transient scattering range. The process uses a paraboloidal scatterer to transform an axially incident plane wave into a spherical wave. Since the magnitude of the scattered field is known analytically, one can simply calibrate a measurement system. In order to calculate the scattered field, we use a sterographic projection that has previously been called the reflector transform.

This technique provides three advantages over traditional calibration with a sphere. First, it is potentially more accurate, since the scattering charateristics of a paraboloid are independent of frequency. There is no need to convert the measured time domain data to the frequency domain in order to deconvolve the characteristics of the scatter; the entire process takes place in the time domain. Second, this technique is simpler to implement. Finally, this technique is appropriate for cerrtain anechoic chambers built of two-wire and four-wire transmisssion lines, where the incident field is not quite uniform.

E1-8
1640

HYPERBOLOIDAL SCATTERER FOR SPHERICAL TEM WAVES

Carl E. Baum
Phillips Laboratory
Kirtland AFB, NM 87117-6008

Everett G. Farr
Farr Research
614 Paseo del Mar NE
Albuquerque, NM 87123

This paper describes a special hyperboloidal scatterer which can be used as a canonical scatterer in a transient scattering range. It has the property of transforming one spherical TEM wave (from a conical wave launcher) into a second spherical TEM wave with no change in temporal waveform. The amplitude and polarization of the second wave are known analytically in terms of the first. This new solution to Maxwell's equation is useful in the calibration of transient scattering ranges.

F2-1
1340

RADIO PHYSICAL OPTICS MODEL OVERVIEW

Herbert V. Hitney
Tropospheric Branch, Code 543
Naval Command, Control and Ocean Surveillance Center, RDT&E Division
San Diego, CA 92152-5000

Split-step parabolic equation (PE) methods have been successfully used in recent years to model radio propagation effects in the lower atmosphere, in particular for cases where the vertical refractivity structure varies with range. Significant disadvantages of these PE models are their extensive computational requirements and limited elevation angle capability. The Radio Physical Optics (RPO) model is a range-dependent hybrid model that uses a combination of ray-optics (RO) and PE methods to overcome these disadvantages and create an efficient radio propagation assessment capability for over-water paths. An overview of the various methods used in RPO is presented along with some examples.

The RPO algorithm is divided into four regions. For short ranges and high angles, a flat earth model is used that ignores earth curvature and refractive effects. At lower angles, a full RO model is used that accounts for refractive effects on spreading and the optical path lengths of direct and sea-reflected rays. For angles below the RO region, and for receiver altitudes up to a certain height, a split-step PE model is used. For points above the PE region, but below the RO region, a method named "extended optics" is used that is initialized by the PE model, but uses RO techniques to propagate to higher altitudes.

The capabilities of RPO are summarized as: frequencies from 100 MHz to 20 GHz; transmitter heights from 1 to 100 m; horizontal, vertical, and circular polarization; several antenna patterns with beamwidths from 0.5 degrees to omnidirectional; multiple vertical refractivity profiles at arbitrary ranges; surface roughness effects based on wind speed; and unlimited maximum range and altitude for the receiver. The figure below is a sample RPO display for a slowly rising duct.

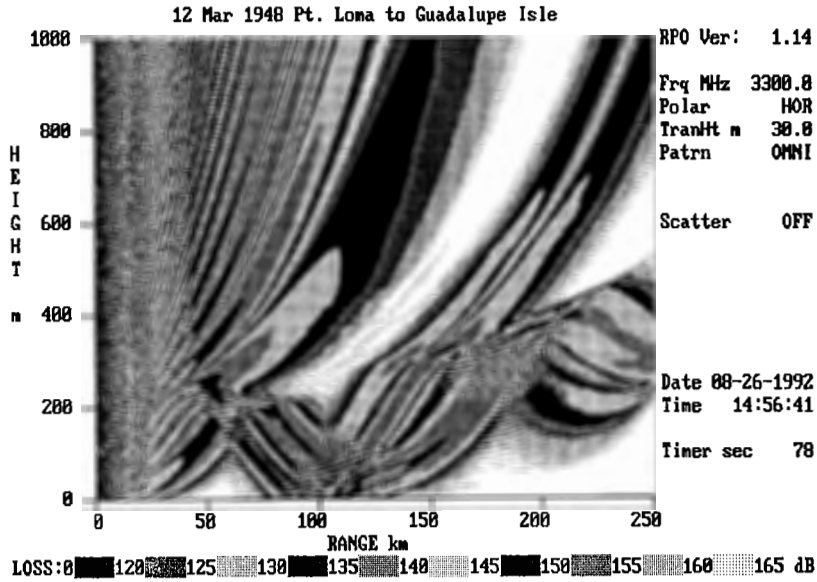

F2-2
1400

IMPEDANCE AND ROUGH SURFACE BOUNDARIES IN PARABOLIC EQUATION/SPLIT-STEP PROPAGATION MODELS

G. D. Dockery, J. D. Huffaker
J. R. Kuttler, C. P. Mrazek
Johns Hopkins University
Applied Physics Laboratory
Johns Hopkins Road
Laurel, MD 20723

The parabolic equation/split-step method has been established as one of the most accurate and general approaches to representing electromagnetic propagation in the troposphere (e.g., G. D. Dockery, IEEE Trans. Ant. Prop., 36(10), 1464-1470, 1988). This method allows specification of virtually any atmospheric refractivity condition, and has been tested successfully for frequencies between 100 MHz and 20 Ghz.

Recent efforts have focused on incorporating impedance boundary conditions at the earth's surface, and representing variable surface heights (e.g., a terrain profile, or sea swell) into PE/split-step algorithms. A method for implementing an impedance boundary using a "mixed-Fourier" transform was described in J. R. Kuttler, et al, Radio Sci., 26(2), 381-393, 1991. This approach allows any modification of the reflection coefficient, such as the simple rough surface models frequently used in radar calculations, to be included as a modification of the surface impedance; examples of such calculations are presented for 10 Ghz where surface roughness effects are evident. The impedance boundary also allows calculations at HF frequencies for which surface wave effects are important. Comparisons with analytic HF propagation calculations are presented for frequencies down to 10 Mhz.

A few different algorithms for accounting for variable height surfaces have also been investigated. The two methods described here involve (1) transforming the problem in each range interval to accommodate the varying surface location, and (2) performing a global conformal map to "flatten" the surface, after which the usual PE/split-step algorithm can be applied. Calculations using these two methods are presented for surfaces representative of sea swells and coastal terrain.

F2-3
1420

A TERRAIN PARABOLIC EQUATION MODEL (TPEM)

Amalia E. Barrios
Naval Command, Control and Ocean Surveillance Center
RDT&E Division, Code 543
San Diego, CA 92152-5000

A numerically efficient method has been developed to model tropospheric radiowave propagation over irregular terrain in the presence of range-dependent, non-standard environmental conditions. The model is based on a modification to the smooth-earth parabolic equation, and uses the split-step Fourier algorithm developed by Hardin and Tappert (*SIAM Rev. 15, p. 423, 1973).*

For radiowave propagation over terrain, the parabolic equation (PE) is subject to a range-dependent boundary condition, specifically, that the field is zero at the surface (assuming horizontal polarization). Since the surface is constantly changing for any arbitrary terrain, this poses a formidable problem. The method developed here is based on "transforming" the PE through a change of variables and determining a new "modified" PE with a new *range-independent* boundary condition that is now easily solved. This transformation is equivalent to defining a new modified refractivity that includes a term based on the second derivative of the terrain. Conceptually, the modified refractivity, which normally accounts for the earth's curvature, is now used with an additional term to take into account the radius of curvature of each segment of the terrain.

Comparisons are made between TPEM and other existing terrain models, and against measured data. The figure below is a coverage diagram from TPEM for a terrain path in Alberta, Canada.

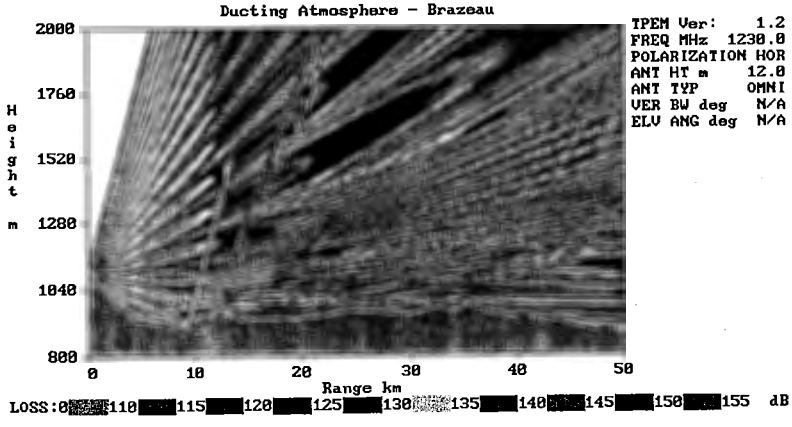

F2-4
1440

PROPAGATION EFFECTS ON RADAR TERRAIN CLUTTER IN COASTAL REGIONS

J. P. Reilly
C. Lin
The Johns Hopkins University
Applied Physics Laboratory
Johns Hopkins Road
Laurel, MD 20723-5099
S. A. Rudie, General Physics Corporation

This paper develops a method for characterizing terrain shadowing and clutter as seen by a ship-board radar in a coastal environment. The method takes into account the location of the ship, the particular terrain topology, the radar parameters, and the propagation characteristics. Terrain contours are defined using a data base known as DTED (Digital Terrain Elevation Data) published by the Defense Mapping Agency. The data base provides terrain elevations on a 100 m grid for much of the earth's land mass. We determine visible terrain by one of two methods: one method uses an optical ray-trace program; a second method uses an electromagnetic parabolic equation model termed "TEMPER", in which the terrain is a lower boundary. Terrain visibility determined with the two methods agree very well. Whereas both methods account for refraction, the TEMPER method also accounts for diffraction. In either case, propagation calculations use refractivity profiles that can vary with altitude, range, and azimuth. We illustrate our techniques using a simple sea-breeze model, in which the refractivity profile obtained over the sea is modified over land in accordance with the terrain contours. We calculate radar clutter by taking into account terrain slopes, terrain visibility, and radar parameters. The calculated clutter received by the radar is strongly affected by the propagation factor determined with TEMPER, and varies significantly with terrain roughness and radar frequency. The statistical distribution of reflectivity obtained with our method compares favorably with published experimental data obtained in similar environments over a wide range of radar frequencies. We compare land visibility and clutter for various propagation conditions, including a standard (4/3 earth) atmosphere, and an atmosphere with a surface-based duct. The assumptions concerning propagation considerably affect the strength of the clutter returns, as well as the spatial distribution and extent of the clutter.

F2-5
1520

RADAR DETECTION OF LOW-ALTITUDE TARGETS IN A MARITIME ENVIRONMENT

Kenneth D. Anderson
Tropospheric Branch, Code 543
Naval Command, Control and Ocean Surveillance Center, RDT&E Division
San Diego, CA 92152-5000

In recent years there have been numerous instances where maximum radar detection ranges of low-altitude targets have been less than expected. Analytical propagation models, notably the JHU/APL TEMPER program and the NRaD Radio Physical Optics (RPO) program, have been used to model the reduced detection ranges. Over the ocean, the evaporation duct refracts radio frequency energy downward from the direction it would flow in a normal or standard atmosphere. It is predicted that the evaporation duct would (1) move the location of the last optical interference null (Lloyds mirror effect) outward in range, (2) decrease the amplitude of the signal return at the peak of the last interference maximum, and (3) decrease the slope of the signal falloff with respect to range at ranges beyond the last interference maximum.

Results from an analytical and experimental effort to assess low-altitude, short-range propagation effects over the ocean are presented. A moderate power X-band radar was used to measure signal return from a set of calibrated targets which were carried on a high-speed ocean-going boat. In addition, surface and upper air meteorological sensors were used to monitor both vertical and range dependent refractivity conditions. From these observed refractive conditions, the NRaD RPO model is used to predict maximum target detection ranges for comparison to measured ranges.

For an X-band radar with a free-space detection range of 8 km (130 dB propagation loss threshold), the expected maximum target detection range in a standard atmosphere is 13.5 km. Measured detection ranges varied from a minimum of 6 km to a maximum of 34 km. The reduced detection ranges were caused by evaporation ducts which is consistent with theory. Detection ranges much greater than standard were caused by surface based ducts created by elevated trapping layers which are not observable from surface meteorological measurements.

F2-6
1540

A PRACTICAL TROPOSPHERIC SCATTER MODEL USING THE PARABOLIC EQUATION

Herbert V. Hitney
Tropospheric Branch, Code 543
Naval Command, Control and Ocean Surveillance Center, RDT&E Division
San Diego, CA 92152-5000

A simple, semi-empirical method is presented that allows tropospheric scatter effects to be included in parabolic equation (PE) radio wave propagation models. This method has been implemented in the hybrid Radio Physical Optics (RPO) propagation model, and several comparisons of RPO results to experimental measurements are presented.

In the PE model, field strength is computed at equally-spaced vertical points separated by a height interval δz. The model adds a small random fluctuation to the mean refractivity profile at each of these points to simulate tropospheric scatter. These fluctuations are taken from a uniform distribution whose mean is zero and normalized such that the variance of the difference between adjacent values is equal to the one-dimensional refractive-index Kolmogorov spectrum in the inertial convective subrange at the wavenumber associated with δz. An effective mean refractive-index structure parameter is included to account for variation with altitude.

This model was developed because it is very simple to implement in the PE model. However, the model lacks a sound physical basis in several areas. For example, δz is chosen based on issues related to the numerical solution of the PE, and not on the turbulent wavenumbers that should contribute to scatter. Also, the Kolmogorov spectrum is not realistically modeled, since the random fluctuations are uncorrelated with height and perfectly correlated with range. In spite of these shortcomings, the comparisons of modeled results with experimental measurements and with the semi-empirical model of the Engineer's Refractive Effects Prediction System (EREPS) is quite good, as shown in the figure below.

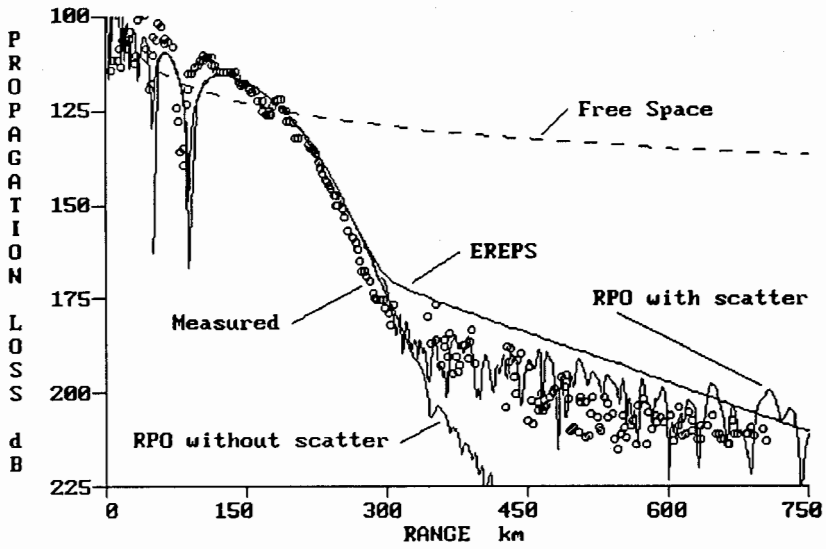

F2-7 1600 MEAN DYADIC GREEN'S FUNCTION OF A RANDOMLY ROUGH SURFACE

Saba Mudaliar
Rome Laboratory
Hanscom AFB, MA 01731

Two most widely adopted approaches for studying scattering from randomly rough surfaces are the Kirchhoff method and the perturbation method. Both are first-order approximations and hence have their inherent limitations. Any attempt to go beyond these approximations and seek a more rigorous solution is confronted with formidable difficulties. Nevertheless several such attempts have been made over the last decade and they have considerably enriched our understanding of the basic problem. In this paper we adopt a multiple scattering approach and derive the mean dyadic Green's function of a random surface.

The rough surface under consideration is plane on the average; it is smooth enough so that derivatives of all orders exist; it obeys Gaussian statistics; it is also statistically homogeneous and isotropic. The Green's dyadic satisfies the inhomogeneous wave equation and the boundary condition corresponding to the perfectly conducting rough surface. So we have a stochastic boundary value problem.

We first use the property of analyticity and obtain an approximate boundary condition on the mean surface. On using the Green's theorem in conjunction with the unperturbed Green's dyadic we readily obtain an integral equation for the Green's function. Expansion of this integral equation by succesive iteration leads to the Liouville-Neumann series where we identify the n'th term as the n'th order scattering. The first term leads to the well known perturbation result. It is impractical and not worthwhile to go beyond and compute higher order terms in this series. However we may involve multiple scattering by renormalizing the series. In this context it is expediant to use diagram techniques. We thus obtain an integral equation for the mean dyadic Green's function. This equation is now solved using the Bourret approximation. It may be noted that in spite of the simple approximation multiple scattering is implicitly involved in our results. Moreover our procedure offers a clear physical picture of the kind of multiple scattering processes taken into account.

F2-8
1620

SPATIAL DECORRELATION PROPERTIES OF MULTIFREQUENCY RADAR BACKSCATTER FROM ROUGH SOIL SURFACES

Ram M. Narayanan and Duane T. Hickenbottom
Dept. of Electrical Engineering and Center for Electro-Optics
University of Nebraska-Lincoln
Lincoln, NE 68588

When a distributed target is illuminated by a coherent electromagnetic wave, the magnitude of the scattered signal is equal to the phasor sum of the returns from all scatterers illuminated by the incident beam. As the radar antenna spatially scans a rough surface, the backscattered power follows a probability distribution, which is subject to spatial decorrelation. The fading statistics, such as the coefficient of variation and the decorrelation distance of the radar backscattered power are functions of the statistics of the rough surface such as the rms roughness and the roughness correlation length, as well as the wavelength. A knowledge of the decorrelation characteristics of radar backscatter is essential in computing the total number of independent samples achieved during a backscatter coefficient measurement. A simple rule of thumb generally followed assumes that the radar signals decorrelate after the antennas have translated by one-half the aperture diameter.

In order to explore this phenomenon experimentally, the radar backscatter from a variety of rough surfaces were investigated as a function of frequency, incidence angle, polarization and illuminated footprint size. Spatial samples of radar backscatter were acquired from bare soil over a scan length of approximately 2.6 m every 1.6 mm using a truck-mounted network-analyzer based scatterometer. Measurements were made at different frequencies (9 and 14 GHz), incidence angles (0° and 35°), polarizations (VV, HH, and VH) and footprint sizes (0.3 and 0.6 m). The statistics of the bare soil surface were determined using a specially designed profilometer that scanned the entire surface over which the radar data were acquired.

Our measurements indicate that, in general, radar signals decorrelate at distances smaller than the "rule-of-thumb" formula. Diffuse scatter, such as cross-polarized backscatter or backscatter at intermediate incidence angles, yielded decorrelation distances that were smaller than those obtained from coherent scatter, such as co-polarized backscatter at normal incidence. Decorrelation distances were also observed to increase with increasing wavelength, all other parameters remaining constant, while spot size had no measurable effect. These results indicate that an understanding of the decorrelation characteristics of radar backscatter will help provide realistic estimates of the reduction in fading variance.

F2-9
1640

SEA SURFACE MEAN SQUARE SLOPE MEASUREMENTS USING THE FALLOFF OF BACKSCATTERED POWER WITH INCIDENCE ANGLE MEASURED BY THE 36 GHz SCANNING RADAR ALTIMETER

Edward J. Walsh, Code 972
NASA/GSFC/Wallops Flight Facility
Wallops Island, VA 23337

The Southern Ocean Waves Experiment (SOWEX) was conducted in June 1992 with collaborators from NASA/Goddard, the University of Massachusetts, the University of New South Wales, and the Australian CSIRO Division of Oceanography and the Division of Atmospheric Research. The NASA 36 GHz Scanning Radar Altimeter (SRA) acquired extensive data under conditions varying from gale force wind with 9-m wave height down to light-and-variable wind conditions. This paper concerns the ability of the SRA to measure the total mean square slope (MSS) of the sea surface in a fashion analogous to the optical technique of Cox and Munk (J. Optical Soc. America,44,838-850,1954).

Several types of data were collected in sequence at 245 m altitude on each flight to demonstrate the MSS measurement capability. Initially, pulse-limited waveforms were acquired at a rate of about 700 Hz for 1 minute using a low-gain horn (39° beamwidth) at nadir. The wide beamwidth used with this technique makes the return pulses insensitive to variations in aircraft pitch and roll attitude. These pulse-limited data azimuthally integrate the backscattered power at each off-nadir angle and measure the backscattered power falloff with angle simultaneously at all incidence angles (Hammond, Mennella and Walsh,IEEE Trans. Antennas and Propagation,AP-25,61-67,1977). The SRA was then quickly switched to its scanning mode (1° two-way beamwidth scanning across the ground track ±22° relative to the orthogonal to the aircraft wings at 10.6 Hz). For 1 minute the aircraft was held straight and level with the SRA scan direction upwind-downwind. Then the aircraft was placed in a 5° bank (scanning from 17° off-nadir to the left, to 27° off-nadir to the right) while the aircraft (and the scan direction) slowly turned azimuthally through two and a quarter revolutions. The aircraft then rolled out to fly straight and level while scanning in the crosswind direction for 1 minute. The SRA mode was then switched back to the low-gain horn mode for 1 min.

This sequence provided the instantaneous, azimuthally integrated MSS measurements from the low-gain horn, the azimuthal dependence of the fall-off of scattering from the turn data, and the straight and level scanning data. The various determinations of MSS are intercompared under a variety of wind conditions to assess the ability of the fixed direction scanning data to determine MSS. These data would allow the SRA to simultaneously characterize the high frequency waves which are most sensitive to the local wind at the same time it measures the energetic portion of the directional wave spectrum through its wave topography measurements.

H1-1
1340

IONOSPHERIC PLASMA SIMULATION LABORATORY EXPERIMENTS WITH THE VTF

D.T. Moriarty, M.C. Lee, and R.R. Parker
Plasma Fusion Center, MIT, Cambridge, MA 02139

Laboratory experiments with the Versatile Toroidal Facility (VTF) have been conducted to investigate the microwave propagation and attenuation in the ECRH generated plasmas. These experiments are aimed at simulating the anomalous absorption of radio waves in turbulent ionospheric plasmas.

The location of the upper hybrid resonance layer as determined by Langmuir probe data agrees qualitatively with the location determined by the transmission diagnostic. Discrepancies between the two methods have been complicated by the small signal to noise ratio near the important regions due to turbulent scattering. Low frequency density fluctuations commonly observed in toroidal plasmas are believed to be produced by the drift wave instabilities. They can significantly scatter incident diagnostic waves when $\delta n/n >> \rho_i/L_n$ where $\delta n/n$ is the fractional density fluctuation, ρ_i is the ion Larmour radius, and L_n is the scale length of the density gradients.

A hot cathode electron beam steady state current drive system recently installed can allow for simulation of auroral field aligned currents.

H1-2
1400

COMPARATIVE STUDIES OF LANGMUIR WAVES EXCITED BY VERTICALLY AND OBLIQUELY TRANSMITTED HF WAVES

M.C. Lee[1,2], L.A. Sanchez[2], S.P. Kuo[3], D.T. Moriarty[1], M.P. Sulzer[4], and K.M. Groves[5]
1. Plasma Fusion Center, MIT, Cambridge, MA 02139
2. ECS Engineering Dept., BU, Boston, MA 02215
3. Polytechnic University, Farmingdale, NY 11735
4. Arecibo Observatory, Arecibo, PR 00613
5. Phillips Laboratory, Hanscom AFB, MA 01731

In our recent ionospheric heating experiments at Arecibo, Puerto Rico, we investigated the spectral characteristics of HF enhanced Langmuir waves among other phenomena. The obliquely propagating HF waves were transmitted from a tilted heater in experiments during August 5 - 11, 1992, while the vertically propagating HF waves were employed in experiments during September 17 - 22, 1992. In the "oblique heating" experiments, the main beam of the HF heater waves was tilted by 12 ^{0} to the north, while the first sidelobe pointed 13 ^{0} to the south. The radiated power of the first sidelobe was estimated to be only slightly different ($\sim 1dB$) from that of the main beam (D.B. Muldrew, personal communication, 1992). Thus, the illuminated ionospheric region was presumably much greater than that with the vertically transmitted waves from the heater. The cascading spectra of the PDI (parametric decay instabilities) produced Langmuir waves were observed in the vertical heating experiments as expected. The radar measurements of the HF enhanced plasma lines in the oblique heating experiments also showed the excitation of PDI; however, the cascading spectrum was not seen. Rather, a broad, highly structured spectrum separated from the PDI produced spectrum by 15 kHz or so with higher power was generated. It indicates that other process(es) excited by the obliquely propagating heater waves can compete with the PDI. Our comparative studies of Langmuir waves produced by the vertically and obliquely transmitted HF heater are aimed at invesitigating the source mechanisms responsible for the generation of HF enhaced Langmuir waves. Parametric instabilities and nonlinear scattering processes will be examined as the potential mechanisms.

H1-3
1420

STUDIES OF ARTIFICIAL SPREAD F PHENOMENON WITH TILTED HF HEATER AT ARECIBO, PUERTO RICO

L.A. Sanchez[1], M.C. Lee[1,2], M.P. Sulzer[3], S.P. Kuo[4], Y.R. Dalkir[2], J.L. Scali[5], and B.W. Reinisch[5]
1. ECS Engineering Dept., BU, Boston, MA 02215
2. Plasma Fusion Center, MIT, Cambridge, MA 02139
3. Arecibo Observatory, Arecibo, PR 00613
4. Polytechnic University, Farmingdale, NY 11735
5. University of Massachusetts, Lowell, MA 01853

Ionospheric heating experiments were conducted at Arecibo, Puerto Rico with a tilted HF heater during August 5 - 11, 1992. The main beam of the HF heater wave was tilted by 12 ^{0} to the north, while the first sidelobe pointed 13 ^{0} to the south. The radiated power of the first sidelobe was estimated to be only slightly different ($\sim 1dB$) from that of the main beam (D.B. Muldrew, personal communication, 1992). Thus, the illuminated ionospheric region was presumably much greater than that with the vertically transmitted waves from the heater. Both the 430 MHz radar and a digisonde were used to monitor the heated ionospheric region and to measure the plasma temperature, density, and the drift velocity. Artificial spread F echoes and wideband absorption phenomenon were seen on the ionograms, indicating the generation of large-scale and short-scale ionospheric irregularities. The radar measurements of the HF enhanced Langmuir waves showed the excitation of the parametric decay instabilities. These results indicate that the tilted HF heater can still partially transmit the vertically propagating pump waves into the ionosphere and produce ionospheric density irregularities.

H1-4
1440

SUSPECTED VLF-WAVED INDUCED PARTICLE PRECIPITATION EVENTS IN IONOSPHERIC HEATING EXPERIMENTS AT ARECIBO, PUERTO RICO

L.A. Sanchez[1], M.C. Lee[1,2], M.P. Sulzer[3], K.M. Groves[4], and S.P. Kuo[5]

1. ECS Engineering Dept., BU, Boston, MA 02215
2. Plasma Fusion Center, MIT, Cambridge, MA 02139
3. Arecibo Observatory, Arecibo, PR 00613
4. Phillips Laboratory, Hanscom AFB, MA 01731
5. Polytechnic University, Farmingdale, NY 11735

Our ionospheric heating experiments at Arecibo, Puerto Rico have indicated that large -scale field-aligned ionospheric ducts created by HF heater waves may support the propagation of VLF waves from the lower ionosphere into the radiation belts. Suspected events of particle precipitation were observed, which give rise to enhanced radar backscatter at altitudes near 90 km or so. Our theoretical analyses suggested that the VLF waves produced by lightning or injected from a ground-based naval transmitter near Arecibo can be guided by the HF induced ionospheric ducts to reach the radiation belts at L = 1.47 and effectively interact with energetic electrons through the pitch angle scattering. These precipitated energetic electrons can reach the lower E region and cause anomalous ionization, leading to intense backscatter radar echoes. Other possibilities which may also produce similar radar signals at Arecibo such as sporadic Es, meteor shower, and natural precipitation of particles have been examined with the radar measurements of the auto-correlation functions (ACF).

H1-5
1520

ANALYSIS OF TSS-1 ELECTRODYNAMIC TETHER SWITCHING TRANSIENTS MEASURED WITH THE SETS EXPERIMENT

S. G. Bilén, B. E. Gilchrist, V. M. Aguero
Space Physics Research Laboratory
University of Michigan
2455 Hayward
Ann Arbor, MI 48109-2143
D. S. Lauben, S. D. Williams
EERA/STARLAB
Durand Building
Stanford University
Stanford, CA 94305
D. C. Thompson
Center for Atmospheric and Space Sciences
Utah State University
Logan, UT 84322-4405

The first mission of the Tethered Satellite System (TSS-1) deployed an electrically conductive 1.6m diameter Italian built satellite to a maximum distance of 256m above the Space Shuttle Atlantis. Because the satellite was connected to the shuttle via an electrically conducting tether, the system induced an EMF across the tether. Using a high impedance voltage monitor, the Shuttle Electrodynamic Tether System (SETS) experiment was able to make high resolution measurements of this induced EMF. In addition, the SETS experiment selectively placed resistive loads between the tether end and the Shuttle's electrical ground. Due to the large inductance presented by the tether reel (≈ 12H fully wound), large transients (≈ -500V for tether current of 15mA) occurred as the resistive loads were switched out. The SETS experiment measured these transients by selectively sampling in high speed (32kHz) bursts. The figure below shows a typical transient (time: 218/00:20:22 GMT, tether length: 179m, altitude: 299km, latitude: 2.4°, longitude: 177.5°).

In this work we present typical measurements of switching transients generated by the system and comparison to our pre-mission model and measurements. These switching transients provide the only high voltage data for the TSS-1 electrodynamic tether system operating in a space plasma. Aspects for the accurate prediction of switching transients — vital to system health — are also identified.

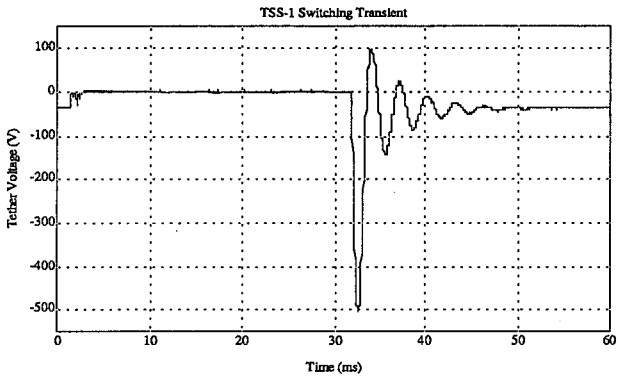

H1-6
1540

ELF AND VLF WAVE GENERATION IN HF HEATER-MODULATED POLAR ELECTROJET

S. P. Kuo
Weber Research Institute, Polytechnic University,
Route 110, Farmingdale, NY 11735
M. C. Lee
Plasma Fusion Center, Massachusetts Institute of Technology,
Cambridge, MA 02139

The report of the successful generation of the ULF radiations by HF heater with modulation of a 10 minute on-off period (P. Stubbe and H. Kopka, J. Geophys. Res., 86, 1606, 1981) stimulated a series of a new experiments. Encouraging results led to the plan of constructing a new super heating facility in Alaska aimed primarily at the further study of the generation of ELF/VLF radiations (P. Kossey and R. Brandt, National Radio Science Meeting, Colorado, Jan. 7-10,1992). The potential generation mechanisms include the modulation of the electrojet current (P. Stubbe and H. Kopka, J. Geophys. Res., 82, 2319, 1977; J. Fejer and E. Krenzien, J. Atmos. Terr. Phys., 44, 1075, 1982; K. Papadopoulos and C. Chang, Geophys. Res. Lett., 12, 279, 1985), the thermal filamentation instability of the HF heater (S. P. Kuo and M. C. Lee, Geophys. Res. Lett., 10, 979, 1983) and the parametric excitation of the Alfven waves (K. Papadopoulos et al., J. Geophys. Res., 87, 1491, 1982; K. Ko et al., J. Geophys. Res., 91, 10097, 1986) and the whistler waves (S. P. Kuo and M. C. Lee, J. Atmos. Terr. Phys., 51, 727, 1989), etc. Presently, the main concern of the research in this subject is how to enhance the generation efficiency. A technique of beam painting is suggested by Papadoulos, et al. (Radio Science, 25, 1311, 1990).

In this work, we discuss an instability process for the ELF/VLF geneartion. As the HF heater wave deposits heat into the elctrojet plasma, the elctron-neutral collision frequency is enhanced. If the heating of the elctrojet is modulated, a positive feedback through the elctron-neutral collisional heating process can cause the transient response of the plasma to the elctrojet current modulation to grow and copnsequently, lead to an instability. Considering a sinusoidally modulated HF heater wave having it field amplitude proportional to $|\cos \omega_1 t/2|$, the threshold fields of the thermal instability under normal electrojet conditions are determined for the o-mode and x-mode operation respectively. For a super heater wave field of 1.5 V/m, the instability can be excited by the x-mode heater whithin a few tens of a millisecond, and can not be excited by the o-mode heater. This instability process which depends upon not only the free energy of the HF heater, but also that of the electrojet current, has the potential to generate ELF/VLF radiations much effectively.

H1-7
1600

CHAOTIC ION MOTION CAUSED BY THE KINETIC ALFVEN WAVE IN THE MAGNETOSPHERE

S. P. Kuo and Antony Y. Ho
Weber Research Institute, Polytechnic University,
Route 110, Farmingdale, NY 11735

The kinetic Alfven wave appears frequently in the magnetosphere and is characterized by a sizable component of electric field parallel to the background magnetic field. This parallel field component of the kinetic Alfven wave (KAW) can significantly affect the motion of energetic protons which are confined by the earth's dipolar magnetic field and execute bouncing motion about the equatorial plane. Similarly, it can also effectively perturb the motion of those energetic electrons trapped in the lower magnetosphere. Such a perturbation on the motion of charged particles provides a possible cause of charged particle precipitation observed in the polar region (B. Hultqvist, Space Sci. Rev., 23, 581, 1979) and provide a source mechanism of low-altitude trapped energetic protons in the equatorial region (T. G. Guzik et al., J. Geophys. Res., 94, 145, 1989). The KAW can be excited through mode conversion of surface MHD waves at magnetospheric boundaries (A. Hasegawa, J. Geophys. Res., 81, 5083, 1976) or by bouncing electron beams (A. Hasegawa, Geophys. Res. Lett., 6, 664, 1979).

In this work, the interaction between a bouncing proton and a kinetic Alfven wave in the magnetosphere is studied using a simplified model and a Hamiltonian averaged over the gyration period of the protons. Both transverse and parallel components of the wave electric fields are included in the formulation. Significant chaotic motion is observed for relatively small wave amplitudes, which may explain observed effects. The results also show that the chaotic level increases considerably when protons bounce resonantly with the wave.

H1-8
1620

OBSERVATIONS OF NATURAL AND MAN-INDUCED ULF/ELF NOISE SIGNATURES OBSERVED AT THE LOW FREQUENCY ELECTROMAGNETIC SIGNATURES OBSERVING STATION OF NCCOSC/NRaD, AT POINT LOMA, SAN DIEGO, CALIFORNIA

Wolfgang-Martin Boerner
THE UNIVERSITY OF ILLINOIS AT CHICAGO
EECS, Communications and Sensing Lab., M/C 154
CHICAGO, IL 60680-4348, USA
Tel/**Fax**: +[1](312)996-5480/**2456** or **413-0024**

Jack Y. Dea and Peder M. Hansen
Naval Command, Control and Ocean Surveillance Center
NRaD (formerly NOSC), Communications Systems Development
NCCOSC/NRaD,Code 832,SAN DIEGO,CA,92152-5000, USA Branch
Tel/**Fax**: +[1](619)553-5781/**6457**

Arthur William Green, Jr.
USGS GOLDEN RESEARCH FACILITIES
INTERMAGNET, 1711 Illinois Street, Rm 234
Golden, CO 80401
(USGS Denver Fed. Centr, PO# 25046, MS 968, Denver, CO)
Tel/**Fax**: +[1](303)273-8482/**8450**

A Low Frequency Monitoring Network has been under development at NRaD (formerly NOSC), San Diego, U.S.A., for the last three years. The original intent was to monitor space vehicle induced signatures in the 5 to 12 Hz region. These narrow-band signatures are thought to be signals derived from different layers of the ionosphere. More recently, our interest has expanded to include monitoring of anomolous broadband signals in the 0.1 to to 20 Hz region that often precede the occurrence of nearby earthquakes. Observations of such events have led to a hypothesis that geological signals are normally present in the ULF (Ultra-Low Frequency, 3 Hz) and ELF (Extremely Low Frequency, 3 to 3000 Hz) bands in addition to the generally accepted signals from micropulsations and lightning discharges. In Southern California, the geological signals are best observed in the "polarimetric window" regions of (i) 2 to 5 Hz using horizontally oriented magnetic sensors and, (ii) 2 to 20 Hz using vertically oriented magnetic sensors. To determine the significance of anomolous events, we conducted a statistical study of the background noise levels. Observations of daily records over a span of several months indicated that the background level in the 1 to 20 Hz region is stationary. Stationarity is not true below 1 Hz. The APD (Amplitude Probability Density) of 2 to 12 Hz signals was found to be surprisingly close to a Gaussian distribution. These two results indicated that a determination of long term averages and variances would be meaningful. Long term averages and variances were obtained and were used to develop alert level criteria. The alert level criteria are used as input parameters in our newly developed Automated Monitoring System (AMS), a computerized monitoring and real-time analysis system. High alert levels in conjunction with the fulfillment of several other factors often presage the occurrence of an earthquake or volcanic eruption, which include: (i) persistence of the elevation of the signals, (ii) the existence of resonance lines in the window region of the power spectrum, and (iii) the Schumann peaks remaining relatively normal. Several examples of broadband precursor emissions are shown as well as a table listing all nearby moderate/large quakes that occurred during the past three years and also listing the correlations with our data base.

H1-9
1640

The TSS-1 Electrodynamic Tether Mission: Early Results and Future Opportunities

B. E. Gilchrist
University of Michigan, Department of Electrical Engineering and Computer Sciences, 1301 Beal, Ann Arbor, MI 48109-2122
Nobie H. Stone
NASA Marshall Space Flight Center, Space Science Laboratory, Huntsville, AL 35812
Marino Dobrowolny
Instituto Fisica Spazio Interplanetario
CNR, Frascati ITALY

The Tethered Satellite System was developed by NASA and theItalian Space Agency to provide the capability to deploy satellites on long, gravity gradient stabilized tethers from the Space Shuttle. The goals of the TSS-1 mission (launched July 31, 1992) were to demonstrate the feasibility of deploying and controlling long tethers in space, and to evaluate some of the unique applications of the TSS as a tool for research by conducting exploratory experiments in space plasma physics. TSS-1 was supposed to have deployed the Italian satellite 20 km above the Orbiter. During the mission, the deployer jammed at 256 m and, as a result, TSS-1 did not achieve its primary objectives.

In spite of the problems experienced, several results were obtained in near proximity to the Orbiter that demonstrate TSS to be safe, stable and easy to control. Moreover, at TSS-1's shortened tether length, the electrodynamic tether system was still operational, allowing investigation of low voltage system characteristics and natural global variations of the tether current flow. Further, the unique ability of the electrodynamic tether to provide a remote electrical reference for local plasma perturbations and their measurement was clearly demonstrated. In addition, numerous measurements were made of electron beam interactions with the nearby plasma environment. The mission also provided unique data on tether dynamics and dynamic stability, as well as verification of science instrumentation and tether current control hardware

In this presentation, the TSS-1 scientific and technological goals will be presented and the extent the objectives were met by the return obtained from this first tethered satellite mission. The need for a reflight to assure the ultimate success of the TSS-1 mission goals and ultimately to tether technology in general will be discussed.

J1-1
1340

Advances in Lightwave Communication

Tingye Li
AT&T Bell Laboratories
Crawford Hill Laboratory
Holmdel, New Jersey 07733

Summary

Twenty two years have passed since the attainment of the first low-loss optical fiber intended for telecommunication applications. The rapid research progress in the lightwave field that ensued has led to the widespread deployment of optical fibers in telecommunications systems throughout the industry. Optical fiber transmission systems are now in commercial use under the ocean to link continents, on land to join cities, and in metropolitan areas to connect telephone central offices and to distribute broadband services. Indeed, optical fiber has emerged as the undisputed transmission medium of choice in almost all areas of telecommunication, because it offers unrivaled transmission capacity at a lower cost compared to other media.

Research continues today on many fronts to explore the efficient uses of the wide bandwidth of low-loss single-mode fibers for long-distance transport as well as for local networks and distribution. Monolithic integration of photonic and electronic devices is being pursued for both transmission and switching, to enhance subsystem performance and functionality, and to reduce overall system cost. The continuing interest in higher-speed devices and systems is evident in demonstrations of transmission experiments at data rates beyond 20 Gb/s. Coherent detection offers high receiver sensitivity and efficient means for channel election in a densely-packed wavelength-multiplexed system, but noncoherent techniques involving optical amplifiers and tunable optical filters are an attractive alternative. Various coherent and noncoherent experimental systems have been demonstrated for transmission and networking. Recent developments in erbium-doped fiber amplifiers are evoking intense interest, as wavelength-multiplexed systems employing optical amplifiers as non-regenerative repeaters can provide a cost-effective means to upgrade the transmission capacity of the embedded long-distance network by at least an order of magnitude. Such systems promise significant benefits in operational flexibility, network functionality, and overall cost for both terrestrial and undersea long-haul transmission. When distances between regenerative repeaters become very large, nonlinear effects in the transmission fiber are of great interest, as these effects may impair signal transmission. Nevertheless, amplified transmission of conventional NRZ (non-return-to-zero) signals at multigigabit-per-second rates has been demonstrated over distances beyond that required for transoceanic applications (>10,000 km). Refractive-index nonlinearity in the transmission fiber and amplified spontaneous emission noise from the EDFAs are the limiting factors that determine the system performance. Already, amplified transoceanic systems are being developed for installation and service by 1995. Looking ahead, optical solitons that exploit both the nonlinearity and dispersion of the fiber medium have the potential to increase further the capacity of ultra-long distance systems. Soliton transmission may very well be used in the future as demand increases.

As amplifiers become less costly, they will be used in shorter-distance but higher-volume applications, such as high-speed data networks and distribution of broadband services. Hence, the widespread use of optical amplifiers will hasten the realization of the full potential of lightwave technology. It can be said that lightwave communications is now passing from a replacement phase to a revolutionary phase, and the fiber optical amplifier is the catalyst in this transformation. This talk will review present lightwave systems and discuss various research results that will have great impact on the future of telecommunications.

J1-2
1400

FIBER OPTIC TECHNOLOGY FOR RADIO ASTRONOMY APPLICATIONS

C.M. Gee, T.R. Chen and G. Grimes
Ortel Corporation
2015 W. Chestnut St, Alhambra, CA 91803
R.T. Logan Jr, M.D. Calhoun and G. Lutes
NASA/Jet Propulsion Laboratory
4800 Oak Grove Dr, Pasadena, CA 91109

Fiber optic technology using semiconductor lasers and high-speed photodiodes offers remoting capabilities with wide bandwidth, large dynamic range and phase stability for radio astronomy applications.

In this paper, we will present the performance of fiber optic links used to transmit analog signals from 10 MHz to 15 GHz over many kilometers. With commercial directly modulated, distributed-feedback (DFB) semiconductor lasers, RF signals up to 15 GHz may be transmitted over 10 km distances with 118 dB-Hz signal to noise performance. At IF frequencies from 50 to 550 MHz, third order spurious-free dynamic range of 120 dB-$Hz^{2/3}$ can be achieved. Single-sideband phase noise of -95 dBc/Hz at 1 Hz offset frequency from an 8 GHz carrier has been measured with a noise floor of <-130 dBc/Hz at offset frequencies >10 kHz from the carrier. We will also present thermal coefficient of delay (TCD) results for optical fiber and fiber optic terminal equipment and delay variations due to cable flexure.

In addition, we will review various fiber optic link techniques, including DFB lasers, Fabry Perot lasers and external modulators. Noise contributions such as laser relative intensity noise, receiver thermal and shot noise will be defined and related to equivalent input noise (noise figure), phase noise and dynamic range of the link.

J1-3
1420

CURRENT APPLICATIONS OF ANALOG FIBER OPTICS IN THE NASA/JPL DEEP SPACE NETWORK*

George Lutes
Jet Propulsion Laboratory
4800 Oak Grove Drive
Pasadena, California 91109

The performance and cost effectiveness of the NASA/JPL Deep Space Network (DSN) have been greatly enhanced by the use of ultra stable, wideband, low loss analog fiber optic systems. These systems have permitted centrally located frequency and timing facilities, the use of special equipment by any station regardless of its location within the complex, and new test capabilities.

In this paper we will describe these applications and their implementation. They include transmission of ultrastable 100 MHz frequency references from a central frequency and timing facility to stations located up to 29 km away, transmission of wideband, 100 to 800 MHz, intermediate-frequency signals to be processed by equipment located up to 29 kms away, and transmission of a 12 GHz microwave signal to measure antenna contribution to system frequency stability to a level of less than 1×10^{-15} for 1,000 seconds averaging time.

* This work represents the results of one phase of research carried out at the Jet Propulsion Laboratory, California Institute of Technology, under contract with the National Aeronautics and Space Administration.

J1-4
1440

THE CSO–JCMT SUBMILLIMETER–WAVE INTERFEROMETER

J. E. Carlstrom and T. G. Phillips
MS 105-24, Caltech, Pasadena, CA, 91125
R. E. Hills and O. P. Lay
MRAO

A linked submillimeter–wave interferometer between the JCMT and CSO telescopes, located near the summit of Mauna Kea at 4,200 m, has been built and tested. The interferometer exploits fiber optics to transmit the local oscillator reference signal and the receiver IF signals. A fiber optic delay line is implemented in the IF transmission from the receivers to a 1024 channel, 1 GHz bandwidth, digital correlator. Commercial wideband (10 GHz) fiber optic transmitters and receivers are used. Fibers with extremely low thermal coefficient of expansion are used for the local oscillator reference to minimise thermal drifts of the interferometer phase response.

The frequency modulation is designed so that the fringe rotation is stopped for one sideband and at 2 MHz for the other sideband, making the correlated output sensitive to only one (selectable) sideband. The narrow spectrometer channels and the single sideband response allow only three delay steps to be used for each receiver IF, as long as the integration time is kept short (< 10 s). Compensation for the remaining delay error is made in software post–processing.

The local oscillator system was designed for high coherence at wavelengths as short as 350 μm. Currently, receivers covering the 1 mm and 800 μm windows are available at both telescopes. Receivers at 600 μm should be available this winter.

First observational tests of the interferometer were made in 1992 June and September in both the 1 mm and 800 μm atmospheric windows. We were able to measure continuum and spectral line emission. The design of the interferometer and observational results will be presented.

J1-5
1520

AN OPTICAL FIBER IF TRANSMISSION SYSTEM AND TRACKING DELAY FOR THE OWENS VALLEY MILLIMETER ARRAY

S. Padin and S.F. Soares
California Institute of Technology
Owens Valley Radio Observatory
Big Pine, CA 93513

A wide-band optical fiber IF transmission system and tracking delay have been developed for the Owens Valley Millimeter Array. The IF system processes two 1-2 GHz IF bands from two SIS mixers in each telescope. This allows simultaneous dual wavelength observations in the 2.7 and 1.3-mm bands and dual polarization observations in either band.

The 1-2 GHz IF signals from the receivers in a telescope are frequency multiplexed, one band being shifted to 2.5-3.5 GHz. This multiplexed signal is transmitted to the array control building via a 1310-nm singlemode optical fiber link with a bandwidth of ~10 GHz. The optical link provides wide-band transmission with small passband errors (typically ±1 dB and ±5 ° over the 1-6 GHz band). However, the link components are expensive so frequency multiplexing two IF signals is attractive despite the added complexity. The link uses phase-stabilized optical fiber which has a liquid crystal polymer coating with a thermal expansion coefficient that compensates for that of the silica fiber. In the Owens Valley Array the largest temperature induced diurnal delay change in summer is ~5 ps. This results in a phase change of ~6 ° at the correlator output for IF signals at the top of the 2.5-3.5 GHz band. At lower temperatures the phase-stabilized fiber has better performance and in winter the largest delay change in the Owens Valley system is ~1 ps.

The three longest segments (512, 256 and 128 ns) of the tracking delay are included in the optical link. This avoids the difficulty of compensating for dispersion in long coaxial cable delay segments. The optical delay also has smaller delay variations with temperature because phase-stable fiber is used. Fiber delay segments are inserted using mechanical fiber switches. The switches have losses of ~1 dB per delay segment and this limits the number of fiber segments since optical loss in the link degrades the signal-to-noise ratio. The remaining segments in the tracking delay are realized in coaxial and microstrip transmission lines. The complete delay has a length of 1 μs and a resolution of 1/128 ns. At the tracking delay output the two IF signals are demultiplexed and sent to continuum correlators and a digital spectral line correlator.

J1-6 1540 FIBER-OPTIC APPLICATIONS TO RADIO TELESCOPES AT NOBEYAMA RADIO OBSERVATORY

M. Nishio, M. Ishiguro, C. Torii, T. Miyaji, S. Kawashima and T. Kanzawa
Nobeyama Radio Observatory, National Astronomical Observatory, Nobeyama, Minamisaku, Nagano, 384-13 Japan

At Nobeyama Radio Observatory, fiber-optic devices are widely used to a new interferometer, the Nobeyama Radioheliograph, constructed at 1991 and 1992. For the Nobeyama 45m Telescope and the Nobeyama Millimeter-wave Array, applications of fiber-optic devices are in progress to broaden their IF-signal bandwidth. We will describe the present status of fiber-optic applications at Nobeyama Radio Observatory.

The Nobeyama Radioheliograph consists of 84 small antennas of 80-cm diameter, which are aligned on T-shaped baseline of 490m east-west and 220m north-south. Observation frequency is 17 GHz. The fiber-optic devices are used as transmission lines of IF signals, reference signals of phase-locked local oscillators and control data. A reference signal of a master oscillator in an observation building is distributed to phase-locked local oscillators installed in the antennas by using a 1-to-84 optical divider and optical fiber cables. This phase-lock network is of open loop type. We use phase-stabilized optical fibers with temperature coefficient of less than 0.2 ppm/C and O/E converters installed in temperature controlled boxes. Phase stability of the phase-locked network is 3deg/6hours in rms. Additional phase noises are generated in the E/O converter of the phase-locked local oscillator. The coherent loss caused by the phase noise is about 0.1% at the correlator outputs, which is negligibly small.

The Nobeyama 45m Telescope is a single paraboloidal dish with the diameter of 45m, which has superior performance in millimeter wave range. At present, received signals are transmitted from the receiving room of the 45m Telescope to an observation building via coaxial cables. Frequency range of the IF signals is from 2.2 GHz to 2.7 GHz. By replacing the coaxial cable system to fiber-optic system, the analog IF signals from 5 to 7 GHz are transmitted without equalizations of band-pass characteristics. Developments of 5x5 multi-beam receivers with a digital spectrometer is in progress. The fiber-optic system is beneficial to these receivers and spectrometer because of broad frequency responses and reduction of cabling spaces. The fiber-optic system is in test stage and will be used at late 1993. The new signal transmission system will be also applied to a new VLBI observation mode using high-speed sampling and recording unit of 2 GHz bandwidth.

The Nobeyama Millimeter-wave Array is a interferometer with six movable 10m dishes. There are 30 stations on east-west and north-south baselines and the antennas are moved from a station to other station in order to change antenna spacing. Signals received by the antennas are transmitted to an observation building through phase stable coaxial cables installed in a tunnel under the ground. Fiber-optic devices are planned to be used to transmit IF signals. The optical fiber cables are installed from each of 30 stations to the observation building and connected to the antennas with optical connectors. Frequency range of the transmitted IF signals is from 5 GHz to 7 GHz. The phase-stabilized optical fiber cables will be used. At present, the fiber-optic system has been tested and will be applied to the Millimeter-wave Array at late 1994. At the same time, developments of ultra wideband correlators with 2 GHz bandwidth are in progress.

J1-7
1600

HIGH RESOLUTION IMAGING AT MM-WAVELENGTHS WITH THE HAT CREEK ARRAY

L.G. Mundy, W.C. Erickson, A.W. Grossman, and L. Blitz
Astronomy Deptartment
Uinv. of Maryland
College Park, MD. 20742

The Hat Creek mm-wavelength array, operated by the Berkeley-Illinois-Maryland Association (BIMA), is planning an operational mode in which two of its telescopes can be placed at outrigger sites located 0.6 and 1.0 km from the main array. Use of these outrigger telescopes will yield angular resolutions of 0.45 arcseconds at 3.0 mm wavelength and 0.20 arcseconds at 1.3 mm wavelength. When nine telescopes are operational, reasonable image quality will be obtained with a 12-hour observation. The maximum sidelobe amplitude depends upon source declination, but is about 16%.

Communication with the outrigger telescopes will be by means of high-quality, analog, optical links. Links will be used both for transmission of LO signal to the antennas and return of the data IF signal from the antennas. We have tested the operation of these links on the existing telescopes; fringes were obtained on astronomical sources on September 18, 1991. The link was operated using both normal single-mode optical fiber and special phase-stable fiber. The phase-stable fiber was found to show a factor of 10 less temperature sensitivity in the phase compared to normal fiber. A line-length measurement system, instituted at radio frequencies, was successfully used to compensate for temperature dependent phase variations within the cable.

The extended array will be used to map star forming regions and protoplanetary nebulae on spacial scales as small as 30 AU. It will also be used to make high resolution maps of active galactic nuclei and solar flare regions. We plan to use self-calibration techniques to correct for atmospheric phase variations and to explore an alternative possibility which uses variations in atmospheric emission to estimate these phase variations.

J1-8
1620

FIBEROPTICS AT THE SAO SUBMILLIMETER ARRAY

Martin W. Levine and Colin R. Masson
Smithsonian Astrophysical Observatory
60 Garden Street
Cambridge, MA 02138

The Smithsonian Astrophysical Observatory (SAO) is constructing a submillimeter wavelength interferometer to operate in the range 0.3 to 1.3 mm. The submillimeter array (SMA) is compromised of six movable 6-m diameter telescopes to be installed near the summit of Mauna Kea on the island of Hawaii. The maximum baseline is 500 m, which corresponds to a resolution of 0.53 arcseconds at 1.3 mm and approximately 0.1 arcseconds at 0.3 mm. Each of the six antennas of the SMA contains a set of six cryogenically-cooled SIS mixers, any two of which can be selected to operate simultaneously.

Fiberoptic technology was factored into the design of the SMA from the beginning, to address the basic issues of reference phase stability and low-dispersion IF transmission. The implementation of this technology into the architecture of the reference signal distribution system, with its emphasis on symmetry, commonality of optical paths and component temperature control, is described in this paper. The reference signals are transmitted in the 6 to 8 GHz range as amplitude modulation of the 1.3μ optical carrier. A prototype of the reference distribution system, which includes active temperature control of the laser diode transmitter and photodiode receiver has been fabricated and preliminary testing in the laboratory has been completed. Test data at a reference frequency of 6.7 GHz show that the temperature sensitivity of the overall system, including 100 m of temperature-compensated fiber, is less than 0.06 ps/C. A detailed block diagram of the complete IF and reference signal distribution system design which evolved from these considerations is presented.

A basic building block of the signal distribution system is phase-stable transmission media; optical fiber for the longer distances and coaxial cable for internal connections. Data from SAO measurements of temperature stability of a variety of fibers and cables is included in this paper. In particular, the widely-used Sumitomo temperature-compensated fiber was found to exhibit a point of inflection of the temperature coefficient of phase at approximately 10 C; the measured value at this temperature was in the order of 0.0003 to 0.0005 ps/m per degree C.

Session B-4 0835-Thurs. CR2-28
NUMERICAL METHODS
Chairman: Ronald J. Pogorzelski, General Research Corp., Santa Barbara, CA 93160-6770

B4-1
0840

SPARSE MATRIX TECHNIQUES AND SOLUTIONS OF MAXWELL EQUATIONS

L. J. Bahrmasel
McDonnell Douglas Research Laboratories
St. Louis, MO 63166-0516, U.S.A.

The numerical solution of partial differential equations naturally lead to a sparse matrix regardless of whether the problem at hand is transient or not. If we consider the solution of Maxwell equations in the frequency domain, we are led to solving a Helmholtz equation in two dimensions or a curl-curl type of equation in three dimensions. Regardless of the type of spatial discretization method (finite difference, finite element, etc.), we obtain a system of linear equations to solve. The structure of this linear system of equations will in general be sparse and possibly banded. If one attempts to solve this linear system using standard LU decomposition techniques, such as those available in LINPACK (J. J. Dongarra et al, *LINPACK User's Guide*, 1979), one will quickly find that storage space and speed will be a problem, particularly in three dimensional applications.

An alternative to storing either the entire matrix, or even the banded portion, is to only store the nonzero entries. In other words, only keep track of the important matrix entries, the nonzero ones. This is the basis for all sparse matrix techniques. The standard methods of solving the linear systems may then be used, either direct (S. C. Eisenstein et al, *Yale Sparse Matrix Package* I & II, Yale Univ. Dept. of Comp. Sci. RR#112 and RR#114) or iterative (D. J. Evans, *Software for Numerical Mathematics*, 49-83, 1974). In implementing these standard methods, one only performs arithmetic operations on the nonzero entries, thus saving considerable computational time. An important frequency domain application involves finding the largest or smallest eigenvalues related to a wavequide. This too can be accomplished using sparse techniques.

Aside from applying sparse matrix techniques in the frequency domain, they can also be utilized in the time domain. For instance, an implicit method is required to solve Maxwell equations when stiffness occurs. In the course of using an implicit method to solve a partial differential equation, one is required to solve a system of linear equations. This system involves the Jacobian matrix associated with the spatial discretization of the partial differential equation. The structure of this Jacobian matrix is sparse, hence it would advantageous to take advantage of the sparsity as is outlined above for frequency domain solutions.

An overview of sparse matrix techniques applied to the solutions of Maxwell equations will be given, for both frequency and time domain.

B4-2
0900

A THREE DIMENSIONAL FINITE VOLUME TIME DOMAIN SOLVER FOR MAXWELL'S EQUATIONS*

M.R. Axe Specialist, M. Shu Research Associate, R.K. Agarwal Director
McDonnell Douglas Research Laboratories
P.O. Box 516, St. Louis, MO 63166

It is well known that Maxwell's equations can be written as a set of first order partial differential equations in hyperbolic conservation law form. As a consequence the well-developed computational fluid dynamics (CFD) algorithms developed for the solution of the compressible Euler equations can be applied for the numerical solution of these equations. In the present work, Maxwell's equations are solved in the time domain using the method of lines, which decouples the temporal terms from the spatial terms. An explicit finite-volume algorithm is developed wherein the spatial terms are discretized using a second order central difference operator while the time-integration is carried out using a five stage Runge-Kutta time-stepping scheme. A fourth order dissipation operator is added to stabilize the algorithm. A second order Engquist-Majda type of boundary condition is used in the far field. The code has been validated by comparing the calculations with known analytical solutions and the work of other investigators for the electromagnetic scattering from perfectly conducting spheres (Figure 1), cone-spheres (Figure 2), finite cylinders, and almonds (Figure 3).

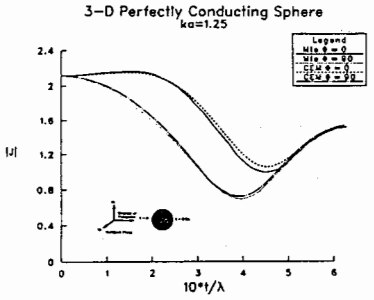

Figure 1

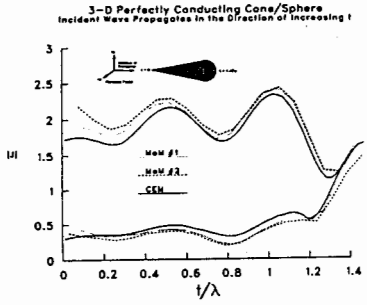

Figure 2

Figure 3

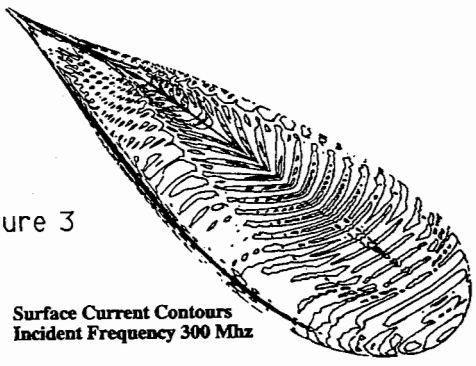

* This research was conducted under the McDonnell Douglas Independent Research and Development program.

B4-3 0920 INSIGHTS CONCERNING THE CONDITION NUMBER OF THE MATRIX RESULTING FROM A NEAR-FIELD LOCALIZATION FORMULATION

R. J. Pogorzelski
General Research Corporation
5383 Hollister Avenue
Santa Barbara, CA 93160-6770

It has recently been suggested that the computational efficiency of a numerical solution of the integral equations which arise in electromagnetics can be enhanced by inducing a local behavior in the interaction among the various current elements. One method of achieving the desired localization has been described by Canning [IEEE AP-S Mag., 32, 18-30, Oct. 1990]. Canning's technique involves combining the current elements into phased arrays which produce beams of radiation thus limiting the interaction to those elements lying within a given beam. More recently, it was noted that this is a far field concept whereas, in fact, the interactions very often occur in the near zone of the sources. [R. J. Pogorzelski, 1992 National Radio Science Meeting Digest, pg. 430.] A formulation was introduced which achieves the localization in the near zone by means of focused equivalent sources. Being equivalence based, this formulation is currently limited to closed bodies.

A problem which arose during the development of Canning's approach was the matter of the condition number of the resulting matrix. Early versions of Canning's method caused a deterioration of the matrix conditioning. Newer versions involve only unitary transformations and therefore do not change the condition number from that of the original method of moments matrix. Thus, it is natural to inquire as to the condition number properties of the near-field localization technique. In particular, one might ask whether near field localization induces poor conditioning by virtue of eliminating direct interactions among certain of the current elements. The two dimensional case of an infinitely long circular conducting cylinder affords a convenient opportunity to address this question because the resulting matrix is circulant. The eigenvalues of a circulant matrix can be obtained very readily via the discrete Fourier transform. Moreover, the spectral content of the solution can be inferred from the cylinder diameter and the properties of the Bessel functions in the eigenfunction solution. In the present work, it is shown by means of this example that the degree of localization and the matrix condition number are directly related. That is, a more localized basis results in a better conditioned system of equations.

B4-4
0940

Parameter Estimation for Characterization of Microwave Structures

B. Houshmand and T. Itoh
Department of Electrical Engineering
University of California, Los Angeles
Los Angeles, CA 90024-1594

ABSTRACT

Characterization of microwave structures such as micorstip lines, slot-lines, coplanar waveguides for a range of frequency has been possible by employing the well know Finite-Difference Time-Domain (FDTD) method. The main feature of the FDTD approach is the efficient implementation even for three dimensional structures with arbitrary metalizatian, and layered structure. In addition, the FDTD algorithm may be derived directly from the integral or differential forms of the Maxwell's equation. These features, as well as, the recent advances in implementation of accurate Absorbing Boundary Conditions (ABC) have made the FDTD method a practical analysis tool for complex microwave structures. The main drawback, however, has been the excessive computation time required to simulate the wave propagation throughout the structure which is required in order to characterize various structure parameters such as the S-parameters for a range of frequencies. In addition, it is known that the Fourier Transform based methods for parameter computation are quite sensitive to small numerical errors which arise from reflections from the absorbing boundaries and the spatial-temporal discretization of the Maxwell's equations. Recently, there has been an attempt to utilize the Parameter Estimation techniques which have been developed in the signals and Systems area to alleviate the disadvantages of the FDTD method. For example, an Auto-Regressive Moving Average (ARMA) model is matched to the input-output signals of the microwave structure by utilizing a System Identification (SI) algorithm. This method could potentially reduce the computational time since the structure is completely characterized when the system parameters are computed. In addition, the sensitivity of the structure parameters to numerical errors can be reduced. In this talk several promising SI algorithms are presented. The savings in the computation time, and the robustness of the structure parameters to numerical errors are discussed.

B4-5
1020

MULTI-WAVELENGTH 3-D SCATTERING WITH DUAL-SURFACE INTEGRAL EQUATIONS ON VECTOR AND PARALLEL SUPERCOMPUTERS

Margaret B. Woodworth
ARCON
Waltham, MA 02154

Arthur D. Yaghjian
Rome Laboratory
Hanscom AFB, MA 01731

The dual-surface magnetic field integral equation (DMFIE) has been applied to compute scattering from three-dimensional perfect conductors up to several wavelengths across, using the conjugate gradient iterative method (Woodworth and Yaghjian, Ch. 4 in PIER 5, Ed. Sarkar, 1991). More recently, access to large vector and parallel computers has enabled us to solve scattering from electrically larger bodies (up to 15 wavelengths across for a perfectly conducting cube).

We begin with an overview of the dual-surface integral equation for solving multi-wavelength scattering problems. Comparisons will be shown between the bistatic scattering computed with the DMFIE and a uniform high-frequency solution applied to cubes 15 wavelengths on a side.

Various configurations of vector and parallel supercomputers will be discussed along with strategies for obtaining optimum performance from each computer architecture. Actual computer run times and memory requirements versus the size of the scatterer will be presented for the vector and parallel supercomputers.

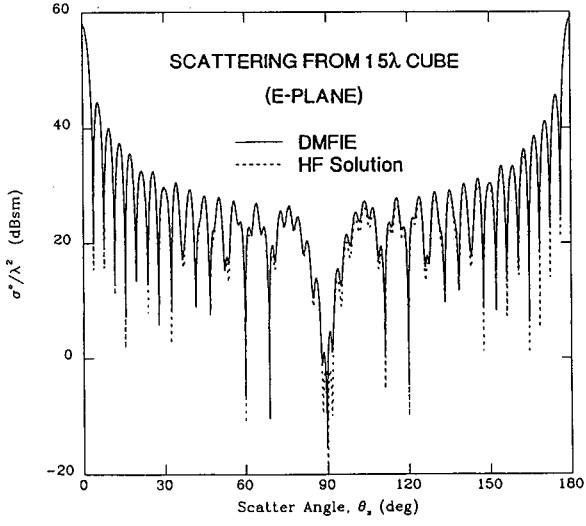

B4-6
1040

USING THE HYBRID MOM/GTD TO STUDY THE EFFECT OF A CONDUCTING SCATTERER ON AN APERTURE ANTENNA

John Silvestro
Electrical and Computer Engineering Department
Clemson University
Clemson, SC 29634-0915

The Method of Moments (MOM) has been used successfully in the past to analyze the effect of electrically small conducting scatterers on an antenna. For large scatterers this technique becomes computationally intensive. One way to overcome this limitation is to use a hybrid Method of Moments/Geometrical Theory of Diffraction (MOM/GTD) technique, where the field scattered by the conductor is calculated using the GTD. In such solutions, the equivalence principle is used to close the aperture and the equivalent magnetic currents that result are the unknowns of the problem. The antennas of interest are rectangular waveguides and it is often easier to use entire domain basis functions when working with such antennas. A problem with this choice though, is how to use the GTD to calculate the scattered field for cases where the conductor is not in the far zone of the antenna. The proposed solution to that problem is to divide the basis function under consideration into small piece-wise sinusoidal pulses and then to calculate the field scattered by each of these pulses using the GTD. In this way, the conductor is in the far zone of each pulse and the scattered field due to a given entire domain basis function is equal to the weighted sum of the fields due to these smaller pulses. By using this approach, entire domain basis functions can be used in a MOM/GTD solution of the interaction of a large conducting scatterer with an aperture antenna for cases where the scatterer is not in the far zone.

As a test of this idea, a computer code that implements this procedure for a long conducting cylinder of circular cross section that is near a rectangular waveguide has been developed. A network analyzer has been used to measure the reflection coefficient of a waveguide near a long conducting cylinder for a variety of cylinder sizes and spacings. Comparisons of the computed data with the measured data show an excellent agreement for cylinders that are in the radiating near field region of the antenna. Representative examples of this data will be presented.

B4-7
1100 **A NUMERICAL STUDY OF THE ILL-POSED NATURE OF HALLEN'S EQUATION**

Richard C. Booton, Jr.
Center for Microwave/ Millimeter-Wave Computer-Aided Design
Department of Electrical and Computer Engineering
University of Colorado
Boulder, CO 80309-0425

Many investigators have observed the tendency for numerical solutions of Hallen's equation to exhibit "instability". Tikhonov and Arsenin (Solutions of Ill-Posed Problems, V.H. Winston and Sons, Washington, DC, 1977) have pointed out that any Fredholm integral equation of the first kind is ill posed. Sarkar (Radio Science 18, 29-38, 1983) has emphasized the applicability of this result to Hallen's equation with the implication that the trouble frequently is in the equation not in the numerical method.

The purpose of this talk is to explore numerically this ill-posed nature and to relate it to specific properties of the Green's function. The situation is illustrated by numerical solutions for a plane wave normally incident on a thin cylinder. Triangular basis functions and several weighting functions are used. The solutions for the current are shown to be well-behaved until one tries too fine a grid. This is illustrated by the figures below for 32 and 128 basis functions.

The Green's function and its derivatives are examined to determine the conditions for which spurious solutions should be expected. The essence of the approach is to determine current solution components that are consistent with the basis functions but that produce only small additions to the electric field. These conditions are shown to agree with the results of the moment-method solutions.

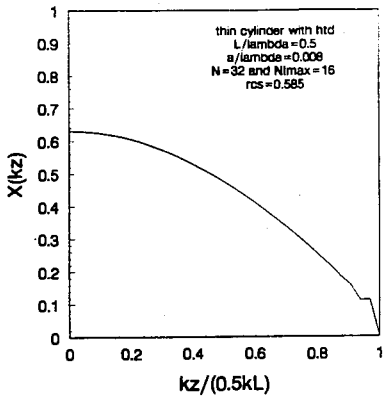

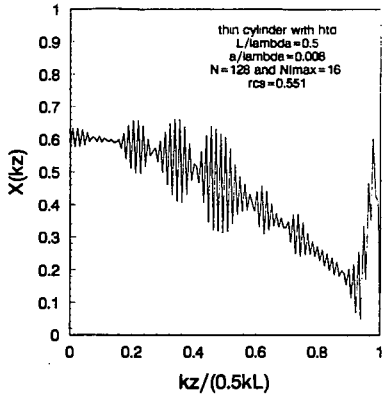

B4-8
1120

THE MAXIMAL RANGE STEP IN TROPOSPHERIC WAVE PROPAGATION USING THE PARABOLIC EQUATION METHOD

Vic Dannon
Office of Naval Technology,
Naval, Command, Control and Ocean Surveillance Center, RDT&E Division
San Diego CA 92152-5000.

The parabolic equation method had been introduced to wave propagation models to facilitate the computation of the wavefield. The wave equation may be approximated by a diffusion equation where the range r has the role of the time variable t and the height z is the spatial variable x. Then, the wavefield computed at some range r serves as "initial" condition for the computation of the wavefield at "time" $r + dr$. To quickly obtain the power loss coverage diagram, we wish to sweep the range in the largest possible range steps.

F. Tappert has used in his simulations a fixed increment $\Delta r \approx 2k(\Delta z)_N^2$ where $k=2\pi/\lambda$ is the wavenumber and $(\Delta z)_N = \lambda_o / 2\theta_{\max}$ is the z increment used in computing the values of the wavefield $u(r,z)$ at the range r. However, at higher frequencies the run times with the fixed increment become impractical.

The truncation error of the parabolic equation is often mentioned with the expectation that it would determine the maximal increment but we demonstrate that this doesn't work. That is, the truncation error of the equation is inadequate for the purpose of determining the maximal range step for a given wavefield error.

However, by analyzing the wavefield error, we obtained a formula that relates the range increment to the wave field error, the gradients of the refractive index n (with respect to range and height) and to the wavefield and its gradients. We show that given a wavefield error of δ, the maximal range step Δr allowed is given by $\Delta r \approx \delta \left|1+(\Delta_i u_{ij} + \Delta_j u_{ij})/u_{ij}\right| / k\left|\Delta_i n_{ij} + \Delta_j n_{ij}\right|$. where $n_{i,j}$ is the refractive index and u_{ij} is the field at the i,j (height, range)grid point.

The formula had been tested successfully on homogeneous and range-dependent ducting environments. We obtained run time speed-up of 300-900% compared to the use of a fixed increment.

B4-9
1140

SELECTIVE COMPUTATIONS OVER A WIDE BANDWIDTH

Randy L. Haupt
Christopher J. McCormack
Department of Electrical Engineering
HQ USAFA/DFEE
2354 Fairchild Drive Suite 2F6
United States Air Force Academy, CO 80840
E. K. Miller
Group MEE-3, MS J580
Los Alamos National Laboratory
Los Alamos, NM 87545

Considerable computer time is necessary to run numerical electromagnetic models that are broadband or have resonances over a wide range of frequencies. Traditionally, the models are run using very small frequency increments so none of the important frequency features are skipped. This talk presents an adaptive rational function/polynomial interpolation technique for reducing the number of computations needed to accurately characterize an electromagnetic model over a broad bandwidth.

Assume the electromagnetics model is programmed on a computer and returns the desired characteristic as a function of frequency. A good example is antenna impedance vs. frequency. The impedance is calculated at five equally spaced frequency values across the bandwidth. Next, the interval is broken in two and the error checked in each interval. If the error is too large in an interval, then two more equally spaced data points are added between the three existing data points and the process repeated. This adaptive scheme lends itself well for recursive programming. Interpolated impedance values are found using Bulirsch-Stoer rational function interpolation combined with Neville's polynomial interpolation. These algorithms calculate interpolated values for the impedance without calculating the coefficients of the rational function model. In addition, these algorithms calculate an error estimate at each interpolated point over the interval. Although these algorithms tend to be slow, they are numerically stable and provide an error estimate for the adaptive intervals. Speed is not a necessity in these calculations, because the impedance calculations take far more time then the interpolation process.

We will present results from a Numerical Electromagnetics Code model of the impedances of a tilted terminated folded dipole (broadband) and a trap dipole (two resonances) using the adaptive interpolation methods described above.

Session E-2 0855-Thurs. CR1-40

INITIATIVES AND TRENDS IN SPECTRUM MANAGEMENT

Chairman: R.D. Parlow, National Telecommunications and Information Administration, U.S. Dept. of Commerce, Washington, DC 20230

Organizers: R.D. Parlow and D.J. Cohen, National Telecommunications and Information Administration, U.S. Dept. of Commerce, Washington, DC 20230; and G.H. Hagn, SRI International

E2-1 0900 AN OVERVIEW OF INITIATIVES AND TRENDS IN SPECTRUM MANAGEMENT

R.D. Parlow, Associate Administrator
National Telecommunications and Information Administration, Room 4009
U.S. Department of Commerce
14th & Constitution Avenue, N.W.
Washington, D.C. 20230

This paper presents an overview of various trends and initiatives that are taking place in the spectrum management community. During the past several years a number of events have taken place that have influenced the direction of spectrum management decisions, initiatives and policies.

The recommendations from the National Telecommunications and Information Administration (NTIA) study on future spectrum management issues and processes are progressively being implemented. Bills in Congress that direct the reallocation of 200 MHz from the government to the private sector are still pending. This proposed legislation also contains Administration proposals for incorporating market based principles, i.e. auctions, into the spectrum attribution process. This topic continues to generate considerable debate.

The NTIA has issued an NOI on national spectrum requirements which is intended to help identify future requirements, trends and actions for the spectrum management community. Coupled with this effort is the development of a national database of spectrum use -- both government and private sector users. In addition the FCC has made some significant decisions regarding the development of new mobile and wireless radiocommunication services and has issued several experimental licenses for Low Earth Orbit (LEO) mobile experiments.

Internationally, a number of significant events have occurred. The World Administrative Radio Conference (WARC 92) occurred in Malaga-Torremolinos, Spain between February 3 - March 3, 1992 where significant spectrum reallocation decisions were made. These will shape the future for numerous radio services. An additional Plenipotentiary Conference of the International Telecommunication Union (ITU) was held in December, 1992 to consider recommendations for a major restructuring and reorganization of the Union.

This paper will touch briefly on these and other events and their implications on the spectrum management community.

E2-2
0920

THE 1992 WORLD ADMINISTRATIVE RADIO CONFERENCE: OUTCOMES AND IMPLICATIONS

David P. Wye, Project Director
Office of Technology Assessment
United States Congress
Washington, DC 20510

In February 1992, the International Telecommunication Union (ITU) held a World Administrative Radio Conference (WARC-92) that reallocated radio frequencies to expand the use of existing radiocommunication services such as mobile telephony and high frequency broadcasting and to permit the development of innovative radio-based technologies and services such as high definition television and digital audio broadcasting. WARC-92, which was the broadest reallocation conference in 12 years, set the rules and regulations governing international, and influencing domestic, radiocommunications well into the next century.

However, the implications of the decisions made at WARC-92 are not yet clear. The conference did not agree on global allocations for several important services, and the footnotes and resolutions associated with the allocations that were made will require years to interpret and negotiate between the countries of the world. In the United States, the allocations made at WARC-92 are now being considered by the FCC and NTIA, and private companies are moving ahead with plans to deploy new systems and services. However, the limitations placed on these new systems at the conference may constrain their ability to deliver services, and the viability of (all) the new systems is still an open question.

This paper is based on a study being conducted by the Office of Technology Assessment in response to requests from the House Committee on Energy and Commerce and the Senate Committee on Commerce, Science, and Transportation. The study is a follow-on to a previous OTA background paper released in November 1992, *The 1992 World Administrative Radio Conference: Issues for U.S. International Spectrum Policy*. That paper looked at the issues to be considered by WARC-92 and the U.S. preparation process for the conference. As subsequently requested, the present assessment will: 1) examine the decisions agreed to at WARC-92; 2) analyze the impacts these decisions could have on the development of domestic radiocommunication policies, technologies, and services; 3) evaluate the outcomes of the conference vis-a-vis the domestic WARC preparation process; and 4) examine possible improvements in the WARC preparation process in light of changes in the structure and timing of future world radio conferences.

E2-3 SPECTRUM SHARING CONSIDERATIONS FOR ULTRAWIDEBAND (UWB) SYSTEMS
0940

David J. Cohen and D. S. Anderson

National Telecommunications and Information Administration
179 Admiral Cochrane Drive
Annapolis, Maryland 21401

Changes in technology have made it possible to manufacture equipments that radiate "ultrawideband" (UWB) short pulses containing a few cycles (1-10) of the carrier. These ultrawideband radiators are proposed for a variety of applications including radar, sensors and Personal Communication Services (PCS). The bandwidths of these systems are quite large ranging up to 10 GHz. Depending upon the application, the power spectrums from ultrawideband systems can easily span over a number of allocated bands. The spectrum management community therefore has considerable interest in predicting the impact on the existing electromagnetic environment of overlaying emissions from ultrawideband devices.

The NTIA, has initiated a ultrawideband (UWB) spectrum sharing study comprising both analyses and measurements. This paper discusses the current findings of this study.

The findings of the NTIA study to be presented include:

(1) The development of an analysis model to assess the electromagnetic compatiblity of ultrawideband devices. The technical analysis indicates that the technical parameters most important for sharing are the peak value, PRF of the ultrawideband emission and the impulse bandwidths of receivers.

(2) The results of a measurement program to gain familiarization with the spectral characteristics of ultrawideband devices and to assess the validity of the analysis model.

(3) An examination of ITU and U.S. Radio Regulations and how they relate to ultrawideband devices.

E2-4
1020

AUTOMATION FOR FREQUENCY MANAGEMENT IN DEVELOPING COUNTRIES - CONSIDERATIONS AND CRITERIA.

John P. Murray
Applied Spectrum Research
2975 Valmont Road, Suite 100
Boulder, CO 80301

Dramatic increases in radio spectrum demand are being felt in developing countries as they are elsewhere, perhaps more so for some services. The well known approaches to planning and administering spectrum efficiently increasingly require automation. They also require some adaptation to meet the needs of individual administrations or special frequency-use groups.

The paper presents basic criteria for planning for the acquisition and use of automated techniques and equipment for frequency management in developing countries. Planning criteria are suggested which consider management, engineering, administrative and operational requirements. Criteria place emphasis on a consideration of the practical resources available to the frequency manager, especially staffing and support.

Emphasis is also placed on the integration of the several aspects of the frequency management process, including long-range planning, day-to-day administrative operations, and radio frequency monitoring.

Requirements for automated techniques are reviewed based on experience with CCIR, frequency management automation applications in developing countries and related applications in the US.

E2-5
1040

DEVELOPMENTS TOWARD LESS FUTURE SPECTRUM CROWDING

Robert J. Matheson
National Telecommunications and Information Administration
Institute for Telecommunication Sciences
Boulder, Colorado 80303

It is common knowledge that the radio spectrum is under continuously-increasing pressure from a growing number of new services that are vying for a fixed amount of spectrum. What is seldom noticed, however, is that there are some powerful factors at work in the opposite direction.

The development of optical fiber has already partially de-populated the microwave bands used by the common carriers. The continued development of fiber may also remove many video signals from the microwave bands, while undersea optical cables compete with international satellites. Digital compression techniques for video and voice are allowing as much as 10:1 improvements in the number of signals carried in a given bandwidth. Not only does this allow high definition TV to be carried in a 6 MHz channel, but it will allow a massive increase in the number of signals to be carried by existing cable and satellites. Although there is almost explosive growth today in the number of transmitters, most of these are very short range, using efficient frequency re-use architectures. For example, 40 million cordless phones successfully share 10 pair of frequencies. Similar efficiencies are possible for PCS, wireless LANS, and many other systems. Finally, there has been a breakthough in the practical use of higher frequencies. In only a few years, the maximum frequency for consumer products has moved from 1 GHz to 18 GHz, thus greatly increasing the amount of highly-usable spectrum.

Frequency management policies that encourage the use of these new technologies may actually result in a decrease in spectrum crowding.

E2-6
1100

THE GENERAL SATELLITE SERVICE-A TOOL FOR SPECTRUM MANAGEMENT IN THE 1990s

J. Kiebler
MITRE Corporation
409 Third St. SW
Suite 300
Washington, DC 20024

D. Olmstead
Hughes Aircraft Co.
Bldg. S64, MS B433
P.O. Box 80002
Los Angeles, CA 90009

M. Sue
Jet Propulsion Laboratory
MS 161-228
4800 Oak Grove Drive
Pasadena, CA 91109

This paper introduces the concept of a General Satellite Service (GSS) as a means to adapt to the rapid introduction of new space applications, to cope with changing markets over the lifetime of a satellite system, and to facilitate implementation of multifunction satellites.

An overview of the Advanced Communications Technology Satellite (ACTS) and the ACTS Mobile Terminal (AMT) is given to illustrate the technology development that is creating pressure to consider fresh approaches to management of the radio spectrum.

With introduction of a GSS, entry into a frequency band would be based on technical compatibility, measured by application of a set of technical standards which are discussed in the paper. A technical description of the GSS is given and the potential benefits that could result from its adoption are reviewed. Factors are explained that make frequencies above 20 GHz particularly favorable for implementation of a GSS that can encompass a mix of mobile, personal, and traditional point-to-point communications services . Sharing and efficient use of the orbit/spectrum resource are important issues to be addressed in connection with the GSS. The results of studies of these topics are presented.

It is concluded that introduction of a General Satellite Service could provide the flexibility needed to keep pace with the rapid changes in satellite communications applications and in markets. Study results show that technical standards can be introduced that preserve efficient use of the orbit/spectrum resource.

E2-7 1120 THE NEW NTIA SPECTRUM MANAGEMENT MEASUREMENT SYSTEM (RSMS): F. Saunders

Session F-3 0835-Thurs. CR2-6
PROPAGATION MEASUREMENTS AND SIMULATION
Chairman: Julius Goldhirsh, Applied Physics Laboratory,
The Johns Hopkins Univ., Laurel, MD 20723-6009

F3-1
0840 **INITIAL ANALYSIS RESULTS FROM THE VIRGINIA TECH OLYMPUS SATELLITE 12, 20, AND 30 GHz PROPAGATION EXPERIMENT**

W.L. Stutzman, T. Pratt, and A. Safaai-Jazi
Satellite Communications Group
Bradley Department of Electrical Engineering
Virginia Polytechnic Institute & State University
Blacksburg, Virginia 24061-0111

Propagation data were collected from August 1990 to August 1992 at Blacksburg, Virginia, from the Olympus satellite at an elevation angle of 14°. Separate earth terminals were constructed and operated at the three spacecraft beacon frequencies of 12.5, 19.77, and 29.66 GHz, plus a fourth portable terminal at 20 GHz. Each frequency has a total power radiometer which shares the antenna and RF sections of the beacon receivers. The radiometers are used to set absolute levels, permitting separation of clear air losses. This paper reports on initial analysis of data.

The experiment is the only one performed in North America to date which simultaneously spans the Ku- and Ka-band frequencies along the same path. This control feature permits direct inference of frequency variation effects of clear air loss, scintillation, and rain attenuation. An especially significant result from the experiment is the scaling of attenuation between frequency pairs. This is possible because of the controlled nature of the measurements with frequency being the only variable between terminals. Results show that average values are close to that predicted in available models and that scaling is relatively stable with little variation during a storm up to about 10 dB of fading.

In addition to statistical studies, the experiment investigated particular applications. One study is the use of the portable terminal in a microdiversity configuration. It was found that baseline separations of 50 m or less will provide improvement for moderate to severe scintillation events, but no improvement for rain. A study on an adaptive uplink power control experiment showed that 20 GHz beacon fade measurements can be scaled to effectively compensate for 30 GHz fading.

F3-2
0900

FADING INTO VEHICLES ON SATELLITE-EARTH PATHS AT L-BAND

W. J. Vogel
G. W. Torrence
The University of Texas at Austin
Austin, Texas 78758
N. Kleiner
Motorola, Inc.
Chandler, Arizona 85249

Personal portable transceivers designed for use in satellite based communication systems may be required to operate inside vehicles. Research was carried out to determine the propagation loss of a line-of-sight satellite signal penetrating into a variety of vehicles. One feature of a low earth orbiting (LEO) satellite based communication system is the continuously changing elevation angle when viewed from the perspective of the portable unit. Thus it is believed important to characterize propagation effects as a function of elevation angle. Elevation angles from 8° to 90° were selected. Three different transceiver antennas (a micro strip patch mounted on a pager unit, and a quadri-filar helix or a stacked loop mounted on a hand set) were used. These were held by a person sitting inside the vehicle in their respective natural orientations; namely at the belt for the pager antenna and between mouth and ear for the hand set. Positions inside the vehicle were those of the driver (alone in the vehicle), and the front and rear passenger (with driver present). Key findings of these measurements are that (1) instantaneous signal amplitudes have a Rayleigh distribution with only a small dependence on elevation angle, vehicle type, or seat position and (2) the 1 s mean signal levels follow a lognormal law. Excess loss due to signal penetration into the vehicle is defined as the difference between the in-vehicle measured value and the outside-vehicle calibration value. Losses over 360° of vehicle rotation are described in percentage categories ranging from the 25th to the 99.9th percentile. At the 90th percentile, typical penetration loss is less than 17 dB between 8° and 73° elevation with either the helix or the loop antenna. For 90° elevation the loss increases to 20 dB. Measurements recorded using the patch antenna reflect different characteristics due to its relatively higher directivity. In this case, the loss at 8° is greatest, 22 dB, decreases to 17 dB at 73° elevation, and then increases to 18.5 dB at 90° elevation.

F3-3
0920

EXPERIMENTAL PERFORMANCE OF SHF COMMUNICATIONS REQUIRING THE USE OF THE EVAPORATION DUCT

L. Ted Rogers and Kenneth D. Anderson
Naval Command, Control and Ocean Surveillance Center
RDT&E Division
Code 543
San Diego, CA 92152

Results from an experiment to evaluate the performance of an over-water, over-the-horizon, SHF digital communication system are presented. Two simplex microwave digital communication circuits (similar to commercial line-of-sight microwave links) are used on an 83 km transmission path that is twice the line-of-sight distance. One circuit is operating at 7.5 GHz. The other circuit operates at 14.5 GHz. Both transmitters output a quasi-random bit stream at 1.544 mega-bits per second (DS-1) that is analyzed at the receiver site.

In a standard atmosphere, the expected received signal level (RSL) is approximately 60 dB below the receiver noise threshold. However, at these frequencies, propagation modeling shows that, more than half of the time, trapping by the evaporation duct can increase RSL by at least 60 dB. At 7.5 GHz, we expect nearly error free communications approximately 63 percent of the time. At 14.5 GHz, we expect successful communications approximately 78 percent of the time.

The propagation path is instrumented at both ends to record surface meteorological conditions and RF characteristics. RSL measurements are compared to predicted levels which are derived from the measured surface meteorology. Percent Error Free Seconds (%EFS), Bit Error Rate (BER) and other industry standard parameters are measures to assess the effect of RSL variation on link performance. Additionally, results from high-speed sampling of RSL are made to assist in channel characterization.

F3-4
0940

MEASUREMENT OF SPECULAR AND DIFFUSE MULTIPATH REFLECTION COEFFICIENTS OF TERRAIN AT MILLIMETER WAVELENGTHS

Ram M. Narayanan*, Daniel D. Cox* & James M. Ralston**
*Dept. of Electrical Engineering/Center for Electro-Optics
University of Nebraska, Lincoln, NE 68588
**Institute for Defense Analyses, 1801 N. Beauregard St.
Alexandria, VA 22311

Multipath data were obtained at a frequency of 95 GHz over pathlengths of 250 to 500 m by measuring height-gain interference patterns over various types of terrain. The transmit antenna was kept fixed at 1.0 m height, while the receive antenna translated over a range of heights between 0.5 and 4.0 m. The grazing angles for this geometry varied between approximately 0.2 and 1.0 degrees. The transmitter consisted of a fixed-tuned Gunn oscillator operating at 95 GHz with a power output of 40 mW, while the receiver front-end consisted of a 13 dB noise figure balanced mixer pumped by another fixed-tuned Gunn oscillator at 85 GHz. The 10 GHz IF was further downconverted to 60 MHz, and amplified in a narrow 10 MHz bandwidth pre-amplifier prior to detection. The transmit and receive antennas were standard gain horns of 21 dB gain and 17 degree beamwidth. The broad antenna beamwidth ensured full illumination of the Fresnel zones on the ground. The interference pattern was sampled every 0.7 mm as the receiver was translating vertically.

Measured interference patterns indicate the presence of both specular as well as diffuse multipath components in the received signal. Our analysis indicates that these components can be separated by filtering in the spatial Fourier transform domain by appropriate choice of the cut-off frequency. The cut-off frequency, i.e, the spatial frequency at which the separation is performed, is chosen such that the resultant specular component decorrelates in accordance with the system geometry considerations, while simultaneously ensuring that the diffuse component has a very small decorrelation distance, typically of the order of a wavelength (3.16 mm in our case). Using this separation technique, specular and diffuse multipath reflection coefficients can be deduced for various terrain conditions.

F3-5
1020

SIMULATED DIVERSITY SYSTEMS ON MICROWAVE LINE-OF-SIGHT LINKS

Alan R. Webster,
Department of Electrical Engineering,
The University of Western Ontario,
London ONT. N6A 5B9
CANADA.

Simulated results are presented for various optional diversity systems using combinations of antennas employing both space and angle diversity. The data base used in the simulation has been accumulated over a number of years on three separate microwave links in Ontario. The system employed uses 16 antenna elements, arranged vertically and equally spaced, to cover an aperture of about 660 wavelengths at the operating frequency of 16.5 GHz. The complex amplitude across this array is measured at a rate of one complete set per second, and such data are available on a more or less continuous basis for the fading season. Some preliminary results were presented earlier (A. R. Webster, URSI/N. Amer. Rad. Sc. Mtng, p.447, 1991) and the results of expanded analysis are presented here.

An initial estimate of space diversity effectiveness is directly available from the amplitude measurements and these indicate that two relatively broad beam antennas attain maximum diversity quite rapidly as the vertical separation between them is increased, with little further improvement thereafter.

Angle diversity is also readily simulated by Fourier transforming the array complex amplitude and the results from the use of antennas of different beam-width and pointing angle, combined also with simultaneous space diversity, are presented. Significant gains in overall performance are indicated.

F3-6
1040

SPACE DIVERSITY AND FADE DURATION STATISTICS AT C-BAND FOR OVER-WATER LINE-OF-SIGHT LINKS

Julius Goldhirsh, G. Daniel Dockery, Bert H. Musiani
The Johns Hopkins University, Applied Physics Laboratory
Johns Hopkins Road, Laurel, Maryland 20723-6099

Space diversity and fade duration statistics are characterized for two over-water, line-of-sight, propagation links operating at 4.7 GHz in the Mid-Atlantic coast of the United States. The links consist of a transmitter radiating a CW signal simultaneously to two receiver sites located at distances of 39 km (Lookout Tower) and 44 km (Lighthouse). The receiver antennas are at widely different heights of 13.7 m and 45.5 m, respectively, and are displaced 5.5 km from one another. Annual and monthly fade statistics have been reported by the authors for the year period June 1, 1989 through May 31, 1990 (J. Goldhirsh, G. D. Dockery, B. H. Musiani, Radio Sci. (in press)). In this paper we report on monthly and annual single and joint probability "fade" and "fade duration" distributions derived from simultaneously acquired time-series of attenuations measured at both receiver sites. The distributions were heavily biased by the presence of "Sustained Deep Fade" (SDF) events which were arbitrarily defined as fades which exceeded 20 dB relative to free space conditions for periods of two hours or more. They are believed to be generally caused by warm, moist air flowing at altitude over cold water causing extreme subrefractive conditions. Such mesoscale events have been associated with Bermuda highs. The major results were as follows: (1) Annual diversity gains derived from the single and joint distributions showed highest levels at 3.5 dB and 10.8 dB at the 10% level relative to the Lighthouse (higher receiver site) and Lookout Tower, respectively. The proximity of the joint and Lighthouse distributions implied that on an annual basis, the Lighthouse is the better link, receiving generally the larger signals. (2) The monthly joint probabilities were far removed from the Lighthouse distributions during the months July–October (warmer water) and were near coincident with these distributions during November–June (colder water). The statistics during the latter monthly interval were dominated by SDF events. (3) The annual fade duration statistics are dominated by SDF events which result in the joint distribution nearly coinciding with the Lighthouse case and negligible probability changes in the fade durations over the first 120 seconds. (4) During the months July–October, large changes in the fade duration probabilities occurred over the first 120 seconds. Small changes in fade duration probabilities occurred during the months November–June because of the prominence of SDF events.

F3-7
1100

MODULATED MULTIPATH PROPAGATION EFFECTS FOR PERSONAL COMMUNICATION IN THE OFFICE ENVIRONMENT

W. J. Vogel
H. Ling
G. W. Torrence
Electrical Engineering Research Laboratory
The University of Texas at Austin
10100 Burnet Road
Austin, Texas 78758-4445

Currently, personal communication systems operating at a frequency near 1 GHz are being designed for use inside office buildings. The propagation environment in such spaces is usually defined by head-high attenuating partitions, an abundance of multipath scatterers, and a relatively unobstructed ceiling. Most office ceilings consist of suspended arrays of sound absorbing tiles and fluorescent lights. Considering the potential blockage of the direct line-of-sight path, communication links are often established via an attenuated direct path and a few indirect paths.

When a dominant multipath component at the receiver derives from a reflection off a metallic fluorescent light fixture, its effective path is length-modulated by the plasma-like column inside the fluorescent tube. Measurements will be presented which demonstrate that, under the right circumstances, deep line-frequency synchronized fading can be observed.

A simple model is constructed to explain the observed 120 Hz modulation on the received signal when the fluorescent lights in a room are turned on. The gas discharge in a fluorescent light bulb can be considered a plasma which is turned on and off at a frequency of 120 Hz. Assuming that the frequency of the transmitter is well below the plasma frequency of the bulb, the bulb will be perfectly reflecting to the transmitter signal during the on-cycle of the lamp and perfectly transparent during the off-cycle. Consequently, the phase of the received multipath signal changes at a rate of 120 Hz. When combined with the direct and other multipath contributions in the indoor environment, this results in a 120 Hz modulation of the received signal.

F3-8
1120

POLARIZED TRANSMISSION AND EMISSION IN THE MIDDLE ATMOSPHERE (25 - 150 km) NEAR THE ZEEMAN-SPLIT MICROWAVE O_2 LINES

Hans J. Liebe, George A. Hufford, and Michael Cotton
Institute for Telecommunication Sciences
National Telecommunications and Information Administration
325 Broadway, Boulder, CO 80303-3328, U.S.A.

Gaseous atmospheric attenuation and delay properties in the 50 to 75-GHz band and near 119 GHz are dominated by the fine structure lines of molecular oxygen. With increasing altitude the complex refractivity displays spectral patterns which change from an unstructured band to the isolated shapes of about 35 lines. The earth's magnetic field (22 - 65 μTesla) splits each line into many sublines. The anisotropic nature of these Zeeman components causes polarization discrimination and Faraday rotation.

The "Zeeman-effect" Propagation Model ZPM estimates the path transmission and emission that originates between 25 and 150 km near isolated O_2 lines. Many aspects of how polarized, plane radio waves propagate through a spherically stratified model atmosphere are evaluated (i.e., complex refractivity tensor, path-specific attenuation rates, Faraday rotation, polarization, and optical depth). Related to the absorptive line properties is thermal emission. The example below shows emission near the 61.150-GHz line frequency, as seen by a linearly polarized (HL/VL) pencil-beam antenna looking from outer space into the atmosphere to minimum heights of 65 and 90 km above sea level at either the equator or the north pole. Radiometers of limb-sounding experiments conducted from space platforms (e.g., UARS-MLS and ATLAS-MAS) are able to detect such emissions features, which reveal information on O_2 density, ambient temperature, and pressure.

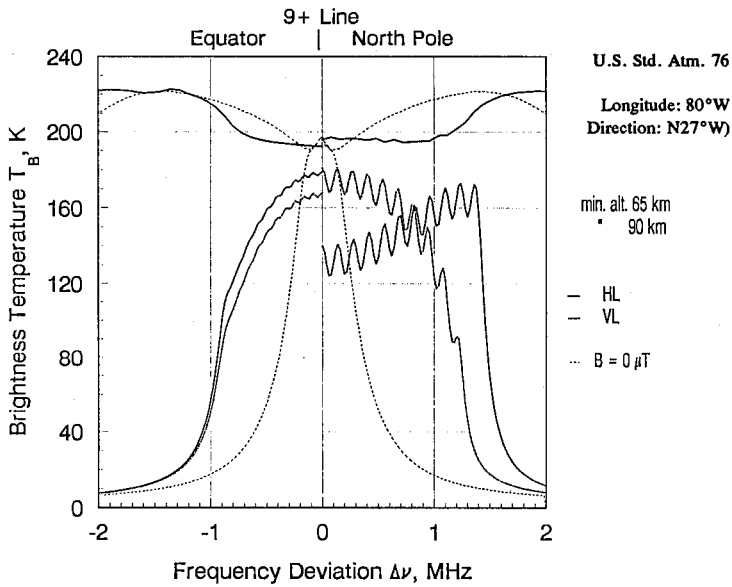

F3-9
1140

Laboratory Measurements of Water Gravity Wave Characteristics Using Full Polarization Microwave Radiometry

D.B. Kunkee, A.J. Gasiewski
School of Electrical Engineering
Georgia Institute of Technology
Atlanta GA, 30332-0250

To demonstrate the usefulness of the full Stokes vector (T_v, T_h, $T_U = 2Re\langle E_v E_h^* \rangle$ and $T_V = 2Im\langle E_v E_h^* \rangle$) in determining the characteristics (i.e. direction) of ocean waves from satellite-based passive observations, radiometric emissions from a striated water surface under clear air background conditions were observed at 92 GHz. A Dicke-switched dual-polarized radiometer with additional circuitry to provide estimates of the four Stokes parameters (A.J. Gasiewski and D.B. Kunkee, "Calibration and Applications of Polarization Correlating Radiometers", accepted for publication in *IEEE Trans. Microwave Theory Tech* July, 1992) was used to obtain calibrated full polarimetric measurements over the entire range of water wave azimuthal angles ϕ_s. The measurements were compared to theoretical calculations based on the Kirchoff approximation (KA) for a sinusoidal surface. The KA models the surface as a distribution of specularly reflecting facets, each of which contributes to the total observed radiation in accordance with the Fresnel reflectivity relations.

For sinusoidal water waves of $h/\Lambda = 0.05$ (where h is the peak amplitude and Λ is the water wavelength), the measured T_U amplitude is approximately $\pm 10^\circ K$ over $0^\circ \leq \phi_s \leq 360^\circ$ at an observation angle of $\theta_s = 65^\circ$ (see figure). The peak-to-peak variation of T_U is comparable to the measured variations of T_v and T_h. For near-nadir observations the T_U response decreases, but could be significant for some remote sensing applications. The wave tank measurements suggest that ocean wave direction will be observable (modulo 180°) using T_v, T_h, and T_U.

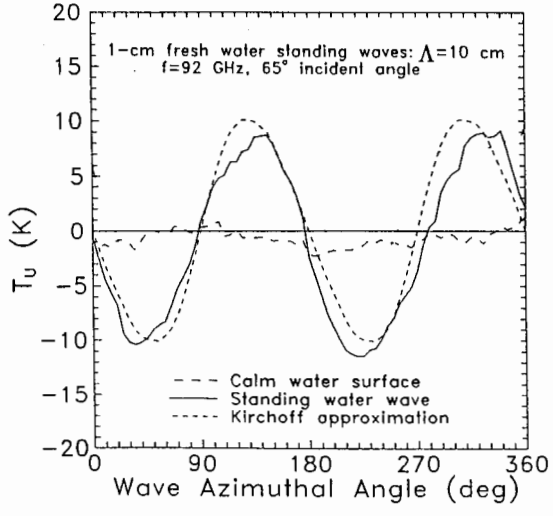

Session G-3 0855-Thurs. CR0-30
LOW AND MID-LATITUDE PHENOMENA
Chairman: David Anderson, Ionospheric Effects Division,
Phillips Laboratory, Hanscom AFB, MA 01731-5000

G3-1
0900 COMPARISON BETWEEN CALCULATED AND OBSERVED F-REGION ELECTRON DENSITY PROFILES AT JICAMARCA, PERU

Amanda P. Creamer
Phillips Laboratory/Staff Meteorology
Kirtland Air Force Base, NM 87117-6008
Patricia H. Doherty
Institute for Space Research
Boston College
Newton, Massachusetts
Bela G. Fejer
Center for Atmospheric Space Sciences
Utah State University
Logan, Utah
David N. Anderson
Ionospheric Effects Division
Phillips Laboratory
Hanscom Air Force Base, Massachusetts

Electron density profiles and isodensity contours derived from Jicamarca incoherent scatter radar observations in Peru (1 degree N dip latitude) for 30 Sep to 3 Oct 1970 are compared with results from the Anderson time-dependent ionospheric specification model. The parameterized physical model solves the ion continuity equation for O^+ concentration through production, loss, and transport of ionization. A primary factor controlling the peak plasma density at Jicamarca is the vertical **ExB** drift which drives the ionization upward during the day and downward at night. The **ExB** drift in the model was varied to represent conditions of no vertical drift, a climatological equinoctial vertical drift, the actual drifts recorded for the observation days, and 50% of the actual drift for these days. The comparisons will illustrate the sensitivity of the low latitude plasma density calculations to changes in the vertical **ExB** drift for magnetically quiet, solar moderate equinoctial conditions at the magnetic equator. We also show the agreement between the model and the data for the various drifts with emphasis on the agreement between the data and the model profiles when the actual drift is used in the model calculations.

G3-2
0920

TIDAL EFFECTS ON THE LOW LATITUDE IONOSPHERE

C G Fesen
Thayer School of Engineering
Dartmouth College
Hanover, NH 03755

Tidal effects on the ionosphere are investigated with the National Center for Atmospheric Research thermosphere-ionosphere general circulation model (TIGCM). The model incorporates predictions from the lower atmosphere model of Forbes and Vial to parameterize the waves originating in the lower atmosphere which penetrate the thermosphere. To isolate the effects of these upward propagating tides on the ionospheric structure, model simulations were made which included and which omitted the contribution from the tidal waves generated in the lower atmosphere. Emphasis is on the possible tidal influence on the model simulations of the peak electron density n_{max} and the height of the peak h_{max}. The results indicate that the tides do affect the simulated n_{max} and h_{max}. The response is typically largest in the afternoon and evening hours and at low latitudes. The effect is apparently due to tidal perturbations on the horizontal neutral winds.

G3-3
0940

IONOSPHERIC ROCKET TOMOGRAPHY TO RECONSTRUCT EQUATORIAL IRREGULARITIES FROM MEASUREMENTS OF TOTAL ELECTRON CONTENT

P.A. Bernhardt, J.D. Huba and P.K. Chaturvedi
Space Plasma Branch
Code 6780, Plasma Physics Division
Naval Research Laboratory
Washington, DC 20375-5000

A technique is described to obtain ionospheric electron densities from transionospheric, rocket-beacon total electron content (TEC) data. When the line-of-sight from a ground receiver to the rocket beacon is tangent to the flight trajectory, the electron concentration at the rocket can be obtained by differentiating the TEC with respect to the rocket distance. A similar method may be used to obtain the electron density profile if the layer is horizontally stratified. In a structured, time stationary ionosphere, computerized tomography (CT) can be used to analyze TEC data obtained along a chain of ground-based receivers aligned with the plane of the rocket trajectory. CT analysis of TEC data is used to reconstruct a tow-dimensional image of a simulated equatorial plume. With TEC data from nine receivers with spacings ranging from 100 to 200 km, we obtain an F-region reconstruction having spatial accuracy of 15 km. Ionospheric rocket tomography (IRT) may also be applied to rocket assisted measurements of amplitude and phase scintillations and airglow intensities.

G3-4
1000

DIRECTION FINDING IONOGRAMS OBTAINED ON MID LATITUDE PATHS

Q. R. Black, J. F. Wood, Jr., and W. M. Sherrill
Southwest Research Institute
6220 Culebra Road
P.O. Drawer 28510
San Antonio, Texas 78228-0510

A direction finding ionosonde consisting of an interferometer using 7-element, 50 and 150 meter crossed baselines, has been developed to provide group path delay, azimuth, and elevation of each resolved mode over the sounding frequency range. DF ionograms have been acquired automatically, using various non-cooperative compatible sounder transmissions.

Diurnal sequences of DF ionograms were obtained for mid-latitude paths at nominal ranges of 1000, 2000 and 3000 km. Data measured to characterize the DF properties of each path include group delay, azimuth, and elevation vs frequency, as well as an AZ/EL scatter plot showing the distribution of angular occupancy for the path. The results show modes arriving closest to the great circle bearing (i.e., with lowest azimuth error) arrive via the lowest elevation angles and with least group delay. Fractional degree per MHz linear and quasi sinusoidal azimuth gradients with frequency were observed at various times of day. One hop F region high rays showed smoothly varying elevation as a function of frequency, increasing with group path delay as expected. Variable lateral deviation from the great circle plane was observed for high rays up to 5 degrees in azimuth equatorward at various times of day.

G3-5
1040

PLASMA FREQUENCY PROFILES IN THE F_1 REGION

Leo F McNamara[1] and Bodo W Reinsich[2]
[1]ANDREW SciComm Inc, 2916 National Drive, Garland, Tx 75041
[2]University of Massachusetts Lowell, Center for Atmospheric Research, 450 Aiken St, Ma 01854

Empirical models of the F_1 region are generally regarded as inadequate, even at mid latitudes. Models which appear as components of programs for the prediction of HF propagation support by the ionosphere are very crude, and virtually undocumented. In some applications, these limitations of the F_1 models are not a major concern, since the effects of the F_1 ionogram cusp or ledge in the profile are minimal. However in applications such as the Single Station Location of remote HF transmitters, the F_1 layer assumes a greater importance, and requires more accurate models.

Plasma frequency profiles derived automatically from Digisonde observations at Millstone Hill are therefore being analyzed with a view to providing more reliable models of the mid-latitude F_1 region. Observations of variations of f_oF_1, h_mF_1 and y_mF_1 will be presented, and compared with current models.

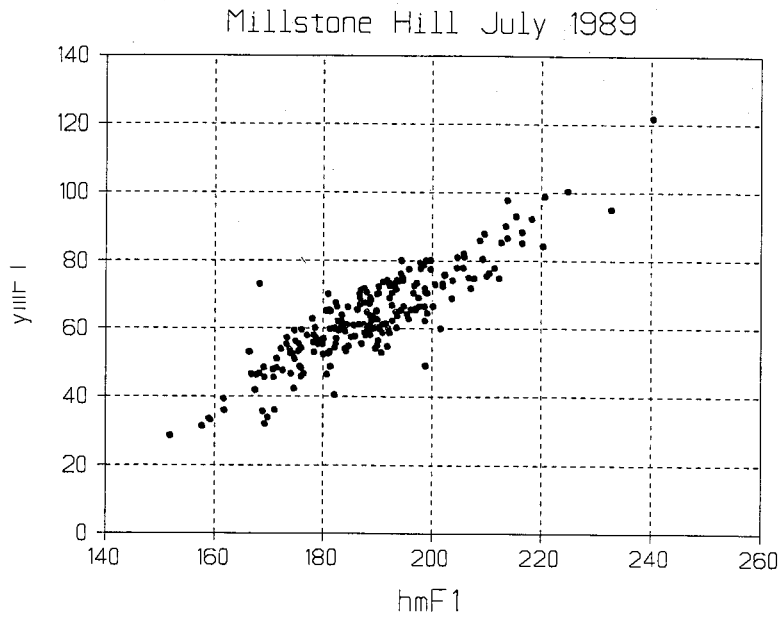

G3-6
1100

CHAOTIC IONOSONDE ECHOES REVEAL NEUTRAL AND PLASMA INSTABILITIES

J.W. Wright, 1915 Spruce Ave. Longmont, CO 80501;

In quiet conditions most ionogram echoes demonstrably occur by total internal reflection at critical plasma-density contours; this is attested by their high amplitude and by temporal stability and broad radio bandwidth for the characteristic Doppler, echolocation and polarization echo parameters. The continuous 'traces' on ionograms, comprised of such echoes, describe the bottomside structuring of the ionosphere in considerable detail. Lateral structures of large scale (defined as scales comparable to and exceeding the reflection height) are likewise quantified without ambiguity by the multiparameter diagnostics of fully-configured digital ionosondes.

There are, however, other classes of echoes best described as more or less chaotic in the parameters mentioned above. Some of these (e.g. 'Spread F' and 'Sporadic E') are well recognized indicators of specific neutral- and plasma-dynamic processes. In this paper I call attention to another class of chaotic echoes which has been neglected heretofore; it occurs from the E-region and seems clearly identifiable with neutral instabilities in mid-latitude examples and with plasma instabilities at auroral latitudes. Valuable diagnostic opportunities are therefore promised by these echoes, but it is important to determine the irregularity scales and intensities responsible for them. Some ambiguity arises in attempting to decide between total reflection and Bragg scatter for these echoes; an equatorial-electrojet example of the latter is described for perspective on this question.

G3-7
1120

ON THE DETAILED STRUCTURE OF IONOSONDE ECHOES: A NEW DIAGNOSTIC HORIZON

J.W. Wright, 1915 Spruce Ave. Longmont, CO 80501; and M.L.V. Pitteway, Dept. Computer Science Brunel University, Uxbridge UB8 3PH, UK.

We describe the basis and motivation for a development yielding a ten- to fifty-fold improvement in the precision with which echo phase-dependent parameters (mainly 3-dimensional echolocation and Doppler) can be determined by digital ionosondes. Improved resolution is achieved of the medium-scale irregularities which cause overlapped and therefore interfering contributions to measured echo waveforms. The work also provides the basis for an improved phase-dependent method of impulsive noise rejection and echo recognition, with (as a side benefit) the availability of echo physical parameters in real time.

The approach extends, and is dependent on, the use of "pulse sets" in the dynasonde, as described in various recent publications by the authors. We do not depend on conventional amplitude thresholding or other envelope characterizations for echo recognition on a pulse-to-pulse basis. Instead, we employ phase information throughout the envelope and among the members of a small set of pulses (closely spaced in time, frequency, receiving-antenna location and orientation) to define individual ionospheric 'glints' as echoes. A phase residual EP serves to quantify the success of this process and to assign confidence limits on each parameter. EP is typically 5° to 15° near the peak amplitude of the usual ionosonde echo, composed of several overlapping glints; for an individual glint resolved by our approach, EP may be reduced to a few times 0.1°.

J2-1
0840

THE FUNDAMENTAL CELESTIAL REFERENCE FRAME DERIVED FROM VLBI

Chopo Ma, NASA Goddard Space Flight Center
David B. Shaffer, Interferometrics Inc.
Jane L. Russell, Naval Research Laboratory

The goal of the astrometric VLBI effort of NASA, NRL, USNO and other cooperating organizations is to establish the fundamental celestial reference frame using ~400 extragalactic radio sources with positions accurate to better than 1 milliarcsecond. The majority of the sources are quasars with identified optical counterparts. The ~110 core sources of the catalog are those used regularly in the VLBI programs for geodynamics and Earth orientation, which began dual frequency Mark III VLBI observations in 1979. The remaining sources have been observed primarily in sessions devoted to astrometry, which constitute less than 5% of the total observations. While the reference frame sources are distributed uniformly on the sky, the southernmost sources have significantly fewer observations than the more northerly sources. Modification of the standard IAU precession/nutation model is necessary for best catalog accuracy. Tropospheric propagation and source structure are probably the chief sources of error. The orientation of the frame axes is arbitrary, and several choices will be discussed.

J2-2
0900

THE RADIO/OPTICAL REFERENCE FRAME LINK

J. L. Russell (ARC/NRL)
K. J. Johnston, A. L. Fey (NRL)
C. de Vegt, N. Zacharias (Hamburger Sternwarte)
C. Ma (NASA)
D. L. Jauncey, J. E. Reynolds (ATNF)
D. B. Shaffer (Interferometrics, Inc)
G. Nicolson, A. Kemball, G. MacLeod (HartRAO)
N. Kawaguchi, Y. Takahashi (CRL)
E. A. King, P. M. McCulloch (Univ. Tasmania)
D. F. Malin (Anglo-Australian Observatory)
G. L. White (Univ. of Western Sydney, Nepean)

In 1987 we began a program to establish a global radio reference frame of about 400 compact and flat spectrum radio sources with optical counterparts. So far, with the cooperation of the NASA, USNO and NOAA groups, as well as that of astronomers from South Africa, Australia and Japan, we have attempted observations of about 450 sources using Mark III VLBI. We now have compiled a preliminary list of 400 sources, forming a radio reference frame which provides a nearly uniform global distribution, with the most sparse coverage in the galactic plane. This cooperative effort has allowed the formation of a radio reference frame which has pole to pole coverage, although the southern sources have fewer observations per source than those in the north.

One of our goals is linking the radio and the optical reference frames. A parallel observing and data reduction effort is continuing to obtain positions of the optical counterparts of the radio sources, based on astrometric measurements from photographic plates. So far we have published about 50 optical positions; plate measuring is in progress to provide positions for an additional 200.

J2-3
0920

High-Accuracy Astrometry of Weak Radio-Emitting Stars by Phase-Referenced VLBI Observations

J.-F. Lestrade, Observatoire de Meudon and JPL
R.B. Phillips, Haystack Observatory/MIT
D.J. Jones, Jet Propulsion Laboratory/Caltech
R. A. Preston, Jet Propulsion Laboratory/Caltech

We are conducting astrometric VLBI observations of radio emitting stars to link the Hipparcos optical frame to the stable radio VLBI celestial frame at the milliarcsecond level. The flux densities of radio-emitting stars are in the milliJansky range which is very weak by VLBI standards. But the technique of phase-referencing can enhance the sensitivity of a VLBI array, and allow the use of phase, which is the most accurate observable for high-accuracy astrometry.

We shall report on recent results demonstrating that submilliarcsecond astrometry over several years is achieved by this technique for radio-emitting stars as weak as 2 milliJanskies. We shall discuss the astronimcal applications of these high-accuracy positions, proper motions and trigonometric parallaxes measured during a long-term program. Applications envisioned so far are for the Hipparcos link, the distance scale in the Galaxy, detection of deflecting unseen mass and detection of planets around radioluminous stars.

J2-4
0940

ASTROMETRY WITH OPTICAL INTERFEROMETERS

C.A. Hummel, A. Quirrenbach, D.F. Buscher
NRL/USNO Optical Interferometry Project
University Space Research Associates
R.S. Simon, D. Mozurkewich, K.J. Johnston
Remote Sensing Division
Naval Research Laboratory
D.J. Hutter, N.M. Elias
Astrometry Department
United States Naval Observatory
J.T. Armstrong
NRL/USNO Optical Interferometry Project
Sachs Freeman Associates, Inc.

We report five years of measurements of stellar positions in a selected field of the FK5 catalog with an accuracy of about 10 mas in declination and 20 mas in Right Ascension. We used the north-south and east-south astrometric baselines of the MK3 Optical Interferometer on Mt. Wilson, each about 12 meters in length. The MK3 measures and compensates the geometrical delay, which is proportional to the dot-product of the source-vector and the baseline-vector, and tracks the stellar interference pattern using piezo-electrically activated mirrors in LASER-controlled optical delay lines. Drifts of the baseline length due to temperature variations were measured and compensated for by monitoring the delay of an artificially produced white light interference pattern. A method using three different observing wavebands in order to overcome turbulent spectral index fluctuations in the
atmosphere was also employed.

The Naval Research Laboratory and the US Naval Observatory have started to build a new Astrometric Optical Interferometer on Anderson Mesa, Arizona (part of the Navy Prototype Optical Interferometer at Lowell Observatory). Four siderostats will be located in a Y-shaped configuration, with one element in the array center and three arms each 20 meters in length. This instrument will feature a real-time zeroth-order fringe tracking algorithm, a full-array LASER metrology system and a limiting magnitude of 10. With it, we will be able to maintain the HIPPARCOS reference frame with matching accuracy over the next few decades.

J2-5
1020

VLBI MEASUREMENT OF SOLAR GRAVITATIONAL BENDING OF RADIO WAVES

B.E. Corey
Haystack Observatory
Westford, MA 01886
J.L. Davis, D.E. Lebach, M.I. Ratner, and I.I. Shapiro
Harvard-Smithsonian Center for Astrophysics
Cambridge, MA 02138

We have measured the deflection of radio waves by the solar gravitational field to an accuracy of 0.1 percent (standard error) by means of very long baseline interferometry (VLBI) on a transcontinental baseline.

In October 1987 we used two antennas at the Owens Valley Radio Observatory, Big Pine, CA, and two at the Haystack Observatory, Westford, MA, to observe the quasars 3C273B and 3C279 at 2, 8, and 22 GHz during an 11-day period spanning the solar occultation of 3C279. On days when 3C279 was more than one degree from the sun, the antennas alternated between the sources, which are 10 degrees apart, with an 8-minute cycle time. Phase calibration equipment measured changes in the instrumental phases and delays between the receivers and the MkIII VLBI recording terminals. Water vapor radiometers, solar hygrometers, and standard meteorological sensors were employed at each site.

Cross-correlation yielded group-delay estimates for the separate frequency bands, from which we estimated group delays free of the dispersive effects of plasma. Constraints on the non-dispersive atmospheric delay were inferred from the atmospheric data, and constraints on earth orientiation parameters were estimated by interpolating from measurements on operational geodetic VLBI networks. These delays and constraints are being analyzed with a Kalman-filter program to estimate the Parameterized Post-Newtonian parameter γ. We will present our results and discuss the limiting error sources.

J2-6 1040

PROPER MOTION OF SGRA*

D. C. Backer
Astronomy Department
601 Campbell Hall
University of California
Berkeley, CA 94720

and

R. A. Sramek
National Radio Astronomy Observatory
Array Operations Center
Socorro, NM 87801

A proper motion of the compact, nonthermal radio source in the galactic center, known as SgrA*, has been determined with differential astrometric observations at 6cm on the NRAO VLA, 1981-89. The technique involves sequential observations of SgrA* and three reference, presumably extragalactic sources spread in a triangle around SgrA*, and spaced by about 0.7° with a time cycle of two reference sources and one SgrA* observation in 10 minutes. The data are phase calibrated hourly with observations of 1748-253. The dominant effect in the phase calibrated data is slow tropospheric refraction of SgrA* and the three reference sources with an amplitude of 0.1″ and a time scale of one hour. Some observations are corrupted by much stronger tropospheric turbulence.

We determine a premlimary (to final publication) proper motion $(\mu_\alpha, \mu_\delta) = (-3.25 \pm 0.50, -5.50 \pm 0.80)$ mas y^{-1}. These can be rotated into galactic coordinates (by PA 31.53°) to $(\mu_l, \mu_b) = (-6.39 \pm 0.74, -0.11 \pm 0.60)$ mas y^{-1}. The errors here represent firm upper limits to the uncertainty in the measurements obtained by altering the weighting of reference sources and data differently. An object at rest in the galactic center would have a proper motion, formally a secular parallax, in galactic coordinates of $(-(A-B) - Y_\odot/R_o, -Z_\odot/R_o)$ where the standard nomenclature for Oort's constants and solar peculiar motion and distance are used. Evaluation yields (-220 km s^{-1} / 8.5 kpc -15.3 km s^{-1}/8.5 kpc, -7.4 km s^{-1}/8.5 kpc) = (-5.84,-0.18) mas y^{-1}. The distance to the galactic center has been determined by statistical parallax of H_2O masers as 7.6 ± 0.6 kpc (Moran, Reid, & Gwinn, 1992 Maser Conference). Use of this value results in a predicted secular parallax of (-6.53,-0.20) mas y^{-1}.

We conclude that the peculiar velocity of SgrA* is no larger than our uncertainties in both coordinates, (27,22) km s^{-1} at 7.6 kpc. If SgrA* has the same kinetic energy as the 10 $M_\odot$ objects buzzing around in the center with radial velocity components of 100 km s^{-1}, then we can infer that the mass of SgrA* exceeds 160 $M_\odot$. Given that this source is smaller than 10 AU in diameter, we surmise that SgrA* contains a massive black hole.

J2-7
1100

VLBI MASER PROPER MOTION STUDIES AND DISTANCE DETERMINATIONS

Karl M. Menten
Harvard-Smithsonian Center for Astrophysics
60 Garden Street/MS 42
Cambridge, MA 02138

Multi-epoch VLBI observations of astrophysical masers have led to proper motion determinations for a number of these sources. In the past, most such measurements were made for water vapor (H_2O) masers, which arise in high velocity molecular outflows emanating from newly formed stars. Distances to these masers can be determined either by modeling the source kinematics with the observed proper motions, radial velocities, and positional information as input parameters or by using the method of statistical parallax. Maser proper motion parallaxes have been used to measure the distance to the Galactic Center. Currently, studies targeted at H_2O masers in external galaxies are under way that will result in an independent determination of the extragalactic distance scale.

We shall review the existing proper motion measurements, report on work in progress, and examine future developments. In particular, the potential of the recently detected very strong and widespread interstellar methanol (CH_3OH) masers for studies of galactic kinematics will be discussed.

J2-8
1120

ASTROMETRY FOR SPACECRAFT TRACKING

Robert N. Treuhaft
Jet Propulsion Laboratory, MS 238-700
California Institute of Technology
4800 Oak Grove Drive
Pasadena, California 91109

This paper will review techniques for the astrometric tracking of spacecraft at radio, infrared, and optical frequencies. Astrometric tracking involves the development of observation strategies to locate objects in reference frames of radio sources, stars, or planets. For radio tracking, very long baseline interferometry observation strategies will be described which were used on the Deep Space Network to measure the gravitational deflection of a natural radio source by Jupiter with 200-microarcsecond (μas) accuracy. These observation strategies, with minor conceptual modifications, are the same as those which would be applied to a spacecraft target. Spacecraft astrometry is characterized by short (~1 hour) passes which are designed to differentially cancel measurement errors. Atmospheric refractivity fluctuations were treated stochastically and were the dominant error in the final results. Calibration strategies for future 20-μas measurements will be discussed.

Infrared interferometry is being considered as a potential technique for supporting spacecraft tracking, if laser-based telemetry replaces radio telemetry in the next 10-20 years. Infrared reference frames as well as spacecraft observation strategies will be developed. Presently, astrometric measurements are being made on the U.C. Berkeley Infrared Spatial Interferometer on Mt. Wilson. The current performance of the interferometer, which is limited by both atmospheric fluctuations and system noise, will be illustrated with data taken in October 1992. The immediate ground-based astrometric accuracy goal is 10 milliarcseconds.

Optical astrometry is also being considered as a technique for future spacecraft tracking. Narrow-field (~1 degree), filled-aperture astrometry experiments on the U.C. San Diego Ronchi telescope at Table Mountain will be described. The Ronchi technique, which involves subdividing the focal plane of an optical telescope in order to achieve few-milliarcsecond accuracy, is another candidate technology for future spacecraft astrometry. The application of the Ronchi technique to apparently faint (~11^{th} magnitude) laser-carrying spacecraft at outer planets will be discussed. Recent Ronchi phase data acquired with the Table Mountain telescope will be shown to demonstrate the dominant astrometric errors, which, for this device as well, are atmospheric fluctuations and system noise.

J2-9 PRECISION OPTICAL INTERFEROMETER IN SPACE (POINTS)
1140 James D. Phillips, Robert W. Babcock, John F. Chandler, M. Charles Noecker, and Robert D. Reasenberg
Smithsonian Astrophysical Observatory
Harvard-Smithsonian Center for Astrophysics, MS 63
60 Garden St., Cambridge, MA 02138

POINTS is a proposed spaceborne astrometric interferometer with 5 microarcsec (μas) accuracy for a single 1½ minute measurement on a pair of m=10 stars, a 1000-fold improvement over currently available accuracy. It comprises two Michelson stellar interferometers with 25 cm subapertures and 2 m baselines, observing targets separated by 90°+Δ, where $|\Delta| \leq 3°$. Several measurements at the nominal accuracy on a target at 1 kpc would yield distances accurate to 2.5 pc, and proper motions to 0.6 μas/yr (3 m/sec).

Applications include (a) a distance scale based on direct parallax determinations for a large number of Cepheids; (b) a thorough search for planets around other stars sensitive to an astrometric signature 1/100 that of Jupiter at a distance of 10 pc; (c) a determination of the masses of stars in binary systems and those close enough to apply the method of perspective acceleration; (d) parallax measurements yielding both absolute stellar magnitudes and, in conjunction with mass estimates and other data, a sharpened mass-color-luminosity relation; (e) a vastly improved global reference frame and a tie to existing ones; (f) the study of the mass distribution in the Galaxy; (g) a strictly geometric (*i.e.*, coordinate and parallax) determination of the membership of star clusters; (h) a bound on or a measurement of quasar proper motions; (i) solar-system studies; (j) proper motion of Rigel, the guide star for the Gravity Probe-B experiment; (k) the evolution of interacting binary systems; (l) elucidating the problem that some age determinations for globular clusters result in greater ages than those determined for the universe; (m) stellar dynamics of globular clusters; (n) stellar dynamics of the Galaxy; (o) isotropy of central sources of, and motion of knots in, Active Galactic Nuclei; and (p) the position shift due to microlensing. [R.D. Reasenberg, Bull. Am. Astron. Soc. **16**, 758 (1984); R.D. Reasenberg, *et al.*, Astron. J. **96**, 1731 (1988); "TOPS: Toward Other Planetary Systems," report by NASA's Solar System Exploration Division, due to be published Sept. 1992; and Astrometric Interferometry Mission Strawman Science Program, developed by the Space Interferometry Science Working Group, S. Ridgway, chair, 5 July 1992.]

Control of systematic error is central to the instrument design. The approach has three levels: stable materials, real-time metrology, and post-measurement bias detection and correction using closure. (Heuristically, 4 measurements around a great circle should add to 360°.) The effect of optical aberrations is minimized by maintaining each telescope boresighted on its target within a few arcsec. The measurement of the angle between the targets is divided into three parts: two offsets from the interferometer axes, and the *articulation angle* between the interferometer axes (90°+Δ). The offsets are determined from dispersed interferometer fringes (*channelled spectra*). Dispersing the fringe allows operation at substantially increased target offsets, simplifying pointing requirements, and captures information that would be lost with white-light fringe detection. Full Aperture Metrology is used to hold the starlight optical path difference constant with respect to *fiducial points* located in front of each subaperture. The pair of fiducial points corresponding to each starlight interferometer defines its *pseudobaseline*. The articulation angle, which is between the real baselines, is closely related to the angle between the pseudobaselines. The latter is measured with picometer-accuracy laser gauges of a novel design.

Session B-5 1335-Thurs. CR2-28
COATED STRIPS, MICROSTRIPS AND TRANSMISSION LINES
Chairman: Tatsuo Itoh, Dept. of Electrical Engineering,
Univ. of California, Los Angeles, CA 90024-1594

B5-1
1340

BOUNDARY INTEGRAL SOLUTION TO SCATTERING FROM COATED GROOVES AT OBLIQUE INCIDENCE

J. Moore[1], H. Ling[1] and C. S. Liang[2]
[1]Department of Electrical and Computer Engineering
The University of Texas at Austin
Austin, TX 78712-1084
[2]General Dynamics, Fort Worth Division
P.O. Box 748
Fort Worth, Texas 76101

A boundary integral approach to the study of two-dimensional conductor-backed coated gratings under oblique incidence is presented. The grating is assumed to be infinite and periodic in only one dimension. Because of the underlying periodicity of the grating, it is sufficient to consider just one groove (or period) of the whole structure. The approach taken here is to subdivide this single groove into a homogeneous top region consisting of air and a bottom region made up of the groove, coating, and conductor backing. The grating lies in the x-z plane, and the aperture boundary along which the top and bottom regions meet lies along the x-axis. For the top region, the periodicity of the structure allows the fields along the aperture to be expanded into a sum of Floquet harmonics. The bottom region which consists of the groove in the presence of a dielectric coating and a conductor backing is divided into a number of homogeneous sub-regions. The fields within each sub-region are expressed in terms of an integral equation of the tangential fields along the boundary enclosing that sub-region. Because the incident field is oblique (has a z-dependence), the formulation needs to take into account coupling between the TM_z and TE_z polarizations. The method of moments with pulse expansion and point matching is used to discretize the boundary integral equation into a matrix equation. By enforcing the metal conditions and matching the fields across the boundaries of all the bottom sub-regions and across the aperture boundary, the unknown tangential fields on the aperture are found. The various modes excited by the grating are then extracted from the aperture fields. This method was validated against results for grooves along a dielectric half-space presented in (R. Janaswamy, IEEE Trans. Antennas Propagat., 40, 162-169, 1992) and (S. L. Chuang and J. A. Kong, Radio Science, 17, 545-557, 1982). Results for various groove profiles are investigated.

B5-2
1400

SCATTERING BY GAPS IN COATED STRIPS

J. Moore and H. Ling
Department of Electrical and Computer Engineering
The University of Texas at Austin
Austin, TX 78712-1084

We have recently developed two numerical solutions to the problem of scattering from gaps in infinite conductor-backed material coatings. They include a boundary integral equation formulation and a spectral integral equation formulation. In the boundary integral formulation, the discretization domain of the infinite structure is reduced to a localized region near the gap by removing the specular solution and surface wave contributions from the boundary integral equation. The spectral integral formulation utilizes the Green's function for the conductor-backed coating in a volume integral equation. We obtained both the numerical diffraction coefficients and surface wave excitation coefficients due to the isolated gap. The two solutions agree quite well with one another.

The goal of this work is to take advantage of these numerical solutions by employing a UTD-style solution building process in order to predict and understand the effects of gaps in complex coated bodies. In this paper, the scattering from a coated strip with a gap in the material coating is investigated. The approach is to systematically account for the isolated contributions and the interactions of the different scattering mechanisms. The isolated scattering mechanisms include as shown below (a) diffraction due to the gap, (b) surface waves excited by the gap, (c) diffraction at the strip edge, and (d) surface waves excited at the strip edge. The solutions to (c) and (d) are found using the technique presented by Moore and Ling (J. Moore and H. Ling, International IEEE AP-S Symposium, 305-308, 1992). We can then construct the total scattered field by systematically building up the multiple interactions.

We will show that (i) gaps in material coatings can significantly alter the scattering characteristics of the composite structure; and (ii) good results can be obtained from this "component" approach in that it compares favorably with the brute-force method of moments solution. This methodology is attractive in that the building block approach taken here allows one to pinpoint the dominant scattering mechanisms present in the overall RCS and through this process gain insight into the complex scattering physics of coated structures.

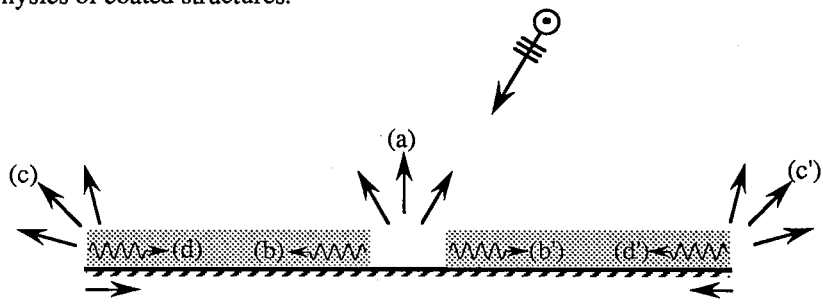

B5-3
1420

MODELING OF SPURIOUS RADIATIONS FROM FEED LINE DISCONTINUITIES IN MICROSTRIP ARRAYS

Abdelaziz Benalla* and K. C. Gupta
Department of Electrical and Computer Engineering
University of Colorado, Boulder CO 80309.

Microstrip line discontinuities are commonly encountered in feed networks in linear and planar microstrip arrays. Figure below shows a T-junction and a right-angle chamfered bend discontinuities. The effects of microstrip line discontinuities are: junction reactances, excitation of surface waves and spurious radiations. For microstrip arrays where the amplitude distribution is controlled by the feed network (such as for corporate-fed arrays), the effect of discontinuity reactances is to cause errors in both the amplitude and phase distributions. The effects of the spurious radiations are: unwanted coupling among discontinuities, increase in side lobe level and contribution to cross-pol radiation. Therefore, inaccurate modeling of these discontinuities leads to poor array performance (such as increase in SLL level, shift in main beam pointing, etc...).

The multiport network model (MNM) has been successfully used for microstrip patch antennas and arrays (A. Benalla and K.C. Gupta, Electromagnetics, Jan. 1991, Vol. 11, pp. 89-106). In the present contribution, the MNM approach is extended to the analysis of microstrip feed line discontinuities. The use of a single approach for modeling the radiation from both the patches and the feed line discontinuities is very convenient. The MNM approach includes both the effects of junction reactances and spurious radiations. Comparison of the results for scattering parameters obtained using this approach with the full-wave moment method will be presented. The effects of discontinuity radiations on the radiation pattern of a typical linear microstrip array will be discussed.

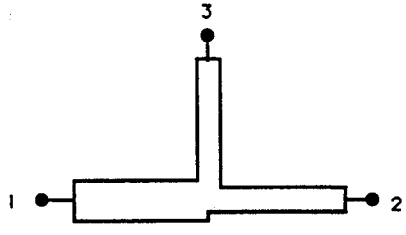

T-junction

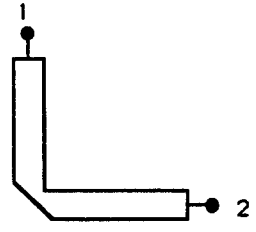

Right-angle chamfered bend

B5-4
1440

EM CHARACTERIZATION OF MATERIALS IN A MICROSTRIP SUBSTRATE ENVIRONMENT

D.P. Nyquist, B. Kzadri, D.J. Infante and J.M. Grimm
Department of Electrical Engineering
Michigan State University
East Lansing, Michigan 48824-1226

The dielectric (complex permittivity ϵ) and magnetic (complex permeability μ) characteristics are deduced for materials located in the substrate of a tri-layered conductor/substrate/cover microstrip environment. The principal EH_0 microstrip mode is quantified using a full-wave integral-operator formulation for its currents. Scattering parameters of the substrate-loaded microstrip region are de-embedded from measured (using an automatic network analyzer) terminal S-parameters by a method recently developed by the authors. The sample-region phase constant β_m and interfacial reflection coefficient Γ_m are subsequently deduced from the measured S-parameters. Equating the analytical full-wave solutions for those quantities to their measured values leads to a pair of complex transcendental equations $\beta(\epsilon,\mu,\omega) - \beta_m = 0$ and $\Gamma(\epsilon,\mu,\omega) - \Gamma_m = 0$, which are solved numerically for the desired constitutive parameters $\epsilon(\omega)$ and $\mu(\omega)$. This technique is valuable for the characterization of substrate materials in both practical microwave integrated circuits and microstrip-like field applicators designed for the study of material properties.

It was found that, for the field applicator utilized, transverse microstrip currents were negligible, and a full-wave description of longitudinal current k_z is provided by the axial-transform-domain integral equation

$$\int_{-w}^{w} g_{zz}(x|x';\zeta)\, k_z(x')\, dx' = 0 \quad \ldots \forall\ |x| < w$$

where w is the strip half-width, g_{zz} is an electric Green's function in Sommerfeld-integral representation and ζ is the axial transform variable. A rapidly convergent MoM numerical solution is implemented using entire-domain Chebychev basis functions. Non-trivial principal-mode current solutions exist only for discrete values $\zeta = \beta$. Based upon the full-wave current solution, characteristic impedance Z_c is computed using the average-voltage/current definition

$$Z_c = \frac{V_{avg}}{I} = \left[\int_{-w}^{w} dx\, k_z^*(x) \int_{-t}^{0} -e_y(x,y)\, dy\right]\left[I \int_{-w}^{w} k_z^*(x)\, dx\right]^{-1}$$

where e_y is computed from k_z and t is the substrate thickness. Finally, $\Gamma = (z_c - 1)/(z_c + 1)$ where z_c is the characteristic impedance normalized to that of the unloaded region. This formulation provides the necessary analytical relations for β and Γ.

Extensive numerical results will be presented based upon measurements for both low-loss and dissipative substrate materials.

B5-5
1500

MULTICONDUCTOR TRANSMISSION LINES IN MIXED DIELECTRIC MEDIA

Ching-Chao Huang
IBM East Fishkill ★
D/16S, B/640, Z/AR1
Hopewell Junction, NY 12533
Phone: (914) 892-3150, FAX: (914) 892-3039

★ with IBM Raleigh, D/36D, B/061, 3039 Cornwallis Road, Research Triangle Park, NC 27709 after 10/23/92.

The accurate characterization of capacitance in electronic equipments is esstial in that the capacitance can affect impedance, delay, and noises.

The method of moments has been widely used in the past to compute capacitances in various environments. Based on the image theory, Weeks computes the capacitance matrix of 2D conductors embedded in dielectric layers (Weeks, IEEE-MTT, 18, 35-43, 1970). The free-space Green's function, together with the concept of bound charge, were used in (Wei et al, IEEE-MTT, 32, 439-449, 1984) and (Venkataraman et al, IEEE-MTT, 33, 952-959, 1985) to handle arbitrary dielectric interfaces.

This paper combines the above two approaches (i.e., layered Green's functions and bound charge technique) so that the CPU time and storage can be minimized when arbitrary dielectric interfaces are mixed with dielectric layers. In so doing, we found it necessary to exploit several new algorithms as follows.

When no infinite ground plane is present, Venkataraman et al applied the constraint that the sum of all free and bound charges is zero. In using the layered Green's function to account for planar dielectric interfaces, we need to apply the constraint that the sum of all free charges is zero.

In accounting for arbitrary dielectric interfaces, Wei et al and Venkataraman et al integrated the gradient of a free-space Green's function over each line segment. In those cases where arbitrary dielectrics are sandwiched between two parallel ground planes, however, we found it more efficient to numerically differentiate the integral of a closed-form parallel-plate Green's function, than to sum up the integrals of the gradient of a free-space Green's function for each image term.

It is also noted that the papers cited above all used the point-matching method. (Weeks actually combined the least-square method with point-matching method that resulted in a normal equation.) The Galerkin's method is used in this paper for better accuracy.

Session B-6 1535-Thurs. CR2-28
INVERSE SCATTERING
Chairman: Weng Cho Chew, Dept. of Electrical and Computer Engineering,
Univ. of Illinois at Urbana-Champaign, Urbana, IL 61801

B6-1
1540

VARIABLE-DENSITY LINEAR ACOUSTIC INVERSE PROBLEM †

M. Moghaddam[1] and W. C. Chew[2]

[1] Jet Propulsion Laboratory
California Institute of Technology
Pasadena, CA 91109

[2] Department of Electrical and Computer Engineering
University of Illinois at Urbana-Champaign
Urbana, IL 61801

ABSTRACT

The linear acoustic inverse problem is solved for density (ρ) and compressibility (κ) using the basic ideas of diffraction tomography (DT). The key to solving this problem is to utilize frequency diversity to obtain the required independent measurements. The receivers are assumed to be in the far field of the object, and plane wave incidence is also assumed. Born approximation is used to arrive at a relationship between the measured pressure field and two terms related to the spatial Fourier transform of the two unknowns, ρ and κ. The term involving compressibility corresponds to monopole scattering and that for density to dipole scattering. Measurements at several frequencies are used and a least squares problem is solved to reconstruct ρ and κ. It is observed that the low spatial frequencies in the spectra of ρ and κ produce inaccuracies in the results. Hence, a regularization method is devised to remove this problem. Several results are shown. Low contrast objects for which the above analysis holds are used to show that good reconstructions are obtained for both density and compressibility after regularization is applied.

† This work was supported by the Army Research Office under contract DAAL03-87-K0006 to the University of Illinois Advanced Construction Technology Center, the National Science Foundation under contract ECS-85-25891, and the office of Naval Research under contract N00014-89-J1286. The computation time was provided by the National Center for Supercomputing Applications at the University of Illinois through the Cray Research and Development grant.

B6-2 1600

Design of Planar Optical Waveguides with Prescribed TM Modes

Lakshman S. Tamiland **Yun Lin**
Erik Jonsson School of Engineering and Computer Science, and
Center for Applied Optics
The University of Texas at Dallas
Richardson, TX 75083
(214) 690–2197

Abstract

An inverse scattering approach to designing optical waveguides with prescribed propagation characteristics of TM modes is presented here. The refractive index profile is formulated as a solution to a nonlinear differential equation whose forcing function is the potential obtained from the application of inverse scattering theory. The method is capable of reconstructing smooth refractive index profiles for planar waveguides that support single mode or multi modes. Both the cases of zero and non-zero reflection coefficients characterizing the transmission properties of waveguides are discussed here.

The conventional method of designing optical waveguide structures is to assume a refractive index profile and solve the governing differential equation to find the various propagation modes and their propagation characteristics. This is an iterative procedure and is time consuming. The procedure discussed in this paper as opposed to the direct method, starts with the required propagation characteristics of the waveguide and obtain the refractive index profile as the end result. This is achieved by transforming the wave equation for both the TE and TM modes in the planar waveguides to a Schrodinger type equation and then applying the inverse scattering theory as formulated by Gelfand, Levitan and Marchenko. The TE mode case has been done by Jordan and Tamil.

We verify the results here using a direct technique based on finite differences.

B6-3
1620

Synthesis of Optical Channel Waveguides: An Inverse Scattering Approach

Lakshman S. Tamil
Erik Jonsson School of Engineering and Computer Science, and
Center for Applied Optics
The University of Texas at Dallas
Richardson, TX 75083
(214) 690–2197

Abstract

We discuss in this paper an inverse scattering approach to synthesizing refractive index profiles of a two dimensional optical channel waveguide from a specified propagation characteristics. The scalar wave equation describing the channel waveguide can be separated into two one dimensional wave equations under the condition that the refractive index can be written in the additive form$n^2(x,y) = n_0^2 + n_x^2(x) + n_y^2(y)$. The wave equations can then be transformed into a Schrodinger type equation whose potential functions are related to the refractive index profile of the waveguide. The propagation characteristics of the waveguide are characterized either by the reflection coefficient or by the transmission coefficient. The Gel'fand-Levitan- Marchenko inverse scattering theory is used to obtain the unique solution of the potential function from the scattering coefficients. An alternative technique using Darboux transform will also be discussed.

G4-1
1400

A STUDY OF THE OCTOBER 1989 IONOSPHERIC STORM

S. Y. Ma*, K. H. Lin and K. C. Yeh
Department of Electrical and Computer Engineering
University of Illinois at Urbana-Champaign
Urbana, IL 61801-2991
R. O. Conkright
National Geophysical Data Center
National Oceanic and Atmospheric Administration
Boulder, CO 80303-3328

A large solar flare of class 4B/X13 occurred at 1229 UT on October 19, 1989. The arrival of particles associated with this flare triggered a magnetic storm with a sharp increase in the horizontal component of the geomagnetic field (SSC) at 0917 UT on October 20, 1989. The magnetograms taken in Japan showed the magnetic storm underwent two periods of maximum activities associated with the storm-time ring current development. In response to these magnetic activities the ionosphere showed remarkable effects. Both positive and negative storm effects were observed. Additionally global propagation of traveling disturbances were seen. The ionospheric behavior based on the data collected from more than 40 ionosonde stations and 14 TEC stations will be shown and reported.

*Permanent address: Department of Space Physics, Wuhan University, China.

G4-2
1420

THE PUZZLING DIFFUSE RESONANCE BETWEEN THE ELECTRON PLASMA FREQUENCY AND THE UPPER HYBRID FREQUENCY

Robert F. Benson, Code 692
NASA/Goddard Space Flight Center
Greenbelt, Maryland 20771

One of the most puzzling of the large number of ionospheric responses stimulated by topside sounders that are extremely dependent on the ambient ratio of the electron plasma frequency f_N to the electron gyrofrequency f_H is the diffuse resonance named DNT (because it occurs between f_N and the upper-hybrid frequency $f_T = (f_N^2 + f_H^2)^{1/2}$). When $f_N/f_H<1$, the DNT resonance appears to "float" away from the ionogram zero time-delay baseline. When $f_N/f_H>1$ the resonance has a more normal appearance, i.e., it is present as soon as the sounder receiver is turned on following the transmission of the sounder pulse (Benson, Radio Sci., 17, 1637-1659, 1982). In the present paper, knowledge of the DNT resonance will be reviewed and it will be shown that the stimulation of this resonance is strongly dependent on the antenna orientation relative to the ambient magnetic field direction.

G4-3
1440

A STUDY OF HF TERRESTRIAL COMMUNICATION SIGNAL LEAKAGE THROUGH THE IONOSPHERE

Marisa McCoy, John P. Basart, Nestor J. Escalera
Dept. of Electrical and Computer Engineering, Iowa State University, Ames, IA, 50011

Astronomy has exploited most of the electromagnetic spectrum, with the distinct exception of the HF frequency band (1 - 30 MHz). Low frequency radio astronomy from the Earth's surface is not easily done because of the ionosphere's characteristics. While data may sometimes be collected using only one radio telescope, long baseline interferometry is nearly impossible due to perturbations in the amplitude and phase fronts from ionospheric variations. No reliable corrections exist for the extremely decorrelated data.

The solution is to observe from above the Earth's ionosphere. However, in the 1 - 30 MHz band of interest, the ionosphere is neither a perfect reflector nor is it a perfect transmission medium. Terrestrial signals leak through and increase the background radio noise or introduce spurious signals into the measurements, making the detection of faint sources difficult. Ideally, radio telescopes on the moon's far side would provide a perfectly shielded environment, but at much greater cost and difficulty than a similar system in Earth orbit. The ultimate goal of this research is to determine if there are times when the radio leakage is sufficiently low to permit high-resolution low-sensitivity radio astronomical measurements from Earth orbit, and to be able to predict those times using solar and geophysical parameters.

Most ionospheric propagation models deal with point-to-point communication paths. These models assume the HF signals reflect off the ionospheric E and F regions according to geometric considerations. Our propagation model must take a different approach. All terrestrial HF communications signals, especially over-the-horizon radar, are potential interferers to low frequency radio astronomy. We propose to model the signal leakage to help determine if periods or frequency bands exist in which the background terrestrial radio noise is sufficiently low to allow radio astronomy observations from Earth orbit.

We have initiated a preliminary investigation into predicting signal strengths at the top of the ionosphere with respect to time, frequency, and solar behavior. Existing ionospheric models will provide a description of the general, global state of the ionosphere. This information will then be used as an input to our model of a randomly varying, turbulent medium, through which communication signals propagate. We anticipate using available space data to verify these initial predictions.

G4-4
1500

USING CONTOUR PLOTTING TO FIND THE MOST FREQUENTLY OCCURRING MODEL OF IONOSPHERIC CONDUCTIVITY AT VERY LOW FREQUENCIES.

J. A. Ferguson (Code 54)
Naval Command, Control and Ocean Surveillance Center, RDT&E Division
San Diego, CA 92152–5000

In cases where a large number of data samples is available, spread over a large range of time, a graphical technique may be used to select an optimum ionospheric conductivity profile. This technique fits the samples of measured values of signal strength with calculations determined from a sample set of ionospheric conductivity profiles. The technique is applied to measurements and the most frequently occurring model profile is found.

J3-1 1340 ACCELERATION OF PSR 1620-26 IN THE GLOBULAR CLUSTER M4

D. C. Backer
Astronomy Department
601 Campbell Hall
University of California
Berkeley, CA 94720

and

R. S. Foster
Remote Sensing Division
Code 7210
Naval Research Laboratory
4555 Overlook Avenue, SW
Washington, DC 20375-5000

Brinklow *et al.* (1987, *IAU Circ.* No. 4470) announced the discovery of the second pulsar in a globular cluster – PSR 1620-26, an 11-ms pulsar in M4. We added this object to our Pulsar Timing Array experiment at the NRAO GB 140ft telescope in 1988 January. Lyne *et al.* (1988, *Nat.*, **332**, 45) and McKenna and Lyne (1988, *Nat.*, **336**, 226) reported that this pulsar is in a binary system with 0.3 $M_\odot$ companion and a 191-d orbital period and a highly significant eccentricity, 0.025.

Reduction of our data using the McKenna and Lyne model always fell short of reducing the residuals to white noise. In late 1991 our conclusion was that the neutron star had perhaps experienced a "glitch" which is unexpected given the excellent timing record of the other millisecond pulsars. In 1992 March a solution was obtained that satisfied all data well with the addition of a single parameter, a large period second derivative, $\ddot{P} = -2.3 \times 10^{-27}$ s s^{-2}. In comparison, simultaneous observations of the 3ms pulsar in M28 show no irregularities.

The ratio $\dot{P}/\ddot{P}$ gives a time scale for the change in sign of the period derivative of only 14 years. If the second derivative arises from the gravitational influence of a companion, then the acceleration derivative, or jerk, will be $\dot{a} \simeq 7 \times 10^{-15}$ cm s^{-3}. This $\dot{a}$ is larger by 5 orders of magnitude than the jerks expected from either nearby stars in the cluster or the overall cluster potential. The $\ddot{P}$ could be the result of a third body in a long period orbit about the binary. Periods in the range of 10 to 100 years would be allowed by the present size of $\dot{P}$ without appealing to special geometry. The corresponding companion mass would be 3.3×10^{29} g $(P_{o2}/10\ \mathrm{y})^{7/3}$, where P_{o2} is the second orbital period. However this explanation may run into difficulty owing to the weak binding of such an object to the inner binary in the moderately dense core of M4.

J3-2
1400

MILLISECOND PULSAR POPULATION: NEW DISCOVERIES

Fernando Camilo
Physics Department, Princeton University
Princeton, NJ 08544-0708

Millisecond or "recycled" pulsars are strongly magnetized, rapidly spinning neutron stars emitting a broad-band radio beam that sweeps past our line of sight once with each revolution of the star. These objects are extraordinarily stable clocks, whence high precision timing measurements provide (1) astrometric results of outstanding accuracy, and (2) tests of the long-term stabilities of the best atomic clocks. Those that are found to be in binary systems (approximately half of them) further provide unique opportunities for (3) determining neutron star masses, (4) studying the evolution of close binary stellar systems, and (5) performing high-precision tests of relativistic gravitation theories.

We present results based on continuing searches for millisecond radio pulsars at high galactic latitudes at Arecibo Observatory, Puerto Rico. To date we have surveyed approximately 500 square degrees of sky at high latitudes at 430 MHz, as part of a continuing survey. We have discovered four recycled pulsars and a number of slow ones in this highly sensitive survey reaching a minimum detectable flux density $S_{\rm min} \sim 2$ mJy for fast pulsars. Most of the recycled objects discovered are interesting in their own right (two of them are isolated), and together they add considerably to our knowledge of millisecond pulsars. The consequences of our discoveries for millisecond pulsar population and statistics studies are considered, and objects of particular interest are discussed in detail.

J3-3
1420

THE PULSAR THAT BURST THE BUBBLE

D. A. Frail
National Radio Astronomy Observatory
Socorro, NM 87801

In 1991 Frail and Kulkarni announced the detection of the pulsar PSR 1758-24 on the western edge of the supernova remnant G5.4-1.2. It was argued that the two were physically associated and that the system was an example of a "interacting composite", first suggested by Shull et al., whereby a high velocity pulsar is able to catch up with the decelerating supernova shell, significantly influencing both the dynamical and energetic evolution of the remnant. The requisite pulsar velocity according to this hypothesis was 2500 km/s - the highest velocity for any known pulsar!

We will examine this hypothesis in the light of new observations. These include a wide-field radio continuum image, a distance determination from 21-cm observations, a year-long pulsar timing program, and a proper motion measurement of the cometary nebula surrounding the pulsar.

J3-4
1440 DIFFERENTIAL ASTROMETRY AND THE PROPER MOTION OF THE PULSAR IN THE CTB 80 SUPERNOVA REMNANT

R. S. Foster
Remote Sensing Division
Code 7210
Naval Research Laboratory
4555 Overlook Avenue, SW
Washington, DC 20375-5000
and
D. C. Backer
Astronomy Department
601 Campbell Hall
University of California
Berkeley, CA 94720

A proper motion of the radio pulsar PSR 1951+32 in the supernova remnant CTB-80 has been estimated. Using the Very Large Array, a change in position of $0''.241 \pm 0''.088$ at a position angle of 214 ± 20 degrees has been observed, consistent with the known supernova morphology. This motion is consistent with the idea that the pulsar is moving in the direction of the bow shock which is part of the core of the CTB80 nebula, and which is thought to result from the interaction of the spindown luminosity of the pulsar with the surrounding ISM and SNR material. The measurements were made using a differential astrometry technique to determine the separations between the pulsar and five extragalactic background sources. The initial observations were made on 1989 January 13 and were repeated 2.64 years later on 1991 July 18. The implied annual proper motion of this source is $0''.092 \pm 0''.033$. Combining the astrometric data with pulsar scintillation and optical line velocity measurement we conclude the pulsar is probably at a distance just under 1 kpc and moving at a velocity of slightly under 400 km/s. The closer than previously assumed distance to the CTB-80 remnant indicates that the expected gamma-ray flux from PSR 1951+32 maybe a factor of more than four larger than previously expected. The technique of using differential astrometry to perform proper motion analysis will be reviewed in the context of the observations of the fast motion of the pulsar in the CTB 80 supernova remnant.

J3-5
1500

A NEW MODEL FOR DISPERSION AND SCATTERING IN THE GALAXY

James M. Cordes
Astronomy Department & NAIC
Cornell University
Ithaca, NY 14853

I will summarize a new model for the galactic distribution of free electrons that was developed by the author and J. Taylor (Princeton). The model may be used to (1) infer distances from pulsar dispersion measures; (2) predict dispersion measures for specific positions in the Galaxy; and (3) predict the amplitudes of interstellar scattering effects such as angular broadening and pulse broadening. Future measurements that will improve the model include scattering measurements of sources seen through the galactic center and VLBI of sources in the anticenter direction. The new distance scale implied by the model also has implications for the inferred velocities of radio pulsars, which will be presented both statistically and in particular for a pulsar that is producing a spectacular bow shock nebula from its motion through the interstellar medium (Cordes, Romani, & Lundgren 1993).

J3-6
1540

POSITIONS AND PROPER MOTIONS OF PULSARS

E. B. Fomalont (NRAO), W. M. Goss (NRAO), A. G. Lyne
(Jodrell Bank),R. N. Manchester (CSIRO) and
K. Justtanont (Jodrell Bank)

We have determined accurate radio positions for 40 pulsars using the VLA. Nineteen of these pulsars were observed at three epochs (1984.98, 1986.39 and 1989.08) from which proper motions have been obtained with an accuracy better than 0.01" per year for the stronger pulsars. Proper motions with lower accuracy were also determined for an additional 21 pulsars from a comparison of the VLA positions with previously published positions. Where independent determinations of the proper motions are available, they generally agree within twice the estimated errors, but there are a few notable exceptions. The derived pulsar velocities transverse to the galactic plane are, on average, somewhat larger than those found previously.

Absolute positions have a precision of about 0.05" and, after correction for known proper motions, are in excellent agreement with positions derived from pulsar timing observations. The weighted mean offset between the VLA and timing frames is less than 0.02" in each coordinate.

J3-7
1600

TOWARDS VLBI DETERMINATIONS OF PULSAR PARALLAXES, POSITIONS, AND PROPER MOTIONS

R.M. Campbell (Harvard University),
N. Bartel (York University),
I.I. Shapiro, M.I. Ratner (Center for Astrophysics),
R.J. Cappallo, A.R. Whitney (Haystack Observatory),
W.H. Cannon (Institute for Space and Terrestrial Sciences),
W.T. Petrachenko (Geological Survey of Canada),
J. Popelar (Geodetic Survey of Canada), and
T.M. Eubanks (U.S. Naval Observatory)

Interleaved observations of a pulsar and one or more extragalactic phase-reference sources by VLBI provide a means to determine their differential sky positions possibly with submilliarcsecond accuracy. We have begun a long-term program to determine the parallax distances, positions, and proper motions of about nine pulsars, with anticipated uncertainties in the distances as small as 5% in some cases. Preliminary analysis of the data from one pulsar from one set of observations shows that phase-connection is feasible, thus indicating that our program goals are achievable. These goals include determination of properties of the interstellar medium, partial calibration of the dispersion-based galactic distance scale, and, when coupled with pulse time-of-arrival measurements, provision of a tie between the solar-system and extragalactic reference frames.

This work was supported by NASA grant NGT-50663 and NSF grant AST89-02087. Operations at the Haystack VLBI correlator are supported by the NSF through the Northeast Radio Observatory Corporation.

J3-8
1620

PULSAR OBSERVATIONS WITH THE VERY LONG BASELINE ARRAY

C.R. Gwinn
Physics Dept.
University of California
Santa Barbara, CA 93106

Very-long baseline interferometry (VLBI) of pulsars has proved useful for alignment of reference frames, measuring proper motions and trigonometric parallaxes, and studying interstellar scattering. In the future, VLBI of pulsars may be useful for studying pulsar magnetospheres, and for measuring orbits of binary pulsars. The US Very Long Baseline Array, soon to be operational, will present new capabilities for pulsar observations with VLBI. These include wider recorded bandwidth, improved gating capabilities, and the possibility of frequent, routine observing. I discuss the possibilities for improved observations offered by the capabilities of the VLBA, focusing in particular on the difficulties faced by astrometric and scattering VLBI of pulsars.

J3-9
1640

THE VLBA CORRELATOR'S PULSAR GATE

Jonathan D. Romney
National Radio Astronomy Observatory
Post Office Box O
Socorro, New Mexico 87801-0387

The Very Long Baseline Array (VLBA) is currently nearing completion. Consisting of ten new, dedicated VLBI antennas and a comprehensive control, correlation, and analysis center, it is designed as a multi-purpose instrument, supporting the full range of scientific investigations which can be carried out using VLBI techniques.

Among its capabilities is a gating facility incorporated into the VLBA correlator, intended to enhance the sensitivity of pulsar interferometry, and to permit observations at selected pulse phases. The gate may also be applied as a simple de-disperser for single-dish pulsar observations recorded on VLBA tapes.

The VLBA correlator's 'FX' architecture makes possible the efficient implementation of the gate as a system-wide function of pulse phase and RF frequency only. Subdivisions of the gate control matrix can support observations in multiple RF bands, either contiguous in frequency or in a bandwidth-synthesis mode.

A primary limitation of the correlator for pulsar observations arises from the 131.072-ms ($2^{17}\mu$s) fundamental integration cycle, which limits its applicability to millisecond pulsars. It may be possible, however, to design external equipment to provide shorter integrations.

The basic pulsar gate hardware is complete and has been exercised in test fixtures. Integration into the correlator system and development of control software will begin after the correlator becomes operational for the more common and more straightforward continuum and spectroscopic observing modes.

Session B-7 0835-Fri. CR2-28
TRANSIENTS
Chairman: Carl E. Baum, Phillips Laboratory/WSR, Kirtland AFB, NM 87117-6008

B7-1
0840

REPRESENTATION OF SURFACE CURRENT DENSITY AND FAR SCATTERING IN EEM AND SEM WITH ENTIRE FUNCTIONS

Carl E. Baum
Phillips Laboratory/WSR
Kirtland AFB, NM 87117-6008

In the SEM representation of various electromagnetic response parameters there is in general an entire function included for completeness. Conditions for presence and absence of this entire function are developed here. For the surface current density on a finite-size perfectly conducting object in free space entire-function-free representations are possible in both class-1 and class-2 forms of the coupling coefficients. For the far scattering from such an object, however, the class-1 form leads to the necessary inclusion of such an entire function which can be quantified. This class-1 form is still useful and appropriate for late-time representation and associated target identification. However, for scattering-length (or cross-section) calculations the class-2 form (with no additional entire function) is more suitable. In this case the coefficients are frequency dependent for each pole associated with a natural mode.

B7-2
0900

MEASUREMENT AND CALCULATION OF THE RESONANT FREQUENCIES OF A FINITE DIELECTRIC CYLINDER

Douglas J. Taylor*, Scott L. Browning
Naval Research Laboratory
Washington, DC

Herbert Überall
Physics Department
The Catholic University of America
Washington, D.C. 20064

ABSTRACT

Resonances of a dielectric cylinder with spherical endcaps are measured and compared with predictions based on a Bohr-Sommerfeld quantized surface wave model method. This technique for computing electromagnetic resonances is based on phased matched circumferentially propagating surface waves, and has provided a physical basis for understanding and computing the resonant frequencies of penetrable dielectric objects with non-canonical geometries. Computations are implemented by establishing that the phased matched resonance condition can be written mathematically as,

$$\int \frac{ds}{\lambda(s)} = \frac{1}{2\pi} \int k(s) ds = n + \frac{n'}{4}$$

where a particular surface wave (ray) traverses a closed path which measures n wavelengths plus $\frac{n'}{4}$ advance for each time a caustic is encountered. The surface wave propagation constant, $k(s)$, and wavelength, $\lambda(s)$ vary along the path s, and depend on the surface curvature and dielectric properties of the object. The propagation constants of the surface waves are not known exactly and are approximated with values computed from equivalent spherical and cylindrical canonical geometries.

Predictions of the lowest order (m=0) resonant frequencies of a dielectric cylinder with hemispherical endcaps using this approximate phase matched surface wave method are compared with microwave measurements. A variety of cylinder radii and overall lengths were tested to observe the physical effects of surface wave propagation cutoff and surface wave dispersive phase velocity. While the resonances can be categorized into internal and external modes, only the internal relatively high Q modes are addressed here.

B7-3
0920

TIME-FREQUENCY ANALYSIS OF BACKSCATTERED DATA FROM A COATED STRIP WITH A GAP

H. Ling[1], J. Moore[1], D. Bouche[2] and V. Saavedra[2]
[1]Department of Electrical and Computer Engineering
The University of Texas at Austin
Austin, TX 78712-1084
[2]Commissariat a l'Energie Atomique
Centre d'Etudes Scientifiques et Techniques d'Aquitaine
BP No. 2, 33114 Le Barp, France

It is well recognized that electromagnetic signals backscattered from a target contain information useful for identifying the target. Target characteristics are commonly extracted by analyzing the signal in either the time or the frequency domain. For example, the natural resonances of a target are manifested in the frequency domain as sharp, discrete events and can be attributed to the unique global features of the target. Similarly, scattering centers are manifested in the time domain as distinct time pulses and can be related to the local features on the target. For dispersive phenomena, however, the scattering characteristics are not apparent in either the time or the frequency domain. They are best characterized in the *joint* time-frequency domain. This was recognized in several recent works in which the backscattered data from dispersive waveguide ducts (H. Ling and H. Kim, IEEE Microwave and Guided Wave Lett., 2, 140-142, 1992; A. Moghaddar and E. K. Walton, to appear in IEEE Trans. Antennas Propagat.) and plasma plumes (H. Kim and H. Ling, Elect. Lett., 3, 279-281, 1992) were analyzed in the time-frequency domain. Among the tools which have been used to generate the time-frequency display include the well-known short-time Fourier transform and the Wigner-Ville distribution, as well as the more recently introduced wavelet transform.

In this work, the short-time Fourier transform is used to analyze the backscattered data from a coated plate with a gap in the coating. This structure has recently been characterized from the forward scattering point of view in order to study the basic scattering physics associated with discontinuities in material coatings (J. Moore and H. Ling, to appear in J. Electromag.Waves Applications). The most interesting aspect of the scattering physics in this class of targets is the presence of strong surface wave contributions to the backscattered signal. Since surface waves are dispersive in nature, they are difficult to distinguish in either the time or the frequency domain. The time-frequency display provides a good tool for localizing the various surface wave phenomena. In addition, once the different scattering mechanisms are isolated, it is possible to carry out a two-dimensional gating operation in the time-frequency plane. This is a natural extension of the usual time-gating concept commonly utilized in microwave measurements and allows the original data to be decomposed into a set of fundamental scattering mechanisms in either the time or the frequency domain.

B7-4
0940

WIDEBAND SCATTERING OF A MICROSTRIP PATCH IN TERMS OF SEM NATURAL MODES

Hans Steyskal*
Rome Laboratory
Hanscom AFB,Mass.,USA

Richard C. Hall
Huber+Suhner AG
Herisau, Switzerland

With the present interest in electromagnetic pulses the question arises whether existing frequency-domain computer codes can be used to provide the temporal response of antennas and scatterers. Although time and frequency solutions are related by the Fourier transform, a straightforward numerical transform often is computationally impractical due to the very fine frequency sampling required. Therefore we explore a new approach, based on the Singularity Expansion Method (SEM), which uses additional known, physical characteristics of the solution. It leads to a simple analytic approximation of the frequency spectrum from which a time domain solution is readily obtained.

We applied this approach to scattering from a rectangular microstrip patch antenna. We modified an existing frequency-domain MOM code to accept complex frequencies and then searched for the frequencies where the MOM matrix equation has nontrivial homogeneous solutions. This determines the natural frequencies and the corresponding natural modes. Evaluation of the unknown mode amplitudes generally poses a major difficulty (G.W.Hanson, IEEE AP-S Symp.Digest p 2235, Jul 1992), but is facilitated by the fact that we already have a code which gives a CW solution. We simply determine the amplitudes such that the current expansion gives the best rms match to one (or more) known CW cases.

With the above approach we have obtained an accurate analytic expression for the current on a 4 GHz antenna element. Using a 7-mode approximation we computed the radar cross section over the 1-12 GHz range and these results were found to compare very well with independent computations at closely spaced, real frequencies.

*) temporarily at Ecole Polytechnique Federale de Lausanne, Switzerland.

B7-5
1000

A Dynamically Tunable Optical Filter as Dispersion Compensator

Lakshman S. Tamil and **Yisong Li**
Erik Jonsson School of Engineering and Computer Science, and
Center for Applied Optics
The University of Texas at Dallas
Richardson, TX 75083
(214) 690–2197

Abstract

A detailed analysis of dispersion compensating fiber optic filter proposed by Oullette [Opt. Lett. 16, 303 (1991)] is provided here. Design parameters of the filter that could provide dispersion compensation for wide spectral sources are discussed. The dispersion compensating filter designed here can be dynamically tuned to compensate for the drifts in the laser center frequency due to temperature change and other deteriorations. The filter can be fabricated by exposing the photo-refractive fibers to the ultra violet radiation. A design methodology for fabricating the refractive index variation along the longitudinal direction of the fiber, with appropriate chrip and taper coefficients is also given here. Dispersion compensation capability of the fiber filter is demonstrated by simulating pulse broadening after transmission in a long fiber and the regeneration of the pulse after dispersion compensation. This device can be cascaded to the already buried optical fibers thus enhancing the bandwidth of those fibers.

Session G-5 0835-Fri. CR0-30
VALIDATION OF IONOSPHERIC MODELS
Chairman: Bodo W. Reinisch, Center for Atmospheric Research,
Univ. of Massachusetts, Lowell, MA 01854

G5-1
0840

TDIM Validation

J J Sojka and R W Schunk, (Both at: Center for Atmospheric and Space Sciences, Utah State University, Logan, UT 84322-4405; 801-750-2964; sojka@cc.usu.edu)

The Utah State University Time Dependent Ionospheric Model (TDIM) is a physical model of the terrestrial F-region. It has been used to define the high latitude climatology of the AWS Parameterized Real-Time Ionospheric Specification Model (PRISM). For the past three years it has been one of five physical F-region models being compared in the CEDAR initiative called 'Problems Related to Ionospheric Modeling and Observations' (PRIMO). The main PRIMO objective is to identify specific shortcomings in the physical models of the ionosphere.

We are comparing the TDIM simulations with data from a wide distribution of ground-based ionospheric sounders; specifically, those in the American, Russian, and Indian sectors. These comparisons are of the F-region bottomside profile, N_mF_2, and h_mF_2. The emphasis is to use individual days of data rather than monthly medians. Seasonal and solar cycle dependences are used as selection criteria for these comparisons. How the comparisons can be extended to include TEC and topside N_e measurements. The current status of the USU effort will be discussed.

G5-2
0900

HOW ACCURATE ARE IONOGRAM-DERIVED N(h) PROFILES

C.F. Chen, J.L. Scali, and B.W. Reinisch
University of Massachusetts Lowell
Center for Atmospheric Research
450 Aiken Street
Lowell, MA 01854

M. Buonsanto
Massachusetts Institute of Technology
Haystack Observatory
Atmospheric Science Group
Westford, MA 01886

Q. Zhou
Arecibo Observatory
P.O. Box 995
Arecibo, Puerto Rico 00613

Incoherent scatter radars and ionosondes are the major instruments providing ionospheric electron density profiles. Because the two instruments use different techniques to determine the electron density, it is important to compare the results. By using a large database, detailed hmF2 comparisons have been carried out. The data were obtained by the Digisonde 256 and the Incoherent Scatter Radar operating at Millstone Hill (43N, 72W geographic), Massachusetts. Comparing data from different seasons in 1990 shows a seasonally dependent systematic difference between the F2 peak heights determined by the Digisonde and the radar varying from 4km in winter to 17km in summer. This paper discusses these observations and offers some explanations of the results.

G5-3
0920

IRI PREDICTIONS AND ACTIVITIES PERTAINING TO THE VIM PROJECT

Dr. D. Bilitza
NASA, GSFC, NSSDC, Code 633/HSTX
Greenbelt, MD 20771

A brief overview is given over the goals and activities of the URSI/COSPAR Working Group on the International Reference Ionosphere (IRI), with special emphasis on the parameter and regions that are of interest to URSI's Verification of Ionospheric Models (VIM) project. Results and recommendations of the 1992 IRI Workshop, held during the COSPAR/IAF World Space Congress, are presented and future plans and priorities of the IRI effort are discussed. Recent model improvements and remaining model shortcomings are highlighted and their impact on the electron density in the middle ionosphere is evaluated.

IRI predictions for the VIM periods are presented for comparisons with the VIM data base. In the middle ionosphere the IRI user can choose between several peak and profile options. We illustrate the differences in densities obtained with these different options.

G5-4
0940

DAY TO DAY COMPARISON OF CALCULATED AND OBSERVED ELECTRON DENSITY PROFILES AT MIDLATITUDES

Dwight T. Decker, Institute for Space Research, Boston College,
885 Centre St., Newton, MA 02159
David N. Anderson, Phillips Laboratory, GPIM, Hanscom AFB, MA 01731
B.W. Reinisch, University of Mass Lowell, Center for Atmospheric Research,Lowell, MA 01854
Jurgen Buchau, Phillips Laboratory, GPIA, Hanscom AFB, MA 01731

Over the last couple of years, there has been an increasing effort to validate various theoretical models of the earth's ionosphere. In the work done to date, the focus has been almost exclusively on comparisons with monthly medians of observations. But there is growing interest on how well the day to day 'weather' of the ionosphere can be modeled. With that in mind, we are simulating the day to day variations for several months at three midlatitude stations. The stations are at Bermuda, Wallops Island and Millstone Hill and the months are March, May, June, November, December of 1990 and October of 1989.

Our primary goal is to see how well a theoretical model simulates the ionospheric day to day variability when that model is essentially driven by statistical inputs. For this study, the input we are particularly interested in is the thermospheric neutral wind. This is because the wind is believed to be one of the major sources of ionospheric variability. Our approach is to do four sets of simulations using four different sources for the neutral winds. The first source is the empirical model HWM90 based on satellite and ground-based observations of the thermospheric winds. For our second source, we use the VSH (Vector Spherical Harmonic) Model based on runs of a general circulation model of the thermosphere and ionosphere (the NCAR-TIGCM). In our third set of simulations, we use winds derived from the F2 peak heights contained in the IRI (International Reference Ionosphere). Finally, in the fourth set of simulations we use a 'real-time' input by using the observed F2 peak heights to derive effective winds.

G5-5
1000

COMPARISON OF THE FLIP MODEL DIURNAL ELECTRON DENSITY VARIATION WITH VIM DATA

Phil Richards , Physitron Inc., 3325 Triana Blvd., Suite A, Huntsville, Alabama 35805
B. W. Reinisch, University of Massachusetts Lowell, Center for Atmospheric Research, 450 Aiken Street, Lowell, MA 01854

The Field Line Interhemispheric Plasma model is a comprehensive model of the ionosphere and plasmasphere which includes interhemispheric solutions to the time-dependent continuity and momentum equations for 0+, H+, N+, and He+. the model also provides interhemispheric solutions for the photoelectron fluxes to yield electron heating rates which are used in the time-dependent energy equations to calculate the ion and electron temperatures. Steady state solutions are also obtained for many minor ion and neutral species in each ionosphere. A recent innovation is the ability for the model to take the measured hmF2 and use it to calculate neutral winds that closely reproduce the observed hmF2. This new technique has greatly improved the ability of the model to reproduce the observed electron densities. The agreement between the model and data is generally very good during the daytime but there are still important discrepancies at night. In this paper, the FLIP model calculations are compared with VIM data from 1989 and 1990. These calculations were made in conjunction with the NSF-CEDAR sponsored PRIMO campaign.

G5-6
1040

A COMPARISON OF THE OBSERVED SEASONAL CHANGE IN THE F-REGION DIURNAL VARIATION WITH SIMULATIONS FROM A COUPLED THERMOSPHERE-IONOSPHERE MODEL

T.J. Fuller-Rowell and M. Codrescu
CIRES, University of Colorado and
NOAA Space Environment Laboratory,
325 Broadway,
Boulder, CO80303.

The F-region ionospheric density is controlled by production from solar EUV, loss by reactions with thermospheric neutral molecular species, and transport by diffusion and neutral winds. During the year, although solar flux changes are important, it is the large changes in neutral thermospheric composition and winds which have the dramatic effect on the diurnal variation of F-region ion density. It is essential therefore to have a realistic description of these parameters. Results from a coupled thermosphere-ionosphere model (CTIM) have been compared with the observed diurnal variation of ion density in summer, winter and equinox. The model is able to simulate thermospheric composition and winds self-consistently with the plasma density and temperature. The comparisons have been used to validate the model and to illustrate the importance of a realistic thermosphere in ion density calculations.

G5-7 1100 ESTIMATION OF CONJUGATE ELECTRIC FIELDS FROM *hmF2*

Horng-Yu Wu and Kent L. Miller
Center for Atmospheric and Space Science
Utah State University
Logan, UT 84322-4405
801-750-3592

Thermospheric winds and penetrating electric fields play important roles in the complex phenomena of F2-layer magnetic storms. The combined effect of both on the ionosphere can be inferred using a method based on the non-linear relationship between the neutral winds and the height of the F2-layer. The combination of meridional winds and zonal electric fields in the F2-layer can be thought of as an "effective wind". In this paper we examine three scenarios that may occur in the meridional neutral winds and electric fields during magnetic storm periods. First, a simultaneous change in the height of the F2-layer occurring at more than one conjugate pair of ionosonde stations at all latitudes is expected to occur in the early stages of storms when magnetospheric electric fields penetrate to middle and low latitudes. Second, neutral wind perturbations driven by high latitude heat sources propagate to low-latitude regions with a time-lag of several hours. This would occur in the latter stages of storms when heating in the auroral oval drives enhanced equatorward winds via the traveling ionospheric disturbances. Third, the meridional neutral winds and electric fields during storm periods do not change from the quiet-time patterns. This occurs particularly when the effects of the storm die out in the higher latitudes.

Changes from the quiet-time values of hmF2 occurring simultaneously at one or more pairs of conjugate ionosonde stations are attributed to the penetration of electric fields. By subtracting the quiet-time background determined on the ten most quiet days of the month from the result of the effective wind derivation, an estimate can be made of the strength of the perturbation electric field during this magnetospheric dynamo process. The most pronounced storm effects include a decrease in the F2-layer peak electron concentration and a strengthening of equatorward winds. The effects appear to be greatest when magnetic storm onset occurs at midnight and before midnight. Pre-midnight storms enhance equatorward winds around midnight. However, midnight storm strengthen equatorward winds near dawn. For all storm cases different local starting times were examined to show that the penetrating electric field to min-latitudes normally occurs near midnight periods. The strengths of zonal electric fields at mid-latitudes normally are less than 10 mV/m and decrease with latitude.

G5-8
1120

ESTIMATING THE TOTAL ELECTRON CONTENT FROM IONOGRAMS

C.N. Wang, X. Huang, and B.W. Reinisch
University of Massachusetts Lowell
Center for Atmospheric Research
450 Aiken Street
Lowell, MA 01854

M. Buonsanto
Massachusetts Institute of Technology
Haystack Observatory
Atmospheric Science Group
Westford, MA 01886

Ionograms provide the electron density profiles up to the peak of the F2 layer and the electron content can be calculated directly for the bottom side ionosphere. Using the scale height at the F2 peak, the profile shape in the top side ionosphere can be estimated. Based on different models (IRI, Bent, and Chapman) we have approximated the topside profile shape and compared the extrapolations with incoherent scatter radar observations at Millstone Hill.

G5-9
1140

A SURVEY OF THE TIMES OF DESCENT OF SPORADIC-E LAYERS: IMPLICATIONS OF THE INFLUENCE OF ATMOSPHERIC TIDES

Dr. Kent L. Miller
Center for Atmospheric and Space Science
Utah State University
Logan, UT 84322-4405
801-750-3592

This paper presents results of a global survey of the height of sporadic-E layers. The layer height is indicated by monthly average values of ionosonde measurements of h'Es. Results at each ionosonde typically show two times each day when the sporadic-E layer descends. The descent of the layer is thought to indicate the low-altitude termination of the descent of a so-called "intermediate layer." Intermediate layers are relatively thin plasma layers that are observed to descend through the valley between the E and F regions and to merge with sporadic-E layers near 110 km altitude. The observation of two descending phases of h'Es suggests that the occurrence of the layer is correlated with the semi-diurnal tide. However, the times of descent of the two layers are, in general, not separated by 12 hours. The separation of the two times of descent is strongly dependent on season, with the greatest separation in time occurring in local summer in the mid-latitudes. The two layers merge in the winter at some stations. The times when the two layers are observed is similar at different longitudes. Results from low latitude stations show the two layers to descend within about 6 hours of each other, with the local time dependent on longitude.

Session J-4 0835-Fri. CR2-26
ADVANCED COMPUTING TECHNIQUE
Chairman: Michael Davis, Arecibo Observatory, Arecibo, PR 00613

J4-1
0840

FUTURE OF COMPUTATIONAL ASTROPHYSICS

Prof. Michael L. Norman
Department of Astronomy and
National Center for Supercomputing Applications
University of Illinois at Urbana-Champaign
Urbana, Illinois 61801

Numerical simulation has become a powerful tool to theorists and observers alike as a means for gaining dynamical insights into astronomical phenomena as well as rationalizing increasingly complex observational databases. As highlighted in the recent NRC report of the Astronomy and Astrophysics Survey Committee (the "Bahcall Report"), computer simulations are expected to help solve a number of long-standing problems in astrophysics in the 1990s.

Since the inception of the NSF Supercomputer Centers program in 1985, we have seen the number of projects in astronomy increase fivefold and the CPU utilization increase 30-fold over the first year-end numbers. Figures are not available for how much research is being done on personal workstations and departmental minicomputers, however the Bahcall Report estimates that 10% of all professional astronomers are engaged in theoretical computations. It is clear that we are witnessing explosive growth of a new and powerful methodology in astronomical research.

In this talk I will illustrate the statements above and show examples of significant achievements in computational astrophysics. I will identify the major trends evident in current research and project their potential impact on astronomy assuming advances in computer power continue as expected.

J4-2
0900

OBJECT ORIENTED PROGRAMMING IN RADIO ASTRONOMY: AIPS++

Dr. G. Croes, Associate Director
National Radio Astronomy Observatory
520 Edgemont Road
Charlottesville, VA 22903-2475

The presentation introduces the key concepts of object oriented design and development of computer programs. It discusses the benefits that an organization can gain and various traps one can fall into. We will explain the various tools one needs for this approach, and the reasons why we chose C++ as the programming language for our project rather than the more conservative FORTRAN language.

We will illustrate the concepts involved through a description of the AIPS++ project. We intend AIPS++ not only to succeed AIPS for the processing of interferometric data, but also for the analysis of single dish data.

A consortium of seven radio astronomy organizations currently develops AIPS++ as a cooperative venture. The widespread geographic distribution of these organizations gives rise to interesting project management problems which we also intend to discuss.

J4-3
0920

NCSA RADIO SYNTHESIS IMAGING COMPUTING PROJECT

Richard M. Crutcher
National Center for Supercomputing Applications
University of Illinois
1002 West Green Street
Urbana, IL 61801

The Astronomy and Astrophysics Survey Committee (AASC) recently released its report for the 1990's, "The Decade of Discovery." The 1990's AASC included for the first time a panel specifically devoted to astronomical computing. The AASC report called for a greatly enhanced role for computing and computational resources in astronomy and astrophysics - particularly in the observational area. Among the specific recommendations of the AASC report in the computational area were: 1) Use of upgraded NSF supercomputer centers by astronomers. 2) Development of network links to widely-used observatories. 3) Development of digital data archives available over national high-speed networks. With funding from the National Science Foundation High Performance Computing and Communications initiative, the National Center for Supercomputing Applications has begun a program for the direct implementation of these three recommendations of the Astronomy and Astrophysics Survey Committee. We plan to prototype the next generation of astronomical telescope systems - remotely located telescopes connected by high-speed networks to very high performance, scalable architecture computers and on-line data archives, which are accessed by astronomers using DARPA/NSF Gbit/sec networks.

Specifically, we propose to install a data link between the millimeter-wave synthesis array radio telescope at Hat Creek, California operated by the Berkeley-Illinois-Maryland Association (BIMA) and the National Center for Supercomputing Applications (NCSA) at Urbana, Illinois for real-time transmission of data to the high performance, massively parallel Connection Machine 5 (CM-5). We will port the BIMA data processing system MIRIAD to the CM-5, optimize the very computationally intensive algorithms for calibration and imaging, develop new algorithms which utilize the massively parallel architecture, and use (and make available to the general community) the CM-5/MIRIAD system for processing of data from radio synthesis arrays. We further plan to implement a true distributed processing metacomputer. We will experiment with and develop the techniques for connecting multiple supercomputers for maximum high performance; also, we will connect astronomers' workstations in Madison, Wisconsin over the BLANCA Gbit/sec testbed network to the NCSA supercomputers. Finally, we plan to implement an on-line, digital archive of the BIMA radio telescope database and a digital library of processed images. Astronomers anywhere on the national network may browse through the digital library and download images needed for their own research to their own workstations.

The development of this complete software, distributed computing, and data archive and library solution to the radio astronomy computing problem will advance our expertise in high performance computing and communications technology and ultimately therefore our knowledge of astronomical Universe.

J4-4
0940

VOLUME VISUALIZATION IN RADIO ASTRONOMY

Eric W. Greisen
National Radio Astronomy Observatory
520 Edgemont Road
Charlottesville, Virginia 22903-2475

With the advent of advanced telescope systems and the rapid increase in affordable computer power, radio astronomers have begun to encounter large "cubes" of data which must be examined and understood before any physical conclusions about them may be reached. Examples of such cubes are two-dimensional images of the sky taken at a sequence of times or a sequence of radial velocities. Software engineers will need to develop as many techniques as possible to allow astronomers to discover what lies within their cubes. Interactive slicing on planes or, preferably, bricks, the display and rotation of one or more isosurfaces, and various false-color displays have all proven useful. The most powerful - and expensive - tactic seems to be ray tracing done by assigning each voxel a color, intensity, and opacity and developing the displayed intensities by computing with the equation of transfer. The volume visualization occurs in the human brain upon viewing a rapid andn ordered (e.g., a geometric rotation) sequence of such ray tracings. Examples of such movies done at the Australia Telescope National Facility will be presented as well as a discussion of current trends at the NRAO.

J4-5
1020

APPLICATIONS OF PARALLEL SUPERCOMPUTING IN COMPUTATIONAL ASTRONOMY

Thomas A. Prince
Department of Physics, Mathematics, and Astronomy
and the Caltech Concurrent Supercomputing Facilities
California Institute of Technology
Pasadena, CA 91125

Parallel, or concurrent, supercomputers provide significant performance advantages over conventional serial or vector supercomputers. Current methodologies for parallel programming allow straightforward development of efficient parallel algorithms for typical scientific applications. Several examples of parallel supercomputing applications in astronomy will be discussed including: high-sensitivity radio pulsar searches using giga-point FFTs, detection algorithms for binary accretion-powered pulsars, enhancement of IRAS images, and ground-based diffraction limited IR/optical imaging. Performance of the Intel Touchstone Delta System, a 520-CPU concurrent supercomputer, will be discussed.

This work supported by NSF AST-9020787. Computational facilities provided by the Concurrent Supercomputing Consortium (CSCC).

J4-6 HIGH-RATE PULSAR ACQUISITION AND ANALYSIS NETWORK
1040

R. S. Foster
Remote Sensing Division
Code 7210
Naval Research Laboratory
4555 Overlook Avenue, SW
Washington, DC 20375-5000

and

J. M. Cordes
Astronomy Department
Space Sciences Building
Cornell University
Ithaca, NY 14853

Important problems in observational science are at present limited by the available data recording and computational resources. In astronomy, construction and major upgradings of radio telescopes represent a significant national investment whose benefits can be realized only through a corresponding investment in computational and networking power. Moreover, discoveries of new phenomena and tests of basic physical laws are anticipated to require state-of-the-art signal processing methods applied to large data sets.

The pulsar search problem is an excellent problem for application development under the High Performance Computing and Communication initiative. Under this program we propose to develop the following resources: (1) custom algorithms for transforming, dechirping, and signal detection on several computer platforms, including those with SIMD, MIMD, shared memory, and message-passing architectures; (2) investigate various algorithms for the detection of weak signals (typically 0.0001 times the mean noise); (3) develop methods of fast data acquisition; (4) interface and make optimal use of dense recording media with massively-parallel computer systems; (5) develop algorithms for the dynamic excision of radio frequency interference from wideband, baseband signals; (6) establish fast data links between data collection sites and supercomputing centers. Together, we plan to maximize signal processing performance by use of state-of-the-art hardware along with improved algorithms for signal detection.

The status of this initiative will be discussed with results from code implementation on massively parallel computers. Benchmarks of a search code on a variety of platforms, including serial, vector, and massively parallel architectures will be presented.

J4-7
1100

PRECISION POINTING SYSTEM FOR THE GBT

Donald C. Wells
National Radio Astronomy Observatory
520 Edgemont Road
Charlottesville, VA 22903-2475
dwells@nrao.edu

The 100m GBT [Green Bank Telescope] is under construction, with completion anticipated for January 1995. The GBT will be capable of operating at frequencies higher than 50 GHz, *if* its surface can be controlled and its beam pointed with sufficient accuracy. The 2000 panels of the GBT (75 μm RMS) will have actuators, and three laser rangefinders plus retroreflectors attached to the actuators will be used to actively servo the surface. A test assembly of four panels with overall geometry similar to the GBT is currently operating in Green Bank, and initial surface servo results are quite promising. The rangefinders have RMS errors less than 50 μm in the open air over 50-100 m ranges. The atmosphere is better behaved than many people had feared a priori.

The 8000 m^2 surface of the GBT will only be effective at high frequencies if the narrow beam can be pointed accurately. The plan for pointing is that another set of rangefinders will be mounted on a ring of piers around the telescope to measure retroreflectors attached to the alidade, elevation and backup structures of the GBT. The initial precision pointing implementation is likely to involve measuring a plane fitted through a ring of retroreflectors on the backup structure relative to a plane fitted through the circle of rangefinders on the ground. This (first order) solution for the azimuth and elevation of the dish backup structure will be independent of the alidade structure and the encoders, and its RMS error may be less than 1 arcsec.

Higher order deflections of the structure will be modelled with structural models combined with a variety of other sensor data. We expect to utilize temperature sensors throughout the GBT, a system of autocollimators in the alidade structure, pressure sensors for wind loadings, inclinometers near the elevation bearings and retroreflectors attached to the alidade and feed arm. It is likely that index of refraction variations will be measured with acoustic time-of-flight sensors. If vibrations prove to be an important problem in the GBT, we expect to track them by fitting sensor data to weighted sums of the eigenvectors of the structural models.

The GBT precision pointing system will produce pointing corrections (real alt-az minus ideal alt-az) for the monitor and control system of the telescope. These corrections will be updated several times per second. The 8 m subreflector will have a 6 degrees-of-freedom actuator system with response up to about 1 Hz, so that it will be possible to steer the beam faster than the response of the 100 m structure.

This talk will provide an overview of the present state of plans for the GBT precision pointing system software project, which will begin in January 1993.

J4-8 CONTROL SYSTEM CONCEPTS AT THE NRAO 12 M TELESCOPE
1120 P. R. Jewell, A. V. Dowd, D. T. Emerson, T. W. Folkers,
R. W. Freund, J. R. Hagen, and W. L. Peters
National Radio Astronomy Observatory
Campus Building 65
949 North Cherry Avenue
Tucson, AZ 85721-0655

The control system in use at the 12 m for the last two years employs several novel concepts. The system architecture is such that processing power is distributed among a workstation and several dedicated microprocessors in a well-integrated network. The network utilizes a custom-designed parallel input/output bus for fast synchronization, status, and error information. Finally, observing procedures and the user interface employ a language interpreter for C-like syntax that allows development and experimentation by staff astronomers without requiring the compiling and linking of essential system code.

The principle feature of the 12 m system is the distributed processing architecture. This architecture was chosen because it allows a modular development environment, and because it allows nearly unlimited expansion capabilities, without the difficulties of real time programming in a single large machine whose operating system may not be designed for such a task.

The computing network consists of a Sun Sparc 2 - class workstation, and four single-board microprocessors running the VxWorks real-time operating system. The microprocessors are Motorola MV-147s using the 68030 processor chip. Standard command and data transfer are via Ethernet using TCP/IP protocols. Unix "socket" connections are used extensively for communications between processors, and for inter-task communication in a given processor. The central workstation runs several tasks, including the user interface, the high-level system executive, status and monitor displays, and the data writers. One of the VxWorks microprocessors handles antenna tracking and closes the servo loop, another controls the digital continuum backend, a third controls two spectrometers, and a fourth drives synthesizers and performs a few miscellaneous input/output tasks, including GPIB network communications with commercial instruments. Most of the tasks in the workstation and in the microprocessors produce error and diagnostic logs.

The custom status and monitor bus (SAMBUS) has been a particularly successful feature of the system. It consists of 16 parallel input/output lines. Reading and writing of the SAMBUS is done by real-time device drivers in the VxWorks machines. This bus allows error conditions to be flagged very quickly so that, for example, data-taking can be suspended to protect data integrity.

The language interpreter allows a very flexible way for non-specialists (e.g., staff astronomers) to develop observing procedures without exposing the system to corruption and crashes. The interpreter understands virtually all C syntax structures and math library functions, except for pointers (basically, it is C without pointers). The interpreter was developed, in part, through use of the "yacc" and "lex" utilities of Unix. Procedure code is interpreted very quickly, and a rudimentary debugger is available.

J4-9
1140

Aperture Synthesis with the Tethered Satellite System

I.R. Linscott, Center for Radar Astronomy
Stanford University, Stanford, CA 94305
B.E. Gilchrist and T. Neubert
Space Physics Research Laboratory,
University of Michigan, Ann Arbor, MI 48109-2143

The first mission of the Tethered Satellite System (TSS-1), aboard the space shuttle Atlantis deployed, while in low Earth orbit, an electrically conductive 1.6 m diameter Italian built satellite upward to a maximum distance of 256 m above the shuttle. The satellite remained electrically connected to Atlantis via a conducting tether. During this operation, the Shuttle Electrodynamic Tether System (SETS) experiment collected high resolution samples of the tether voltage from the payload bay using a high impedance, low noise voltage monitor.

This configuration allowed the TSS-1 tether to be treated as a VLF radio antenna. Of particular interest is the synthesis of global scale apertures using the tether as a single antenna element. The performance of this synthesis technique is presented for the TSS-1 tether, based on the aperture response for the geometry of the TSS-1 Mission. Estimates for the associated beam response as well as sensitivity estimates to radio signals in the VLF radio band will be discussed. Although Atlantis's orbit was inside the ionosphere and locating sources is complicated, the tether aperture response and sensitivity to VLF signals are very interesting and they do provide an unusual perspective of any sources.

In addition to the tether antenna, the SETS experiment carried a magnetic antenna, consisting of a 0.2 x 0.4 m loop, mounted in Atlantis' cargo bay. Synoptic measurements were made using the magnetic antenna during the TSS-1 mission and these data afford an additional means of constructing a single element synthetic aperture at VLF frequencies. The magnetic antenna's aperture response will be evaluated and compared with the tether's electrical antenna aperture response for VLF radio signals.

Session J-5 1335-Fri. CR2-26
SEARCH FOR EXTRATERRESTRIAL INTELLIGENCE
Chairman: Jill C. Tarter, SETI Project, NASA/ARC, Moffett Field, CA 94035

J5-1
1340

A SEARCH FOR INFRARED LASER SIGNALS

Albert Betz
Center for Astrophysics & Space Astronomy
University of Colorado
Boulder, CO 80309-0389

In an effort complementary to NASA's search for microwave signals from an extraterrestrial intelligence, we are searching for possible laser signals of a similar origin. We are surveying ~300 nearby stars in a multi-year effort to detect narrowband laser signals in the 10 μm wavelength region. For this directed search, we are using an available 1.7 m telescope and a heterodyne receiver tuned for discrete CO_2 laser frequencies between 26-30 THz. The bandwidth of the heterodyne receiver allows us to analyze a Doppler velocity range up to ± 60 km s^{-1} around selected laser lines, and thus accommodate the velocity dispersions of hypothesized laser sources orbiting nearby stars. The resolution of the spectrometer is currently 2.4 MHz (24 m s^{-1}) with 10^3 spectral channels available. Although this resolution is somewhat coarse for the intended purpose, any slight indication of a signal could be re-observed at much higher resolution with the type of signal processor developed for the microwave survey.

J5-2 THE SERENDIP III SETI PROGRAM

1400 Dan Werthimer, Stuart Bowyer, Charles Donnelly, and David Ng
Space Sciences Laboratory
University of California
Berkeley, CA 94720

SERENDIP is an ongoing search for narrow band radio signals from extraterrestrial civilizations. SERENDIP systems operate under a piggyback search paradigm in which unobtrusive long term observations are conducted on the world's largest radio telescopes. In this talk we will discuss SERENDIP III, the latest generation of SERENDIP instruments, and results from the first nine months of observations at the NAIC Arecibo Observatory.

SERENDIP III is a four million channel FFT-based spectrum analyzer operating at 0.6 Hz resolution with a 1.7 second integration time. To date SERENDIP III has accumulated 1500 hours of high quality telescope time observing 70% of the sky visible by the Arecibo telescope. Over this nine month period SERENDIP III has analyzed 13 trillion spectral bins, and recorded information of 50 million strong narrow band signals in the 424 - 435 MHz band. A handful of these signals have survived our RFI rejection and signal detection algorithms, and have thus been added to our list of ETI candidate signals. A follow-up observation program will be conducted this year in an attempt to verify each of these candidate signals.

J5-3
1420

INITIAL OBSERVATIONS OF THE NASA HIGH RESOLUTION MICROWAVE SURVEY - THE SKY SURVEY ELEMENT

S. Gulkis, S. Levin, E.T. Olsen, and M.J. Klein
Jet Propulsion Laboratory
California Institute of Technology
4800 Oak Grove Drive
Pasadena, CA 91109

The NASA High Resolution Microwave Survey (HRMS) is composed of two observational modes: a target search of nearby stars and an all sky survey. The objective of the all sky survey is to search the entire celestial sphere over the frequency range 1 - 10 GHz with a spectral resolution of 30 Hz or less. Initial observations of the HRMS - Sky Survey Element were started on October 12, 1992 using a beam waveguide 34 m diameter antenna operating at X-band. A 26 m diameter antenna operating at L-band was also used. Both antennas are located at the NASA/JPL Goldstone tracking station near Barstow, California. A 2 million channel prototype, digital spectrum analyzer is being used. This paper will report on the Sky Survey system performance parameters, and present the results of the first three months of operation.

J5-4
1440

PRELIMINARY RESULTS FROM THE HIGH RESOLUTION MICROWAVE SURVEY TARGETED SEARCH OBSERVATIONS AT ARECIBO

Dr. Peter R. Backus
SETI Institute
2035 Landings Drive
Mountain View, CA 94043

NASA's High Resolution Microwave Survey (HRMS) is part of the Toward Other Planetary Systems (TOPS) program. It is an attempt to detect the presence of planets orbiting other stars through the indirect evidence provided by intelligent, technological life that may have arisen on those planets. The HRMS searches for microwave radio transmissions from technological civilizations in two complementary strategies, a Sky Survey and a Targeted Search.

The Targeted Search will examine approximately 1000 solar-type stars within 100 l.y. for narrowband CW or pulsed transmissions in the frequency range of 1 GHz – 3 GHz that may have frequency drifts of $\Delta f/f \leq \pm 10^{-9}$. To accomplish the search in a reasonable time, a Targeted Search System (TSS) has been developed. The initial TSS consists of an RF/IF processor, a multichannel spectrum analyzer (MCSA), special purpose signal detectors, and a control computer. The MCSA processes a 10 MHz bandwidth into six simultaneous resolutions from 1 Hz to 28 Hz. A CW detector performs an incoherent integration on the 1 Hz or 2 Hz resolution to achieve sensitivity to CW signals with a S/N of 0.25. A pulse detector analyzes all six resolutions for pulses with durations in the range from 25 ms to 1.5 s and a S/N > 10. The data are processed in real-time and the control computer compares potential signals with a database of know interference (RFI). Signals not in the database undergo further tests immediately.

This paper presents preliminary results from the initial deployment of the TSS to the Arecibo Observatory in October, 1992. Planned observations will include 24 stars and cover the 290 MHz of bandwidth provided by the observatory's standard radio astronomy receivers. Frequency bands covered are 1302-1430 MHz, 1566-1678 MHz, and 2355-2405 MHz.

J5-5
1500

TARGET SELECTION STRATEGY FOR HRMS

David Soderblom
Space Telescope Science Institute
3700 San Martin Drive
Baltimore, MD 21218 USA
and
David Latham
Harvard-Smithsonian Center for Astrophysics
60 Garden Street
Cambridge, MA 02138 USA

NASA's High Resolution Microwave Survey consists of two complementary parts: A more or less unbiased All Sky Survey and a Targeted Search Element (TSE). The TSE is intended to examine the nearest ~1000 solar-type stars to a much higher level of sensitivity than is possible in the All Sky Survey. Here we describe a TSE strategy that incorporates several levels so as to explore as much of the target parameter space as possible, while applying astrophysical knowledge of the potential targets to optimize the *a priori* odds of a detection in the dominant portion of the sample. That strategy is:

1. Observe the nearest 100 systems, which are mostly M dwarfs within about 20 ly.
2. Observe all F5 to K5 dwarfs within 30 ly, including binary stars (~64 stars).
3. Observe the old, single G0V to K2V stars out to 150 ly as the prime sample (~1000 stars).
4. Spend additional time on the old, single G0V to G5V dwarfs that are within 60 ly (~20 stars) to detect possible leakage signals.

We will elaborate upon these choices and describe the relevant observational techniques. An important part of our work is the detailed characterization of the target stars, particularly with regard to the presence of low mass companions, and that effort will be described as well.

J5-6
1520

HRMS TARGETED SEARCH SYSTEM HARDWARE

J.W. Dreher for HRMS TS Team
NASA Ames Research Center
MS 244-11
Moffett Field, California, CA 94035-1000

An overview of the hardware to be used in the Targeted Search element of the NASA High Resolution Microwave Survey will be given. The RF system will use dual-polarization, wide-band scalar feeds and cryogenic orthomode transducers, followed by HEMT low noise amplifiers and an upconverter. 400 MHz bandwidth LCP and RCP IFs centered near 700 MHz will be distributed in analog form over singlemode optical fibers, as will the LO and an RF test signal. The 10 MHz bandwidth digital IFs required by the signal processors will be selected from a wideband IF by a hybrid analog-digital frequency conversion and filtering system. The first stage of signal processing is a Fourier Transform spectrometer implemented as a polyphase filter bank with time-overlapped spectra and Han windowing. It will deliver 14 million 1 Hz bandwidth channels every .75 seconds as well as 5 coarser resolutions (each at the same aggregate data rate). Three detector systems will analyze these outputs. A Pulse Detector will search for repetitive pulses using a power-thresholded subset of the spectrometer data; by using multiple resolution data streams it will maintain a nearly optimum performance over two decades of pulse bandwidth. A CW Detector will search the 1 Hz (or 2 Hz) resolution power data for continuous signals drifting up to 1 (or 4) Hz/sec. Another detector will use the complex amplitudes from the 1 Hz resolution to perform a search for non-drifting CW signals with 3 dB more sensitivity than the drifting CW detector. The results of these detectors will be analyzed and placed into a database by a high-performance workstation; this computer will also control the system in an unattended mode, including automatic reobservation of signals if required. Four dual-polarization, 10 MHz bandwidth signal processing units will be housed in two transportable, RF-shielded shelters. A pre-production version of this system was sucessfully deployed at Arecibo from September to November 1992.

J5-7
1600

HRMS SKY SURVEY STRATEGIES FOR INTERFERENCE REJECTION

E. T. Olsen, S. Levin, C. Backus and S. Gulkis
169-506
Jet Propulsion Laboratory
California Institute of Technology
4800 Oak Grove Drive
Pasadena, CA 91109

The Sky Survey component of the NASA HRMS program will utilize the DSN 34m antennas to observe the entire celestial sphere over the RF range 1.0 GHz to 10.0 GHz at a resolution 30 Hz or less. In the absence of RFI, the probability of detection of a CW signal will exceed 90% if the received flux level exceeds 4 x 10^{-23} x f_{GHz} Wm^{-2}. No more than 25% of the available telescope time will be devoted to reobservation of candidate signals. Thus RFI must be efficiently rejected to ensure that the limited observatory resources are not squandered in following up signals of human origin.

Strategies for RFI rejection have been developed and are being tested in the field at 8.4 GHz, 2.7 GHz and 1.7 GHz. We are using a prototype 2^{21} channel FFT system which spans an instantaneous IF bandpass of 40 MHz at a resolution of 19 Hz and which achieves the planned operational HRMS Sky Survey limiting sensitivity.

The rejection strategies currently being tested are scheduling, scan strategy, beam chopping, frequency breadth, signal duration and detection statistics. They are being applied in the areas of antenna control, signal detection hardware, near-real time signal detection software and post processing. The goal is to identify those methods which are most efficient and least costly to implement in the future operational Sky Survey system while at the same time allowing the largest fraction of the RF bandpass to be searched for signals of extraterrestrial intelligent origin.

A condensed database of the RFI encountered is being compiled to keep track of the frequencies which it obscures and to compare the RF occupancy at operational limiting sensitivity with that encountered in previous surveys with a less sensitivity instrument.

J5-8
1620

INTERFERENCE REJECTION STRATEGY FOR THE NASA HRMS TARGET SEARCH

Gary Heiligman
Sterling Federal Systems
NASA Ames Research Center, MS 244-11
Moffett Field, CA 94035-1000

Many types of man-made RF interference (RFI) possess some of the hypothesized characteristics of an ETI signal. The Targeted Search System (TSS) incorporates several complementary techniques for rejecting RFI. Predetection methods include these:

- RF shielding
- low-distortion RF/IF components
- high dynamic range A/D converters
- narrow (1-28 Hz) spectral bin width
- high out-of-band rejection
- detectors that identify bad bands
- masking of known RFI frequencies

Once detections are made the preliminary reports are passed to the System Control Subsystem (SCS), a fast workstation computer. The SCS rejects detections caused by RFI using three techniques:

- RFI database queries, e.g., does the RF, IF, or baseband frequency correspond to an entry in a database containing known RFI-generated detections?
- A priori criteria, e.g., is the topocentric drift rate exactly 0?
- Statistical tests, e.g., did the average power in the band change significantly?

Detections that pass these tests are declared to be unresolved and are queued for a series of reobservations. These include slight changes in local oscillator frequencies (to ensure that the detection is not an image sideband or distortion product), pointing the telescope on and off source, and recording the complex amplitudes of a 643 Hz-wide subband centered on the detection (to enable reconstruction of the time series). The result is a system capable of finding signals in near-real time that has a relatively small (<10%) reobservation overhead.

J5-9
1640

THE GEORGIA TECH SPACEBORNE TRANSMITTER DATABASE AND ITS USES IN SETI AND RADIO-ASTRONOMY

David R. DeBoer and Paul G. Steffes
Georgia Institute of Technology
School of Electrical Engineering
Atlanta, GA 30332-0250

To address the increasing problem with space-based interference in SETI searches and radio-astronomy, a database and search system have been developed which characterize spaceborne transmitters including geostationary communications satellites, low earth orbiting governmental satellites and deep space exploration probes. Two databases have been developed for this work. The first, called GEOSAT, contains 470 spacecraft of which 407 are geostationary and primarily commercial. GEOSAT operates using the dBASE III Plus software package. The second database was developed by the Space Frequency Coordination Group (SFCG) and is called SSDB. SSDB contains 153 government-owned spacecraft and uses a software/database management package called Clipper.ver87. All listings are non-classified.

The top-level search system is called SETI RFI Search (SRS) and searches GEOSAT and SSDB for a match to given parameters. The parameters consist of a sky window in right ascension/declination or azimuth/elevation, and a frequency range. The observer's location is also entered as well as the date and time (UT) of the observation. An on-line catalog of locations and observatories and their positions is included. The spacecraft found to lie within the search space are written to an ASCII output file along with the parameters and spacecraft characteristics.

SRS has another menu with helpful astrometric routines as well as on-line help. Programs are included to convert SSDB data for use with SRS (DCSS) and GEOSAT data for use with SRS (DCGEO). All of the above runs in the MS-DOS environment, however SRS can easily be adapted for other operating systems such as UNIX and VMS.

J5-10
1700

SPECTRAL LINE RADIO ASTRONOMY AS PART OF THE HRMS ALL-SKY SURVEY

Woodruff T. Sullivan, III
Dept. of Astronomy, FM-20
University of Washington
Seattle, WA 98195 USA

The Sky Survey portion of NASA's High Resolution Microwave Survey (HRMS) will scan the entire sky at all frequencies from 1 to 10 GHz with a resolution of 30 Hz and beam sizes ranging from about 25 arcmin to 3 arcmin. The effective integration time per beam will be only 1-2 sec during the main survey, but it is still anticipated that useful astrophysical results will come from 1 kHz and 78 kHz "radio astronomy" spigots that are part of the spectrometer design (not to speak of the possibilities for unprecedented, but natural phenomena of sub-100 Hz bandwidth that may be serendipitously discovered).

Examples of anticipated all-sky astronomical surveys include: (1) interstellar masers, both those known (such as hydroxyl and methanol) and new ones (note that the 6 GHz methanol masers recently surprisingly discovered by Menten would have been easily found in the HRMS), (2) strong absorption lines, especially in the 21 cm H I line, against continuum sources both in the Galaxy and extragalactic, and (3) a search for the expected radio lines produced by the decay of axions, a candidate particle to explain the dark matter in the Galaxy; the frequency of this line depends on the (unknown) mass of the axion.

Until the full 300 MHz spectrometer is available in 1996, observations are now being carried out with a prototype of 40 MHz bandwidth and 2.1 million channels. It is planned to conduct one or more "deep" surveys in the 1400-1700 MHz range at low galactic latitudes using the 40 meter dish of Caltech's Owens Valley Radio Observatory. These surveys of much higher sensitivity would not only be useful for SETI, but also for searching for H I emission from galaxies hidden behind Galactic dust in the zone of avoidance and for searching for time-variable continuum sources.

J5-11
1720

CONTINUUM RADIO ASTRONOMY WITH THE HRMS ALL-SKY SURVEY

Dayton L. Jones
Mail Code 238-600
Jet Propulsion Laboratory
4800 Oak Grove Drive
Pasadena, CA. 91109

The sky survey element of NASA's High Resolution Microwave Survey will scan the entire sky at frequencies between 1 and 10 GHz. One of the astronomical benefits of this survey will be a catalog of continuum radio sources at higher frequencies than existing all-sky surveys. Although the total observing time per beam area will be very short ($\sim$ one second), the wide frequency coverage will allow total power averaging over multi-GHz bandwidths. The resulting sensitivity will be comparable to the MIT-GB 5-GHz surveys with the NRAO 300-foot antenna. A catalog at $\approx$ 10 GHz will be particularly useful for selecting very compact sources with inverted spectra.

At frequencies near 1 GHz, the sky survey will produce maps of extended galactic emission covering all galactic latitudes. The wide instantaneous bandwidth ($\approx$ 320 MHz) of the spectrometer will permit continuum sources showing strong interstellar scintillation to be readily detected.

Data obtained during the sky survey will be archived as raw spectra with approximately 100-kHz resolution, along with antenna pointing, amplitude calibration, and RFI information. A limited frequency range can also be archived at higher spectral resolution ($\approx$ 1 kHz). Algorithms for selecting the frequency bands to be archived at kHz resolution are currently under development.

This work was carried out at the Jet Propulsion Laboratory, California Institute of Technology, under contract with the National Aeronautics and Space Administration.

J5-12
1740

RADIO ASTRONOMY AND THE HRMS: TRANSIENT & SCINTILLATING SOURCES

James M. Cordes
Astronomy Department & NAIC
Cornell University
Ithaca, NY 14853

The High Resolution Microwave Survey (HRMS) has, as one component, an all sky survey between 1 and 10 GHz. Single-pass coverage of sky positions will be made over time and frequency spans ~ 1 - 3 sec x 320 MHz with resolutions of 50 ms and 30 Hz. Tentative plans also include a galactic plane survey in L band (eg. 1.4 to 1.72 GHz) with greater dwell times and multiple passes on sky positions. Strategies for detecting transient sources on a wide range of time scales will be discussed. Potential objects include long term variables similar to Cygnus X-3, flare stars, and pulsars that emit occasional giant pulses like the Crab pulsar. The ability to use interstellar dispersion delays as a signature for source detection will be discussed. Interstellar scintillations pose both difficulties and opportunities for finding compact sources of high spatial coherence. We will discuss strategies that take scintillations into account, in both the strong and weak scattering regimes that apply for distant and local sources, respectively. Before the sky survey spectrometer is available in 1996, a prototype system with 40 MHz bandwidth is available. Search strategies for this system will also be presented.

This work was supported by NASA Grant NAG 2-697 and by the National Astronomy and Ionosphere Center, which operates the Arecibo Observatory under cooperative agreement with the NSF.

INDEX

A

Adams, J.W., 43
Adler, R.W., 75
Agarwal, R.K., 53, 132
Aguero, V.M., 118
Anderson, D.N., 24, 156, 201
Anderson, D.S., 142
Anderson, K.D., 109, 149
Armstrong, J.T., 166
Arsenieva, A.D., 48
Axe, M.R., 132

B

Babcock, R.W., 171
Baca, E.A., 13, 102
Backer, D.C., 168, 184, 187
Backus, C., 222
Backus, P.R., 219
Bahar, E., 46
Bahrmasel, L.J., 131
Baker-Jarvis, J., 86
Banerjee, A.K., 40
Barnes, F.S., 40
Barrios, A.E., 107
Bartel, N., 190
Basart, J.P., 182
Basu, S., 23
Basu, Su., 23
Bauhahn, P., 89
Baum, C.E., 99, 103, 104, 193
Benalla, A., 174
Benson, R.F., 181
Bernhardt, P.A., 27, 28, 36, 158
Betz, A., 216
Bhapkar, U.V., 91
Biernacki, P., 17
Biggs, A.W., 13, 87, 102
Bilén, S.G., 118
Bilitza, D., 200
Black, Q.R., 159
Bleszynski, E., 52
Bleszynski, M., 52
Blitz, L., 129
Boerner, W.-M., 121
Bolton, S.J., 38
Booton, R.C., Jr., 51, 137
Bouche, D., 195
Bowyer, S., 217
Browning, S.L., 194
Buchau, J., 23, 201
Buetow, J., 95
Bundy, S., 16
Buonsanto, M., 199, 205
Buscher, D.F., 166

C

Calhoun, M.D., 124
Camilo, F., 185
Campbell, R.M., 190
Cannon, W.H., 190
Cappallo, R.J., 190
Carlstrom, J.E., 126
Chandler, J.F., 171
Chang, D.C., 51
Chaturvedi, P.K., 158
Chen, C.F., 199
Chen, K.Y., 17
Chen, T.R., 124
Chew, W.C., 177
Clancy, C.T., 76
Codrescu, M., 203
Cohen, D.J., 142
Compton, R.C., 55
Conkright, R.O., 180
Cooper, Henry F., 83
Cordes, J.M., 188, 212, 227
Corey, B.E., 167
Cotton, M., 154
Cox, D.D., 150
Cramer, P.W., 49
Creamer, A.P., 156
Croes, G., 208
Crowe, T.W., 90
Crutcher, R.M., 209
Curran, D.B., 81

D

Dabberdt, W.F., 64
Dalkir, Y.R., 29, 116
Dannon, V., 138
Davis, J.L., 167
Davis, W.A., 1, 3
de Pater, I., 31, 38, 77
de Vegt, C., 164
Dea, J.Y., 121
DeBoer, D.R., 224
Decker, D.T., 24, 201
DeSanto, J.A., 45
Ditz, M.W., 1
Djuth, F.T., 27, 28
Dobrowolny, M., 122
Dockery, G.D., 106, 152
Doherty, P.H., 156
Donnelly, C., 217
Dowd, A.V., 214
Dreher, J.W., 221
Duncan, L.M., 27, 28
Dunn, J.M., 51

E

Ecklund, W.L., 64
El-Ghazaly, S.M., 96
El-Sharawy, E.-B., 19
Elias, N.M., 166
Emerson, D.T., 214
Erickson, W.C., 129
Escalera, N.J., 182
Eubanks, T.M., 190

F

Fainberg, J., 78
Fairall, C.W., 62
Falco, F., 50
Farr, E.G., 103, 104
Fejer, B.G., 156
Feng, W., 57
Ferguson, J.A., 183
Fesen, C.G., 157
Fey, A.L., 164
Folkers, T.W., 214
Fomalont, E.B., 189
Ford, P.G., 34
Foster, R.S., 184, 187, 212
Frail, D.A., 186
Franke, P.M., 69
Freund, R.W., 214
Fuller-Rowell, T.J., 203

G

Gage, K.S., 64
Gardner, R.L., 100
Gasiewski, A.J., 155
Gaynor, J.E., 65
Gee, C.M., 124

Gelmont, B., 94
Genco, S.M., 95
Geyer, R.G., 88
Gilchrist, B.E., 118, 122, 215
Giri, D.V., 98
Gitin, M.M., 55
Glisson, A., 50
Goetz, M.P., 2
Goldhirsh, J., 152
Goss, W.M., 189
Gossard, E.E., 60, 61
Green, A.W., Jr., 121
Greenwald, R.A., 25
Greisen, E.W., 210
Grider, D., 89
Grimes, G., 124
Grimm, J.M., 175
Grossman, A.W., 80, 129
Groves, K.M., 115, 117
Gulkis, S., 38, 218, 222
Gupta, K.C., 15, 174
Gurnett, D.A., 37
Gwinn, C.R., 191

H

Hagen, J.R., 214
Haines, D.M., 73
Hall, R.C., 196
Hansen, P.M., 121
Harmon, J.K., 32
Hartwick, P.J., 40
Haupt, R.L., 139
Hecksher, J., 71
Heelis, R.A., 24
Heiles, C., 38
Heiligman, G., 223
Hickenbottom, D.T., 112
Hill, D.A., 11
Hills, R.E., 126
Hitney, H.V., 105, 110
Hjelme, D.R., 20, 54
Ho, A.Y., 70, 120
Hooker, H.B., 57
Houshmand, B., 134
Huang, C.-C., 176
Huang, X., 205
Huang, Y., 71
Huba, J.D., 36, 158
Huffaker, J.D., 106
Hufford, G.A., 154
Hummel, C.A., 166
Hunsucker, R.D., 75
Hunton, D.E., 28
Hur, K.Y., 55
Hutter, D.J., 166

I

Imbriale, W.A., 49
Inan, U.S., 30
Infante, D.J., 175
Ishiguro, M., 128
Itoh, T., 92, 134

J

Jankovic, D., 51
Jauncey, D.L., 164
Jensen, M.A., 9
Jevremovic, V., 56
Jewell, P.R., 214
Johnk, R., 41
Johnston, K.J., 164, 166
Jones, D.J., 165
Jones, D.L., 226
Justtanont, K., 189

K

Kanda, M., 39, 41
Kanzawa, T., 128
Kawaguchi, N., 164
Kawashima, S., 128
Keller, A.E., 37
Keller, D.M., 1
Kelley, M.C., 27
Kemball, A., 164
Kiebler, J., 145
Kim, D., 63
King, C.W., 65
King, E.A., 164
Klein, M.J., 38, 218
Kleiner, N., 148
Kleinman, R.E., 84
Knepp, D.L., 68
Kobayashi, H.K., 42
Koh, P.J., 90
Koppel, D., 50
Kuklinski, W., 73
Kunkee, D.B., 155
Kuo, S.P., 70, 115, 116, 117, 119, 120
Kurth, W.S., 37
Kuttler, J.R., 106
Kwiatkowski, S.L., 54
Kzadri, B., 175

L

LaBelle, M.S., 51
Latham, D., 220
Lauben, D.S., 118
Lay, O.P., 126
Lebach, D.E., 167
Lee, B.S., 46
Lee, M.C., 29, 70, 114, 115, 116, 117, 119
Lestrade, J.-F., 165
Levin, S., 218, 222
Levine, M.W., 130
Li, T., 123
Li, Y., 91
Li, Yi., 197
Liang, C.S., 172
Liebe, H.J., 154
Lin, C., 108
Lin, K.H., 180
Lin, S., 57
Lin, Y., 178
Lindell, I.V., 84
Ling, H., 153, 172, 173, 195
Linscott, I.R., 215
Logan, R.T., Jr., 124
Lott, G.K., 75
Lubecke, O.B., 92
Lutes, G., 124, 125
Lyne, A.G., 189

M

Ma, C., 163, 164
Ma, M.T., 44
Ma, S.Y., 180
MacDowall, R.J., 79
MacLeod, G., 164
Mader, T., 18
Malin, D.F., 164
Manchester, R.N., 189
Maradudin, A.A., 47, 48
Marks, R.B., 2
Martin, C.L., 64

Martinez, E., 89
Martinez, J., 99
Martner, B.E., 64
Masson, C.R., 130
Masterson, K.D., 39
Matheson, R.J., 144
Matini, A., 58
Mattauch, R.J., 91
Maurer, M.J., 35
McAdoo, J.A., 93
McCormack, C.J., 139
McCoy, M., 182
McCulloch, P.M., 164
McGurn, A.R., 48
McKinnis, J., 16
McLemore, D., 99
McNamara, L.F., 160
Megahed, M.A., 96
Méndez, E.R., 47
Menietti, J.D., 81
Menten, K.M., 169
Meriwether, J.W., Jr., 26
Meyer, J., 66
Mickelson, A.R., 17, 20, 54, 56, 57, 95
Miller, E.K., 139
Miller, K.L., 204, 206
Miller, R., 66
Mitchell, D.L., 31, 77
Miyaji, T., 128
Moghaddam, M., 177
Moore, J., 172, 173, 195
Moriarty, D.T., 114, 115
Mozurkewich, D., 166
Mrazek, C.P., 106
Mudaliar, S., 111
Muhleman, D.O., 80
Mundy, L.G., 129
Murray, J.P., 143
Musiani, B.H., 152

N

Nabulsi, K.A., 85
Narayanan, R.M., 112, 150
Neubert, T., 215
Ng, D., 217
Nickisch, L.J., 69
Nicolson, G., 164
Nishio, M., 128
Noecker, M.C., 6, 171
Nogradi, I., 22
Norgard, J., 58
Norman, M.L., 207
Novotny, D.R., 39
Nyquist, D.P., 175

O

Oliker, V., 12
Olmstead, D., 145
Olsen, E.T., 218, 222
Olsen, R.G., 101
Ondrejka, A., 41
Orman, M., 50
Ostro, S.J., 77

P

Padin, S., 127
Palmer, P., 77
Pan, D.-S., 92
Parker, R.R., 114
Parlow, R.D., 140
Parrikar, R.P., 15
Paul, A.K., 72, 74
Paulus, R.A., 59
Peatman, W.C.B., 90
Peters, W.L., 214
Petrachenko, W.T., 190
Pettengill, G.H., 34
Pfaff, R.F., 27
Phillips, J.D., 6, 171
Phillips, R.B., 165
Phillips, T.G., 126
Pitteway, M.L.V., 162
Pogorzelski, R.J., 133
Pollack, C.J., 28
Popelar, J., 190
Popovic, Z.B., 16, 17, 18, 20, 56, 57, 95
Prather, W., 99
Pratt, T., 147
Preston, R.A., 165
Primas, L.E., 56
Prince, T.A., 211
Pucic, S.P., 5

Q

Quirrenbach, A., 166

R

Radisic, V., 20
Rahmat-Samii, Y., 9, 98
Ralston, J.M., 150
Ratner, M.I., 167, 190
Reasenberg, R.D., 6, 171
Reilly, J.P., 108
Reiner, M.J., 78
Reinisch, B.W., 23, 73, 116, 160, 199, 201, 202, 205
Reynolds, J.E., 164
Richards, P., 202
Rodriguez, P., 28
Rogers, L.T., 149
Romero, H.A., 28
Romney, J.D., 192
Rose, R.B., 75
Rowland, H.L., 36
Rowland, J., 66
Rudie, S.A., 108
Russell, J.L., 163, 164

S

Saavedra, V., 195
Safaai-Jazi, A., 147
Sailors, D.B., 97
Sales, G.S., 71
Sanchez, L.A., 115, 116, 117
Sanders, F., 146
Scali, J.L., 116, 199
Schennum, S.D., 101
Schlicher, R.L., 87
Schoenberg, J., 18
Schroeder, J.A., 63
Schuermeyer, F., 89
Schunk, R.W., 198
Sega, R., 58
Shaffer, D.B., 163, 164
Shapiro, I.I., 167, 190
Sheehan, R., 24
Shen, B., 7, 8
Sherrill, W.M., 159
Shu, M., 53, 132
Shur, M., 89, 90, 94
Siefring, C.L., 28
Siegel, P., 91
Silvestro, J., 136
Simon, R.S., 166
Simpson, R.A., 35

Snyder, L.E., 77, 82
Soares, S.F., 127
Soderblom, D., 220
Sojka, J.J., 198
Sower, G., 99
Sprague, R.A., 72
Sramek, R.A., 168
Stankov, B.B., 63, 64
Steffes, P.G., 224
Steyskal, H., 196
Stone, N.H., 122
Stone, R.G., 78, 79
Strauch, R.G., 64
Stutzman, W.L., 7, 8, 147
Sue, M., 145
Sullivan, W.T., III, 225
Sulzer, M.P., 115, 116, 117
Szuszczewicz, E.P., 27

T

Takahashi, Y., 164
Tamil, L.S., 178, 179, 197
Taranenko, Y., 30
Taylor, D.J., 194
Telikepalli, R., 14
Thompson, D.C., 118
Thompson, T.W., 33
Torii, C., 128
Torrence, G.W., 148, 153
Towe, E., 93
Tran, H.B., 52
Tran, T., 99
Tranquilla, J.M., 14
Treuhaft, R.N., 170
Tyler, G.L., 35

U

Überall, H., 194

V

Valladares, C.E., 23, 24
Voelker, R.H., 21
Vogel, W.J., 148, 153

W

Wait, D.F., 4
Wait, J.R., 85
Walsh, E.J., 113
Wang, C.-M., 35
Wang, C.N., 205
Weber, E.J., 27
Webster, A.R., 151
Wells, D.C., 213
Werthimer, D., 217
Westwater, E.R., 63, 64
White, A.B., 62
White, G.L., 164
Whitney, A.R., 190
Williams, D.F., 2
Williams, S.D., 118
Winglee, R.M., 81
Wise, F.W., 55
Wolfe, D.E., 65
Wood, J.F., Jr., 159
Woodworth, M.B., 135
Wright, J.W., 161, 162
Wu, H.-Y., 204
Wuertz, D.B., 64
Wye, D.P., 141

Y

Yaghjian, A.D., 10, 135
Yeh, K.C., 180
Yeomans, D.K., 77

Z

Zacharias, N., 164
Zhou, Q., 199
Zrnic, D.S., 67

Wednesday, 6 January (cont.)

1700-1800

Commission B Business Meeting	CR2-28
Commission E Business Meeting	CR1-40
Commission F Business Meeting	CR2-6
Commission H Business Meeting	CR1-42
Commission J Business Meeting	CR2-26
Commission K Business Meeting	CR1-46

Thursday, 7 January

0835-1200

B-4	NUMERICAL METHODS	CR2-28
F-3	PROPAGATION MEASUREMENTS AND SIMULATION	CR2-6
J-2	HIGH PRECISION ASTROMETRY	CR2-26

0855-1200

E-2	INITIATIVES AND TRENDS IN SPECTRUM MANAGEMENT	CR1-40
G-3	LOW AND MID-LATITUDE PHENOMENA	CR0-30

1335-1520

B-5	COATED STRIPS, MICROSTRIPS AND TRANSMISSION LINES	CR2-28

1335-1700

J-3	PULSARS	CR2-26

1355-1700

G-4	IONOSPHERIC PHENOMENA	CR0-30

1535-1700

B-6	INVERSE SCATTERING	CR2-28

Friday, 8 January

0835-1200

B-7	TRANSIENTS	CR2-28
G-5	VALIDATION OF IONOSPHERIC MODELS	CR0-30
J-4	ADVANCED COMPUTING TECHNIQUE	CR2-26

1335-1800

J-5	SEARCH FOR EXTRATERRESTRIAL INTELLIGENCE	CR2-26